

PB275526



INELASTIC BEHAVIOR OF ECCENTRICALLY BRACED  
STEEL FRAMES UNDER CYCLIC LOADINGS

by

Charles W. Roeder  
Research Assistant  
University of California, Berkeley

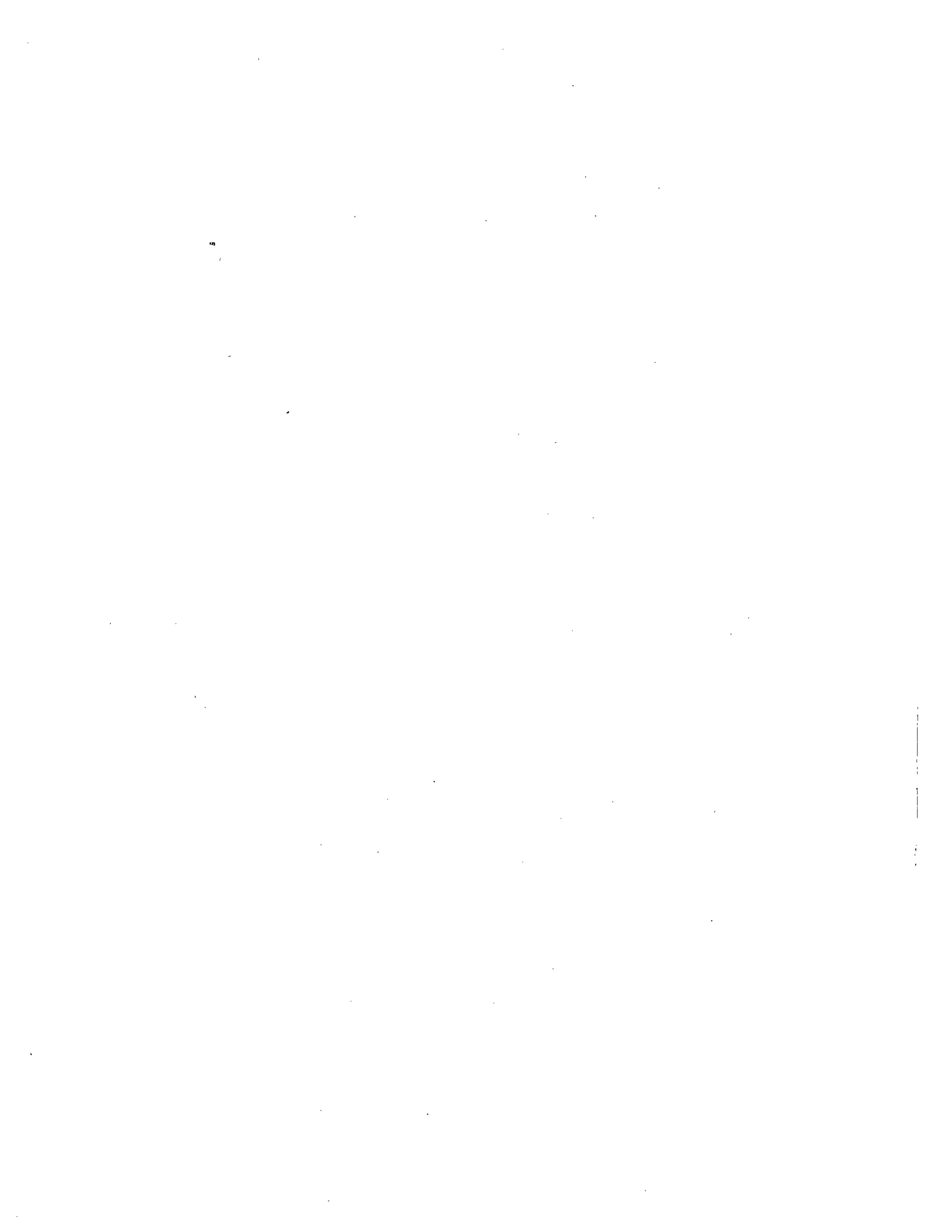
Egor P. Popov  
Professor of Civil Engineering  
University of California, Berkeley

Report to Sponsors  
American Iron and Steel Institute  
National Science Foundation

Report No. UCB/EERC-77/18  
Earthquake Engineering Research Center  
College of Engineering  
University of California  
Berkeley, California

August 1977

REPRODUCED BY: **NTIS**  
U.S. Department of Commerce  
National Technical Information Service  
Springfield, Virginia 22161



## **GENERAL DISCLAIMER**

**This document may be affected by one or more of the following statements**

- **This document has been reproduced from the best copy furnished by the sponsoring agency. It is being released in the interest of making available as much information as possible.**
- **This document may contain data which exceeds the sheet parameters. It was furnished in this condition by the sponsoring agency and is the best copy available.**
- **This document may contain tone-on-tone or color graphs, charts and/or pictures which have been reproduced in black and white.**
- **This document is paginated as submitted by the original source.**
- **Portions of this document are not fully legible due to the historical nature of some of the material. However, it is the best reproduction available from the original submission.**



## ABSTRACT

A unique, practical structural system, the eccentric bracing system, which possesses many advantages in the seismic design of steel structures, is described in this work. This system employs diagonal braces with deliberately large eccentricities with respect to the beam-column joint. The eccentricity is introduced to provide a ductile fuse which will prevent brace buckling at extreme loads, such as those that may occur during a severe shake, and to avoid the poor energy dissipation characteristics which result from this buckling. The system is also a very stiff structural system, since linear elastic analysis indicates that the lateral stiffness remains essentially constant over a wide range of small to moderate eccentricities. Therefore, eccentrically braced frames offer the elastic strength and stiffness of a braced frame and the energy dissipation of a steel moment-resisting frame. Hence, the system is very suitable for the design of earthquake-resistant structures, and it has numerous potential applications.

Short beams which initially yield in shear are tested in cyclic loading. These beams were designed to simulate the behavior of an eccentric element. It was found that cyclic shear yielding of the eccentric element is the most desirable energy dissipation mechanism because of its greater stability during large cyclic deflections. An analytical model for predicting the behavior of such beams is developed from the test results. The model is based on sandwich beam theory, which includes the effect of cross-sectional warping caused by shear yielding. The inelastic model is used to perform inelastic dynamic analysis of a 20-story eccentrically braced prototype structure under the 1.5 times

El Centro and unreduced Pacoima Dam acceleration records. The results of these analyses are compared with the computed response for similar ordinary braced and moment-resisting frames. The eccentric bracing system performs very well in this comparison because it combines strength, stiffness, and energy dissipation. The moment-resisting frame did not have sufficient strength or stiffness and the ordinary braced frame lacked good energy dissipation, so the alternate structures did not perform as well as the eccentric system.

Two one-third scale model eccentrically braced test frames were designed and tested. The frames were three-stories high, and they were modeled to represent the lower corner of the 20-story prototype structure. The loading program simulates the response of the eccentrically braced frame under the 1.5 times El Centro and unreduced Pacoima Dam acceleration records in sequence. The tests indicate that the eccentrically braced frame can be expected to survive two such sequential earthquakes without a structural failure. Further, for severe earthquakes of this intensity, the frames exhibit very sound, unpinched hysteresis loops which do not deteriorate in strength or stiffness. The tests are also compared with the inelastic model, and the comparison indicates that the behavior predicted by the model is in very close agreement with the test results.

Finally, design recommendations are made. The combination of these, the analytical procedures, and the test results can be used to produce structures which are able to withstand very severe earthquake excitations. In addition to applications in building design, which were emphasized in this work, the eccentric bracing system offers attractive possibilities for supports of water towers, large span roofs, and other systems in areas with severe seismic activity.

## ACKNOWLEDGEMENTS

The research reported herein is the major phase of Project 193 on "Earthquake Bracing of Multistory Steel Frames" sponsored by the Committee of Structural Steel Producers and the Committee of Steel Plate Producers of the American Iron and Steel Institute (AISI). Some support in developing this report was also provided by the National Science Foundation (NSF) under Grant ENV-7604263 on "Seismic Behavior of Structural Components". Mr. Albert C. Kuentz of AISI and Drs. S. C. Lin and J. B. Scalzi of NSF provided much encouragement in carrying out this work. It is a pleasure to acknowledge with gratitude this support which made this work possible.

The preceding three reports issued on this project are:

"Structural Steel Bracing Systems: Behavior under Cyclic Loading," by E. P. Popov, K. Takanashi, and C. W. Roeder, Report No. EERC 76-17, June 1976, Earthquake Engineering Research Center, University of California, Berkeley, California;

"Capacity of Columns with Splice Imperfections," by E. P. Popov and R. M. Stephen, Report No. EERC 76-21, September 1976, Earthquake Engineering Research Center, University of California, Berkeley, California;

"Tensile Capacity of Partial Penetration Welds," by E. P. Popov and R. M. Stephen, Report No. EERC 76-28, October 1976, Earthquake Engineering Research Center, University of California, Berkeley, California.

The Task Force on Project 193 offered much valuable advice and

significantly contributed to the practical orientation of the project. The authors sincerely thank the following members of this group: A. L. Collin, S. E. Ault, L. H. Daniels, J. L. Fox, R. D. Hanson, R. H. Hofer, Jr., J. C. Kariotis, H. A. Krentz, L-W. Lu, M. A. Mark, W. A. Milek, Jr., J. O. Robb, D. R. Strand, E. J. Teal, and L. A. Wyllie, as well as H. J. Degenkolb, who was an early advocate of the structural system studied herein.

A number of graduate students assisted with the project among whom Ed Ong competently and with dedication helped throughout the study, and Perry Chin was involved on special assignments. Barry Lotz and Don Clyde of the laboratory research staff helped in testing the frames, Beverly Bolt edited the manuscript and Robin Cranford did the typing. Leona Rambeau and Gail Feazell prepared the drawings. The help of these people is greatly appreciated.

The authors also wish to express their gratitude to Professor V. V. Bertero who freely gave advice and cooperated to the utmost in the smooth running of this project.



## TABLE OF CONTENTS

	<u>Page</u>
Abstract . . . . .	i
Acknowledgements . . . . .	iii
Table of Contents . . . . .	v
List of Tables . . . . .	ix
List of Figures . . . . .	xi
List of Symbols . . . . .	xvii
Chapter 1. Introduction . . . . .	1
General . . . . .	1
Background . . . . .	2
Scope and Objectives . . . . .	5
Chapter 2. Design and Linear Elastic Analysis of the Prototype . . . . .	7
Design of the Prototype . . . . .	7
Linear Elastic Analyses . . . . .	10
Overall Plane Frame Analysis . . . . .	11
Detailed Linear Elastic Analysis . . . . .	15
Summary . . . . .	16
Chapter 3. Cyclic Shear of Wide Flange Beams . . . . .	19
General . . . . .	19
Test Set-up . . . . .	20
Design of the Beam Specimens . . . . .	22
Beam Specimen 1 . . . . .	24
Beam Specimen 2 . . . . .	27
Beam Specimen 3 . . . . .	28
Beam Specimen 4 . . . . .	29
Beam Specimen 5 . . . . .	30
Beam Specimen 6 . . . . .	32
Beam Specimen 7 . . . . .	33
Beam Specimen 8 . . . . .	35
Beam Specimen 9 . . . . .	36
Summary of Conclusions of Cyclic Beam Tests . . . . .	38
Analytical Model for Cyclic Shear Yielding Beams . . . . .	41
Simple Shear Deflection Theory . . . . .	44

Table of Contents (cont'd)	<u>Page</u>
Sandwich Beam Theory . . . . .	46
Cyclic Shear Model . . . . .	53
Fit of the Cyclic Shear Model . . . . .	55
Summary of Cyclic Shear Yield Behavior . . . . .	57
Chapter 4. Inelastic Dynamic Analyses . . . . .	59
General . . . . .	59
DRAIN-2D Dynamic Analysis Program . . . . .	59
Post Buckling Brace Element . . . . .	61
Alternate Structures . . . . .	62
Input Parameters . . . . .	63
Results From 1.5 Times the El Centro Excitation . . . . .	65
Results From the Pacoima Dam Excitation . . . . .	69
Comparison of the Member Behavior . . . . .	72
Floor Deformations in the Eccentrically Braced Frame . . . . .	75
Problem Noted in Eccentric Frame Dynamic Analysis . . . . .	77
Dynamic Response of the Entire Structure . . . . .	81
Summary of Dynamic Analysis Results . . . . .	82
Chapter 5. Design of One-Third Scale Model Frames and Test Setup . . . . .	85
General . . . . .	85
Design of One-Third Scale Model . . . . .	85
Selection of Model Member Sizes . . . . .	86
Additional Design Parameters for Test Frame 1 . . . . .	88
Design of Test Frame 2 . . . . .	90
Test Setup . . . . .	93
Loading Beam . . . . .	94
Lateral Support System . . . . .	96
Instrumentation . . . . .	98
Loading Program . . . . .	102
Total Lateral Load on the Test Frame . . . . .	104
Summary . . . . .	105
Chapter 6. Braced Frame Test Results, Evaluation and Comparison to Inelastic Analytical Model . . . . .	107

Table of Contents (cont'd)	<u>Page</u>
General . . . . .	107
Results for Test Frame 1 . . . . .	107
Evaluation of Test Frame 1 . . . . .	113
Test Frame 2 . . . . .	119
Comparison of the Tests . . . . .	126
Comparison of the Analytical Model with Test Results . . . . .	129
Summary . . . . .	132
Summary, Design Recommendations and Conclusions . . . . .	133
Summary . . . . .	133
Design Recommendations . . . . .	134
Conclusions . . . . .	137
References . . . . .	141
Tables . . . . .	145
Figures . . . . .	149
Appendix A . . . . .	247
Appendix B . . . . .	257
Appendix C . . . . .	275
Appendix D . . . . .	289
Appendix E . . . . .	303



LIST OF TABLES

	<u>Page</u>
Table 1 - Design Parameters of Beam Specimens . . . . .	145
Table 2 - Comparison of Data Points Between ANSR-I and Test Frame 1 . . . . .	146
Table 3 - Comparison of Data Points Between ANSR-I and Test Frame 2 . . . . .	147

**Preceding Page Blank**



## LIST OF FIGURES

	<u>Page</u>
Figure 1 - Typical Load Deformation Relationship of a Slender Bar . . . . .	149
Figure 2 - Typical Pinched Hysteresis Loops for a Concentrically Braced Frame [4] . . . . .	150
Figure 3 - Alternate Eccentrically Braced Elements . . . . .	151
Figure 4 - Eccentric Bracing System of This Study . . . . .	152
Figure 5 - Prototype Structure . . . . .	153
Figure 6 - Normalized Stiffness of the Prototype Structure as a Function of its Eccentricity . . . . .	154
Figure 7 - Computation of the Lateral Stiffness Provided by the Brace . . . . .	155
Figure 8 - Variation in the Lateral Stiffness Provided by the Brace . . . . .	156
Figure 9 - Lateral Stiffness of a Single Story Frame . . . . .	157
Figure 10 - Subassemblage Used in the Detailed Linear Elastic Analysis . . . . .	158
Figure 11 - Photograph of the Test Apparatus and Cycling Procedure	159
Figure 12 - Design Options of the Test Specimens . . . . .	160
Figure 13 - Force-Displacement Relationship for Monotonic Test . . . . .	161
Figure 14 - Cyclic Force - Deflection Behavior of Specimen 1 . . . . .	162
Figure 15 - Photograph of the Photogrammetric Grid for Specimen 1 . . . . .	163
Figure 16 - Cyclic Force - Deflection Behavior of Specimen 2 . . . . .	164
Figure 17 - Cyclic Force - Deflection Behavior of Specimen 3 . . . . .	165
Figure 18 - Cyclic Force - Deflection Behavior of Specimen 4 . . . . .	166
Figure 19 - Cyclic Force - Deflection Behavior of Specimen 5 . . . . .	167
Figure 20 - Photograph of the Tear in the Doubler Plate in Specimen 5 . . . . .	168
Figure 21 - Cyclic Force - Deflection Behavior of Specimen 6 . . . . .	169
Figure 22 - Cyclic Force - Deflection Behavior of Specimen 7 . . . . .	170

List of Figures (cont'd)	<u>Page</u>
Figure 23 - Photograph of the Failure in Specimen 7 . . . . .	171
Figure 24 - Cyclic Force - Deflection Behavior of Specimen 8 . . . . .	172
Figure 25 - Cyclic Force - Deflection Behavior of Specimen 9 . . . . .	173
Figure 26 - Idealized Bilinear Stress-Strain Diagram for Steel . . . . .	174
Figure 27 - Shear Stress Distribution and Cross-Sectional Warping Due to Shear Deformation in a Wide Flange Section . . . . .	175
Figure 28 - Comparison of the Shear Yield Theories With Experimental Data . . . . .	176
Figure 29 - Components of Deflection of a Sandwich Beam Element . . . . .	177
Figure 30 - Proportion of Incremental Shear Carried by the Web and Flange . . . . .	178
Figure 31 - Comparison of the Cyclic Shear Yield Model with Test Specimen 2 . . . . .	179
Figure 32 - Comparison of the Cyclic Shear Yield Model with Test Specimen 6 . . . . .	180
Figure 33 - Comparison of the Cyclic Shear Yield Model with Test Specimen 8 . . . . .	181
Figure 34 - Linear Approximation of the Post-Buckling Brace Behavior . . . . .	182
Figure 35 - Acceleration Record for 1.5 Times El Centro N-S Component 1940 . . . . .	183
Figure 36 - Acceleration Record for Pacoima Dam 1971 . . . . .	184
Figure 37 - Maximum Relative Displacement Due to the 1.5 Times El Centro Base Excitation . . . . .	185
Figure 38 - Maximum Story Drift Due to 1.5 Times El Centro Excitation . . . . .	186
Figure 39 - Deflected Shape at the End of 8.0 Seconds of the 1.5 Times El Centro Excitation . . . . .	187
Figure 40 - Maximum Relative Displacement Due to the Pacoima Dam Excitation . . . . .	188
Figure 41 - Maximum Story Drift Due to the Pacoima Dam Excitation . . . . .	189
Figure 42 - Deflected Shape at the End of 15.0 Seconds of the Pacoima Dam Excitation . . . . .	190



List of Figures (cont'd)	<u>Page</u>
Figure 43 - Time-History of the Roof Displacement of the Moment-Resisting and Eccentrically Braced Frames Due to the Pacoima Dam Excitation . . . . .	191
Figure 44 - Components of Braced Frame Deflection . . . . .	192
Figure 45 - Maximum Floor Deformations of the Eccentric Elements . . . . .	193
Figure 46 - Time-History Plot of the Eccentric Element During 1.5 Times El Centro Excitation . . . . .	194
Figure 47 - Time-History of the Eccentric Element During Pacoima Dam Excitation . . . . .	195
Figure 48 - Damping Forces on the Elastic Central Bracing System . . . . .	196
Figure 49 - Location and Free Body of the Test Frame . . . . .	197
Figure 50 - General Design of Test Frame 1 . . . . .	198
Figure 51 - Beam-to-Column Connection Used on Test Frame 1 . . . . .	199
Figure 52 - Brace-to-Beam Connection Used on Test Frame 1 . . . . .	200
Figure 53 - General Design of Test Frame 2 . . . . .	201
Figure 54 - Beam-to-Column Connection Used on Test Frame 2 . . . . .	202
Figure 55 - Brace-to-Beam Connection Used on Test Frame 2 . . . . .	203
Figure 56 - Layout of the Test Apparatus . . . . .	204
Figure 57 - Photograph of the Key Components of the Lateral Support Frame . . . . .	205
Figure 58 - Placement of the SR 4 Strain Gages . . . . .	206
Figure 59 - Placement and Deformation Geometry of Clip Gages in Eccentric Elements . . . . .	207
Figure 60 - Placement of Clip Gages on the Test Frames . . . . .	208
Figure 61 - Placement of Miscellaneous Instrumentation . . . . .	209
Figure 62 - Load Program for the Inelastic Cycles of Testing . . . . .	210
Figure 63 - Load Program for the Elastic Cycles of Testing . . . . .	211
Figure 64 - Effect of the Frictional Force on the Force-Deflection Hysteretic Curves . . . . .	213

List of Figures (cont'd)	<u>Page</u>
Figure 65 - Component of Lateral Force Induced by Vertical Load Cells . . . . .	213
Figure 66 - Photograph of the Test Frame and Test Facility . . . . .	214
Figure 67 - Lateral Force - Third Floor Deflection Hysteretic Behavior for the Elastic Cycles at the Start of Test 1 . . . . .	215
Figure 68 - Lateral Force - Third Floor Deflection Hysteretic Behavior for the Inelastic Cycles of Test Frame 1 . . . . .	216
Figure 69 - Lateral Force - Third Floor Deflection Hysteretic Behavior for the Elastic Cycles After LP 12 . . . . .	217
Figure 70 - Lateral Force - Third Floor Deflection Hysteretic Behavior for the Elastic Cycles After LP 22 . . . . .	218
Figure 71 - Photograph of the Torn South Eccentric Element of Test Frame 1 . . . . .	219
Figure 72 - Photograph of Test Frame 1 After Completion of the Test . . . . .	220
Figure 73 - Lateral Force - First Floor Deflection Hysteretic Behavior for the Inelastic Cycles of Test Frame 1 . . . . .	221
Figure 74 - Lateral Force - Second Floor Deflection Hysteretic Behavior for the Inelastic Cycles of Test Frame 1 . . . . .	222
Figure 75 - Lateral Force - First Floor Deflection Hysteresis Loops for Inelastic Cycles of Test Frame 1 After Correction for Brace Connection Slippage . . . . .	223
Figure 76 - Lateral Force - Second Floor Deflection Hysteresis Loops for the Inelastic Cycles of Test Frame 1 After Correction for Brace Connection Slippage . . . . .	224
Figure 77 - Lateral Force - Third Floor Deflection Hysteresis Loops for the Inelastic Cycles of Test Frame 1 After Correction for Brace Connection Slippage . . . . .	225
Figure 78 - Lateral Force - Third Floor Deflection for the Elastic Cycles After LP 22 After Correction for Brace Connection Slippage . . . . .	226
Figure 79 - Axial Force - Brace Slippage Hysteresis Loops for the First Floor Brace of Test Frame 1 . . . . .	227
Figure 80 - Photograph of a Typical Yielded Eccentric Element . . . . .	228
Figure 81 - Lateral Force - Floor Deflection of the First Floor South Eccentric Element of Test Frame 1 . . . . .	229

List of Figures (cont'd)	<u>Page</u>
Figure 82 - Lateral Force - Floor Deflection of the First Floor North Eccentric Element of Test Frame 1 . . . . .	230
Figure 83 - Components of Lateral Deflection for Test Frame 1 . . . . .	231
Figure 84 - Test Frame 1 - Column Flange Buckling . . . . .	232
Figure 85 - Lateral Force - Third Floor Deflection Hysteretic Behavior for the Elastic Cycles at the Start of Test 2 . . . . .	233
Figure 86 - Lateral Force - Third Floor Deflection Hysteretic Behavior for the Inelastic Cycles of Test Frame 2 . . . . .	234
Figure 87 - Lateral Torsional Buckling in Test Frame 2 . . . . .	235
Figure 88 - Photograph of the Torn Eccentric Element of Test Frame 2 . . . . .	236
Figure 89 - Lateral Force - Third Floor Deflection Hysteretic Behavior for the Elastic Cycles After LP 26 of Test 2 . . . . .	237
Figure 90 - Buckled Third Floor Brace in Test Frame 2 . . . . .	238
Figure 91 - Lateral Force - First Floor Deflection Hysteretic Behavior for the Inelastic Cycles of Test Frame 2 . . . . .	239
Figure 92 - Lateral Force - Second Floor Deflection Hysteretic Behavior for the Inelastic Cycles of Test Frame 2 . . . . .	240
Figure 93 - Lateral Force - Floor Deflection of the First Floor South Eccentric Element of Test Frame 2 . . . . .	241
Figure 94 - Lateral Force - Floor Deflection of the First Floor North Eccentric Element of Test Frame 2 . . . . .	242
Figure 95 - Photograph of Test Frame 2 After Completion of the Test	243
Figure 96 - Comparison of the Analytical Model with the Third Floor Test Results of Test Frame 1 . . . . .	244
Figure 97 - Comparison of the Analytical Model with the Third Floor Test Results of Test Frame 2 . . . . .	245



## LIST OF SYMBOLS

$A$	- cross-sectional area
$b$	- flange width
$d$	- depth of the wide flange section
$E$	- modulus of elasticity
$G$	- elastic shear modulus
$G_p$	- plastic shear modulus for a web yielding in pure shear
$h$	- story height
$I$	- moment of inertia of the cross section
$I_f$	- moment of inertia of the flange
$I_w$	- moment of inertia of the web
$K$	- lateral stiffness
$M$	- bending moment
$M_f$	- bending moment of a flange
$M_p$	- full plastic moment
$M_p^*$	- reduced plastic moment contributed by the flanges
$P$	- load applied by the lateral load cell
$P_T$	- total corrected lateral force
$Q$	- total shear force
$Q_f$	- shear force carried by a flange
$Q_w$	- shear force carried by the web
$S_f$	- shear area of the flange
$S_w$	- shear area of the web
$t_f$	- thickness of the flange
$t_w$	- thickness of the web
$V_p$	- plastic shear force

- $w_t$  - total deflection of a sandwich beam
- $w_b$  - partial deflection due to beam bending
- $w_{bf}$  - deflection due to flange bending
- $w_s$  - partial deflection due to shear
- $w_{st}$  - deflection due to shear in the flange
- $\Delta_3$  - lateral deflection of the third floor of the test frame
- $\Delta P$  - correction for the lateral force
- $\delta_a$  - lateral deflection due to elongation of the brace
- $\delta_b$  - lateral deflection due to elongation of the column
- $\delta_c$  - lateral deflection due to deformation of the eccentric element
- $\rho$  - uniaxial strain hardening ratio
- $\delta_y$  - yield stress in tension
- $\phi$  - beam curvature

## CHAPTER 1. INTRODUCTION

### General

Structures which are located in seismic regions must be designed to resist considerable lateral inertial loads. The design of such structures requires a balance between strength, stiffness and energy dissipation. This report describes a new structural system, an eccentric bracing system, which meets the above requirements for earthquake-resistant steel structures. The system employs deliberately large eccentricities between the brace connection and beam-column joint, chosen to assure that the beam yields in shear. It is believed that this is the first application of cyclic shear yielding as the primary energy dissipation mechanism of a structure. The results of this study show that the system is well-suited to earthquake-resistant design.

Any structure which is designed to withstand earthquakes must fulfil two basic criteria. The first is that it must sustain no structural damage and only limited non-structural damage during shakes which may occur at frequent intervals in the life of the structure. This criterion is usually met by assuring that the structure remains elastic and has sufficient stiffness to prevent excessive deflections.

The second criterion is the necessity of preventing a disaster during an extreme, infrequent earthquake. Here the primary concern is to assure that the structure does not collapse or suffer major structural damage. This is accomplished by examining the inelastic force-deflection hysteresis loops of the structure. The area enclosed within these loops is a measure of the ability of the structure to dissipate energy. If the loops are full and do not deteriorate under repeated and reversed loadings, the structure is much more likely to survive a strong quake. Energy dissipation is

poorer in structures with pinched or deteriorating hysteresis loops. The safety of such structures can be appraised only from a detailed evaluation of the inelastic response of the structure. As a result of the many uncertainties in response evaluations, designers tend to avoid structural systems which exhibit pinched or deteriorating hysteresis loops in favor of other systems with better hysteretic behavior.

Concentrically braced structures are very economical structures with more than enough stiffness to satisfy the first criterion. However, these structures have not been as successful in satisfying the second criterion because they often have strongly pinched hysteresis loops. On the other hand, moment-resisting frames have full, unpinched hysteresis loops but tend to be relatively flexible structures, and sometimes it is uneconomical to develop the desired stiffness in these frames.

It is apparent that the best system for earthquake resistant structures would economically combine the strength and stiffness of a braced steel frame with the excellent energy dissipation of a moment-resisting frame. The eccentric bracing system which is described in this report appears to be such a system. While its initial cost in terms of design and connection details may be slightly higher than for a moment-resisting frame, it may more than make up for this in the considerably lighter steel and small weld sizes required.

### Background

Historically steel moment-resisting frames have been highly regarded by structural designers for their earthquake-resistant behavior. These structures performed very well during the 1906 San Francisco Earthquake and in other more recent earthquakes. However, the 1972 Managua Earthquake showed that stiff shear walls offer many advantages during a severe shake. Since then a strong interest has developed in stiffer



structures for earthquake-resistant construction. Since moment-resisting frames tend to be flexible, braced frames are considered as a means of providing increased structural stiffness. Concentrically braced frames can easily provide the needed stiffness, but their cyclic inelastic behavior is questioned by many designers. Hence, there is strong interest in better understanding and improving the performance of braced frame structures.

Reports on a number of studies which investigated the cyclic inelastic behavior of braced frame structures are available in the literature. Many of the findings and conclusions are summarized by Popov, Takanashi, and Roeder [1]. All of these studies confirm that the cyclic inelastic behavior of concentrically braced frames is strongly influenced by the cyclic post-buckling behavior of the individual braces. This brace behavior has been experimentally and analytically studied by a number of investigators [2,3,4,6,7,8] who obtained cyclic axial force-deflection relationships of the type shown in Figure 1. The general behavior, shown in Figure 1, can be classified into several distinct zones. Zone O-A starts with linear elastic shortening of the brace but, because of initial imperfections, becomes increasingly nonlinear as the stability load is approached. Zone A-B has steadily decreasing axial force with increasing axial shortening, because of the large plastic rotation forming at the center of the brace. The loading is reversed at Point B in Figure 1 (a), so zones B-C and C-D consist of elastic restraightening of the severely deformed brace. Zone D-E consists of inelastic restraightening of the brace, since the tensile, axial force is large enough to form a reversed plastic hinge in the middle of the brace. At point E, the brace is essentially restraightened. Therefore,  $P-\Delta$  moments become

nearly zero and further elongation, zone E-F, is purely a plastic elongation of an axially loaded member. The loading is reversed at point F in Figure 1 (a), and the slope of zone F-G is very similar to the initial slope of zone O-A. Later cycles exhibit the same characteristics as the first cycle, but the compressive buckling loads may be substantially reduced because the brace is not perfectly restraightened after each cycle.

A number of experimental and analytical attempts have been made to translate the inelastic cyclic behavior of an individual brace into the behavior of a braced frame [4,8,9,10,11,12,13,14]. The earliest analytical studies [9,10,11] used variations of the slip model [1] of brace behavior to predict the behavior of braced frames. The later analytical studies [4,8,12] used more accurate mathematical models which simulated more closely the behavior shown in Figure 1. All of the studies produced cyclic inelastic frame behavior which is characterized by strongly pinched hysteresis loops; a typical result is shown in Figure 2. The pinching is caused by the large lateral deflections of the frame, which are necessary to restraighten the brace and regain the brace stiffness after buckling.

Because concentrically braced frames exhibit pinched and deteriorating hysteretic behavior, there is an interest in developing structural bracing systems which exhibit better energy dissipation characteristics. This should be possible, since steel as a material is known to have excellent energy dissipation characteristics. Steel by itself is very ductile and it generates unpinched hysteresis loops with very slow deterioration in strength and stiffness. Steel moment-resisting frames exhibit these same desirable energy dissipation properties [15,16]. Thus, several bracing systems [17,18] have been proposed, which can be designed so

that the inelastic activity is restricted to bending yield as in moment-resisting frames. Since brace buckling is avoided in such designs, desirable energy dissipation characteristics can be achieved. Fujimoto et al [17] tested several frames of the eccentric K-brace type shown in Figure 3(a), and found that they exhibited no pinching of the hysteresis loops. Hisatoku [18] studied several frames of the inverted Y-bracing shown in Figure 3(b) and found that the hysteresis loops could be pinched or full depending upon the length of the vertical strut. The staggered truss system was studied by Gupta [19] and Hanson, Goel and Berg [20]; in this system the center bay is not braced and the plastic behavior is limited to bending of the chords of the center bay. This type of structure may have good hysteretic behavior but it has never been studied experimentally.

Although studies of the behavior of these alternate bracing systems have been limited and incomplete, the results give strong indication that eccentric bracing is a viable alternative to the usual concentric bracing system. This study concentrates on the behavior of eccentrically braced frames. The eccentric bracing concept is employed in diagonally braced frames with deliberately large eccentricities with respect to the beam-to-column joint. The behavior of this type of bracing is quite different from the typical concentric bracing where the centerlines of beams, columns, and braces intersect at the same point.

#### Scope and Objective

The objective of this study is to evaluate thoroughly the eccentric bracing system of the type shown in Figure 4 with particular regard to its applicability in earthquake-resistant design. The proposed system is unique in that the energy dissipation is provided by shear yielding of the eccentric beam element. Since the yield capacity of such an element

can be determined a priori, the braces can be sized so as to prevent their buckling, thereby eliminating pinched deteriorating hysteresis loops. The best connection details and design parameters for this system are determined from a large number of linear elastic analyses. A detailed experimental study of the inelastic behavior of the key eccentric element is made, and an analytical model for predicting its inelastic behavior is developed. A series of inelastic dynamic analyses are carried out to determine the performance of this structural system and to compare it with other structural systems. Quasi-static cyclic tests are performed on two one-third scale model frames to verify that the structure does perform as predicted in the analysis. The predicted inelastic analyses are shown to be in excellent agreement with the experimental results. Finally, conclusions and design recommendations are given to aid in the design of structures of this type.

## CHAPTER 2. DESIGN AND LINEAR ELASTIC ANALYSES OF THE PROTOTYPE.

### Design of the Prototype

The selected prototype structure is the square 20 story - 4 bay office building shown in Fig. 5. The bay width is 24 ft (7.3 m) and the story height is 12 ft (3.6 m) for all stories except the first, which is 15 ft (4.6 m). The structure was designed by using the following gravity load specifications:

Dead load of roof . . . . .	67 psf (3.21 kN/m <sup>2</sup> )
Dead load of floors and interior partitions . . .	85 psf (4.07 kN/m <sup>2</sup> )
Dead load of curtain walls. . . . .	15 psf (.72 kN/m <sup>2</sup> )
Live load of roof . . . . .	20 psf (.96 kN/m <sup>2</sup> )
Live load of floor. . . . .	50 psf (2.40 kN/m <sup>2</sup> )

The earthquake lateral loads of the structure were determined by the 1976 UBC recommendations [21,22]. The natural period of the structure was estimated at approximately 1.24 seconds. It was assumed that the structure rests on a shallow, stiff layer of soil so that the period of the soil is approximately one second and the Soil Interaction Factor is 1.47. This Soil Factor is a new provision to the UBC code. For a structure of this type an Importance Factor of 1.0 is applicable, resulting in an equivalent horizontal acceleration of approximately 7% of gravity. The equivalent acceleration was applied to the dead load plus 25% of the live load to produce a total base shear of 1483 kips (6599 kN). It was assumed that the external bays were braced as shown in Fig. 5(b). The bracing was shifted from the outside bays to the interior bays for the upper levels as shown in Fig. 5(b) to reduce the likelihood of excessively high tensile loads developing in the lower columns [23]. It is quite possible that the bracing would have to be moved to an interior frame or that the

bracing would have to be confined to a single bay within the frame for architectural reasons. However, this should not cause a problem, since the proposed system is not limited to these design assumptions. The code recommended torsional effect was computed and as a result, the braced frames were designed to carry 52.5% of the total base shear. The design of the frames was essentially controlled by these lateral loads, since the tributary area for the gravity loads of the exterior frames was small.

The eccentrically braced frames were designed by plastic methods, where the force distribution was determined by a lower bound technique, moment balancing [24,25,26]. The key concept to the moment balancing approach is that, if the designer chooses any moment diagram, which satisfies statics and the external loading condition of the structure, and also proportions the structure so that there are enough plastic hinges to form a mechanism, the upper and lower bound plastic theorems are both satisfied. An initial assumption of individual member force and moment distribution is made for the structure. This assumed distribution is based on the desired structural performance and the collapse mechanism. The individual nodes of the structure are then checked for force and moment imbalances, and any nodal imbalance is distributed throughout the structure by a prescribed balancing scheme which depends on the desired collapse mechanism of the structure. Appendix A gives an example of a possible balancing scheme for a 3 story eccentrically braced frame structure. Since members will probably be sized with slightly more strength than required by the final moment diagram, the factored design loads become a lower bound for the actual strength of the structure.

This type of procedure was applied to the factored design loads of the structure. The members were then sized in 5-story increments to

simplify the design and analysis of the structure. Structures were designed in this way with a number of connection and design details including eccentrically braced frames with moment-resisting beam-to-column connections, beams oriented for weak axis bending, bolted beam-to-column connections, and several other connection details. The final design had strong axis beam bending and moment-resisting beam-to-column connections. This system was chosen after considerable elastic analysis as the most satisfactory; the other systems were studied and analyzed but the analyses are not included in this report. Unless otherwise specified, all conclusions and results given in this report will apply to the final design.

There are several comments that should be made about this design. The moment-resisting beam-to-column connection details add considerable cost to the design, when compared to bolted connections. However, substantial savings are made by the greatly reduced weight of steel. These savings in weight are realized because of the smaller beam and column sizes. Further, the smaller member sizes result in greatly reduced weld sizes, and the moment resisting connections are not nearly as expensive as the moment-resisting connections of a heavier moment-resisting frame. The beams are smaller because the moment diagram of the beam is in triple or quadruple curvature. The columns are smaller because they are designed by the weak beam-strong column concept, and smaller beam sizes require smaller column sizes. Since the beam is designed as the weak element of the system, the brace must be oversized to prevent buckling due to strain hardening or variability in the yield stress of the beam. Although the brace must be oversized, it contributes very little to the total weight of steel in the structure. The degree of conservatism to be applied

to the brace design will be discussed in greater detail later in this report.

The final design of prototype structure is not covered in great detail in this report, because it was a very preliminary design. This design was established without benefit of the analysis and experimental study performed later in this program. These later studies greatly influenced the selection of the final recommended design procedure, hence more detailed design recommendations are given in a later chapter. The design of the interior unbraced frames is not covered in this report; however, they were designed for their share of gravity loads plus minimum lateral loads as required by the Uniform Building Code (UBC).

#### Linear Elastic Analyses

There are many unusual features in the design of an eccentrically braced structural system, so a substantial program of linear elastic analyses was undertaken after completion of the initial design. This program of analyses was performed to determine which of the alternate designs was most suitable, to further refine the design, and to determine and evaluate the key parameters affecting the elastic behavior of the system. The linear elastic analysis was performed by using the computer program GENFEM3 [27,28]. This program is very suitable for the analysis of structural systems with this geometry. The input data are always input with respect to a local coordinate system. The program also contains provisions for declaring some nodes as "slaves" to the displacement of other "master" nodes. As a result of these features, very complex connection details can be analyzed with relatively simple input and output. Further, substantial changes in the geometry can be made with few input changes, because of the nodal coordinate generation capabilities of the



program. GENFEM3 has both beam element capabilities for performing overall plane frame analysis of the braced frame structure and plate bending and membrane elements for analyzing local effects such as connection details. The program has one major limitation in that the beam type elements do not include deformability due to shear.

This program was used to perform two separate programs of linear elastic analyses. The first program was an analysis of the overall braced frame, which was performed to study the deflections, member forces, and overall behavior of the frame. The results of the overall analysis were then used to determine boundary conditions for detailed analyses of a sub-assembly, which were performed by using the plate membrane and bending elements to model the detailed connection subassembly. This latter analysis was used to study alternate connection details.

#### Overall Plane Frame Analysis

The overall linear elastic plane frame analyses were performed on a frame as shown in Fig. 5(b). All of these analyses were performed with the full design gravity loads and the design earthquake loads applied. Then various alternative initial designs were elastically analyzed under the same loading conditions. This overall elastic analysis program was very useful in refining the design of the structural system. This program was also instrumental in the elimination of design alternatives which employed bolted beam-to-column connections. These alternatives were dropped from consideration because of the high shear force, which is predicted in the eccentric element. Careful evaluation of possible bolted beam-to-column connection details indicated that it was not possible to develop this high shear force in the eccentric element with any of the bolted beam-to-column connections commonly used in steel

structures. The shear force is so large in the eccentric elements that the web would fail in bearing on the bolt, unless a very large number of bolts were inserted. It was not possible to insert such a large number of bolts into a single row while maintaining the minimum bolt spacing. If multirows of bolts are used, the danger of connection failure is greatly increased, because of the large deformations which must occur in the eccentric element during yielding. Therefore, the alternative designs employing bolted beam-to-column connections were rejected for this eccentric bracing system.

The alternatives with moment-resisting beam-to-column connections were carried one step further. A number of separate analyses were made where the loads and member sizes were held fixed while only the eccentricity was varied. This series of analyses led to several conclusions. First, the eccentricity chosen affected the predicted stress levels and the design of the frame. The lateral loads were held constant for all eccentricities, but the UBC design earthquake loads were expected to decrease with increasing eccentricity due to the increasing period. This reduction in lateral loads would make the stress level less sensitive to variation in eccentricity, so the actual UBC design should be less sensitive to variation in eccentricity. Secondly, the elastic floor deformation increased with increasing eccentricity. At eccentricities in excess of 5 ft (1.52 m) the elastic floor deflection was expected to exceed the deflection allowable by the Uniform Building Code.

The third and most surprising observation concerns the variation of lateral stiffness of the frame. For this comparison, the lateral stiffness of the braced frame was defined as the total base shear divided by the lateral deflection of a given point at the top of the structure.

Since the loads were held constant, the total base shear was the same for all eccentricities. The stiffness terms were then normalized by dividing through by the stiffness of a concentrically braced frame (i.e. eccentricity equals zero). The plot of this variation for the acceptable alternative design is shown in Figure 6. At an eccentricity of zero, the lateral stiffness is that of a concentrically braced frame. At an eccentricity of 12.0 ft, the brace is standing vertically, and the stiffness is essentially the stiffness of a moment-resisting frame. The really surprising result is that the stiffness increases for small to moderate (less than 4 ft) eccentricities. This slight increase means that the eccentric system under discussion is not a stiffness reduction or "soft story" scheme, since the stiffness remains relatively constant even for moderately large eccentricities of up to 4 ft (1.22 m). This stable stiffness retention is explained by the geometry of the system.

For a simple explanation of the stability of the lateral stiffness consider the stiffness provided by the brace in a single story braced frame, which is derived by computing the horizontal load necessary to produce a unit horizontal displacement when all other displacements are fixed. This computation is shown in Fig. 7 and

$$K = \frac{AE}{h} \cos^2 \theta \sin \theta \quad (1)$$

In the plane frame analysis, the member sizes and all geometry except the eccentricity were held constant, so A, E, and h are constant and K is a function of  $\theta$ . Figure 8 is a plot of the variation in brace stiffness as a function of  $\theta$ . In the prototype frame, the minimum value of  $\theta$  is approximately  $26^\circ.6$ . The curve in Figure 8 for  $\theta > 26^\circ.6$  exhibits very similar characteristics to the curve of Figure 6. The stiffness

provided by the brace is very stable over a range of small to moderate eccentricities. Further, this will generally be true for other structures using this bracing system, since the ratio of the bay width to story height falls into a relatively well-defined range for most structures. The stiffness is not likely to be stable for other bracing systems, such as the eccentric K brace, since the minimum angle is likely to be in the range of  $40^\circ$  to  $55^\circ$ . Minimum angles in this range fall on the sharply dropping portion of the stiffness curve.

A second factor in the increase in stiffness is the contribution by the rotational restraint of the beams. Figure 9(a) shows a comparison of the lateral stiffness of two moment-resisting frames. If the rotational resistance of the beam is infinite, the lateral stiffness of the frame is 4 times higher than if the rotational restraint is zero. In the eccentrically braced frame system, the eccentricity induces an extra constraint upon the deflected shape of the beam, which is now in triple or quadruple curvature as opposed to double curvature, and the rotational restraint of the beam ends is increased. The added constraint, simulated by the springs in Figure 9(b), together with the increased rotational resistance of the beams, increases the lateral stiffness for small to moderate values of eccentricity.

In summary, the stiffness of the eccentric bracing system is stable up to moderate eccentricities (to approximately 4 ft for the prototype structure). The stability can be attributed to two geometric effects. (a) The lateral stiffness of the brace is stable or increasing over the same range of eccentricities. (b) The eccentric brace adds constraints to the deflected shape of the beam, and the lateral stiffness due to the moment-resisting connections is increased accordingly.

### Detailed Linear Elastic Analysis

After completion of the elastic plane frame analysis, the remaining designs were analyzed in more detail to evaluate the local effects and to refine further the design of the connection. These analyses were performed on subassemblages taken from the structure as shown in Fig. 10. The subassemblage was modeled as a series of plate bending and membrane elements. The forces and bending moments acting at the interfaces of the subassemblages were determined from the overall linear elastic plane frame analysis. It was also assumed that plane sections remain plane at these interfaces. These analyses were performed on subassemblages with the beam oriented for bending in the strong axis and weak axis. The eccentricities were varied from 2 to 4.5 ft (0.61 to 1.37 m), and the effectiveness of stiffener plates, doubler plates, and bolted gusset plates was considered.

Finally, the design with strong axis beam bending and welded moment-resisting beam-to-column connections was chosen because it exhibited the most promising yield and energy dissipation characteristics while still utilizing practical connection details. The design with weak axis bending resulted in a system which did not exhibit very promising energy dissipation, so it was rejected.

A further result was that a single stiffener plate is necessary at the brace-to-beam connection of the subassemblage to assure a uniform distribution of shear stress in the web of the eccentric beam element. The stiffener also prevents the build-up of high stress concentrations at the brace-to-beam connection, and the possibility of local yielding or web crippling is eliminated. The effect of other stiffeners in the beam-to-column and brace-to-beam connections were analyzed, but the analyses did not appear to indicate a strong consistent justification for their use.

The elastic analyses showed that the shear stress was very high in the web of the beam. For wide flange sections with unreinforced webs, the shear stress was high enough that shear yielding of the web would necessarily be the primary energy dissipation mechanism. Since the cyclic inelastic behavior of wide flange beams was not well understood, possible methods of eliminating this shear yielding were studied. It was found that increasing the eccentricity increased the magnitude of bending stresses as compared to shear stresses; but shear yielding of the web could be eliminated only when a substantial doubler plate was added to the web. To eliminate shear yielding completely, the thickness of the doubler plate must be of the order of the thickness of the web. The doubler plates would be quite thick and shear stress would still be high. Hence, it was felt that the inelastic behavior of the eccentric elements required a great deal of study to evaluate the inelastic performance of beams which yield in shear or have large doubler plates.

#### Summary

In this chapter, the initial design of the prototype structure was discussed. The design was considered for a variety of design details. The alternates were then analyzed as plane frame structures, and it was discovered that the elastic system under discussion is not a "soft story" or stiffness reduction scheme. More detailed analyses were then performed on subassemblages of the braced structure. These were helpful in evaluating the alternate designs and determining the best. The alternative selected was a frame with strong axis beam bending, welded moment-resisting beam-to-column connections, and a centerline eccentricity of approximately 3.5 ft (1.07 m). This type of system dissipated energy by cyclic shear yielding of the web. At least one beam stiffener was required to develop

the shear stress in the web of the eccentric element, and although doubler plates reduced the shear stress level in the eccentric beam, they had to be very thick.





## CHAPTER 3. CYCLIC SHEAR OF WIDE FLANGE BEAMS

### General

The general design and linear elastic analyses of the prototype eccentrically braced frame were discussed in the preceding chapter. One of the major findings of the elastic analysis is that the primary yielding of the system will be shear yielding of the web unless thick doubler plates are added to the web of the eccentric beam element. However, neither the cyclic inelastic behavior of beams which yield in shear nor the cyclic inelastic behavior of beams with thick doubler plates is well understood. The only known experiments on wide flange beams yielding in shear have been reported by Newmark and Hall [29]. Their tests were performed by monotonically increasing the load on beams, which yield in shear, to determine if the beams would develop their full plastic moment,  $M_p$ . It was found that the full plastic moment was attained after considerable strain hardening due to shear yielding. These beams, which yielded in shear, can be thought of as exhibiting 3 separate force-deflection behavior zones. The beam is very stiff in the first zone, because the beam is fully elastic. The second zone is a zone of intermediate stiffness due to the elastic flanges and plastic web. The third zone is a very soft zone, because both the web and flanges are fully plastic. Newmark and Hall presented an empirical equation for estimating the stiffness of the intermediate shear yielding zone. These tests indicate that wide flange beams which yield in shear perform well under monotonic loading, but they give no information about the cyclic inelastic behavior of beams which yield in shear.

The cyclic behavior of a panel zone with thick doubler plates has been reported by Popov, Bertero and Chandramouli [30]. A number of beam-

column subassemblages of moment-resisting frames with doubler plates in the connection panel zone of the column were tested under cyclic loads in this study. It was found that the doubler plates performed well in these tests except for one partial failure due to an inadequate weld. These results are applicable to the eccentric elements, but at least one major difference must be expected. This difference is that the eccentric elements of the prototype design will undergo much larger inelastic deformations than the panel zone of a moment-resisting frame, because the eccentric element is the primary energy dissipation mechanism. A program of testing was undertaken to simulate the cyclic behavior of these eccentric elements; the test specimens were 1/3 scale models of these elements of the prototype. This program of testing was undertaken to answer several questions. First, the tests would determine the effectiveness of shear yielding of the web of a wide flange as an energy dissipation mechanism. Secondly, the program would resolve any question of whether the doubler plates were capable of withstanding the required cyclic inelastic deformations. Finally, several specimens, which yielded in bending, were tested so that the behavior of shear yielding beams could be compared with the better understood cyclic behavior of beams yielding in bending.

The test setup, procedure, and results of these tests are discussed in this chapter. The results indicate that shear yielding of the web is a very desirable energy dissipation mechanism for the eccentric beam element. This type of yielding is desirable primarily because of the great stability it exhibits. The development of an analytical model using the results of these tests, is also discussed.

#### Test Set up

Nine specimens were fabricated from a W6x12 section of A36 steel. The actual material properties and residual stresses of the section are

shown in Appendix B. The W 6x12 section was chosen as the closest standard section to a 1/3 scale model of the W 16x64 section used for the beams of the lowest stories of the prototype.

These specimens were tested by quasi-statically cycling the center line load on a simply supported beam. A simply supported beam was chosen because the simple supports simulate the inflection point which must occur at some midpoint of each eccentric element, and because the center line moment simulates the high bending moment at the face of the column in beam-to-column connections. The specimens were tested on a 400 kip Baldwin hydraulic testing machine. The quasi-static cyclic effect was simulated by loading the specimen until achieving the desired deflection, unloading the specimen, turning the specimen upside-down, and again loading in the opposite direction until the reversed deflection is achieved. The centerline deflection of the beam was continuously recorded by a Honeywell XY Recorder connected to 2 Daytronic LVDTs (Linear Variable Displacement Transducers). The readings of these LVDTs were averaged to eliminate any torsional movement of the beam. A photogrammetric grid was applied to the web [15]. This was accomplished by drawing a grid of 0.75 in (18.7 mm) squares on the web of the beam with a 1 mm ink drawing pen while the beam was undeformed. Photographs were taken of the deformed grid at various intervals of the test. The photographs were taken on glass plates which could then be compared to a reference plate, and the grid displacements could then be determined to reasonable accuracy. These displacements serve as a check of the LVDT readings and permit the measurement of local deformations within the web. The remainder of the specimen was whitewashed to better exhibit yielding of the metal. Figure 11 presents two photographs of this test setup and demonstrates the simulated cyclic effect which was produced by turning the specimen upside-down.

## Design of the Beam Specimens

Nine specimens were designed and tested. The purpose of these test specimens was to evaluate the relative performance of beams which yield in shear during cyclic loading. The first six specimens were designed prior to any testing, and the last three were modified in response to questions raised in the first six tests. The specimens were designed by three design options, which were intended to simulate various boundary conditions and connection details. These options are shown in Fig. 12. Option A consists of two beam segments with flanges and the web welded to a center plate with full penetration welds. The connection of the beam segments to the center plate simulates the connection of an eccentric beam element to the face of the column. A tail is left on the beam beyond the simple supports to reduce the possibility of local buckling problems and to provide warping restraint at the simple supports. Option B also has a tail extending beyond the simple supports. However, the specimen is made up of one beam segment with a stiffener plate welded into the centerline position. This detail simulates the brace-to-beam connection, since the beam is continuous and the moment is high at this location. Option C does not have a tail extending beyond the simple support. The supports are formed by a single plate, which is welded to the beam segment by a full penetration weld along the web. The flanges are not connected to the end plate, and so, these end connections simulate the connections which would result if the eccentric beam element were connected to the column by a bolted, non-moment-resisting connection. As a result of this detail, the cross section may warp at this interface, because of different shear strains in the web from those in the flanges.

The primary variable of the design options was the half-span dimension,  $B$ , which had values of 6 and 12 in (152 and 304 mm). The

smaller dimension of 6 in represented the 1/3 scale model of one-half the eccentric element of the prototype. Beam specimens of this length were ordinarily expected to yield primarily in shear of the web. The larger dimension of 12 in (304 mm) was chosen, because it was large enough to assure that the beam yielded in bending before the web yielded in shear. Doubler plates were applied to the webs of Specimens 4 and 5, to check the performance of the plates and to reduce the importance of shear yielding while increasing the significance of bending yield. The latter occurs because the doubler plate greatly increases the shear area of the web. Cover plates were added to the flanges of Specimen 8, to increase the moment of inertia and section modulus of the cross section. This reduces the significance of bending yielding and increases the significance of shear yielding. Thus Specimen 8 was designed primarily as a shear yielding specimen. Specimen 7 had stiffeners added to the web and flanges. These stiffeners were added to prevent flange buckling, and were not expected to affect the balance between bending and shear yielding.

The design of the beam specimens is summarized in Figure 12 and Table 1. The actual yielding of the specimens is a complex problem since each beam is loaded under combined bending and shear. However, Specimens 1, 2, 6, 8 and 9 were designed to yield primarily in shear. Specimens 3, 4 and 7 were designed to yield primarily in bending. Specimen 5 with its doubler plate was proportioned so that yielding in bending and shear occurred at approximately the same loading. From this series of experiments, it is possible to evaluate the relative merits of various types of yielding by comparing results from various test specimens. The tests also permitted a determination of the effectiveness of doubler plates and alternate connection details. Thus, the tests enabled a study to

be made of a wide range of related problems even though the number of tests was small and the tests were fairly simple.

#### Beam Specimen 1

Specimen 1 had a 6 in (152 mm) half span and was designed by Option A with no doubler plates. As a result, it was expected to yield primarily in shear of the web. This specimen was tested basically under monotonic loading, with cycles later added after obtaining the initial results. The monotonic load was applied until a deflection of 1.2 in (27.9 mm) was achieved; a plot of the monotonic behavior is shown in Fig. 13. This specimen produced the same general characteristics reported by Newmark and Hall [29] in that there were three distinct zones of force-deflection behavior and the full plastic moment was achieved only after considerable plastic shear deflection had occurred. Strain gages were mounted on the web of this specimen in an effort to predict the start of web buckling. However, these gages were ineffective because the specimen exhibited the characteristics of an initially imperfect specimen and had no apparent bifurcation of equilibrium. Nevertheless, a visible buckle in the web was observed at 0.6 in (15 mm) center line deflection, but the web buckling did not cause a decrease in load due to the formation of a diagonal tension field. Yielding of the flange was noted at approximately 0.4 inches (10 mm).

After monotonically loading the specimen, several cycles of loading were applied to it. The cyclic behavior of Specimen 1 is shown in Fig. 14. Two small cycles were applied from the deformed configuration after the monotonic loading. These two cycles are essentially repetitive with no deterioration in stiffness despite the severe deformation. Then the loading was reversed to a very large negative displacement, -1.78 in

(-45 mm). During this reversal the web buckle from the monotonic cycle restraightened itself and another severe buckle in the opposite direction formed due to the displacement reversal. The load remained stable during this transition, because the diagonal tension field again formed after the web buckled, but a very slight decrease in strength began after the specimen was deflected through -1 in (25 mm). After the displacement of -1.78 in (-45 mm) the loading was reversed, and the web buckle restraightened again. However, the web buckle formed more quickly and severely for this cycle, because of the very severe strain history. The load began to drop off rapidly and the test was stopped at a deflection of 0.7 in (17.8 mm). The specimen had probably the most severe accumulation of plastic strain of all 9 specimens, but it did not fail. The total energy dissipated by Specimen 1 was 816.6 in-kips (92.3 kN-m).

In the initial monotonic portion of the test, the force-deflection curve first exhibited non-linear behavior at a load of approximately 80 kips (356 kN). Since the yield point in shear is likely to be the same in either direction of loading, this results in a range of approximately 160 kips (712 kN) for the linear elastic zone of the virgin curve. The range of the linear elastic zone is approximately 190 kips during the first cyclic reversal between LP1 and LP3. This represents a significant growth in the linear elastic zone during monotonic loading. This growth indicates that the monotonic portion of the test obeyed an isotropic hardening model [31], since the yield surface grew significantly larger during the strain hardening. Figure 14 also indicates that the elastic zone did not exhibit any visible growth during the later cycles between LP3 and LP13, and so these later cycles exhibited kinematic hardening, which permits translation but no growth in the yield surface [31].

During the monotonic portion of Test 1, three zones of behavior were noted in Fig. 13; a very stiff linear elastic zone; a large transitional zone of intermediate stiffness due to shear yielding of the web; and, finally, a very flat zone due to the formation of a plastic hinge in flexure. The cyclic behavior after LPI did not exhibit this translational shear yielding zone. The force-deflection curves flattened very quickly after leaving the linear elastic zone, and shear yielding is not apparent in the force-deflection hysteretic curves of the cycles after LPI. This phenomenon also adds credibility to the idea that the monotonic loading was strongly influenced by isotropic hardening, since a growth in the size of the yield surface would raise the yield point in shear.

A photograph of the photogrammetric grid is shown in Fig. 15, and this indicates that the yield behavior of the specimen was dominated by shear yielding. Note that the elements in the center of the rectangular grid have deformed into nearly perfect parallelograms, which are associated with pure shear strain. The grid elements near the centerline of the beam and the beam supports do not exhibit quite the same behavior. At these interfaces, the grid also indicates shear strain, since the right angles of the grid change slightly, but the magnitude of the shear strain becomes increasingly smaller closer to these interface lines. The reduction in shear strain is caused by the warping restraint provided at these interfaces. The beam center line is a line of symmetry in geometry and loading, and the beam supports have a tail section extending beyond the support. Therefore, warping cannot occur on either of these lines, so shear strain must be constant along these interfaces. The constant shear strain requires that the flanges must also deform in shear, and the shear area is effectively increased near these interfaces. In the central



portion of the grid, there is no such restraint against warping due to shear deformation; the web carries nearly all of the shear and experiences much larger shear strains.

### Beam Specimen 2

Specimen 2 was of identical design to Specimen 1, but the loading was purely cyclic. The cyclic force-deflection hysteretic curves for Specimen 2 are shown in Fig. 16. This specimen was first subjected to three cycles of gradually increasing deflections to one side of the origin, then the next cycles were larger and were to both sides of the origin. Web buckling became very apparent during this fourth cycle, but the load on the specimen steadily increased, because a cyclic diagonal tension field formed during cyclic loading. The test was terminated at a deflection of -1.55 in (-39.4 mm), because it was believed that little useful information could be obtained from further cycles. There was no deterioration in strength or stiffness and no specimen failure occurred. The total energy dissipated by this specimen was 554 in-kips (62.6 kN-m).

During the early cycles of this test, there was a very marked growth in the linear elastic zone due to isotropic strain hardening, but the later cycles exhibited relatively constant size for the elastic zone; this is typical of kinematic strain hardening. The slopes of the inelastic parts of the force-deflection curves were generally much larger for the early cycles than they were for the later cycles. This indicates that the intermediate shear yielding zone again became less visible on the force-deflection curves after substantial strain hardening had occurred. The photogrammetric grid indicated the same shear deformation and warping resistance behavior as noted for Specimen 1.

### Beam Specimen 3

Specimen 3 was of the same design as Specimens 1 and 2 except that it had a 12 in (305 mm) half span. Since the span length was doubled, the specimen was designed so that shear yielding was less prevalent and deflections could be doubled. Figure 17 shows the cyclic force-deflection relationship for Specimen 3. The first two cycles were between  $\pm 0.4$  in ( $\pm 10$  mm). They generated very repetitive force-deflection curves, but significant flange buckling was already noted during these two cycles. These buckles formed in the compression flange and restraightened when the flange was in tension. The specimen was then loaded until it reached a deflection of 1.25 in (32 mm) at load point LP9. Very large flange buckles were observed during this cycle, and a slight decrease in load was noted just before reaching the cycle reversal point at LP9. The load was reversed, and the displacement was cycled to -1.5 in (-38 mm) at LP11. During this cycle, it was observed that the buckled tensile flange was not restraightening properly, and the load dropped off sharply due to specimen failure at LP11. A tear was noted propagating across the flange and up the web along a line approximately 0.5 in (13 mm) from the center plate. The energy dissipated for this specimen was 497 in-kips (56 kN-m) which is only 61% of the energy dissipated by Specimen 1. The maximum deflection of 1.5 inches is 83% of the maximum deflection obtained by Specimen 1.

The size of the linear elastic zone appeared to grow slightly in the early cycles, but the growth did not appear to be as significant as the growth noted for Specimens 1 and 2. The rectangular grid did not exhibit the parallelograms noted in Specimens 1 and 2. Therefore, shear yielding of the web was not significant in this test.

#### Beam Specimen 4

Specimen 4 was the same design as Specimen 3 except that it had an 0.1875 in (4.8 mm) doubler plate applied to the web of the beam. This specimen was designed to yield only in flexure, because of the long span and doubler plate. Specimen 4 was tested with the same cyclic displacement program as Specimen 3. The cyclic force-deflection hysteretic curves for Specimen 4 are shown in Fig. 18. The first two cycles exhibited the same repetitive hysteresis loops and flange buckling behavior as noted for Specimen 3 except that the loads were higher due to the increased section modulus. On the third cycle, the specimen was loaded until it reached a deflection of 1.25 in (32 mm); very large flange buckles and a decrease in load were noted during this half cycle. Loading reversal was made at LP9, and it was noted that the buckled tension flange was not restraightening properly. The load began to drop off slowly at a deflection of 0.2 in (5 mm), and very small hairline cracks were seen forming in the weld connecting the doubler plate to the beam. The formation of these cracks was accompanied by soft "pinging" sounds and buckling type distortion between the web and doubler plate. This cycle continued until the load dropped off suddenly at -0.95 in (24 mm) to specimen failure. Examination of the test specimen showed that a tearing type failure had occurred at the same location as Specimen 3. The failure of Specimen 4 occurred well before attaining the deflection at which Specimen 3 failed. However, its load carrying capacity was 28% larger. The energy dissipated by this specimen was 570 in-kips (67.5 kN-m), which is 70% of the energy dissipated by Specimen 1, and the maximum deflection was only 69% of the maximum deflection of Specimen 1.

Examination of the photogrammetric data verified that shear yielding of the web was of little importance to the overall specimen behavior, because the doubler plate prevented excess shear deformation. However, there was some evidence that the doubler plate did not perform well in this test. At the end of the test, the whitewash on the doubler plate was virtually unmarred, whereas the whitewash on the web was cracked and peeled. This clearly showed that there was no yielding in the doubler plate, while the web had experienced yielding. The web and the doubler plate were not deforming together. This is known because of the inconsistency in yield behavior and the cracks in the weld of the doubler plate. This cracking in the weld of the doubler plate has also been observed in doubler plates applied to the panel zones of beam-column subassemblages [30].

#### Beam Specimen 5

Specimen 5 was designed similar to Specimens 1 and 2 except that it had a 0.1875 in (4.8 mm) doubler plate welded to the web. This specimen was designed so that plastic shear deformation of the web was less significant than for Specimens 1 and 2 but more significant than for Specimens 3 and 4. The cyclic force-deflection behavior of Specimen 5 is shown in Fig. 19. The first one and one-half cycles of loading were between deflections of  $\pm 0.125$  in ( $\pm 3.1$  mm). After these one and one half cycles, the specimen was turned over, and the load was applied in the opposite direction. However, the load dropped off suddenly while the beam was behaving elastically. This sudden drop in load was accompanied by a loud noise. The specimen was then unloaded to zero load at LP6. Examination of the specimen revealed that a number of fine cracks had formed in the weld around the doubler plate. It was suspected that the weld might be defective, so the test was stopped, and the specimen was returned to the shop. The weld metal was gouged out and inspected for possible

defects, but no weld defects were found. Therefore, the doubler plates were rewelded with full penetration groove welds, and a fillet weld was extended over the groove weld and the doubler to provide added strength to the weld. The test was restarted at LP6. Then the specimen was cycled to -0.125 in (-3.1 mm) at LP7 and 0.125 in (3.1 mm) at LP9. The beam exhibited increased stiffness during the cycle, which can be attributed to greater compliance between the web and doubler plate. The next cycle varied between deflections of -0.4 in (-10 mm) at LP11 and 0.4 in (10 mm) at LP13. The deflection was then reversed to a deflection of -1.16 in (-29.5 mm) at LP16. All cycles up to LP16 exhibited very stable repetitive behavior with no deterioration in strength or stiffness. However, the strength began to deteriorate rapidly after the load was reversed from LP16 and the deflection passed through zero. A ductile tearing type failure was noted between the doubler plate and the web, see Figure 20. The test was stopped at a deflection of 0.72 in (18 mm).

In the early cycles up to LP13, a very significant growth in the strength of the specimen and in the size of the linear elastic zone was noted for each cycle. Much of this growth must be attributed to isotropic strain hardening during these early cycles; however, a significant portion which occurred after LP6, must be attributed to increased compatibility between the web and doubler plate, which was caused by the increased weld size. The performance of the doubler plate in the test indicated that it would be very unlikely that doubler plates would perform satisfactorily on the eccentric elements of the prototype bracing system. The doubler plates greatly increased the strength of the beam, but the doubler plate and its welds were not capable of withstanding the large inelastic deflections necessary in this system.

An examination of the photogrammetric data shows that this specimen exhibited evidence of shear yielding during the test. However, the deflections due to shear yielding were not nearly as great as for Specimens 1 and 2, since the photogrammetric grid did not show the sharp parallelograms noted for Tests 1 and 2. Shear yielding is also apparent in Fig. 19 for the early cycles. For cycles up to LP13, the slope of the inelastic zone was quite steep as was typical of the shear yielding zone. After LP13, the shear yielding zone is not apparent in Fig. 19, because there is a very rapid transition between the linear elastic zone and the very flat zone. The energy dissipated by this specimen was 839 in-kips (94.8 kN-m). This is 103% of the energy dissipated by Specimen 1 and 169% of the energy dissipated by Specimen 3. However, this increase in energy dissipation was caused by the increased strength, since the deflections attained by the specimen were small compared to Specimen 1.

#### Beam Specimen 6

Specimen 6 was designed to be identical to Specimens 1 and 2. Its inelastic behavior was dominated by shear yielding of the web. Since the span length was 1/2 the span length of Specimens 3 and 4, the loading program for the earlier cycles was taken as 1/2 the displacements applied to Test 3 and 4. Later cycles were taken to deflections greater than those attained for Specimens 3 and 4. No failure resulted from this test. The experiment was terminated because little useful information on shear yielding could be obtained by further cycling. The total energy dissipated by this specimen was 624 in-kips (70.6 kN-m). The force-deflection hysteresis is shown in Fig. 21.

A detailed description of this test is not given, because the results are essentially identical to Tests 1 and 2. The inelastic behavior was dominated by shear yielding. Shear yielding, web buckling, and cyclic

diagonal tension formed with no pinching of hysteresis loops or degradation in strength or stiffness. The early cycles up to LP9 exhibited a steady growth in the linear elastic zone due to isotropic hardening. The cycles after LP9 showed no significant growth in this zone, which in general is typical of kinematic hardening. The key conclusion which can be drawn from this test, is that the shear yield energy dissipation mechanism of this specimen was much more stable than the bending yield mechanism of Tests 3 and 4. This stable behavior can be attributed to the restraint provided by the elastic flanges to the yielded and buckled web. This restraint is seen as the cyclic diagonal tension field.

#### Beam Specimen 7

Specimen 7 was designed using Option B with a half span dimension of 12 in (305 mm). It also had 2 pairs of 0.25 in (6.4 mm) stiffeners spaced 2.5 in (63.5 mm) on center on each side of the center plate; no doubler plates were provided. The additional stiffeners were added to reduce the extreme flange buckling noted in Tests 3 and 4 and to delay the premature failure which resulted. The stiffeners were placed at the predicted location of the peak of the wave forms due to flange buckling. The half wave lengths were determined using equation 6.21 of the ASCE Manual 41 [26] and observations of Specimens 3 and 4.

The cyclic force-deflection relationship for this specimen is shown in Fig. 22. The early cycles of loading were of identical displacement to those applied to Specimens 3 and 4. The first two cycles had very repetitive hysteresis loops with force levels nearly identical to those obtained for Specimen 3; however, no visually observable flange buckles occurred during these two cycles. The specimen was then deflected to approximately 1.25 in (32 mm) at LP10. During this half cycle flange

buckling was observed, but the amplitude and wave length of these buckles were much smaller than those observed earlier in Specimens 3 and 4. Thus, the stiffeners forced the flange buckling to exhibit a higher mode effect. The load was then reversed, and the deflection was increased 0.8 in and 0.4 in (20 and 10 mm) beyond the failure points for Specimen 4 and 3, respectively. The flange buckling becomes more severe throughout this half cycle, and at a deflection of -1.7 in (-43 mm) the load dropped off sharply because of the severe flange buckling. The specimen was then carefully examined and no crack or failure could be detected. Therefore, the specimen was unloaded and reversed up to the deflection of 0.72 in (18 mm) with no loss in strength. However, at LP16 the load dropped off very sharply to LP16A, and the test was stopped. The sharp drop in loading was caused by a tearing failure across the tensile flange and up the web. This failure is typical of the failures of Specimens 3, 4 and 7, and is shown in the photograph of Fig. 23. The wave length of the flange buckles was approximately one-half the wave length observed in Tests 3 and 4.

The photogrammetric data verified that this specimen was only minimally affected by shear yielding. The specimen attained much larger deflections and energy dissipation than Specimens 3 and 4, because of the delay in failure caused by the added stiffeners which restricted flange buckling and assured more ductile behavior. However, the added cost of these stiffeners cannot be justified since the energy dissipation and maximum deflection of this specimen were nearly identical to Specimen 1, which had a shorter span and no added stiffeners. The total energy dissipated was 788 in-kips (89.0 kN-m) which was 96% and 159% of that dissipated by Specimens 1 and 3, respectively.



### Beam Specimen 8

Specimen 8 was designed by Option B and had a 12 in (305 mm) half span and four 0.375 in x 1.25 in (9.5 mm x 31.8 mm) cover plates attached to the flange and web by 0.1875 in (4.8 mm) fillet welds. This specimen was also designed after observing the results of the first 6 tests. It was noted that Specimens 1, 2, and 6 which yielded in shear, generally exhibited more desirable behavior. They were superior because they withstood larger deflections, exhibited more stable post buckling strength with no failure, and dissipated more energy. Therefore, Specimen 8 was also designed to yield primarily in shear. This was accomplished by adding cover plates of sufficient size to raise the plastic moment enough to develop shear yielding of the web. As a result of this design, Specimen 8 was strongly influenced by plastic shear deformations but not as strongly as were Specimens 1, 2 and 6.

The load program for the early cycles was identical to that experienced by Specimens 3, 4, and 7. The cyclic force-deflection behavior of Specimen 8 is shown in Fig. 24. The first two cycles exhibited repetitive hysteresis loops with a slight growth in the linear elastic zone due to strain hardening. Web buckling was observed in these cycles but no flange buckling occurred. The deflection was increased to 1.2 in (30.5 mm) at LP11 and then reversed reaching a deflection of -1.9 in (-48 mm) at LP14. At LP14, the specimen had been deflected beyond the point of failure of Specimens 3 and 4 and the point of sharp drop in loading due to flange buckling in Specimen 7. The loading was reversed to a deflection of 2.7 in (69 mm) at LP17. This deflection level is well beyond the point of failure for all flexural yield specimens (Specimens 3, 4 and 7). However, Specimen 8 experienced no failure or loss in strength or stiffness. The test was

stopped at this point because little information on cyclic shear yielding could be attained by further testing. At the conclusion of the test, the specimen was still in very good condition.

The photogrammetric data indicated the yield mechanism was primarily shear yielding of the web because the deformed grid displayed the classic parallelogram shapes with warping restraint noted for Specimens 1, 2 and 6. The maximum deflections attained by this specimen were in the order of twice the maximum values of Specimens 1, 2 and 6. This doubling of maximum deflections was anticipated but not achieved for the bending yield specimens (3, 4 and 7), and this again emphasizes the very stable behavior of the shear yielding beams (Specimens 1, 2, 6 and 8). The beams which yielded in shear, performed well and attained larger deflections despite yielding and buckling of the web because of the cyclic diagonal tension field which was provided by the flanges. The beams which yielded in bending, experienced flange yielding and buckling, but the beam performance was not very stable, because the web provides no restraint to the buckled flanges. The total energy dissipation of Specimen 8 was 1162 in-kips (131 kN-m), which was 234% of that dissipated by Specimen 3.

#### Beam Specimen 9

Specimen 9 was the only specimen designed by Option C. It had a 6 in (152.4 mm) half span with no tail left on the beam for warping resistance at the simple supports and with no flange connection to the end plates. This specimen was designed to yield in shear, but the design was to provide added insight into the desirability of warping resistance and flange restraint, upon the cyclic behavior of beams which yield in shear. The question is significant, because eccentric elements with a bolted beam-to-column connection would lack the warping resistance and flange restraint at the bolted connection.

The cyclic force-deflection hysteresis loops for the specimen are shown in Fig. 25. The first cycles were taken at one half the displacements used in cycling the bending yield specimens (3, 4, and 7). The first two cycles were between deflections of  $\pm 0.2$  in ( $\pm 5.1$  mm). These cycles show very repetitive hysteresis loops, but the stiffness of the shear yielding zone is much smaller than that obtained in Specimens 1, 2 and 6. This loss in stiffness can be seen by comparing the slope of the elastic portions of these early cycles of Fig. 25 with the comparable slopes in Figs. 16 and 21. This loss in stiffness can be attributed to the lack of warping restraint at the simple supports in Specimen 9. The flanges are not connected to the end plates or a beam tail, and so the shear strain is not uniformly distributed at the simple supports. Therefore, cross-sectional warping takes place.

The next cycles were between  $\pm 0.6$  in ( $\pm 15$  mm). During these cycles, considerable twisting of the flanges was observed because of the lack of flange restraint. However, these cycles still exhibit repetitive behavior with no deterioration in strength. The deflection was then reversed to  $-0.9$  in ( $-22.5$  mm) at LP15. The web buckling and twisting of flanges was very severe at this point, and a slight decrease in strength had started to occur. The load was reversed until a deflection of  $1.4$  in ( $35$  mm) was attained at LP18. During this half cycle, web buckling and flange twisting became steadily worse, and the strength began to drop off slowly after a deflection of  $0.2$  in ( $5$  mm) because of these buckling effects. The test was terminated because of the severe web buckling. The total energy dissipated was  $804$  in-kips ( $91$  kN-m).

The photogrammetric grid indicated that the specimen was predominately influenced by shear yielding, but the warping restraint was very different

from Specimens 1, 2, 6 and 8. Web buckling was visibly more severe for this specimen than for any other specimen. The more severe web buckling occurred because the lack of flange restraint prevented proper formation of cyclic diagonal tension field. It is well known from deep plate girder design [32] that a trussing action between the flanges and stiffeners is needed to form a monotonic diagonal tension field. The cyclic diagonal tension field requires the same trussing action, but this action was not possible in Specimen 9, because the flange was not connected to the end plate. The behavior was better than Specimens 3, 4 or 7, but it was not nearly as good as Specimens 1, 2, 6 or 8. The behavior of the specimen indicates one of the additional problems, which must be overcome before bolted beam-to-column connections can be used in the eccentric bracing system.

#### Summary of Conclusions of Cyclic Beam Tests

One primary conclusion, which can be drawn from these tests, is that shear yielding of the web is an excellent energy dissipation mechanism for an eccentrically braced frame. The specimens which yielded in shear (1, 2, 6, 8 and 9) were able to withstand larger inelastic deflections and dissipate larger amounts of energy than the specimens which yielded due to bending (3, 4 and 7). Further, all of the specimens which yielded in bending resulted in fracture of the specimen. None of the shear yielding specimens fractured, although two shear yield specimens (1 and 9) developed web buckling such that they could no longer maintain their full load. However, these two specimens both represent special cases in that Specimen 1 was tested under an unusually severe strain history and Specimen 9 was designed so that it could not develop the cyclic diagonal tension field. The remaining three shear yielding specimens

exhibited no undesirable buckling or fracture problems at the conclusion of the tests. This does not imply that bending yield is a poor energy dissipation mechanism, since it is well known [15,30] that the inelastic behavior of steel moment-resisting frames is very good. The difference is that the eccentric bracing system experiences very large inelastic deformations in the eccentric element, and these inelastic deformations are larger and more concentrated than those encountered in a moment-resisting frame. These results imply that eccentric elements which yield in shear are better able to withstand the large inelastic deformations and remain effective for further cycling.

The reason for this better behavior of shear yielding beams is the greater stability under local buckling, which shear yielding beams exhibit. Since the shear is the slope of the bending moment diagram of a beam, beams with very high shear will have only a very short section of flange, which is plastic, even after considerable strain hardening due to plastic hinge formation has occurred. The formation of flange buckles generally requires flange yielding over a sufficient flange length to form a wave length of buckling [26]. As a result, flange buckles and the associated lateral torsional buckling do not occur in conjunction with shear yielding of the web. Very substantial web buckles form, but the unbuckled flanges provide considerable restraint to the buckled web. Therefore, a cyclic diagonal tension field can form and the load is maintained. Further, these tests indicate that the cyclic diagonal tension field can form and reform without producing any observable pinching of the hysteresis loops or degradation in strength or stiffness. The beam must be designed to develop this cyclic diagonal tension field by adding stiffeners to develop a trussing action between the flanges, stiffeners and the web. Specimen 9 did not have these required stiffeners, and

the cyclic diagonal tension field did not form properly. The design of these stiffeners is similar to the design of stiffeners for deep plate girders [32], since plate girders also require stiffeners to develop a diagonal tension field under monotonic or static load. The beams, which yielded in bending, had a lower shear and moment gradient, and greater length of flange yielded during strain hardening at the plastic hinges. Flange buckling occurs after a sufficient length of flange has yielded, but the web is not able to provide much restraint to the buckled flange, so the flange buckles deform dramatically and eventually fracture after several reversals. This underscores the need for moment-resisting beam-to-column connections. As is verified by comparing Specimen 9 to Specimens 1, 2, 6 and 8, the cyclic diagonal tension field, which is needed to assure stable performance after web buckling, is formed only when the flanges and stiffeners are properly restrained.

The cyclic loading which was applied to these test specimens was primarily to examine cyclic behavior at large deflections. As a result, none of the specimens were subjected to a large number of cycles. The limited number of cycles significantly reduced the amount of energy which could be dissipated by the specimens. A much larger amount of energy could have been dissipated by each of the specimens had it been cycled through a large number of small or moderate inelastic deflections. However, for these nine specimens the beams which yielded in shear were the better dissipators of energy. They were better because they dissipated larger amounts of energy during the test and did not fracture, so that they would have been capable of dissipating more if additional cycles had been run. This better dissipation can be attributed to the distribution of plastic strain over a larger area of the web. Beams, which yield in

bending and have flange buckles, experience very large plastic strains locally and so the specimen fails. The shear yield specimens had a more uniform distribution of plastic strain, and the specimens did not fail.

Finally, these tests indicate that doubler plates should not be applied to the web of eccentric beam elements. The specimens which used doubler plates (4 and 5) resulted in a failure of the doubler plate weld. Moreover the doubler plates did not deform in unison with the web, unless a very large weld was used. This is not to say that doubler plates should never be used, because they may be very effective in elements which remain elastic or undergo only small inelastic deflection. However, doubler plates do not appear to be effective on eccentric elements which undergo very large inelastic deflections, and they are not worth the high cost of installation.

#### Analytical Model for Cyclic Shear Yielding Beams

After it was determined that shear yielding exhibits the best inelastic cyclic behavior, it was necessary to develop an analytical model which would predict the inelastic response of shear yielding beams. The desired model was not one which would predict the local stresses or strains within the elements but a global model which adequately defines the nodal displacement of a beam. The model could then be used to predict the gross overall behavior of eccentrically braced frame structures as opposed to the details of individual connections.

The model developed averages over and ignores many local effects within the beam such as web buckling and diagonal tension, but remains consistent with the general concepts of inelastic behavior and the test results. It is a piecewise linear approximation of the true inelastic force-deflection relationship. The beam is assumed to have rotational

restraint at both ends, and rotational plastic hinges may form at either end as well as shear yielding of the web of the entire element. Hence there are eight possible linear zones of behavior in this model. These zones are

1. Fully elastic beam
2. Elastic web with plastic hinge due to bending at left end
3. Elastic web with plastic hinge due to bending at right end
4. Elastic web with plastic hinges due to bending at both ends
5. Web yielded in shear but no plastic hinges due to bending
6. Web yielded in shear with plastic hinge due to bending at left end
7. Web yielded in shear with plastic hinge due to bending at right end
8. Web yielded in shear with plastic hinges due to bending at both ends

The beam element may fall into any one of these eight zones depending on its strain history and state of stress. The stiffness of the element is computed for each of these zones based on material with bilinear material hardening. This bilinear material was modeled by a variation of the parallel component approach [33, 34]. In this method, an elasto-plastic component is combined with a fully elastic component to model bilinear strain hardening. The fully elastic component simulates the strain hardening of the fully yielded element, and the elasto-plastic component provides the remainder of the elastic stiffness. The slope and yield point of the elasto-plastic component are usually taken as fixed, but in this model these values are adjusted to permit the yield surface to grow during strain hardening and to account for the shear yielding phenomenon. The effect of plastic hinge formation is very easily accounted for by this method [34]. This is done by arbitrarily setting the elasto-plastic component of the bending moment at the plastic hinge to zero and partitioning and condensing the  $2 \times 2$  generalized



stiffness matrix to a single value. When plastic hinges form at both ends, the elasto-plastic component of stiffness is reduced to zero.

Therefore, the calculation of the stiffness of the eight zones of behavior essentially reduces to the problem of determining the 2 x 2 generalized stiffness matrix for a fully linear elastic beam and the 2 x 2 generalized stiffness matrix for a beam with a shear yielded web and no plastic hinges. The stiffness of the linear elastic element depends only upon the geometry of the beam, and the linear elastic properties of the material, Young's Modulus, E, and the Shear Modulus, G. The stiffness of the beam with a shear yielded web requires the definition of the inelastic strain hardening properties of the material. To define these properties a bilinear strain hardening material model was used as is shown in Fig. 26. With this idealization the total uniaxial stress-strain curve is determined by three variables, Young's Modulus, E, the uniaxial strain hardening ratio,  $\rho$ , and the yield stress,  $\sigma_y$ . All three of these parameters can be empirically determined from a tensile coupon test, as shown in the diagram of Fig. 26. It was further assumed that the web strain hardens in pure shear. Therefore, a plastic shear modulus,  $G_p$ , was found using the Prandtl-Reuss equation [31], assuming that the volume of material is constant during plastic deformation. As a result of these conditions, the slope,  $G_p$ , or the strain hardening portion of the bilinear stress-strain idealization in pure shear is

$$G_p = \frac{\rho E}{3} \quad (2)$$

This plastic shear modulus,  $G_p$ , was used in place of G when the beam web had yielded in shear.

In addition to a plastic flow rule, a yield surface had to be defined for the beam. This was done by assuming that the web yields in pure shear and obeys the von Mises yield criterion. Based on this criterion, the shear force at yielding of the web,  $V_p$ , is

$$V_p = t_w d \frac{\sigma_y}{\sqrt{3}} \quad (3)$$

where  $t_w$  is the thickness of the web of the wide flange section and  $d$  is its total depth. Equation 3 predicts an average shear yield stress of  $0.577 \sigma_y$ . It was also assumed that the flange yielded purely by uniaxial stress due to bending. This simplification is a reasonable approximation of the beam bending behavior. To be consistent with this assumption and the test results, the reduced plastic moment contributed by the flanges,  $M_p^*$ , was used in place of the full plastic moment,  $M_p$ .

$$M_p^* = t_f b (d - t_f) \sigma_y \quad (4)$$

where  $t_f$  is the thickness of the flange and  $b$  is the width of the flange. It should be noted that the use of  $M_p^*$  is consistent with the test results of the new cyclic tests as well as those by Newmark and Hall [29]. The earlier tests indicated that the full plastic moment could be developed in beams which yield in shear, but only after considerable strain hardening had occurred. Therefore, the point of first bending yield was taken as  $M_p^*$  for cyclic behavior. The full plastic moment can still be achieved but only after considerable strain hardening.

#### Simple Shear Deflection Theory

The stiffness matrix was determined by computing the combined bending and shear deflection of the beam under unit forces to calculate the flexibility matrix; then the flexibility was inverted to obtain the

stiffness. A simple and commonly used method of computing this combined deflection of an elastic beam is to superimpose the deflection components due to pure bending and pure shear. In the computation of the bending deflections, it is assumed that plane sections remain plane and the material behaves linearly, then the bending deflections and bending stresses in the beam can be computed. The distribution of shear stresses in the beam is determined by applying statics to the bending stress distribution. The shear stress distribution, which results for a wide flange, is a parabolically varying stress with nearly constant shear stress in the web, as shown in Fig. 27(a). This nearly constant stress is approximated by a constant shear stress, as shown in Fig. 27(b). Therefore, the shear deflections can be computed directly from these elastic shear strains.

The above approach is a very direct approach, and it produces satisfactory results if the web of the beam is elastic. This is the procedure used to compute the stiffness terms of zones 1 through 4 in the analytical model. The simplest method of computing plastic shear deflections is to use the same simple shear deflection theory, but to substitute the plastic shear modulus,  $G_p$ , for the elastic shear modulus,  $G$ , when computing incremental shear strain. However, this simplified approach will not produce satisfactory results because it predicts excessive warping. This simple theory assumes that the incremental shear stress and strain are uniformly distributed over the web and are zero in the flanges. Therefore, cross-sectional warping must occur, as shown in Fig. 27(c), since the shear strain is not the same at all points along the cross-section. This warping presents a problem in that warping is prevented at interfaces between shear yielding elements and elastic or bending yield elements. The stiffness of a beam which has

yielded in shear will be underestimated by this simple shear deflection method because the method does not include warping resistance. Figure 28 shows a plot of the monotonic test results from Specimen 1 and the relatively poor fit provided by the application of the simple shear deflection theory. It should be noted that warping also occurs when the web is elastic, but the elastic incremental shear deflections and strain are very small, so the warping is very small. Therefore, it is necessary to develop a theory which will consider the warping restraint provided to a beam with a web which had yielded in shear.

#### Sandwich Beam Theory

A slightly more complex theory, the sandwich beam theory, was used to compute the stiffness of a beam with a web yielded in shear. This theory was used because it is capable of evaluating the effect of warping resistance on the deflections of the beam. The sandwich beam theory variation developed by Plantema [35] and van der Neut [36] was used for this model. In this theory the deflections of the beam are still expressed as the sum of two components.

$$w_t = w_s + w_b \quad (5)$$

but the components are determined as set forth below. The deflections,  $w_s$  and  $w_b$ , are the partial deflections due to shear and bending, respectively, and  $w_t$  is the total deflection of the beam. These components are shown in Fig. 29. The component  $w_b$  can be computed by the ordinary theory of beam bending

$$w_b'' = \frac{M}{EI} = \phi \quad (6)$$

where  $M$  is the bending moment of the beam,  $E$  is Young's Modulus or the slope of the uniaxial stress-strain curve,  $\phi$  is the curvature of the beam, and  $I$  is the moment of inertia of the cross-section. Because of the previous assumptions, the web of the shear yielded beam does not carry any bending stress and thus its bending stiffness is neglected, so that

$$I = \frac{t_f b}{2} (d - t_f)^2 + \frac{1}{6} b t_f^3 \quad (7)$$

This is a reasonable assumption since the bending stiffness of the web is relatively small.

It is necessary to break the partial deflection due to shear,  $w_s$ , into two parts to determine its magnitude. The two parts are obtained because the flanges must undergo the same deflection as the web at all points, and the flange deflection must be composed of flange bending,  $w_{bf}$ , and flange shear,  $w_{sf}$ , components so that

$$w_s = w_{sf} + w_{bf} \quad (8)$$

To simplify the determination of  $w_s$ , it is assumed that there is no distributed load on the beam segment. This simplification is not necessary to obtain a solution, but it simplifies the mathematical solution without affecting the ability of the model to compute the element stiffness.

Since there are no distributed loads, the total shear force,  $Q$ , is constant over the length of the element.

However, this total shear is carried partially by the web and partially by the flanges, so

$$Q = Q_w + 2Q_f \quad (9)$$

where  $Q_w$  is the shear carried by the web and  $Q_f$  the shear carried by a

single flange.  $Q_f$  and  $Q_w$  are not constant over the length of the element. The shear deflection of the web and flanges can be computed by ordinary shear deflection theory.

$$Q_f = G_f S_f w_{sf}' \quad (10a)$$

$$Q_w = G_w S_w w_{sw}' \quad (10b)$$

The  $S_f$  and  $S_w$  terms are the shear areas of the flange and web, and  $w_{sw}$  is the shear deflection of the web, which is also equal to the shear deflection of the beam,  $w_s$ . The terms  $G_f$  and  $G_w$  are the shear moduli terms for the flanges and web; and since the web is plastic and the flanges are elastic, these terms take on the values of the elastic shear modulus,  $G$ , and the plastic shear modulus,  $G_p$ , respectively. The shear area terms are computed by the usual engineering shear deflection theory, and

$$S_w = \frac{(d - t_f)^2}{d - 2t_f} t_w \quad (11a)$$

$$S_f = t_f b$$

The flange bending deflection term,  $w_{bf}$ , is determined analogously to the beam bending term

$$w_{bf}'' = \frac{M_f}{EI_f} \quad (12)$$

where  $M_f$  is the component of bending moment carried by the flange and  $I_f$  is the moment of inertia of the flange.

$$I_f = \frac{1}{12} b t_f^3 \quad (13)$$

Statics requires that the magnitude of the shear be the magnitude of the derivative of the moment diagram with respect to  $x$ , so when the sign convention is considered

$$Q_f = -M_f' \quad (14)$$

$$-EI_f w_{bf}'''' = G_f S_f w_{sf}'$$

and

$$Q = -EI w_b'''' \quad (15)$$

The solution of these equations can be simplified by combining equations and performing algebraic simplification, so that

$$w_{bf}'''' - \alpha^2 w_{bf}' = -\alpha^2 \frac{Q}{S_w G_p} \quad (16a)$$

$$w_b'' = \frac{M}{EI} \quad (16b)$$

$$w_{sf}' = \frac{-EI_f w_{bf}''''}{G S_f} \quad (16c)$$

where

$$\alpha^2 = \frac{G_p S_w G S_f}{EI_f (G_p S_w + 2GS_f)} \quad (17)$$

Equations 16a and 16b can be solved directly since the total shear,  $Q$ , and the total bending moment,  $M$ , come directly from the loading condition. Equation 16a can be solved by separating the solution into its complementary and particular solutions, so that

$$w_{bf} = A_1 e^{\alpha x} + A_2 e^{-\alpha x} + A_3 + \frac{Qx}{3} \quad (18)$$

The constants,  $A_1$ ,  $A_2$  and  $A_3$ , can be determined from the boundary conditions. The boundary conditions used for the solution of Equation 18 depend on the warping of the cross-section as well as the displacement configuration of the beam. Figure 29 clearly indicates that the only

cross-sectional warping that can occur in this system is warping due to different shear strains in the flanges and the web. Since the deflections of the flange are further constrained by Equation 8, warping is prevented if

$$w_{bf}' = 0 \quad (19)$$

at that point. By a similar argument

$$w_{bf}'' = 0 \quad (20)$$

if warping is totally unrestrained at a given boundary. If warping is not, at least partially, restrained at some point in the beam element, the solution of these equations will degenerate into the very simple shear deflection theory, which was discussed earlier in this chapter. Displacement boundary conditions may be more complex since the displacement is the sum of three variables

$$w = w_b + w_{bf} + w_{sf} \quad (21)$$

In all of the test beams, the center line was a line of symmetry, and so no warping could occur. On Specimens 1 thru 8, the beam had a tail section beyond the simple supports, so warping was prevented also at the simple supports. The deflection was zero at the simple supports. Therefore, the boundary conditions used to evaluate the constants of equation 18 are

$$w_{bf}' = 0$$

at center line and simple supports and

$$w_b = w_{bf} = w_{sf} = 0 \quad (22)$$



at the simple supports.

After solving Equation 16a, the solution for Equations 16b and 16c are easily obtained. Equation 16b is the usual beam bending solution, and 16c is dependent upon the solution of Equation 16a. The equations were solved for beams which exhibited shear yielding of the web, and the stiffness of the beam for these shear yielding zones was computed as discussed earlier. The force-deflection relationship for these specimens could then be computed by solving the stiffness formulations in an incremental fashion. In this procedure, the stiffness equations are solved under small load steps and the beam is checked for a change of yield state at the end of each step. If a change in yield state occurs, the stiffness matrix is changed and the incremental solution is continued. Using this approach and a uniaxial strain hardening ratio of 0.75 percent (see Appendix B), the theory was compared with the experimental data from the monotonic portion of Test 1. Figure 28 is a plot of this comparison; the dashed line is the theoretical value and the solid line is the experimental plot. This figure indicates that the theory fits the experiment quite well. The fit is very much better than that produced by the simple shear deflection theory. It should be emphasized that the sandwich beam theory is still a relatively simple theory since it does not consider any of the local effects, such as propagation of yielding, web buckling, or diagonal tension formation. Despite these simplifications, the theory gives a reasonably accurate prediction of the inelastic behavior of the beam elements.

A physical understanding of why the sandwich beam theory produces a better fit than the simple shear deflection theory can be found in Fig. 30. The warping resistance provided by the sandwich beam theory

requires that the shear force in the beam be distributed between the flange and web. Figure 30 consists of three typical plots of this distribution of incremental shear force. These curves are all normalized, and the plotted values are all dimensionless ratios. The upper curve in this figure represents the proportion of incremental shear carried by the flange of the 6 in half span specimens after the web has yielded. Virtually all of the incremental shear is carried by the flanges at interfaces restrained against warping after shear yielding of the web. This warping restraint also affects the interior points so that the flange is always carrying 50 percent of the added shear in all parts of the beam. The middle curve indicates the percentage of shear carried by the flange of a 12 in specimen after the web yielded. This curve is also indicative of the distribution predicted for the prototype eccentric element. Virtually all of the additional shear is transferred to the flanges at the interfaces, but the proportion of shear carried by the flange in the intermediate beam is substantially reduced. Both these curves substantiate the deformation patterns noted in the tests of Specimens 1, 2, 6 and 8. After the web has yielded, virtually all the incremental shear is transferred to the flanges at interfaces where warping is prevented. Therefore, the shear strain of the web becomes small near these interfaces, as noted in Fig. 15. In the central portions of the half spans, the additional shear is still carried primarily by the web, and the plastic shear strain in the web is much larger. The third curve in Fig. 30 is the percentage of shear carried by the flange when the web is fully elastic. The flange carries a greatly reduced percentage of the shear despite the warping restraint at the ends, so the effect of warping is much less severe when the beam is fully elastic. It is then appropriate to use the simple shear deflection theory for the fully elastic beam.

### Cyclic Shear Model

After completion of the monotonic test comparison, the theory was extended to include the cyclic behavior of shear yielding beams. The strain hardening and yield criteria are reasonably well-defined for the monotonic case, but they are not well defined for the cyclic case. There are two simple bilinear strain hardening models for cyclic loading: kinematic and isotropic hardening [31]. Kinematic hardening is strain hardening in which the yield surface is permitted to translate but not grow in size. This is a very popular model because it accounts for the well known Bauschinger Effect. Isotropic hardening permits the yield surface to grow in size but not to translate in the stress space. It is well known that neither of these models accurately represents the cyclic behavior of steel. It was noted in the cyclic tests of the shear yielding beams that the early cycles exhibited considerable growth in the yield surface but later cycles exhibited no growth in this surface.

Dafalias and Popov [37,38] have shown a more complex model that gives a more accurate representation of cyclic stress-strain behavior. This theory produces a particularly good fit on cycles performed at large strains. This model consists of a yield surface and bounding surface. Both of these surfaces may translate and grow in the stress space. The yield surface is allowed to approach and contact the bounding surface, but the yield surface cannot intersect the outer bounding surface. Later studies by Petersson and Popov [39] indicate that this model could be refined by a weighting function. This refinement improves the accuracy of the cyclic stress-strain prediction at smaller strain levels. The weighting function takes a combination of the cyclic stress-strain relation and the monotonic coupon test stress-strain relation to

develop the refined model. The addition of the weighting function permitted an increase in influence of the isotropic type hardening in the smaller strain cycles since experimentally these cycles exhibit considerable growth in the yield surface.

The application of the very simple kinematic and isotropic hardening models did not produce a satisfactory fit to the experimental results, and a more refined model was developed. There was no attempt to apply the full sophistication of the above models because of the several simplifications made in the sandwich beam shear yield theory. Instead, an empirical model was developed which satisfied the general yield surface, bounding surface, and strain hardening concepts of the above theoretical models. The proposed empirical model fits the test results reasonably well.

As was discussed earlier, a variation of the two component approach was used to model the plastic element behavior. This model is basically a kinematic hardening model. Isotropic hardening was introduced into the early smaller cycles by allowing the yield stress of the elasto-plastic component to grow larger during strain hardening. This theory was intended only for beams which yielded primarily in shear, and so the growth in yield point was applied only to the shear. This accomplished a dual purpose in that it assured that the earlier and smaller cycles were more significantly affected by isotropic hardening and it provided a bounding surface to the isotropic hardening. Therefore, the shear yield effect will disappear after sufficient strain hardening due to shear yielding has occurred. This agrees well with the test results since the beams which yield in shear exhibit pronounced growth in the elastic zone in the early cycles and masking of the shear yield effect

in later cycles. This growth in the yield surface was permitted only in the direction of yield. It should be noted that no axial softening was applied to this model during shear or bending yield. This was done because there is no known method for predicting this softening, and the axial loads are generally quite low in the eccentric elements. Moreover, the shear beams were tested with no axial loads.

#### Fit of the Cyclic Shear Model

The cyclic shear model was applied to the cyclic shear yield beam Specimens 2, 6 and 8. It was applied to these specimens because they yielded in cyclic shear and had the required warping restraint in the beam. The comparison of these predictions to test results are shown in Figs. 31, 32, and 33. The fit that is obtained by this model is quite good, especially in the more important range of small and moderate deflections. It should be again noted that this model is a very simple model which is intended to predict the gross overall behavior of an element and a structure. It completely ignores local effects such as web buckling, diagonal tension formation, and progression of yielding. Further, the model applies only an empirical approximation of the true cyclic material behavior. The model also uses infinitesimal strain theory. However, at deflections of greater than about one inch (25 mm) for Specimens 2 and 6, or 2 inches (50 mm) for Specimen 8, the strains are quite large and a finite strain theory would be more appropriate. Infinitesimal strain theory is not a severe limitation because deflections which are large enough to require finite strain theory can occur only after an eccentrically braced frame has undergone severe lateral deflections.

Despite these limitations, the fit is quite good. The fit is particularly good for small and moderate deflections. The slope of the elastic zone of the model is consistently stiffer than the slope found experimentally. This is not a limitation of the model, but a limitation of the experimental procedure employed. The test specimens were designed with an 0.375 in (9 mm) radius for a simple support, as shown in Fig. 12, to permit the specimen to rotate freely. This support system accomplished these ends, but it resulted in a contact stress problem at the supports. This problem is well known [40,41], and local yielding must be expected at these points. The deflection due to this local yielding was not monitored during the test, but the maximum values could be determined after the test. The maximum deflections due to this local yielding were found to be in the range of 0.01 to 0.02 in (0.2 to 0.5 mm). This small deflection is apparent in the stiffness of the elastic zone, but it is insignificant in the inelastic deflected beam.

Although the analytical model fits the test results well, there is some room for improvement of the model. There are two general ways in which the model could be improved. The first is to keep the very simple model concept, but to improve the modeling of the cyclic constitutive relations. For example, no isotropic hardening is applied to the yield due to bending. Figures 31, 32, and 33 show that the fit could be improved if the bending yield were allowed to increase because of strain hardening in some of the earlier cycles. Further, a more realistic model of the bounding surface could improve fit by further eliminating or reducing the strain hardening effect at very large deflections. Finally, as the more refined analytical model is better understood, perhaps the refined model could be applied directly to this theory by assuming the

web acts in pure shear and flanges act under pure uniaxial stress.

The second method for improving the analytical model is to improve the sophistication of the model itself. This could be done by dividing the individual shear yielding beam into a number of finite elements which consider the inelastic cyclic constitutive relation of the material. If the elements included plate bending effects, this type of model could take into account propagation a yielding, web buckling, and diagonal tension field formation. The accuracy of the model would be improved if all of these local effects were considered, but the complexity and cost of analysis would also be increased.

No comparisons are made for the other beam specimens, because the cyclic shear theory did not apply to these cases. The theory applies only to beams which yield in shear before plastic hinges form at both ends of the element. This can be assured by designing the beam such that

$$|V_p| < \left| \frac{2M_p^*}{\ell} \right| \quad (23)$$

if the rotational restraint is applied at both ends, or

$$|V_p| < \left| \frac{M_p^*}{\ell} \right| \quad (24)$$

if simply supported at one end. It is essential that the cross-section be restrained against warping at both ends. Thus, a simply supported end requires a tail or other means of providing warping restraint.

#### Summary of Cyclic Shear Yield Behavior

The results of the cyclic beam tests indicate that cyclic shear yielding of the web provides a very desirable energy dissipation mechanism. Beams which yielded in shear dissipated more energy, withstood larger deflections, and exhibited greater stability than beams which yielded in

bending. Beams which yielded in bending had flange buckling problems, while shear yielding beams buckled only in the web. Web buckling is a more desirable buckling form because of the cyclic diagonal tension field. However, shear yielding beams must be designed with stiffeners and flange restraint if the cyclic diagonal tension field is to form.

Based on the results of the beam tests, a simple analytical model of cyclic shear yield behavior was derived. This model fits the experimental results very well, and it coincides with general observations from the individual tests and with the general concepts of cyclic inelastic constitutive theory.



## CHAPTER 4. INELASTIC DYNAMIC ANALYSES

### General

The purpose of this chapter will be to discuss an inelastic dynamic analysis of the prototype structure. In performing this analysis, the analytical model of the shear beam is first incorporated into an existing dynamic analysis program, DRAIN-2D. The eccentrically braced frame is then analyzed under two separate base excitations and the predicted behavior is presented and evaluated. Three alternate structural systems are also analyzed under the same two base excitations, and the responses of these alternate systems are compared with the predicted response of the prototype system. The objective of this series of analyses is to understand better the inelastic behavior of the total eccentric system both with respect to itself and also relative to other structural systems.

### DRAIN-2D Dynamic Analysis Program

The DRAIN-2D program [34] was used to determine the behavior of the prototype frame; the program performs a plane frame inelastic dynamic analysis for structures subjected to a base excitation. The analysis employs a step-by-step procedure with the yield state of each element checked at the end of each time step. The tangent stiffness modifications and the equilibrium corrections for any imbalance due to change in state are applied at the end of each time step; the time step is held constant, and no iteration is used, however, equilibrium corrections are applied at the end of each time step to correct for any imbalance due to change in state. These corrections are applied to prevent the imbalances from accumulating and causing the solution to diverge. Because of the several simplifications used in this procedure, the solution is by no means exact. It will approach the exact solution, however, if a sufficiently small

step is used, but, since the cost of the solution increases with decreasing time steps, it is desirable to perform the analysis with the largest time step which gives sufficiently accurate results. Therefore the results of these analyses are not used to predict minute differences in behavior, but rather to determine general trends of structural behavior.

One of the main advantages of the DRAIN-2D program is the relative ease with which new inelastic elements can be added. This was the primary reason for the selection of this dynamic analysis program. The elements provided with the basic DRAIN-2D program include: (1) a brace type element (Element 1) which yields or buckles as in a variation of the slip model [1]; (2) a beam-column element (Element 2) which includes the interaction between axial force and bending moment; and (3) a beam element (Element 5) which considers only yielding due to bending. The beam and beam-column elements yield only in bending, since there is no axial softening after yielding. The elements also obey a bilinear strain hardening model which is primarily a kinematic hardening model. In the eccentric bracing system under study, it was determined that the primary method of energy dissipation would be cyclic shear yield of the eccentric element. Hence, the cyclic shear yield model discussed in the previous chapter was also programmed for DRAIN-2D. The basic beam element (Element 5) was used to form the cyclic shear yield element. The programming of the shear yielding element was simplified, since a number of parts of the analysis were identical to those used by the beam element. For example, the application of damping effect, initial and fixed end force applications and geometric stiffness application were essentially unchanged from Element 5. However, major changes had to be made in the state determination, bending stiffness calculation and input subroutine. The behavior of

this element coincides with the behavior described in Chapter 3. A listing of the element subroutines, input instructions, and some comments on the use of the element are given in Appendix C.

#### Post-Buckling Brace Element

The only existing brace type element for DRAIN-2D was the slip model element (Element 1). It is well known [1] that the slip model does not accurately represent the inelastic behavior of a brace, because it does not accurately reflect the behavior of a brace after it has buckled. Similarly, a brace, which yields in compression as permitted in Element 1, greatly overestimates the ability of the brace to dissipate energy. Since neither of the post buckling brace models permitted by Element 1 were accurate representatives of true brace behavior, a more realistic brace element was also programmed for DRAIN-2D. This element was programmed by starting with the basic structure of Element 1. As a result, the programming was again simplified since damping effects, geometric stiffness and some other computations remained unchanged. Major changes were made to the stiffness and state determination calculations. The assumed inelastic behavior of the brace, which was used in this element, is very similar to a model developed by Nilforoushan [12]. The model used is a linear approximation as shown in Fig. 34 of the true brace behavior shown in Fig. 1. Nine linear zones, which are defined by the strain history and other critical parameters, are used to approximate the true brace behavior. The critical parameters are input values, and they are determined by making a best fit to the brace behavior, which was determined by experimentation, by theoretical derivation, or by other acceptable means. This provides more flexibility in the analyses, since the brace behavior is not tied

to a specified theoretical model. The critical parameters, input instructions and a listing of the element subroutines are given in Appendix D.

This model also simulates the deterioration in buckling strength of the brace, which occurs in consecutive cycles. Experimentation has shown that the buckling load achieved on later cycles usually is greatly reduced from the buckling load on the first cycle [1]. The reduction takes place because after the brace buckles it inelastically kinks. In principle, it may be possible to restraighthen such a kink completely, when the load is reversed. However, as a practical matter, the brace is not able to restraighthen completely. As a result, it is less perfect in later cycles and buckles at a lower compressive load. Examination of the results of cyclic tests of axially loaded members indicates that the compressive load deteriorates less when the kinking is less severe. These results also indicate that there is a limit below which the buckling load will not deteriorate. The Post-Buckling element which was developed for DRAIN-2D permits the input of an initial and minimum buckling load of the brace, and then the buckling load is varied for later cycles as required. The details of this reduction procedure are also given in Appendix D.

#### Alternate Structures

Four alternate structures were analyzed by DRAIN-2D. These were the prototype eccentrically braced frame, a concentrically braced frame with all bolted connections, a concentrically braced frame with moment-resisting connections, and a moment-resisting frame. All of these frames were designed for the same geometry and the same gravity loads. The braced frames were assumed to be exterior frames which carried the total lateral loads and were therefore designed to resist, individually, 52.5% of the lateral loads and 12.5% of the gravity loads. The moment-resisting frame was assumed to be one of five frames, which carry tributary loads.

Therefore, the interior frames were taken as the critical frames and they were designed for 25% of the total lateral and gravity loads. The natural periods of all three braced structures were very similar, so the design lateral loads were alike. The moment-resisting frame was a much more flexible structure, and its design lateral loads were markedly smaller because of its longer period. However, this did not significantly affect the design, since the design of the moment-resisting frame was controlled by the maximum story drift. The moment-resisting frame was approximately 30% heavier than the braced frames. It should also be noted that the design of the eccentrically braced frame was more refined by the detailed linear elastic analyses which were performed. The other frames were not designed to the same degree of refinement. Therefore, these designs must be considered preliminary, and improvement in the dynamic performance of these three alternates may be achieved if the design is refined. The design of these alternate structures were performed in 5 story increments.

#### Input Parameters

All of the analyses were performed with a 0.01 second time step, which was chosen after several trial runs of the first few seconds of the eccentrically braced frame analyses. Considerable inelastic activity had occurred during this time span, and the results with the larger time step were sufficiently similar to the results with the smaller (0.005 seconds) time step that the cost of the shorter time step was not warranted. All of the alternate structures were analyzed with original stiffness proportional damping where the damping was approximately 5% of the critical damping for the first mode. Original stiffness proportional damping was chosen because it was felt to be more indicative of the true conditions. It is also desirable because it distributes the damping effect throughout the structure and not just at mass points. Further, it was thought

that the bulk of the damping effect would be attributable to cracking of floor slabs, damage to nonstructural walls, and etc. Therefore, it was expected that damping would substantially increase after yielding of the structure. Original stiffness damping results in a substantial increase in damping after yielding, while tangent stiffness damping produces a significant decrease in damping effects. Therefore, original stiffness damping was thought to be more realistic.

The four alternate structures were analyzed under two separate base excitations. The first excitation was 1.5 times the El Centro 1940 N-S component acceleration record shown in Fig. 35. The first 8 seconds of this record were used, since this time period contains nearly all of the high acceleration peaks and the major part of the inelastic activity should occur within this time period. The peak acceleration for this record is approximately 0.5 times the acceleration of gravity. It is believed that this record is a realistic indication of the intensity of shaking that could occur in a moderate to severe earthquake. The second acceleration was the Pacoima Dam record of the 1971 San Fernando Earthquake. This record, which is shown in Fig. 36, has a peak acceleration of approximately 1.2 times the acceleration of gravity. The first 15 seconds of this record were used, because all inelastic activity should be concentrated within this time period. It is well known that the very high accelerations of this record are a result of amplification due to local site conditions. Moreover, this record is associated with a small impulse type loading and was used to determine the relative performance of the alternate structures under such a dynamic loading. It is not intended to imply that a structure should be designed to resist this excitation.

The analyses were performed on the alternate systems with the P- $\Delta$  effect of the frames accounted for by means of the geometric stiffness. The gravity loads which were used for the computation of the geometric stiffness included the frames share of the full dead load plus 10% of the total live load. It should be noted that a fully accurate resolution of the P- $\Delta$  effect requires a 3-dimensional analysis including the gravity effect of all interior frames. This problem will be discussed in greater detail in a later section. The braced frames were designed as exterior frames, so they all carried 12.5% of the total gravity loads. The moment-resisting frames were designed as interior frames, so each one carried 25% of the total gravity loads. The total mass of the structure was also taken as the mass of the total dead load and 10% of the live load. The braced frames were designed to carry all of the lateral loads, and so, each braced frame was assigned 50% of the total mass of the structure. The design lateral loads were distributed among the moment-resisting frames, and so each interior frame was assigned 25% of the total mass. The gravity loads were also distributed elastically throughout the frame, and hence affected the first yielding of each element. This should not greatly affect the performance of the frames, however, once the inelastic behavior of the frame has started.

#### Results from 1.5 Times the El Centro Excitation

The four alternate structures were analyzed under 1.5 times the El Centro excitation. Figure 37 is a plot of the maximum relative displacement of the various story levels for the alternate structures. The solid line in this plot is the eccentrically braced frame. The triangles indicate the bolted concentrically braced frame, diamonds indicate the concentrically braced frame with moment-resisting connections, and the

squares represent data points of the moment-resisting frame. The maximum relative displacement of each story level is the maximum deflection relative to the structures' undeformed configurations. These maximum values do not occur at the same time for all story levels, so the curves plotted in Fig. 37 do not represent the deflected shape of the structure at any one time of the analysis. The maximum relative deflection of the eccentrically braced frame is significantly smaller than those of the other alternate structures. The maximum deflections of the concentrically braced frames were the largest for the upper stories, and the maximum deflections of the moment-resisting frame were the largest for the lower stories. The curve for the moment-resisting frame exhibits a sharp kink at the 10th floor level. The reason for this sharp kink is that the time of the maximum deflection was very different for the top and bottom stories. The large time difference is introduced because the moment-resisting frame is a more flexible, longer period structure, and the higher modes are more apparent.

Figure 38 is a plot of the maximum story drift for each alternative at the various story levels. The various curves are defined by the same legend as for Fig. 37. The maximum story drifts are generally smaller for the eccentrically braced frame and generally larger for the moment-resisting frame than for the other alternatives. The eccentrically braced frame experienced smaller story drifts because it was a stiffer structure with very good energy dissipation capabilities. The moment-resisting frame also had very good energy dissipation but it was considerably more flexible, and so it experienced the largest drift. The curve for the eccentrically braced frame was relatively uniform indicating that the deformation was greater at lower stories but basically well distributed throughout the structure. The curve for the moment-resisting frame



exhibits two zones of high story drift. These two zones apparently indicate that higher modes of vibration play an important role in the response of the moment-resisting frame. The concentrically braced frames had slightly larger story drifts than the eccentrically braced frames, and the curves were somewhat more erratic than for the eccentric and moment-resisting frames. The erratic nature of these curves was most apparent in the lower stories where the buckling of the braces were most severe, so the curves would probably be smoother if the structural members were sized over smaller intervals and if the design were more refined.

Figure 39 is a plot of the deflected shape of the alternate structures at the end of 8.0 seconds. At that point, the inelastic activity produced by the El Centro record was essentially complete, and the analysis was stopped. The velocity at that time was not equal to zero, so Fig. 39 does not represent the final deformed shape of the structure. However, because future deformations would have been primarily elastic, this deflected shape and the individual time histories of the floor levels can be used to infer an approximate final deformed configuration. A study of these curves leads to several conclusions. The first is that all of the four alternate structures will return to a final deformed shape which is close to the original undeformed configuration of the structures, but the eccentrically braced frame should be somewhat better than the other alternatives. It will have smaller permanent lateral deflection than the concentrically braced frames, and it will exhibit a straighter deflected shape than the moment-resisting frame. The moment-resisting frame will assume a kinked final deformed shape because of its larger story drifts and the influence of higher modes of vibration. The second conclusion is that mathematical models predict that the eccentrically braced frame and the moment-resisting frame will regain their full lateral stiffness

at the end of the excitation, because their yielding mechanisms do not exhibit any deterioration during the analyses. The concentrically braced frames will have only a small portion of their initial stiffness because the analyses indicate that most of the braces have buckled. These buckled braces will behave elastically at the end of the excitations, but some of them will be so severely bent that their elastic stiffness is only a small fraction of their initial stiffness. As a result of this great loss in stiffness, the concentrically braced frames must be expected to experience large lateral deflection during even minor windstorms or aftershocks. Since the concentrically braced frames have lost much of their stiffness, they may also require major structural repair to regain this stiffness. The eccentrically braced frames will require repair only for non-structural damage. Further, the alternate structures have suffered larger permanent lateral deflections and these are more likely to be condemned. A final conclusion to be made from this comparison is that the eccentrically braced frame is likely to be repairable at the conclusion of this level of excitation. This desirable attribute occurs because of the good energy dissipation characteristics of the eccentrically braced frame. All of the frames dissipated large amounts of energy, but the eccentric frame and moment-resisting frame dissipated this energy without any degradation in strength or lateral stiffness. As a result of this better dissipation behavior, the eccentric system is predicted to come out of the excitation in better condition.

The comparison of the performance of the alternate structures can be summarized by noting that all of the alternate structures performed satisfactorily under a substantial excitation. However, the eccentric bracing system did perform better. It experienced smaller relative

deflections and story drifts, and the eccentric system appears to be a more repairable structure.

#### Results from the Pacoima Dam Excitation

The four alternate structures were also analyzed under the Pacoima Dam excitation. The plots of maximum relative displacement of the various story levels for the alternate structures are shown in Fig. 40. The legend of Fig. 40 is identical to that of Figs. 37, 38 and 39. For all of the braced frame structures, the maximum relative displacements fall into a very narrow band. The maximum deflection was of the order of 36 in (910 mm) for all of these frames. The moment-resisting frame experienced maximum deflections which were much larger than those of the braced frames. The maximum deflection for the moment-resisting frame was 69.8 in (1.77 m). Further, Fig. 40 indicates that virtually all of the extreme deformations are concentrated in the lowest 5 stories. These large relative displacements are occurring because of the substantial  $P-\Delta$  effect. The moment-resisting frame has considerably less lateral strength and stiffness than any of the braced frames. When a structure is subjected to a prolonged impulse loading, its strength and stiffness are more important than its energy dissipation capabilities. The Pacoima Dam Record induces an impulse type loading in structures, and so, the flexible moment-resisting frame experiences large deflections. These large deflections induce large  $P-\Delta$  moments, and a larger proportion of the frame's strength and stiffness are expended resisting the  $P-\Delta$  effect.

Figure 41 is a plot of the maximum story drift. This figure gives further verification of the significance of the  $P-\Delta$  effect for the moment-resisting frame. The maximum story deformations are concentrated in the

lowest five stories; the bottom story has a maximum story drift of approximately 22 in (560 mm). The story drift of the braced frame structures all fit into a fairly tight band. The story drift is certainly more severe for lower stories in the eccentrically braced frame, but the deformations are far more uniformly distributed than for the moment-resisting frame. It should be noted that none of the DRAIN-2D elements have a criterion for element failure. It is questionable whether the bottom story would be able to withstand a 22 in (560 mm) story drift without experiencing a total or partial failure of the frame.

Figure 42 is a plot of the deflected shapes of the alternate structures at the end of the analyses. The velocity does not equal zero at this time. However, the inelastic activity is complete for the braced frame structures, so the analyses were stopped. It is again possible to infer the final deflected shape of the braced structures by combining Fig. 42 with the individual story level time-history plots. A study of these curves indicates that all of the alternate structural systems will have considerable permanent deflection. A permanent deflection of the order of 15 to 25 inches (380 to 640 mm) can be expected for the braced frames. The concentrically braced frames will have slightly smaller final deflections, because they have slightly larger stiffnesses and strengths due to their slightly larger weights of steel. All of the braced structures experienced very large inelastic deformations, and it is improbable that any of these structures could be repaired. It is not possible to infer a final deflected shape of the moment resisting frame, because this frame has severe stability problems. Since the Pacoima Dam acceleration record has some characteristics of an impulse loading, the response produced by this record were consistently one-sided responses. That is, at some time in the analysis the relative displacement

moved to one side of the initial undeformed configuration and stayed to that side throughout the rest of the analysis. This type of behavior is displayed in Fig. 43, which is a plot of the time-history response of the roof for the moment-resisting and eccentrically braced frame. The eccentrically braced frame is indicated by the solid line, and the moment-resisting frame is identified by the solid line with squares. As was discussed earlier, the plot shows that the response of the eccentrically braced frame reached a peak at approximately 8.5 seconds, and the response then stabilized during the mild excitations which followed. This frame appears to be stabilizing toward a final top story deflection of approximately 22 in (560 mm). The plot also shows that during this period of time the response of the moment-resisting frame is not stabilizing. The moment-resisting frame reaches a very substantial peak in its response at approximately 10 seconds. The deflections are so large at this time that the P- $\Delta$  effect uses up most of the elastic strength and stiffness of the frame. Therefore, it reaches an even higher peak at 14.6 seconds even though the base excitations are very low during this period. It is very possible that this drift would continue with the moment resisting frame, if a longer Pacoima record were used. As a result, this structure would probably collapse during the rest of the excitation or during minor aftershocks.

The one-sided response, which was noted for all structures subjected to the Pacoima Dam acceleration record, is characteristic of the inelastic response of a single degree-of-freedom system to a pulse excitation. Solutions to the single degree-of-freedom problem are well known [42] and the maximum deflections are strongly influenced by the strength and stiffness of the system. The response to the Pacoima Dam excitation was greatly influenced also by the strength and stiffness of the structures.

All the braced frames had about the same strength and stiffness and they experienced similar responses. The moment-resisting frame was not nearly as stiff or strong as the braced frames, and it experienced much larger deflections. Since one cannot know in advance what characteristics an acceleration record of a future earthquake will possess, it is desirable to have structures with stiffness, strength and good energy dissipation characteristics. To meet all contingencies, an eccentrically braced frame should be best. It is stiff and strong like a concentrically braced frame, and it has excellent energy dissipation like a moment-resisting frame. Hence, the eccentric bracing system can be expected to perform well during virtually any earthquake, if it is properly designed. It is not intended to say that the other systems are inadequate. The other braced systems performed satisfactorily, but the moment resisting frame subjected to the Pacoima Dam acceleration was found to be unsatisfactory. The moment-resisting frame developed problems due to excessive deflections thereby increasing the  $P-\Delta$  effect. It should be noted, however, that the design of the moment-resisting frame was a preliminary design, and its performance could be improved by increasing its strength and stiffness.

#### Comparison of the Member Behavior

The purpose of the comparison of the overall structural behaviors of the different systems was to display their relative merits. It was not intended to make a detailed comparison of local behavior such as axial forces in the columns, since this has been done in other studies [11,12,43]. However, a few general comments will be made about the local inelastic behavior. Essentially all of the energy that was dissipated by the eccentrically braced frame was dissipated in the eccentric elements. Every eccentric element experienced some yielding in both the

Pacoima and El Centro excitation. No braces buckled during the El Centro analysis, and only one brace, which was located at the 16th story level, buckled during the Pacoima analysis. The axial forces in the base of the columns were quite high at times in both tension and compression. The maximum column loads were 3080 kips (13.7 MN) in compression and 1460 kips (6500 KN) in tension. It was assumed in the analysis that the foundation was capable of developing these tensile loads. As a result of the high column forces, plastic hinges formed in the columns for short periods of time at several locations. These hinges did not adversely affect the lateral deflections, since the lateral deflections were severely limited by the bracing. However, the yield locations had to be evaluated at the end of each analysis for inelastic axial shortening. The DRAIN-2D beam-column element (Element 2) does not model any axial softening after yielding has occurred. It is shown in reference [30] that this softening does occur in columns with high axial loads, but no numerical model for evaluating this softening has been implemented. The indicated hinge locations were examined, and it appears that axial softening would not be a problem, or, at most, could be prevented by relatively minor increases in column sizes.

The axial forces in the columns were a more severe problem for the concentrically braced structures. The maximum axial loads in the columns were considerably lower for the eccentrically braced frame, because this force was limited by the shear transmitted by the yielding eccentric element. The increase in column loads is limited only by the strength of the brace for a concentrically braced frame. Since the brace was designed in compression, while it can also yield in tension, wide fluctuation in column loads resulted. The maximum column forces in the prototype concentrically braced frames were 4300 kips (19.1 MN) in

compression and 3000 kips (13.4 MN) in tension. Because of these higher axial forces, the plastic moment was reduced, and plastic hinges formed at a few more locations than for the eccentric bracing system. The energy dissipation of the concentrically braced frames was virtually all due to the inelastic shortening and lengthening of axial members. Similar behavior was noted for the concentrically braced frames with both bolted and moment-resisting connections. This behavior appears to contradict the findings of Igarashi and Inoue [4], who found that the inelastic behavior is better in braced frames with moment-resisting capabilities. However, their conclusions were based on inelastic static analysis, and the analyses discussed here are dynamic. Since there are additional factors which affect dynamic response analysis but which do not have any apparent effect in the static analysis, the basic conclusion that it is better to design braced frames with moment-resisting connections appears to be valid.

The energy dissipation of the moment-resisting frame was entirely due to the plastic hinge rotations of the beam ends. The frame was designed by the weak beam-strong column design concept. As a result, all of the beam ends formed plastic hinges at some time in the analysis. The only plastic hinges which formed in the columns occurred at the very base of the columns. The column bases were fixed against rotation, so these plastic hinges must develop before the structure can form the mechanism which is necessary to achieve large lateral deflections and dissipate energy. Any plastic hinge which forms in the column is certainly more dangerous in a moment resisting frame than a braced frame, because there is less restraint against story drift. However, these plastic hinges were not considered to be critical, because the axial loads in the



columns of the moment-resisting frames were quite moderate. The maximum compressive force was approximately 1250 kips (5560 kN). No tensile forces developed in the columns.

#### Floor Deformations in the Eccentrically Braced Frame

In the previous sections, it was indicated that the overall dynamic performance of the eccentrically braced frame is superior to that of the moment-resisting and concentrically braced frames, because it has both excellent energy dissipation characteristics and greater strength and stiffness. It must be noted that, while obtaining these desirable characteristics, the system develops substantial inelastic floor deformations, which are necessary, because this is the intrinsic energy dissipation mechanism of the eccentric bracing system. The floor deformation is related to the lateral deflections which the structure experiences.

The publication, "Plastic Design of Braced Multistory Steel Frames," [44] presents a method of estimating the lateral deflections of a concentrically braced frame as the sum of two components. The components are  $\delta_a$ , the lateral deflection due to lengthening or shortening of the brace, and  $\delta_b$ , the lateral deflection due to lengthening and shortening of the columns. For eccentrically braced frames, a third component,  $\delta_c$ , the lateral deflection caused by the deformation in the eccentric element, can be added, see Fig. 44. Therefore

$$\delta_T \approx \delta_a + \delta_b + \delta_c \quad (25)$$

If the value of  $\delta_a$  or  $\delta_b$  are to change, it is necessary to have a change in the axial loads of the brace or column. Since the eccentric element is designed to avoid brace buckling these axial loads do not change greatly in a structure which is yielding, however, so the two

components remain nearly constant while the structure is yielding. The third component,  $\delta_c$ , is negligible while the structure is elastic, because of the high stiffness of the elastic eccentric element; but  $\delta_c$  changes significantly after the eccentric element has yielded and lost most of its stiffness. These simple kinematic concepts are reflected in the results of the dynamic analysis.

Time history records of the eccentric element floor deformations were maintained for the bottom 12 stories in the DRAIN-2D analyses. Similar records for the top eight stories could not be obtained because of limitations in the program. However, approximate envelope values for these upper stories can be inferred. Figure 45 is a plot of the maximum floor deformations for the eccentric elements on the first 12 stories. The diamonds identify data from the 1.5 times E1 Centro analysis and the triangles, the Pacoima Dam analysis. This figure shows that the deformations are quite uniformly distributed throughout the height of the structure for the E1 Centro analysis. The peak deformation was approximately 6.7 in (170 mm) for the Pacoima analysis. This deformation is very severe when it is recognized that it is concentrated within 35 in (890 mm) of the eccentric element. The maximum deformation due to the E1 Centro excitation was approximately 1.4 in (35 mm). The time-history plots for the most severely deformed eccentric elements are shown in Figs. 46 and 47. The curves corroborate the significance of the three components of deflection shown in Fig. 44. When the structure is elastic the eccentric element deformations are small but very high velocities are attained during the short time the eccentric element is forced to behave plastically. These results indicate that lateral deflections due to deformation of the eccentric element are basically plastic deformations.

Figures 45, 46, and 47 also verify some of the conclusions reached from observation of story drift and maximum displacement. First, Fig. 45 indicates a uniform distribution of plastic deformation in the eccentric elements during the El Centro analysis. This is very desirable, since it implies that the ductility requirement imposed on an individual element is less severe. Further, the resulting permanent deformation of the structure due to El Centro is small as may be seen from Fig. 46. This agrees with the previous conclusions. Figure 47 indicates a very large permanent plastic deformation of the structure is left after the Pacoima Dam excitation analysis. Therefore, it is apparent that any permanent lateral deflection, which remains in the structure after completion of the analysis, must cause permanent inelastic floor deformation in the structure.

The above discussion can be summarized by saying that the inelastic behavior of the eccentrically braced system is directly related to the inelastic deformation of the eccentric elements. Therefore, the eccentric elements must be designed to withstand the inelastic deformations. Since these deformations may be large, this presents a very substantial design problem.

#### Problem Noted in Eccentric Frame Dynamic Analysis

A potential problem was noted in the DRAIN-2D dynamic analysis of the eccentrically braced frames when original stiffness proportional damping was used. This damping was used because it predicted a more realistic distribution of damping effects and did not cause a decrease in damping after yielding occurred; it also offers more computational stability in the analysis. The DRAIN-2D computer program handles this type of damping by augmenting the structural stiffness at the start of

the analysis and adding a load term at the end of each time step throughout the analysis [34]. The load term is added to the unbalanced load vector, which includes unbalanced loads due to change of yield state of correction for nonlinearities due to large deflections. The unbalanced load vector is then added to the next time step, since no iteration is performed within the time step for this program.

The problem was first noted by observing that the member forces, which were output by DRAIN-2D, did not satisfy equilibrium at the eccentric nodes. The axial forces in the brace and central beam segment were considerably higher than was warranted by the shear in the eccentric beam element. Moreover, this imbalance did not start until the eccentric element started to exhibit large amounts of yielding. The imbalance in member forces could not be caused by inertial loads, since there was no mass at these eccentric nodes. Eventually it was determined that the imbalance in member forces was caused by the application of a load through the unbalanced load vector used in DRAIN-2D. A large number of computer runs were made, which showed that this problem was dependent upon the geometry of the eccentric bracing system and the solution procedure used in DRAIN-2D and not a error within the subroutines developed for this analysis. These runs also indicated that the imbalance became significant only when the vertical damping loads on eccentric nodes became large. These vertical damping loads are large only while the eccentric element is plastic, because the vertical velocities of the eccentric node are essentially zero before yielding but are very large during yielding. This is verified by the time-history plots of Figs. 46 and 47.

The problem occurs when the eccentric element has lost most of its stiffness and ability to transmit shear, but the axial stiffness of the brace and central beam segment is still high. Therefore, this stiff,

interior bracing system is essentially isolated from the rest of the structure by the plastic eccentric elements as depicted in Fig. 48. Since the elastic central bracing system is isolated by the plastic eccentric elements, the damping forces which are applied to these eccentric nodes are transmitted by the trussing action as shown in Fig. 48. The direction and magnitude of these damping forces are dependent upon the direction and magnitude of the velocity. These damping forces will always increase the magnitude of both axial tension and axial compression forces. As a result, the axial force in the brace and central beam section are higher than required by the forces in the eccentric element. It must be emphasized that the DRAIN-2D analysis does satisfy equilibrium when damping effects are taken into account. The apparent imbalance in member forces is balanced by the damping loads.

There are several questions as to whether this damping phenomenon simulates true structural behavior. Damping normally includes any dissipative behavior which cannot normally be included as structural element behavior. This includes many things such as viscous material behavior, slippage in bolts in connections, and damage to floor slabs and non-structural infill walls. Some of these damping effects may physically cause higher axial forces in the brace but other effects will not. For example, in an eccentric bracing system with the floor slab integrally connected to the eccentric beam, considerable damping will result from crushing and cracking of the floor slab and infill walls. This damping is likely to cause a substantial increase in the axial loads of the brace. If the same structure were designed with the eccentric beam isolated from the floor slab, the axial force in the brace could not increase. There would still be considerable damping due to slippage in bolts, damage to infill walls, and other causes, but the

axial load in the brace could not increase after the eccentric element yields, because the brace is physically separated from all of these effects. Therefore, it is apparent that the predicted increase in axial loads may or may not be realistic, depending upon the design of the structure.

This increase in axial forces may cause substantial design problems in a structure. For example, it is very important that the brace be designed to avoid buckling, and it is necessary to have a realistic estimate of brace forces to properly design this brace. Another example, the axial force time history of the brace can be used to generate a time history record of the base shear of the structure. Both of these examples require a realistic time history record for the axial force in the brace. A certain amount of engineering judgment must be applied to this problem to determine if the damping and brace time-history record is realistic. If they are both realistic there is no problem. However, if the overall damping is realistic but the brace forces are unrealistically high, it may be necessary to modify the axial force time-history by finding the axial force at each time step which satisfies nodal equilibrium with the shears in the beam.

This problem was evaluated in the prototype structural system, and it was not found to be a severe problem. The maximum increase in axial forces appeared to be approximately 30%. This increase was felt to be reasonable for the 20-story prototype structural system, because the structure was designed to have interaction between the floor slab and the beam. However, the size of this increase depends upon the structure being analyzed. Increases in excess of 100% were noted for several other shorter eccentrically braced frames.

## Dynamic Response of the Entire Structure

The analyses which were performed were plane frame analyses. However, the effect of factors such as the torsional response and the P- $\Delta$  effect on interior unbraced frames depend on the response of the total structure. The dynamic response of the total structure is a 3-dimensional response problem. However, the cost and complexity of such a 3-dimensional analysis make it prohibitive for present investigation. Therefore, this section will consist of a short discussion of how applicable the plane frame analysis is likely to be to the total frame response.

The first factor to be considered in this discussion is the torsional response of the structure. A plane frame analysis includes no torsional response. However, the total frame response may be significantly affected by the inelastic torsional response of the structure. For example, when an individual frame of the total structure softens due to yielding, the shear center of the structure moves. As a result, the torsional effect on the structure may change suddenly. The prototype structure was designed as a structure with a very symmetric distribution of mass, strength, and stiffness. Therefore, it is likely that yielding will progress in essentially a symmetric manner. This implies that the torsional response is not likely to be a serious problem for this structure, but any torsional excitation or variability in the as-built properties of the structure can increase the significance of torsional response. The full impact of torsion can only be determined by a more thorough study.

The second major factor, which would be considered, is the variability of the in-plane behavior of the various frames of the structure. For example, in the braced frame alternatives, the braced frames were designed to provide the full lateral strength and stiffness of the

structure. The interior unbraced frames were designed to resist their tributary gravity loads with a capability to resist the minimum lateral loads required by the design code. These interior frames are designed by the so called "two bit" frame concept. This lateral strength is necessary, because these interior frames must resist minimal overturning moments due to the P- $\Delta$  effect. However, the lateral strength provided to these interior frames affects the dynamic response of the structure.

This variability in in-plane behavior can be approximately accounted for by a method used by Wang [45] in the analysis of shear wall structures. In this method, two plane frames are analyzed while coupled together with a rigid link at each story level. This method assumes that there is no shear lag within the floor system, and all frames deflect the same amount. One of these two frames would have the properties of an exterior braced frame, and the other frame would have the properties of an interior frame.

This coupled frame analysis would be much more costly, because of the increased number of members and degrees of freedom. This type of analysis was not performed on the 20-story prototype structure, because it was thought that this analysis would not add further insight into the behavior of the eccentrically braced frame. These interior frames were thought to be beneficial to the eccentric bracing system, since they provided added strength and dissipation capability to a system which experiences small deflections with no deterioration in strength or stiffness. This type of coupled frame analysis will likely be more useful in the concentric bracing system, because this system does exhibit some deterioration during later cycles.

#### Summary of Dynamic Analysis Results

Two sets of plane frame inelastic dynamic analyses for two significantly different types of earthquakes were performed on the prototype



structure and three alternate structural systems. In all cases, the eccentrically braced system performed well. It performed well, because it is a stiff, strong structure with excellent energy dissipation characteristics. The concentrically braced frame also performed well but not as well as the eccentric system, because of its poorer energy dissipation and deterioration of strength and stiffness. The moment-resisting frame exhibited desirable energy dissipation, but it lacked the strength and stiffness at large deflections to assure its stability under the Pacoima Dam excitation. It should be noted that the three alternative designs were preliminary designs, and improvements could be made in their performance. However, the designs were sufficiently representative so that they displayed the relative strengths and weaknesses of the alternate structural systems.



## CHAPTER 5. DESIGN OF ONE-THIRD SCALE MODEL FRAMES AND TEST SETUP

### General

The prototype structure had been thoroughly analyzed at this point in the study. Also a detailed experimental and analytical study of the inelastic behavior of the eccentric element had been performed. A number of conclusions were reached in the inelastic dynamic analyses. One of the more critical conclusions was that large inelastic deformations are predicted in the eccentric beam element. These large deformations are necessary to the eccentrically braced system, since its sound energy dissipation capability is created by these severe deformations. Experimental studies were then necessary to assure that the eccentric system could withstand the large deformations without a structural failure. It was also necessary to assure that the actual system behaved as predicted by the analytical model. Further, the following experimental studies were desirable as an aid in the development of design criteria for this type of structure.

### Design of One-Third Scale Model

For testing purposes, it was necessary to choose a frame size which would fit well with a testing facility presently in operation at the University of California, Berkeley. This facility had been successfully used in experiments with shear walls [45] and is frequently used for the cyclic testing of subassemblages. Another consideration in the design of the frame size was that it should have more than one level of eccentric bracing in order to simulate earthquake effects on a taller structure.

For these reasons, a one-third scale model of a three story single bay structure was chosen. This three story single bay braced frame sub-assembly was intended to fit into the prototype structure as the three

stories in the lower corner as shown in Fig. 49(a). For testing purposes, this model was then taken as a free body of this lower corner as shown in Fig. 49(b). Therefore, the cyclic loadings, which were applied to the test frame, were the cyclic effects which the free body would experience, if a one-third scale model of the entire prototype frame were tested.

One major simplification was made in the design and testing of the free body test specimens. The bending moments of the beams of the interior bays of Fig. 49(a) were neglected. This simplification was appropriate because the magnitudes of these bending moments were very small when compared to the overturning moment of the free body. It should also be noted these interior bays may employ bolted connections in which case the bending moment would be essentially zero. Further, the inelastic bending of beams is reasonably well understood (15,16), and it can be accounted for in the design and analysis.

#### Selection of Model Member Sizes

A number of parameters influenced the selection of the scale model member sizes. These obviously included the area of the cross section, moment of inertia, and section modulus. Because of the interest in the inelastic behavior and web and flange buckling, the thickness of the web and flange, width of flange, and depth of section were also important. A further consideration was to make use of standard steel sections and to further restrict the wide flange sections to compact sections. Due to these considerations, the final member sizes have properties which vary considerably away from the desired one-third scale. Because of these variances, the model was first scaled, and then an independent design check of the scale model was made. This check was to assure that the basic design concepts which had been developed for the eccentric system were not violated by approximations in the scaling procedure.

Another variance to be noted in the modeling of the test frame is the top beam of the model which was not designed to conform with the prototype. This member was sized considerably heavier, because of the local boundary condition effects. The first of these local conditions is the absence of the 4th story brace on the test specimen. The missing brace reduces the maximum number of plastic hinge locations in the beam, and so the beam size must be slightly larger. The second local condition is the high axial force which must occur in the eccentric element of the third story of the test frame. The cyclic behavior of beams which yield in shear has been studied and was found to be excellent, but the behavior of beams which are subjected simultaneously to shear and axial forces has not been determined. Because of these two factors, the third floor beam was oversized to avoid any problems. This larger beam size was expected to cause slightly larger deformations in the eccentric elements of the lower two stories, because the eccentric element of the top floor would not yield in shear until the other elements had experienced large amounts of strain hardening. This difference was not expected to be significant.

As is usual with multistory buildings, the story height of the lowest story in the model was higher than for the upper stories. This higher story level resulted in a steeper inclination of the brace angle. This steeper inclination forces earlier yielding in the eccentric beam element associated with the first story brace. In this particular case, the earlier yielding at this location was desirable because it assured the the earliest inelastic action would develop at a well-instrumented location. Figure 50 is a sketch of Test Frame 1 with the principal member sizes shown.

### Additional Design Parameters for Test Frame 1

The columns and beam sizes were identical for both Test Frames 1 and 2. The braces, however, varied. In Test Frame 1, the braces and their connections were designed for axial forces, which were approximately twice the design forces. The brace in an eccentrically braced system can develop increased forces due to strain hardening of the eccentric beam element and a possible lack of uniformity in the yield strength of steel. In this design, it is very important to avoid brace buckling in order to force the eccentric elements to yield in shear. For these reasons, the brace was designed very conservatively.

The spacing of the lateral support points also differed between Test Frames 1 and 2. The lateral support spacing requirements are not explicitly defined in the current design codes. The AISC code [32] specifies that wide flange beams should be supported at plastic hinge locations and at specified intervals depending upon the bending moment. These spacing requirements are based on tests of beams under uniform bending moment and monotonic loading. The eccentrically braced test frames were to be loaded cyclically with a highly variable bending moment across the beam. As a result, the realistic lateral support for this structural system was not clearly defined.

Test Frame 1 was supported conservatively since each beam was supported at six points. The beam-column joints were supported by simulating the support provided by the transverse frames. The brace-beam joint panel zones and two interior points of the central beam segment were also supported. These four interior supports simulate the support provided by the floor slab support joists. These joists are assumed to be spaced at approximately fifth point intervals of the beam which is somewhat closer than the spacing a structural designer would

normally employ. However, this spacing fully satisfies code requirements because all plastic hinge locations are supported. This spacing also supported the central beam segment, because at times this segment develops high compressive forces, and the floor system must provide restraint to prevent weak axis buckling.

The connection details for test frame one are shown in Figs. 51 and 52. The beam-to-column connections were moment-resisting connections. A special feature of this connection detail is the fillet weld between the erection plate and the web of the eccentric beam element. The fillet weld was required because of the very high shear force in the eccentric element. If a bolted connection rather than a welded one had been used, a single row of bolts would not have had sufficient bearing capacity in the web to carry the high shear force. Multi-rows of bolts would be capable of carrying the high shear force, but the extra rows would complicate the connection detail. Additionally, under extreme cyclic loadings, the bolt holes in the web would become progressively larger, due to localized yielding, and the energy dissipation of the structure would be reduced.

The brace-to-beam connection is also shown on Fig. 52. As can be seen in the detail, these were bolted connections. The bolts were designed at working stress levels as friction bolts which were tightened by the Turn of the Nut Method. The capacity of the friction connection was approximately 79 kips, but the connection had a much larger capacity when the bolts were in bearing. The bearing stress of the bolts on the gusset plate and web of the channel was checked against acceptable stress levels, because of the likelihood of slippage in the friction connection.

This figure also shows another feature of the brace-to-beam connection of Test Frame 1. There is an eccentricity between the centroid of the welds of the gusset plate to the beam and the center line of the brace, and this eccentricity induces a bending moment which must be considered in the design of the connection. This eccentricity was the result of two factors. First, the gusset plate had to be of sufficient length to transmit the brace force to the beam. Secondly, the gusset plate could not be allowed to extend into the eccentric zone of the beam. This eccentric zone must be kept clear because it is designed to experience very large cyclic deformations. Since the gusset plate had to be quite long and kept back from the eccentric zone, an eccentricity at the connection was introduced.

Test Frame 1 also employed a number of stiffeners in the connection detail as shown in Figs. 51 and 52. Stiffeners were added to the beam-column joint because of the relatively high component of bending moment transferred by the beam. Stiffeners and a doubler plate were added to the brace-beam joint because of the large component of axial force which the brace transmits to the beam. The brace force applies a shear force to the eccentric beam element and develops an axial force in the central beam. The doubler plate and stiffeners are used to distribute the brace force to the beam. These reinforcing details were felt to be necessary because the gusset plate was much thicker than the web of the beam.

This has been a summary of the more important considerations applied to Test Frame 1. The details are shown in the working drawings of the first frame in Appendix E.

#### Design of Test Frame 2

The basic design of Frame 2 was similar to that of Frame 1. The differences were focused upon specific details of the design, in order



to improve them based on the experience gained from testing the first frame. Figure 53 shows the principal member sizes and details of Frame 2. The basic geometry of the second frame was identical to that of the first frame. However, the brace size in this frame was reduced in order to aid in the determination of the safe limits in the brace design. These braces were designed to develop 1.5 times the design force.

Figure 54 shows the details of the beam-to-column connection. The basic connection is again moment-resisting with a fillet weld between the web of the beam and the erection plate. These details were considered necessary for the satisfactory performance of the system. This connection is the same for both frames. Note that no stiffeners were employed in these beam-to-column connections. The cost of these stiffeners is quite high, and they were left off the second test frame. In comparison with Test Frame 1, the number of stiffeners was also reduced at the brace-to-beam joints of Frame 2. Figure 55 shows the details of this connection. Only a pair of stiffeners was used in this detail, compared to two pairs of stiffeners and a doubler plate used in Frame 1. This was also an attempt to evaluate the need for these costly design details. Since the brace of Frame 2 was somewhat smaller, the need for these stiffeners was reduced. It should be noted that a pair of stiffeners is required for the brace-to-beam connection as called out in Fig. 55. These are very important, and they will always be necessary to assure that the cyclic diagonal tension field can form in the web of the eccentric element.

There were also several other differences in the design of the brace-to-beam connection of Frame 2. The first of these differences is that the brace connection is no longer a purely bolted connection. During

severe cycling, very substantial slippage of the bolted brace connection was noted for the first frame. This slippage will be discussed in greater detail in the next chapter, but in order to prevent slippage in the second frame, a small fillet weld was placed between the flanges of the channels and the gusset plate. This modification in the design of Frame 2 permitted a comparison of behavior between a slipping and fixed brace connection.

Another difference between the frames which can be noted from Fig. 55 is the kind of gusset plate attachment provided for the brace-to-beam connection. Test Frame 1 used the conventional gusset plate arrangement, but the second frame used a welded-on T section for a gusset plate. The T-section offers several advantages. First, the flange weld on the T causes the centroid of the welded connection to move toward the flange thereby nearly coinciding with the thrust line of the force in the brace. Thus, the eccentricity noted on Test Frame 1 is nearly eliminated. Secondly, the flange of the T-section can be aligned with the pair of web stiffeners resulting in a more direct transfer of force between the brace and beam. Therefore, the likelihood of local stress concentration and local instability such as web crippling is reduced. Finally, the T-section is also likely to help provide lateral support to the system because of the rigidity of the connection. This rigidity is helpful to both the brace and the beam, since both members in effect support each other in the out-of-plane direction.

The number of lateral support points was significantly reduced for Frame 2. Lateral support was provided only at four points at each floor level. The panel zone of each beam-to-column connection was supported, and two intermediate points of the beam were also restrained. The intermediate supports were placed at approximately the third points of the beam

span, since this was considered to be a more convenient spacing of floor slab joists by normal structural design standards. However, this spacing was somewhat questionable by code requirements, since support was not provided at all plastic hinge locations, although the two interior support points were of considerable help in preventing weak axis buckling of the central beam segment. In using this placement of lateral support points, it is implicitly assumed that lateral torsional buckling is not a serious problem in the eccentric bracing system. This assumption enters because the only available lateral support against lateral torsional buckling is the indirect support provided by the central beam segment. The very steep moment gradient in the eccentric element justifies this assumption. However, one of the objectives of this test was to determine the validity of this assumption.

In general, Frame 2 was designed less conservatively than the first. The final working drawings of both frames are shown in Appendix E. The results of the tests for these two frames can be compared to determine which of the designs produced better results.

#### Test Setup

The primary purpose of these tests was to perform a detailed investigation into the elastic and inelastic mechanical behavior of the eccentric bracing system. The tests were intended to quasi-statically simulate the cyclic effect of an earthquake rather than to apply a dynamic excitation to the system. This is the same basic procedure used in many other tests of structural systems [15,30,45]. The test facility, which was also used in earlier tests of concrete shear wall subassemblages, is shown in Fig. 56 with a braced frame in testing position. A detailed description of the design and construction of this testing facility is readily available [45,46] so only a brief description of this facility will be made

here. The frame was tested in a horizontal position. It was prestressed at the base to large concrete anchor blocks, which in turn were also prestressed to the test floor of the laboratory. The two load cells at the top of the frame are attached to other anchor blocks and are connected to the loading beam, which distributes the load to the test frame. These load cells apply and maintain a constant total force of 200 kips (890 kN) throughout the test to simulate the gravity load. The variable lateral forces are applied to the test frame by the 460 kip (2047 kN) load cell. The overturning effects of the top 17 stories of the prototype are simulated by a couple, which is also applied by the top two load cells, and the magnitude and direction of this couple are a function of the lateral force. The free body is loaded with an overturning moment of 4.375 kip-ft (5.93 kN-m) for every kip of base shear applied by the lateral load cell. It should be noted that the free body overturning moment is only a small part of the total prototype overturning moment, since this is only a one-third scale model of a single bay of a four-bay prototype structure. The three load cells were all electronically controlled by a MTS 406.11 servo-controller. A more detailed description of the basic system can be found in other references [46].

#### Loading Beam

There were several modifications which had to be made to the test apparatus for these particular tests. The first of these required a loading beam, the placement of which is shown in Fig. 56. The actual member forces of members in the test frame will vary greatly depending upon the loading, yield state and deflection history of the frame. Individual members will attract high proportions of force when they are stiff and much smaller forces when they are less stiff because of yielding. The loading beam makes use of this basic concept. The beam was

designed to remain elastic and relatively undeformable, while exerting no significant effect upon the stiffness of the test subassemblage. The individual elements of the frame should be able to deform and distribute their forces in the same manner as they do in the prototype structure. The presence of the loading beam will have a limited, local effect upon the stiffness of the frame, as the member forces will not be indicative of the prototype behavior in locations near the loading beam. However, these local effects dissipate rapidly, and the behavior in the lowest two stories of the test frame should agree well with the behavior of the prototype.

The design of the loading beam was influenced by several factors. The first was that the beam had to be designed to deliver the total load to the test frame, while the beam remained elastic and did not experience significant deflections. This relatively rigid elastic behavior was necessary to assure that the load cell forces were applied to the test frame members in accordance with their member stiffness and not in accordance with the loading beam stiffness. A second requirement of the loading beam design was that it had to fit within a very limited space. The anchor blocks of the test apparatus could be moved only with very great difficulty. Further, the test frames were designed to approximate a one-third scale model as closely as possible. This left very little space between the test frame and load cells for the beam, so it had to be made from an 8 inch (203 mm) deep wide flange section of high strength steel. A number of stiffeners and reinforcing plates were added to the beam to assure that it remained elastic and did not deflect excessively. The final design requirement also relates to the scale of the test frame.

The load cells, which applied the gravity loads, were 7 ft (2.14 m) on center. It was very important to maintain the 8 ft (2.44 m) column

spacing required by the scale of the test frame, and so the loading beam had to be designed to transfer the loads to these columns. The detailed working drawings for the fabrication of the loading beam are shown in Appendix E.

#### Lateral Support System

The second requirement of the test setup was a positive lateral support system for the beams. The compression flange of wide flange beams must be restrained against out-of-plane motion after it yields in compression to prevent lateral torsional buckling of the beams of the test frame. This lateral support is also needed to restrain the weak axis of the frame to prevent weak axis buckling of the column and central beam segment. The lateral support is very necessary in both the prototype and test frame structures, but it is also important to assure that the support provided to the test frame is consistent with the restraint, which will actually be achieved in the prototype. The compression flange alternates between the top and bottom of the prototype, and so both flanges require some restraint. The prototype lateral support is provided by means of the floor joists, which carry the floor slab. These joists will be of a smaller size than the beam, and they are likely to be bolted into place. As a result, the lateral support of the prototype may permit the beam to deflect and rotate out-of-plane a small amount before resistance is encountered, and then the resistance will not be very large because of the flexibility of the system. The lateral support system for the test frame was designed to satisfy the above general description of the prototype support.

The lateral support system of the test frame also had to be designed to withstand large inelastic deflections, such as a maximum

lateral deflection of  $\pm 6$  in ( $\pm 152$  mm) at the top of frame; and the eccentric element was expected to experience vertical deflections as large as  $\pm 3$  in ( $\pm 76$  mm) at the same time. The test frame support system had to provide continuous support during these large cycles. Finally, the restraint system had to be designed to allow versatility in the placement of the supports, since the two test frames were designed to have different spacings of the support points.

Appendix E shows the design working drawings of the lateral support system, which was designed for the test frame, and Fig. 57 is a photograph of the key components of this system. The basic component of the design is a rail type frame, which is bolted to the laboratory floor, and a sliding arrangement, which encloses the rails, as shown in Fig. 57. Teflon was glued onto all contact surfaces between the rails and slides. Therefore, all friction surfaces were Teflon on Teflon and frictional resistance was essentially eliminated. All of the slides were adjustable so that they could move freely in the plane of the rail. A cruciform was chosen to connect the support system to the beam, since this closely simulates the restraint provided by a floor joist to the beam of the prototype. One of these attachments is shown near the top of a threaded stud in Fig. 57. The cruciform was designed to be tack welded to the test frame, and it was made of light steel plates so that it would be very flexible and could not deliver unrealistic lateral restraint. The threaded studs provided a convenient means of connecting the test frame to the supporting system. The size of the rod was chosen to provide the needed support without being excessively rigid or strong.

The loading beam weighed approximately 2.2 kips (9.8 kN), and this weight had to be supported to prevent damage to the test frame and the test apparatus. Thus, a support system was designed to carry the total

weight of the loading beam and to be adjustable in height. The adjustable height was accomplished by the same threaded rod arrangement used in the lateral support of the test frame. This permitted precise leveling of the loading beam and unrestricted movement and support. All friction surfaces were again coated with Teflon to eliminate friction. A copy of the working drawings of both support frames are shown in Appendix E.

### Instrumentation

The bulk of the data taken during these experiments was read and stored by a high speed data acquisition system. This system can read and record approximately 20000 data points per second and has the capability of monitoring 127 channels, although only 72 were utilized in these tests. With this limited number of channels, the data are recorded virtually instantaneously, and the speed at which the test is conducted has no bearing on the accuracy of the data. A Tektronix console was connected to the data acquisition system for the input of initial data and calibration factors, specification of read points, and for visual monitoring of a limited number of data channels during the test. The system also transfers all data directly to a tape, which can be read, plotted and evaluated on the CDC 6400. This system permitted the reading of a large number of data channels at very close intervals of the test. The resulting data produces a nearly continuous recording of events.

A large number of SR 4 gages were mounted to the structure at locations which were expected to remain elastic throughout the test. These locations were chosen to assure that the bending moments, shear, and axial load of any single member could be accurately determined at any time of the test. There was a high degree of redundancy in these



gage locations, so that cross checks could be made for any malfunctioning gage location. Moreover, these gages were often placed in pairs to check for any out-of-plane buckling or instability. The general philosophy of the placement of the SR 4 gages was to accumulate sufficient data to cover any feasible problem which could occur in the test as well as to give force and bending moment estimates for critical members such as the braces. Figure 58 is a sketch of the test frame which shows the placement locations of SR 4 Strain Gages.

Clip gages were placed in locations where large deformations due to yielding were expected, since clip gages are designed to remain linear throughout a wide range of axial elongation. Several gages were mounted to the flanges at locations where plastic hinges were expected to form, and then the average plastic rotation could be determined [15]. A pair of clip gages was also mounted diagonally on both sides of the web of the eccentric zones as shown in Fig. 59(a). The measurements from them can be combined to estimate the deformation and average shear strain of the eccentric element. The geometry of the deformation of the eccentric element is shown in Fig. 59(b). It is implicitly assumed that the stiffener at the end of the eccentric zone is inclined at the same angle,  $\beta$ , as the face of the column. The shear yield tests of Chapter 3 indicate that this is a reasonable assumption. From the geometry shown in Fig. 59(b) it is apparent that

$$t^2 = u^2 + (v + r)^2 \quad (26)$$

and

$$s^2 = u^2 + (r - v)^2 \quad (27)$$

The eccentric element can be expected to deform severely during the test, and small deflection geometry cannot be expected to hold true throughout the test. Therefore,  $u$ ,  $v$ ,  $s$  and  $t$  must be considered variable. However,  $r$  should remain essentially constant throughout the test, since the beam must deform in an unrealistic manner to significantly change its value. Equations 26 and 27 can be combined to eliminate the variable  $u$  then

$$v = \frac{t^2 - s^2}{4r} \quad (28)$$

The variable  $v$  is a measure of the deformation of the eccentric element, and the angle of average shear strain,  $\gamma_{av}$ , of the eccentric element can be estimated as

$$\gamma_{av} = \tan^{-1} \frac{v}{u} \quad (29)$$

The vertical deflection,  $y$ , of the eccentric element can be determined from  $v$  by noting that the rotation angle  $\beta$  will be quite small and applying small angle geometry

$$y = v - u\beta \quad (30)$$

The placement locations of the clip gages are shown in Fig. 60.

A number of linear potentiometers were also used to measure the deflections of specific points of the frame. The linear potentiometers are capable of measuring deflections of up to  $\pm 6$  in ( $\pm 152$  mm). These gages were placed at locations where direct measurements of deflection or elongation were most useful. The first three potentiometers were placed at the three story levels to measure the lateral deflection of each level. Two others were used to measure the vertical movement of the top of each column. The vertical movements of the eccentric nodes on the bottom story were also measured by a pair of such potentiometers. The average reading of a pair of linear potentiometers was also used to

record the elongation and slippage of individual braces for the first test specimen. Figure 61 is a sketch showing the placement of these linear potentiometers.

In addition to the instrumentation shown in Figs. 58, 60 and 61, the three load cells shown in Figure 56 also transmitted an electronic signal which indicated the magnitude of forces acting on the test frame at a given time. The electronic signals provided by the strain gages, clip gages, linear potentiometers and load cells were all received and measured by the high speed data acquisition system. The data system then interpreted the voltage and current measurements by prescribed calibration factors, and recorded the interpreted data. The timing of the data acquisition was manually controlled, and data were collected at very close intervals to assure accurate plotting and interpretation.

In addition to the data recorded by the high speed data acquisition system, data were taken by other means during the test. The Tektronix console, which was directly connected to the data acquisition system was used to monitor the measurements taken on a limited number of channels. The channels of interest were primarily the linear potentiometers and load cells. These data were used solely for the control of the test. Three Esterline X-Y-Y' Recorders were used during the test to continuously record selected data. These data were recorded as force-deflection plots. The recorded force was always the lateral force on the test frame, and was plotted against the lateral deflections of all three story levels and the vertical deflections of the two eccentric nodes of the bottom story.

A number of manual and photographic measurements were taken during these tests. Several dial gages were mounted to the base plate to measure

any movement of the test frame relative to the anchor blocks. These gages were manually read at various intervals. A 16 mm motion picture camera was also used during this test to record some of the observable inelastic behavior. The test frames were whitewashed to make the yielding of the steel observable. The test frame was under continued observation during the test, and a number of still photographs were also taken during the test. A photogrammetric grid was placed on the web of the beams, columns and braces of the eccentric zones of the lowest story as shown in Fig. 61. Photographs were taken on glass plates at critical points of the test. This is the same photogrammetric procedure as was used in the test of the beam specimens, the purpose of which was to evaluate further the local effects within the severely deformed eccentric element.

#### Loading Program

The two frames were tested under the same basic load program. The cycles covered both elastic and inelastic behavior, with the elastic cycles under force control and the inelastic cycles under displacement control. Figure 62 shows the basic load program for the inelastic behavior portion of the test. The load point numbers which were assigned are shown in this figure. This cyclic deflection history was applied at the third story level. The load program was chosen as a simulation of predicted maximum dynamic response predicted for the 1.5 times El Centro and unreduced Pacoima Dam acceleration records. The first 9 cycles are symmetric displacement cycles with increasing magnitudes of displacement of .5, 1.0 and 1.5 inches (12, 25 and 27 mm). The nine cycles are an idealization to the one-third scale of the dynamic response of the prototype structure computed for the 1.5 times El Centro excitation. However, this is an extreme idealization, since the dynamic analysis does not indicate that the structure would experience so many severe inelastic

cycles. The next cycles are an idealization of the one-third scale of the severe inelastic response predicted for the prototype structure during the Pacoima Dam excitation. The first 13 cycles were primarily intended to evaluate the actual behavior of the structure as compared to the performance predicted for the given excitation. It was thought that these cycles formed a very severe test of the structure, but additional cycles were applied to obtain more information on the behavior of the system and to examine its failure and partial collapse. Hence, the remaining cycles were applied at the full displacement capacity of the test apparatus.

The load program in Fig. 62 includes only the inelastic cycles which were applied to the test frame, but the frame was also subjected to three separate sets of elastic cycles. The elastic cycles were force controlled, and Fig. 63 is a plot of the typical elastic cyclic loading. The magnitudes of the cyclic lateral forces are low and the frame remains elastic during the cycles. The first set of the elastic cycles was applied at the start of the test before any yielding had occurred. The second set of cycles was applied after the three 1.5 in (38 mm) cycles. This set of elastic cycles was thought to represent the elastic condition of the structure after experiencing the 1.5 times El Centro acceleration. The third set of elastic cycles was performed after the 3.0 or the 4.5 inch (76 or 114 mm) cycles. This set of elastic cycles was felt to be indicative of the condition of the structure after an extremely severe earthquake.

The test program of elastic cycles was applied to the structure for several reasons. These cycles give a measure of the elastic stiffness of the frame. This information can be very useful in showing any degradation of stiffness that may occur in the structure. The effect of a partial structural failure on the elastic properties of the frame could also be

determined with these cycles. Further, the elastic cycles were expected to provide information on the accuracy of the tests. For example the frictional force exerted by the lateral support system could be determined by these elastic cycles. Figure 64 shows a graphical representation of how this frictional force can be estimated from the elastic hysteretic curves. Information of this type was valuable at intervals throughout the test, since it gives an indication of how well the test frame and the test equipment are performing.

#### Total Lateral Load on the Test Frame

In the description of the test setup, it was noted that the lateral load on the test specimen was applied by a single load cell as shown in Fig. 56. At very small lateral deflections, this load cell provides the total lateral force on the test frame, but at larger deflections the two gravity load simulators contribute a component to the lateral force. The basis of this contribution is shown in Fig. 65. The one end of the gravity load cells are fixed against translation, but the other end translates with the loading beam and the top of the test frame. As a result, the load cells are not quite perpendicular to the loading beam at large lateral deflections. The average length between the rotation points of the load cells is 83 in (2.11 m). This length will vary slightly during the test, but the variation is too small to be significant in these calculations. Therefore, the angular change,  $\psi$ , produced by this deflection is defined by

$$\tan \psi = \frac{\Delta_3}{83} \quad (31)$$

where  $\Delta_3$  is the 3rd story deflection. Since  $\psi$  is always small,  $\cos \psi$  is essentially equal to 1.0, and the net gravity load is always 200 kips

(890 kN), as was discussed earlier. The lateral load, however, must be corrected. The correction,  $\Delta P$ , is

$$\Delta P = 200 \sin \psi \approx 200 \frac{\Delta_3}{83} \quad (32)$$

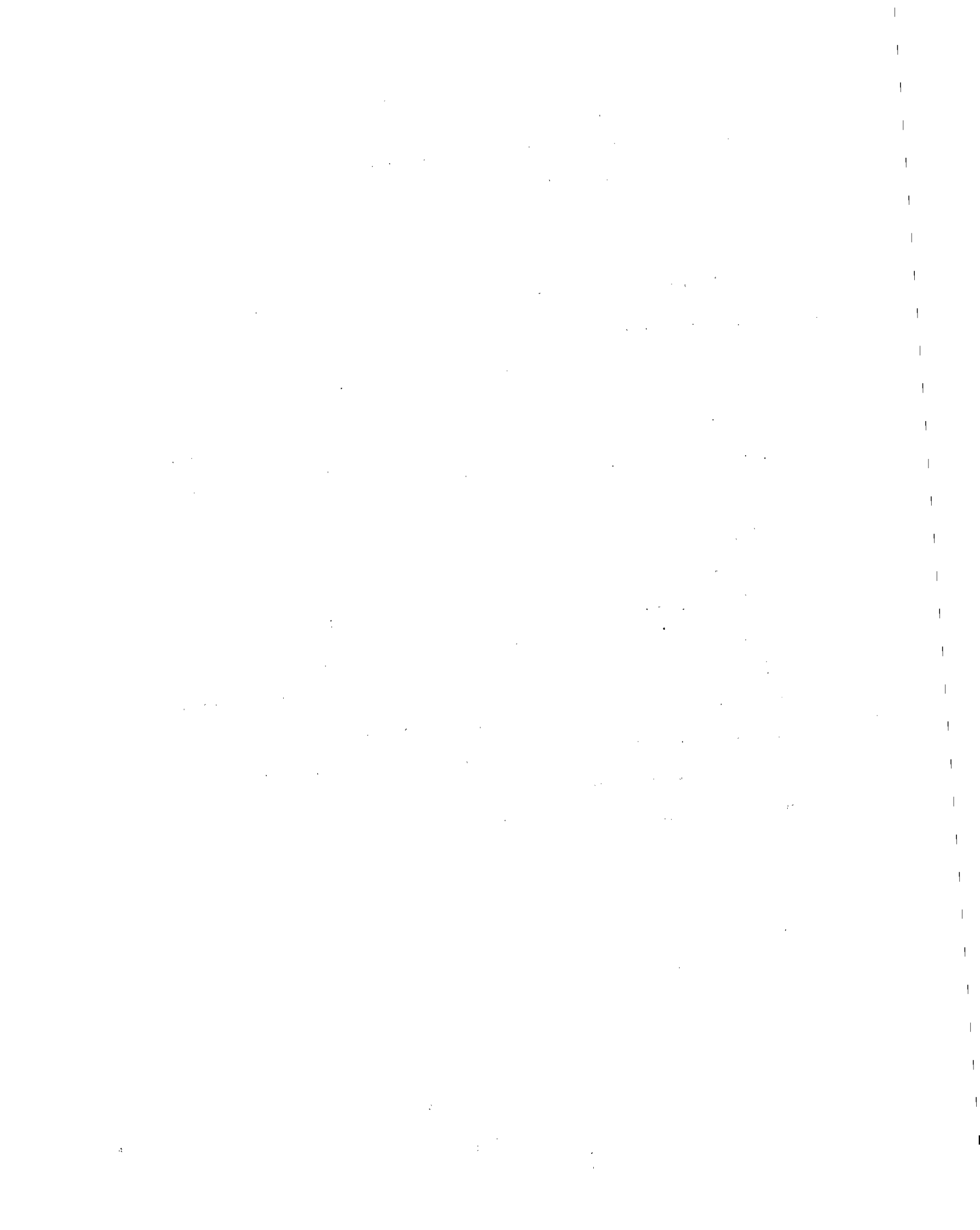
At a lateral deflection of 6 in,  $\Delta P$  is 14.45 kips (64.3 kN), which is very significant. The total corrected lateral force,  $P_T$ , is

$$P_T = P + \Delta P \quad (33)$$

where  $P$  is the load applied by the lateral load cell. All the lateral forces which are presented in this report, are corrected for lateral deflection

#### Summary

The test frames are very complex systems, which are intended to simulate the behavior of a small part of a large structure. Much of the design of the test apparatus centered about the simulation of the total structural behavior. The loading program was intended to produce the maximum amount of useful data, while attempting to simulate a realistic force and deflection history for this small part of the total structure. The instrumentation was applied very liberally, so that maximum information could be obtained from these tests.





## CHAPTER 6. BRACED FRAME TEST RESULTS, EVALUATION AND COMPARISON TO INELASTIC ANALYTICAL MODEL

### General

This chapter contains a discussion of the tests of the two eccentrically braced frames and an evaluation of the results. Comparisons will be made to evaluate the relative performance of the two test frames to aid in determining the best design procedures. The inelastic analytical model, which was discussed in previous chapters, will be compared to the test results.

Reduced copies of the working drawings of the one-third scale models are shown in Appendix E. The two scale model braced frame subassemblages and the loading beam were fabricated at the machine shop of the University of California Richmond Field Station. The lateral support system was fabricated by the University of California Department of Civil Engineering Machine Shop. Tensile coupon tests were taken from the web and flange of each of the main member sizes used in these test frames. The results of these tests and residual stress test results are shown in Appendix B.

### Results for Test Frame 1

Test Frame 1 was tested in the horizontal position with the testing apparatus discussed in the previous chapter. Figure 66 is a photograph of the test frame and the testing facility just prior to testing. The testing began with several cycles of elastic loading as shown in Figure 63. After completion of these elastic cycles, the inelastic displacement controlled loading program shown in Figure 62 was begun. As can be seen from this figure, the frame was first cycled through three cycles of  $\pm .5$  in ( $\pm 12.7$  mm) and then three cycles of  $\pm 1$  in ( $\pm 25.4$  mm) third floor deflection. During the  $\pm 1$  in ( $\pm 12.7$  mm) displacement cycles,

brace bolt slippage was noted. For this reason, a second set of elastic cycles was run to determine the effects of this slippage on the stiffness of the frame. After this, the inelastic displacement was again begun with three cycles of  $\pm 1.5$  in ( $\pm 38$  mm) third floor deflection. One-sided deflections began at 3 in (76 mm). Frame stiffness was then tested with a third set of elastic cycles. Testing proceeded with a 4.5 in (114 mm) one-sided deflection. Eventually, maximum cyclic loading deflection of  $\pm 6$  in ( $\pm 152$  mm) was applied to test the failure mechanism of the frame. Each of these loadings and their effect on the test frame will be discussed.

The initial elastic hysteresis loops shown in Fig. 67 indicate that the lateral support system was not exerting much friction on the test frame. The procedure shown in Figure 64 indicates that the static friction force was approximately 1 kip (4.5 kN). This was less than 1% of the ultimate strength of the test frame, and so, it was neglected. The stiffness of the structure with respect to the prescribed loading and the third floor deflection was 174 kips/in (30.5 kN/mm) during these initial elastic cycles.

The inelastic displacement controlled loading program was then begun. The first three cycles were taken between  $\pm 0.5$  in ( $\pm 12.7$  mm) third floor deflection. The initial shear yielding was expected to occur in the first floor south eccentric element (see Fig. 56) due to the steeper inclination of the first floor brace. The test frame did begin yielding at a deflection of approximately 0.25 in (6.4 mm). Since the first yielding started at this deflection level, the first three cycles can be regarded as a ductility factor of approximately two with respect to first yielding. Figure 68 is a plot of lateral force-third

floor deflection hysteresis loops for these inelastic test cycles. The first three cycles of this figure are completely repetitive with no pinching of the hysteresis loops nor any deterioration in strength or stiffness. The linear elastic portion of these early cycles grew slightly larger with each of these cycles. This growth is indicative of isotropic hardening of the eccentric elements during the early yielding. This growth in yield surface is verified by the fact that the lateral force required to induce a 0.5 in (12.7 mm) deflection increased from 65.8 to 68.6 to 70.3 kips (293 kN, 305 kN, 313 kN) during these three cycles.

The next three cycles were between  $\pm 1$  in ( $\pm 25.4$  mm). During the first one inch cycle, a noise was heard at a load of 78 kips (347 kN). Examination of the test specimen and data indicated that the noise was associated with brace bolt slippage. The test specimen was then cycled through the two additional one inch cycles, and increased slippage of the bolts occurred shortly after each load reversal. The noise increased in duration with each reversal, and the noise and slippage started at a lower load with each reversal. At the end of these one inch cycles, the slippage was starting at a lateral force of approximately 25 kips (111 kN). This slippage did not have any apparent effect upon the hysteretic curves at this time (see Figure 68). The strength of the frame continued to increase due to strain hardening during these cycles. The force required to achieve a 1.0 in (25.4 mm) lateral deflection increased from 85.6 kips to 91.4 kips to 92.9 (381 kN, 407 kN, and 413 kN). Considerable yielding was occurring in the web of the eccentric beam elements of the bottom two stories as evidenced by cracking and flaking of the whitewash.

The plot of the second set of elastic cycles is shown in Figure 69. The effect of the bolt slippage is very apparent in these hysteresis

curves. The stiffness of the frame is essentially the same as the stiffness of Figure 67, when the brace is in full bearing, but the average stiffness is reduced by 11% due to the brace slippage.

The test frame was then cycled for 3 cycles between  $\pm 1.5$  in ( $\pm 38$  mm) and two additional cycles of one-sided deflection where the maximum third floor deflection was 3 in (76 mm) and the minimum deflection was zero. The brace slippage continued to grow more severe during these cycles, and a very small, but distinct, pinching effect was noted in the hysteretic loops for these later cycles. Several of these very small pinched zones are circled in Figure 68. At the end of the 3 in (76 mm) cycles, this slippage was starting as a reversed load of approximately 5 to 10 kips (22.5 - 44.5 kN). The strength of the frame continued to increase during the early part of these five cycles, but it stabilized and showed a very slight decrease in the later cycles. The force required to attain a 1.5 in (38 mm) deflection increased from 99.9 kips to 103.8 kips and 104.3 kips (444 kN, 462 kN, and 464 kN) during the three 1.5 in (38 mm) cycles, but the deflection required to attain a 3 in (76 mm) deflection decreased from 113.5 kips to 112 kips during the 3 inch cycles. This observation indicates that the early cycles are strongly influenced by isotropic strain hardening while the later cycles are predominantly influenced by kinematic hardening. Web buckling in the yielded web of the eccentric beam elements was visible during all of these cycles. However, this buckling did not have a detrimental influence upon the test results, since the cyclic diagonal tension field formed.

The plot of the hysteretic loops of the third series of elastic load cycles is shown in Fig. 70. The average stiffness was 125 kips/in (21.9 kN/mm). This represents a 29% reduction in the average stiffness.

This average stiffness has deteriorated significantly since the last series of elastic cycles after LP12. However, even at this point, the stiffness when the brace and bolt are in bearing is essentially the same as at the start of the test. Figure 70 also indicates that the lateral support system continued to perform well, since the static friction force is still on the order of 1 kip (4.5 kN) despite the large deflections which the frame has experienced.

The test frame was then cycled through two cycles of one-sided deflection with a 4.5 in (114 mm) maximum at the third story level. These two cycles again exhibited repetitive hysteretic behavior. The slippage of the brace was very evident during these cycles, and the hysteretic loops exhibited slight pinching. However, the overall behavior of Test Frame 1 was satisfactory up to LP26. The strength of the frame remained essentially stable during these two cycles with only a very slight deterioration in strength. The force required to induce a 4.5 in (114 mm) deflection decreased from 117.3 kips to 114 kips (522 kN and 507 kN). This further amplifies the significance of kinematic strain hardening during these later cycles. The web buckles also became visibly more severe during these cycles. It should be recalled that the 13 inelastic cycles through LP26 were intended to simulate the behavior of the test frame under sequential 1.5 times El Centro and unreduced Pacoima Dam earthquakes.

The full displacement capacity of the test apparatus,  $\pm 6$  in ( $\pm 152$  mm), was then applied to the specimen to gain insight into the ultimate failure mechanism of the structure. The test frame was first cycled to a maximum deflection of 6 in (152 mm) at LP27, and the frame exhibited no deterioration in strength (see Fig. 68). However, the beam of the first floor south eccentric element (see Figure 56) began

to show signs of imminent failure after reversal from LP27. These signs consisted of the development of shiny slip lines of metal, which began to tear as the displacement was reversed. The tearing of this web began to appear as the deflection reached 1 in (25.4 mm), and it grew worse as the deflection decreased to -5.12 (-130 mm) at LP28. The tear progressed diagonally across the web as shown in the photograph (see Fig. 71). The strength of the frame decreased from -104 kips (-463 kN) at a 2 in (51 mm) deflection to -89 kips (-396 kN) at LP28. This is a relatively small drop, and it indicates that the failure of an individual eccentric element does not mean the total collapse of a frame. However, the plastic deformation progressed more rapidly in the other eccentric elements after the first element started to tear. The south element of the second floor (see Fig. 56) started to tear at a deflection of -2.5 in (-64 mm) after reversal from LP28. This element also tore diagonally across the web. The lateral strength was approximately 81 kips (360 kN) at LP29 after the first two eccentric elements failed. The north eccentric element of the second floor (see Fig. 56) began to exhibit a severe accumulation of plastic deformation at LP29, but this element did not appear to be in danger of immediate failure. The test was stopped at LP29. The specimen was carrying the full 200 kips (890 kN) gravity load, the overturning moment of the upper stories and a lateral load of 81 kips (360 kN) at LP29. This indicates that the test frame retained a very significant proportion of its initial strength despite the failure of two of the eccentric elements. Figure 72 is a photograph of the test frame after completion of the test.

The energy dissipation was relatively uniformly distributed among the eccentric elements of the frame. Figures 73 and 74 are the lateral

force-deflection hysteretic plots for the first and second floor. The areas enclosed within these hysteresis loops together with Fig. 68 are a measure of the cyclic energy dissipation at the various story levels. Comparison of these figures indicate that there is a relatively uniform distribution of energy dissipation within the test frame. At moderate plastic strain levels, approximately 40% of the energy was dissipated within each of the first two stories, and 20% was dissipated within the top story level. The top level dissipated less energy, because the beam at that level was oversize, and this top story was not designed to correctly reflect the behavior of the prototype. The lower stories were sized to simulate prototype behavior, and the energy was dissipated very uniformly within these story levels. This uniform energy dissipation is a very desirable feature, as it indicates that the eccentric beam elements are deforming plastically; and no one element is excessively strained. Figures 73 and 74 also display the very stable and repetitive hysteretic behavior of this eccentrically braced frame.

#### Evaluation of Test Frame 1

The performance of Test Frame 1 was basically very good. It survived cyclic deflections in excess of those predicted for a 1.5 times El Centro base excitation ( $\pm 1.0$  to  $\pm 1.5$  in) with no structural failure and only a modest loss in average stiffness. It is possible that this stiffness could be significant since it implies that the structure will deflect more under lateral load. However, this stiffness loss could be corrected by welding the brace connection to prevent slipping since this test indicates that the loss in stiffness is essentially zero when the brace slippage is prevented. The test frame also withstood cyclic deflections in excess of those predicted for a Pacoima base excitation (up to LP26) without any structural failure. The stiffness

loss was somewhat greater during these larger cycles, but the frame could still be repaired. Several eccentric elements tore during the extreme  $\pm 6$  in ( $\pm 152$  mm) cycles. Nevertheless, the frame retained much of its strength and continued to exhibit ductile behavior. The test was stopped at LP29 where the lateral deflection was 6 in (152 mm). The frame continued to carry the full 200 kip (890 kN) gravity load and an 81 kip (360 kN) lateral load at the conclusion of the test despite the two torn eccentric elements. Thus, this test frame withstood cyclic deflections well beyond those predicted for the 1.5 times El Centro and Pacoima excitations.

Brace slippage was an important factor in the behavior of this test frame. This slippage was measured during the test, and so, its effect can be determined. Since the slippage of the brace is equivalent to an elongation or shortening of the brace, the lateral deflection due to slippage can be computed using the technique [44] discussed in Chapter 4 and shown in Fig. 44. This computation was made for the three floor deflections, and the modified hysteresis curves are plotted in Figs. 75, 76, and 77. These figures indicate that the removal of the deflection caused by brace slip eliminated the small pinching effect, which was noted earlier. Figure 78 is a plot of the modified hysteresis loops for the elastic cycles made after LP22. A comparison of these four figures indicates that the deterioration was caused by brace slippage. They also indicate that the effect of slippage does become more severe for the larger inelastic cycles. The hysteretic loops prior to LP18 are essentially unchanged by the slip correction, but the correction becomes as large as 0.5 in (12.7 mm) for the later cycles. Figure 79 is a plot of the axial force versus the brace slippage plus elongation for the



first floor brace. The area enclosed within these hysteresis loops is the energy dissipation by slippage of the first floor brace. This enclosed area is very small. Further, the loops are extremely pinched, and they deteriorate badly. As a result, the energy dissipation mechanism provided by the brace slippage is very poor. However, the brace and bolted connections were conservatively designed. Thus, the pinching effect due to brace slippage was negligibly small compared to the great dissipation provided by the eccentric beam element.

The test specimen was studied to determine the cause of this deterioration with the bolted brace connections. The nuts were removed from several of the bolts in the first story brace after completion of the test, and it was found that some of the bolt holes had elongated approximately 0.1 in (2.5 mm) to one side. This examination indicates why the slippage dissipation deteriorated. During very early cycles the bolted connection did not slip, because the bolts were tightened down to provide a friction type connection. It should be noted that the first bolt slippage occurred at an axial force of approximately 70 kips. This is somewhat less than the 79.5 kips predicted by the AISC allowable friction connection forces. However, the bolted connection was also designed with the bolts in bearing contact. The ultimate bearing capacity of this connection was approximately 135 kips (599 kN). At slightly larger cyclic inelastic deflections, the frictional resistance of the connection was overcome and the bolts slipped into bearing contact. This slippage continued during a number of cycles, and the friction surfaces became polished. This polishing reduced the frictional coefficient, and the slippage started at a lower reversal load on each succeeding cycle. At the same time, very localized yielding began to

occur due to bearing contact of the bolts in the bolt holes, and so slippage became more severe with each cycle, because the bolt holes grew larger. This local yielding occurred at very low stress levels. The maximum bearing stress was 37 ksi ( $255 \text{ MN/m}^2$ ). This bearing stress is well below the actual yield stress of the brace (42.5 ksi), and it indicates that the bolted connections must be designed very conservatively with respect to bearing stress under cyclic loading to control this localized yielding. If these connections are not designed conservatively, the brace slippage will become more severe, and the structure will eventually suffer severely pinched hysteresis loops which will produce larger deflections.

Figure 80 is a photograph of a typical yielded eccentric element. Note that the eccentric element exhibits complete yielding of the web, but virtually no yielding occurs outside the eccentric zone. This indicates that the bulk of the energy was dissipated by the inelastic strain in the eccentric elements. These eccentric elements behaved like the shear yielding beam elements discussed in Chapter 3. That is, these elements had a photogrammetric grid with very sharp parallelograms in the center of the eccentric element, and less sharply defined shear strain at the edges of the eccentric element because of the warping restraint. Web buckling also accompanied the shear yielding, becoming particularly severe during the cycles between LP18 and LP26. The web buckling did not adversely affect the force-deflection hysteresis loops, because the expected cyclic diagonal tension field formed. This field formed and reformed under cyclic loading without causing any pinching of the hysteresis loops or deterioration in strength. However, the diagonal tension field also restraightened the web on the next half cycle after the web had buckled. This precipitated a failure mechanism where a

tear progressed diagonally across the web through the area which had buckled and restraightened a large number of times. The eccentric node, which is the connection joint of the brace and the beam, experienced very large vertical movements due to the inelastic deformation of the eccentric elements. The test frame was designed so that the early deflections were more severe in the south eccentric element of the first floor. Figure 81 is a plot of the vertical deflection of the eccentric node of this element for the various lateral load levels. This plot is not a hysteretic plot in the full sense, since the area enclosed within the loops has no particular meaning, but this figure indicates that the large inelastic deflections of the eccentric element exhibit very stable, repetitive behavior. The maximum deflection was approximately 2.2 in (56 mm) prior to the element failure. The deflection became more severe after failure of the element. This is a very severe deflection level, since the eccentric element is only 12.5 in (318 mm) long. Figure 82 is the corresponding plot for the north eccentric element. The behavior of this element is similar to that seen for the south element in Fig. 81. The north element experienced some erratic behavior after the south element failed which was caused by the redistribution of forces after failure of the south element.

Figure 83 indicates how the inelastic deflections of the frame are attained. This plot subdivides the deflection into the three components described in Fig. 44 and the component due to slip of the brace connection. This plot clearly indicates that virtually all of the inelastic deflection of the frame is caused by the inelastic deflections of the eccentric element. It also indicates that the component of deflection due to brace slip increases for later cycles at larger deflections, while the component due to elastic elongation of the brace is virtually

constant. The component due to elongation and shortening of the columns increases very slightly in later cycles, because of inelastic shortening in the plastic hinges at the base of the columns. The lateral slippage of the base of the structure was monitored during the test, and it was found that this effect was negligible, since the deflections were always less than 0.001 in (.025 mm).

A very small percentage of the energy dissipation was caused by the formation of a plastic hinge at the base of the columns. The base of the columns were fixed against rotation, and so this point of the column attracted very large bending moments. Therefore, column yielding had to occur before the frame could attain really large deflections. Flange buckles formed in this yielded zone, after the flanges yield. These buckles were first noted at the 3 in (76 mm) deflection. The buckles became progressively more severe during the last cycles of the test. Figure 84 is a photograph of these buckles at the end of the test. The flange buckling did not adversely affect the test, because the plastic rotations at this location were quite small. This flange buckling and the previously noted web buckling of the eccentric beam elements are the only buckling phenomena observed in this test frame.

The results of Test 1 can be summarized by saying that the test frame performed very well. It dissipated large amounts of energy without any significant pinching of the hysteresis loops. The bolted braces did exhibit some undesirable slippage but these effects were severely limited by the conservative design of the bolted connections. The lateral support system performed very well. The results of this test indicate that a well-designed and constructed eccentrically braced frame is able to withstand very severe lateral deflections.

## Test Frame 2

The second test frame was of a less conservative design than the first. The braces were lighter and the lateral support was provided only at the third points of the beams. The number of stiffeners and doubler plates was also reduced. Because of the brace slippage which occurred in the first frame, the brace connections were welded to prevent slippage. These design changes were made to better evaluate the design alternatives for the eccentric bracing system.

The load program and instrumentation were essentially identical to those of Frame 1 except that the elastic cycles were run after  $\pm 1.5$  in ( $\pm 38$  mm) and 4.5 in (114 mm) cycles. The testing began with the elastic load program shown in Figure 63. The lateral force-third floor deflection hysteretic curves for these elastic cycles are shown in Fig. 85. The elastic stiffness of the test frame with respect to the lateral loading and third floor deflection was 164 kips/in (28.7 kN/mm). This stiffness was 6% less than the stiffness of Test Frame 1 because the braces were lighter. Figure 85 again indicates that the frictional force exerted by the lateral support system on the test frame was negligible. The maximum static friction force was 1 kip, and this is less than 1% of the ultimate strength of the test frame.

After completion of the initial elastic cycles, the inelastic displacement controlled loading program shown in Fig. 62 was started. The hysteretic behavior of the lateral load versus the third floor deflection for these inelastic cycles is shown in Fig. 86. The first nine cycles at  $\pm 0.5$  ( $\pm 12.5$  mm),  $\pm 1.0$  ( $\pm 25.4$ ) and  $\pm 1.5$  in ( $\pm 38$  mm) exhibited very repetitive behavior with no pinching of the hysteresis loops, and no deterioration of strength or stiffness (see Fig. 86). The behavior of Test Frame 2 was similar to that of Test Frame 1 during these cycles,

except that the elastic stiffness was 6% greater in the first frame because of the larger braces. Brace slippage was prevented for Frame 2 by both welding and bolting the braces to the gusset plate. The strength of the frame increased steadily during these nine cycles because of the strain hardening in the plastic eccentric elements. The strain hardening in these early cycles was predominantly isotropic hardening. These facts are verified by observing that the force required to induce a 0.5 in (12.7 mm) deflection increased from 64.4 kips to 65.8 kips and 67.3 kips (287 kN, 293 kN, and 299 kN) during the first three cycles. During the 1.5 in (38.1 mm) cycles the strength increased from 99.9 kips to 104.8 kips to 105.5 kips (444 kN, 466 kN, and 469 kN). The whitewash on the web of the eccentric beam elements began to flake during the one inch cycles. This indicates that significant yielding was occurring in the web at this time. Visible web buckling began to occur in the plastic web during the 1.5 inch cycles. However, as can be seen in Fig. 86, this buckling did not have an adverse effect on the strength of the frame.

LP18 marked the end of the first nine inelastic cycles, and a series of elastic cycles were then performed. The hysteretic behavior for these elastic cycles was essentially identical to that shown in Fig. 85. The average elastic stiffness was 158 kips/in (28.0 kN/mm), and the maximum static friction within the test apparatus was less than one kip.

Two cycles of one-sided deflection with a 3.0 in (76 mm) maximum third floor deflection were then run. These cycles also exhibited very good energy dissipation, but the braces began to show severe lateral torsional buckling during these cycles. The brace attracted substantial bending moments because of the welded connections, and so plastic hinges formed in the brace at the base of the structure. Lateral torsional

buckling began to appear during the first 3 in (76 mm) cycle because of the yielded brace. Figure 87 is a photograph of this brace in its ultimate buckled condition. Lateral torsional buckling also occurred in the third story brace because of the high bending moments induced by the heavy third floor beam. However, the local buckling of the third floor brace lagged behind the buckling in the first floor brace. These buckles became steadily worse during the cyclic loading, but they had no apparent effect on any of the hysteresis loops of any of the cycles up to LP22. The behavior during the 3 in (76 mm) cycles showed very little influence due to isotropic hardening and considerable influence due to kinematic hardening. The force required to induce a 3 in (76.2 mm) deflection increased slightly from 107 kips to 110 kips (476 kN to 490 kN) during the 3 inch cycles.

The test frame was then cycled through two 4.5 in (114 mm) one-sided deflections. During these two cycles, the lateral torsional buckles continued to increase. The strength of the frame exhibited moderate deterioration at the end of these cycles since the strength decreased from -109.5 kips to -94.6 kips (-487 kN to -421 kN) when the frame was at zero deflection. However, the hysteretic curves were basically very repetitive. The first web failure occurred in the south eccentric element (see Fig. 56) in the first floor after reversal from LP26. The tear progressed diagonally across the web because of the severe working which it experienced during cyclic buckling and diagonal tension formation. Figure 88 is a photograph of the torn element. The tear was very similar to the initial web tear in Frame 1, except that it occurred one-half cycle sooner.

Another series of elastic cycles was applied to the structure after the web tear. The lateral force-deflection hysteresis loops for these

cycles are shown in Fig. 89. The lateral stiffness indicated by this figure is 134 kip/in (23.5 kN/mm), which is only an 18% reduction from the original elastic stiffness. This is a very important fact, because it emphasizes that the deactivation of one of the eccentric beam elements does not necessarily indicate that the structure will totally collapse. It appears that a number of these eccentric elements must fail before the structure can collapse. The static friction force can also be seen from Fig. 89, and it has remained less than one kip.

The remainder of the load cycles were applied at the maximum deflection capacity of the test apparatus,  $\pm 6$  in ( $\pm 152$  mm). The frame was first deflected to 6 in (152 mm) at LP27. During this half cycle, the maximum lateral strength of the frame was 104 kips (463 kN) which was approximately a 10% reduction in strength from previous cycles. The reduction was primarily caused by the first web tear. The displacement was reversed to LP28 with no adverse effects, but on reversal from LP28 the south eccentric element of the second floor also tore. The strength steadily decreased, while the tear was progressing, to a load of 78 kips (247 kN) at LP29. The third floor deflection was then reversed to -5.46 in (-139 mm) at LP30. The lateral torsional buckling of the third story brace became steadily more severe during each of these cycles. The lateral torsional buckling of the first story brace did not deteriorate much beyond LP26, because it did not carry a very large force after the first eccentric element failed. The displacement was reversed to 6 in (152 mm) at LP31, but the third story brace buckled around its weak axis when the deflection reached 4 in (101 mm). The strength of the frame dropped from 65 kips (289 kN) to 54 kips (240 kN) when the brace buckled in its weak axis. The deflection was continued to 6 in (152 mm) at



LP31, and the test was stopped. The test frame was supporting 57 kips (254 kN) lateral load, 200 kips gravity load, and the overturning moment of the upper 17 stories at the conclusion of the test. It should be noted that the loading beam was designed to have a minimal effect upon the test. However, it is very possible that after the frame had lost significant strength this beam did affect the results of the last cycles. The presence of this rigid loading beam at the top of the structure probably helped the test frame maintain its lateral strength and stiffness after the eccentric elements had failed.

Figure 90 is a photograph of the buckled third story brace. The earliest buckling that occurred in this brace was lateral torsional buckling. This local buckling was first observed during the 3 in (76.2 mm) cycles, and it became more severe with each succeeding cycle. The centroid of the brace section deflected out of the plane of the weak axis because of the severe twisting induced by the lateral torsional buckling. This deflection caused considerable weak axis bending within the brace, which then buckled in a column buckling mode just before LP31. The column type buckling, which is seen in Fig. 90 was caused by large twists induced by the lateral deflections of the compressive flange.

Figures 91 and 92 are lateral force-deflection hysteretic curves for the first and second floor deflections. These figures again show that the hysteresis loops of the eccentric bracing system are very stable and repetitive. This frame has the same good distribution of energy noted for Test 1. That is, the two lower stories each dissipate 40% of the energy and the top story dissipates only 20%. This favorable distribution of energy dissipation indicates that all of the eccentric elements are deforming plastically without causing any one element to deform excessively.

The bulk of the dissipated energy in Test 2 was provided by the eccentric elements. The eccentric elements of Test Frame 2 behaved similarly to eccentric elements of Frame 1 and the shear yield beams described in Chapter 3. They displayed considerable shear yielding of the web, with warping restraint at the interfaces. Web buckles formed, but they did not adversely affect the hysteresis loops, because the cyclic diagonal tension field formed. However, the large inelastic shear deformation again resulted in very significant vertical deflections of the eccentric nodes. Figures 93 and 94 are plots of this vertical deflection as a function of the lateral loads for the north and south eccentric elements of the first floor. These plots amplify the very stable and repetitive characteristics of the inelastic behavior of this eccentrically braced frame. However, the maximum floor deflections are very large, which indicates considerable damage to the floor system. The plots in Figs. 93 and 94 are similar to the curves obtained for Test 1 and shown in Figs. 81 and 82. The only significant difference is that the south eccentric element of Frame 2 experienced slightly larger inelastic deflections than the same element of Frame 1, during the inelastic cycles between LP12 and LP26. Figure 95 is a photograph of Test Frame 2 after completion of the test, which illustrates the many similarities in deflected shape, failure mechanism, and severity of plastic deformations between Frames 1 and 2.

Test Frame 2 experienced its first web tear earlier in the inelastic loading program than Test Frame 1 and the data were examined to determine why this occurred. It was found that the south eccentric element (see Fig. 56) of the first floor had a more severe strain history in Test 2 than in Test 1. This occurred because the loading cycles were displacement controlled and the brace could not slip in Test 2. The more severe strain

history resulted in larger deflections of the south eccentric element of Frame 2. This can be seen by comparing the curves shown in Figs. 81 and 93. These deflections are only slightly larger for each cycle of Fig. 93, but over the total number of cycles this slight difference accumulates into a considerably more severe strain history. If these accumulated strain histories are considered, it is apparent that the eccentric elements fail at approximately the same accumulated strain level.

One of the lateral support points failed in Frame 2 just prior to LP31, when the brace buckled. The cruciform plate tore away from the beam, because neither it nor its welds had sufficient strength or stiffness to restrain the beam after the brace buckled. This failure of the lateral support did not significantly effect the experiment since it occurred just before completion of the test. It can be regarded as being fortunate because it indicated that the lateral support system was performing as intended. The lateral support system was designed to provide adequate lateral support to the frame, while simulating strength and stiffness limits that could be expected in normal building construction.

The results of the second test can be summarized by saying that the frame exhibited the same sound energy dissipation noted for the first frame. The hysteretic loops were repetitive, stable, and unpinched. The primary difference in behavior can be attributed to the behavior of the brace and brace connections. The welded brace connection induced bending moments into the brace which caused the formation of plastic hinges and lateral torsional buckling in the brace. Since Test Frame 2 could not have any brace slippage, it was forced to deform more severely and fail earlier for the same amount of displacement in the eccentric element. The lateral support system performed very satisfactorily during the test. The

results of this test again indicate that a well-designed and constructed eccentrically braced frame can withstand extremely severe lateral deflections.

#### Comparison of the Tests

Although there were several major differences in the design of the two test frames, they both exhibited the same general elastic and inelastic behavior. Their hysteretic loops were very repetitive and stable, and the frames maintained their strength and stiffness well into the failure of individual eccentric elements. Their elastic deflections and energy dissipation were produced by the inelastic deformation of the eccentric elements. These eccentric elements performed well, and their behavior was similar in both frames.

One of the major differences in design of the specimens was the brace-to-beam connection. The first frame had bolted connections. The major advantage of this connection was that it avoided lateral torsional buckling of the brace. A second advantage is that it is an economical connection. Its main disadvantage was that the brace connection slipped. This slippage results in a slight deterioration in the hysteretic behavior, and it caused a loss in the average lateral stiffness of the frame. Because of these two factors, a frame with bolted brace connections can expect slightly larger lateral deflections during severe excitations.

The second frame had welded brace connections. This connection offered the advantage of avoiding brace slippage. A related advantage is that the lateral deflections tend to be less severe. It had the disadvantage of attracting larger bending moments in the brace. These bending moments caused local yielding and the formation of lateral torsional buckling. At severe displacements, the eccentric element will be slightly more severely deformed than with the bolted connection and this may lead

to earlier failure of the frame. However, both connection details are satisfactory since in both cases the frame adequately withstood severe deflections without failing. The undesirable features of each can be minimized if they are designed properly. This means that bolted brace connections should be designed conservatively, whereas welded connections should have good lateral support.

Another difference is the size of the brace. The brace in Frame 1 was designed very conservatively with the factor of safety against ultimate compressive load of greater than two. The brace in Frame 2 had a factor of safety of approximately 1.5. At large displacements of the frame, the braces in the second frame exhibited considerable buckling while those in the first frame did not. In the second test, the buckling problems were induced by the welded brace connection. The brace of Test Frame 2 was strong enough to avoid Euler buckling if the lateral torsional buckling had not damaged the brace. Therefore, the smaller brace size is the more desirable since it is economical while providing adequate strength to the frame.

The lateral support, which was provided to the frame, was also a design variable. Frame 1 was supported at the fifth points of the beam, and the second frame was supported at the third points of the beam. There was no distinguishable difference in the performance of the two test frames with respect to the lateral support. The support used for Test Frame 2 is more economical and consistent with the framing normally used in building construction. From the results of these tests, it appears that lateral torsional stability of the beam is not a severe problem in these eccentrically braced frames. This verifies the results of Chapter 3 where cyclic behavior of short beams is discussed. That is, the high shear

(or moment gradient) of the shear yielding eccentric zone inhibits flange buckling or lateral torsional buckling because the flange cannot yield over a sufficient length to form a buckle. Web buckling occurs but it is more stable because of the formation of the cyclic diagonal tension field.

The gusset plate used in the brace-to-beam connection was also a variable in the design. Test Frame 1 used an ordinary plate type gusset, as shown in Fig. 52. The second frame used a simulated structural T-section for a gusset plate, as shown in Fig. 55. The T-section was used because it provides a better transfer of the axial force of the brace to the beam, since the flange of the T and the beam stiffener can be directly aligned. Further, the centroid of the weld of the T-section coincides with the line of action of the brace, and this simplifies the design. There were no significant differences in the test results, which could be attributed to this design detail. However, the connection detail used in the first frame also required a doubler plate and an additional stiffener to transfer the brace force, as shown in Fig. 52. The additional stiffeners and doubler plate make this a more expensive connection.

The final variation in the design of the test frames was the stiffeners used in the beam-to-column connection. Frame 1 was conservatively designed with column web stiffeners at the level of the beam flanges, as shown in Fig. 51. Test Frame 2 was designed without the use of such stiffeners. There were no apparent differences in the behavior of the test frames that could be attributed to this detail. Therefore, it appears that the eccentric bracing system does not have any special need for stiffeners in the beam-to-column connection. This is not intended to imply that stiffeners are not needed at the brace-to-beam connection. A single stiffener is always required at the brace connection, as shown in Fig. 55, so that the shear can be uniformly transferred to the web and the cyclic

diagonal tension field can form.

#### Comparison of the Analytical Model with Test Results

A static cyclic inelastic analysis was performed on these two test frames and the results were compared to the test results. The DRAIN-2D program is capable of performing only dynamic analysis, and so it was not suitable for this analysis. The ANSR-I [46] computer program was used for this analysis because it was similar to the DRAIN-2D program and it had capabilities for static inelastic analysis. The shear yielding beam element, which was developed for DRAIN-2D, was modified for use in ANSR. The basic element behavior and yield criteria are identical to the listing in Appendix C, but a number of other modifications had to be made to adapt them to the three-dimensional analysis and the iteration and solution procedures used by ANSR. It should be noted that while ANSR is a three-dimensional nonlinear analysis program the shear yielding beam element is still a planar element. It was also necessary to modify the basic ANSR program to create a save-and-restart capability. This capability was necessary because of the iterative nature of the solution and the many cycles to be analyzed.

The entire test frame and loading beam were modeled, and the lateral loads, gravity loads, and overturning couple were applied to the loading beam. The panel zone of all beam-to-column connections were assumed to be rigid. The brace was assumed to be connected to the beam with a pinned connection for Test Frame 1, and a moment-resisting connection for Test Frame 2. The base plates of the test frames were designed to remain elastic throughout the test, and it was necessary to consider the linear elastic deflection of these base plates. This base plate deflection was modeled by using the deflection equation (Equation 147 [41]) of a point load on a plate, which is simply supported on four sides. The base of the

test frame was grouted and prestressed to the anchor block, and the only deflection which could occur was that the column could uplift slightly when it was in tension. This correction reduced the predicted elastic lateral stiffness of the test frame by approximately 9%. The maximum change in deflection caused by this correction was .04 in. (1 mm) at the 3rd floor of the test frame.

The yield stress, Young's Modulus and uniaxial strain hardening coefficient,  $\rho$ , used in this comparison, were obtained from the test results shown in Appendix B. The residual stress distribution of the W 6 x 12 beam section (see Appendix B) was used to produce a modified plastic shear force,  $V_p$ . The yield stress of the web was simply reduced by the average residual stress in the web, and  $V_p$  was computed by Equation 3. The ultimate compressive loads were predicted by the AISC formulas [32], which were modified to the tensile coupon yield stress of the specimen. The interaction between axial force and bending moment was approximated by AISC equation 2.4-3 [32].

Both tests were analyzed for all inelastic cycles up to and including LP23. The ANSR computer program is a load controlled solution, but the test results were displacement controlled. Therefore, the nonlinear analysis was also run as a displacement controlled analysis, but this had to be done by an interactive approach, because of the complexity of the loadings. The interactive analysis was accomplished by first choosing a cyclic loading program and analyzing several cycles. This analysis was examined, and the loading program was adjusted so that the desired cyclic deflection was obtained. After the first displacement cycles were satisfactorily obtained, the results were saved, and the restart capability was used to save the expense of continually reanalyzing the early



cycles. Because of the limitations imposed by manually starting and terminating a run, it was not possible to precisely match the deflection program used in the tests. However, the fit of the analytical model to the experiment was good. Figure 96 is a plot of the lateral force third floor deflection for Test Frame 1. The dashed lines are the curves predicted by the analytical model, and the solid lines are test results. It should be noted that the test curve is corrected for brace slip, since the analytical model has no provisions for brace slip. The curve fit between the experimental and analytical results during the early cycles is extremely good. The later cycles up to LP 23 are also good, but the model displays a common failing during these later cycles. At large deflections, the model consistently undershoots the lower side of the test curve. The model is still satisfactory at LP 23, but it is apparent that the fit will grow worse at larger deflections. The analysis was stopped at LP23 because of the great cost of this analysis in this range, and the limited accuracy to be expected in further cycles. However, Figure 96 indicates that the shear yield model, which was developed in Chapter 3 is a very good model for predicting global deflections of the eccentrically braced frames. This figure also indicates the ways in which the model could be improved. At large deflections, the shear yield model becomes basically a kinematic hardening model, and this causes undershooting shown in Fig. 96. If the shear yielding element could incorporate a more accurate balance between isotropic hardening, kinematic hardening, and bounding surface concept, the fit would be improved for these large deflections.

The analytical model was also compared with the test results in other ways (see Table 2), and the comparison was generally favorable. Table 2 shows that the comparison is by no means exact, but it is good for

inelastic analyses. It should be noted that some of the variables, such as the vertical deflection of the eccentric node, are very sensitive, and this sensitivity makes it difficult to obtain good experimental comparisons.

The plot of the hysteretic comparison of Frame 2 in Figure 97 indicates that the model does a good job of predicting overall inelastic behavior of the frame. Other comparisons are shown in Table 3. The fit obtained for Frame 2 is very similar to the general fit from Test 1.

### Summary

Two eccentrically braced frames were tested and it was found that the eccentric bracing system has excellent energy dissipation capabilities. The hysteretic loops were repetitive and stable, and the frames maintained most of their strength and stiffness even after the first web tear. Hence this system is likely to perform satisfactorily even if one of the eccentric elements fails. A number of design parameters were evaluated. The brace-beam connection was the most sensitive parameter. If the brace is connected by bolts, the brace will slip; if it is welded, the brace will develop lateral torsional buckling problems. Neither of these problems was excessively severe, but the structural design must be attuned to avoid them. An analytical model discussed earlier was compared with these results. The comparison indicated that the analytical model is very good at predicting the behavior of the eccentrically braced system.

## SUMMARY, DESIGN RECOMMENDATIONS AND CONCLUSIONS

### Summary

The eccentric bracing system has many desirable attributes for the design of earthquake-resistant structures. The analyses have shown that this system provides a very stiff structure, and the stiffness provided is stable over a relatively large range of eccentricities. Stiffness is very desirable, because it helps assure a more serviceable structure and tends to limit the  $P-\Delta$  effect during severe earthquake excitations. The eccentric bracing system also offers excellent energy dissipation characteristics and inelastic behavior since the eccentric element is designed to deform inelastically before the brace can buckle.

A study of the inelastic behavior of the eccentric beam element showed that cyclic shear yielding of the web produced superior inelastic behavior. The cyclic behavior was stable during large deflections because a cyclic diagonal tension field formed and prevented deterioration due to web buckling. However, flange restraint and web stiffeners were necessary to develop this tension field. An analytical model of cyclic shear yield behavior was developed from these studies, and the model was used in the inelastic dynamic analysis of a 20-story four-bay eccentrically braced frame. The results of this analysis were compared to results predicted for conventional concentrically braced and steel moment-resisting frames under two very different types of earthquake excitations. The comparison indicated that the eccentrically braced frame performed very well because of its strength, stiffness, and energy dissipation capabilities.

Two one-third scale model test frames were designed to simulate the behavior of the 20-story prototype structure, and they were tested under a loading program which simulated two severe earthquakes sequentially

applied to the structure. These tests verified that the structural system performed as a stiff structure with full, unpinched hysteresis loops and that the loops were repetitive with no deterioration in strength or stiffness. It was further found that this structural system was capable of withstanding both of these earthquake simulations without any structural failure. However, it should be noted that very large floor deflections must be expected during the large lateral deflections. The results of the tests were used also to evaluate various design details. The analytical model was also compared with the test frame results. The predicted behavior from the model was very similar to the actual test results.

The tests and analytical studies indicate that the eccentric bracing system performed well under severe earthquake simulations; the system is very stiff with excellent energy dissipation, and thus performs well elastically and inelastically.

#### Design Recommendations

A number of conclusions were reached during the course of this study which directly affect the design of an eccentrically braced frame. The eccentrically braced system is a framing system where the center line of the brace does not intersect the center line of the beam-to-column connection. The eccentricity is introduced so that the eccentric beam element provides a ductile fuse which assures good inelastic behavior and energy dissipation. Since the plastic behavior is very important to this framing system, the initial preliminary design should be made using plastic design concepts. The technique of moment balancing is suitable for this. The procedure simply requires that the designer obtain a moment diagram which satisfies statics and design the structure accordingly. It is immaterial how this moment diagram was obtained or selected. Two factors are most

helpful in generating the diagram. First, it is useful to understand the general collapse mechanisms which can occur in an eccentrically braced frame. Secondly, because the brace provides approximately 75 to 80% of the lateral stiffness of the structure, it should carry a similar proportion of the lateral shear. An application of this general approach is given in Appendix A.

The beam-to-column connections are also an important feature of the system. They must be designed as moment-resisting connections, because the flanges require this restraint if the diagonal tension field is to form, and the beam must be designed to yield in shear. This is accomplished by assuring that the chosen beam has sufficient web area to develop the plastic shear force,  $V_p$ , required for the eccentric beam elements. The size of the eccentricity is selected so that shear yielding occurs before plastic hinges form at both ends of the eccentric beam element. Moreover, the eccentricity should be chosen to assure a balance between shear and bending yield by having plastic hinges form at both ends of the eccentric beam soon after shear yield. This balance can be accomplished by choosing the eccentricity with the techniques suggested in equations 23 and 24. The beam must be designed for the bending moment at the face of the column, which is considerably less than the bending moment at the center line of the beam-column joint. The plastic moment is reduced to  $M_p^*$  in the eccentric beam segment and is further reduced at the brace connection because of the interaction between moment capacity and high axial load in the central beam segment. It should be noted that doubler plates must not be used to increase the shear area of the web of the eccentric beam element, but cover plates can be applied to the flanges to increase the bending capacity of the beam. The beam design is critical.

It should not be designed too conservatively because the brace and column design depend on the beam design.

The brace itself is designed as a compression member with its ultimate axial design load depending upon the ultimate plastic strength of the beam. The axial design load will be somewhat higher than the load predicted by moment balancing, and it depends on how conservatively the beam is designed. The brace should be designed for this ultimate compressive load with a factor of safety of at least 1.5. The additional factor of safety is necessary to assure that the brace will not buckle despite strain hardening of the eccentric beam element, uncertainty in the actual yield stress of the steel, and the additional force necessary to crack the floor slab. This factor of safety could be modified if an analysis of an individual design indicated that the modification was justified.

The columns are designed by the usual weak beam-strong column design concept employed in steel moment-resisting frames. The beam-to-column connection must be designed as a moment-resisting connection as shown in Figure 54. This type of all-welded connection is necessary because of the high shear in the eccentric element and the required flange restraint, which assures stability of the eccentric beam element. It should be noted that a fillet weld is necessary between the erection plate and the beam web because of the very high shear force in the eccentric beam element.

The brace-to-beam connection is best designed as a bolted joint with a structural T section used for a gusset plate as shown in Figure 55. The flange of the T should be directly aligned with the web stiffeners as shown in this figure. This pair of stiffeners is always necessary to develop the diagonal tension field and to ensure stability of the eccentric beam element. The bolted connection should be designed for the full

ultimate brace load with the additional factor of safety. The connection must be designed with bolts in bearing, and the bearing stress should not exceed the yield stress of the material. The limitation in bearing stress is necessary so that cyclic slippage of the brace does not become too severe and reduce the energy dissipation of the system. It should be noted that brace slippage in the connection will produce a slight deterioration in lateral stiffness during a major earthquake, but the loss in stiffness can be regained later by welding the connection. A welded connection is also an acceptable alternative. Finally, the use of a regular gusset plate as shown in Figure 52 is also acceptable. However, this last detail will generally require additional stiffeners and doubler plates at the brace connection.

### Conclusions

The major conclusions of this report can be summarized as follows:

1. The eccentric bracing system is a very stiff structural system which easily satisfies the serviceability requirements of building codes. The weight of steel required may be of the order of 30% less than that required for steel moment-resisting frames. Further, this lateral stiffness remains stable through a wide range of small to moderate eccentricities.
2. Cyclic shear yielding is a desirable method of energy dissipation for the eccentric element. Shear yielding offers good stability under large cyclic deflections. Web buckles form after the web has yielded, but if the beam is properly designed, a cyclic diagonal tension field forms at large displacement levels, and this tension field prevents any significant deterioration in the inelastic behavior of the frame.
3. The cyclic inelastic behavior of structures with eccentric

elements which yield in shear can be predicted by a simple analytical model which gives a good indication of structural behavior.

4. Inelastic dynamic analyses of the eccentric prototype system and other alternate concentrically braced and moment-resisting frames under two very different severe base excitations indicate that different excitations produce different responses in the structure. Some excitations create a pulse effect, and the structure must have considerable elastic strength and stiffness to limit inelastic deflections. Other excitations exhibit a periodic effect, and the structure must exhibit sound cyclic energy dissipation characteristics to limit inelastic deflections. The eccentric bracing system performs very well because it combines the stiffness of a braced frame with the very desirable energy dissipation of a steel moment-resisting frame.

5. One-third scale models of eccentrically braced frames exhibit large initial elastic stiffness; they also possess very sound energy dissipation characteristics. The hysteretic loops are unpinched and do not deteriorate in strength or stiffness. Further, even beyond failure of the first eccentric element, the structure continues to retain most of its strength and stiffness. Therefore, the premature failure of a few eccentric elements for any reason will not necessarily mean a total collapse of a structure. Apparently a relatively large number of eccentric elements must fail before the structure is in danger of total collapse.

6. The inelastic behavior of the eccentrically braced frame is very good, but very large inelastic floor deflections must be expected through all of the floors of a structure. This is both an advantage and a disadvantage. It is desirable because it distributes the inelastic activity and no one point experiences excessive deformation. However, it



also indicates that considerable floor damage must be expected on all floor levels. The floor damage may be quite severe, but it is also more easily repaired than many other types of damage.

7. The beam-to-column joint must be a moment-resisting connection. This is necessary because the flanges of the eccentric beam element require restraint to develop the cyclic diagonal tension field. A web stiffener is also required at the brace connection to develop this tension field. These connection details are costly, but the weld and member sizes are relatively small. Therefore, the danger of lamellar tearing and the cost of welding should be significantly less than for a steel moment-resisting frame.

8. No doubler plates are required in the web of the column of the eccentrically braced frames. Inelastic strains in this panel zone do not adversely affect the story drift as they do in moment-resisting frames. However, stiffeners may be needed at the beam-column connections.

9. A peripheral conclusion was reached relative to the design of the bolted connections. As is well documented in the test of Frame 1, slippage of bolted connections can have a very detrimental effect upon the hysteretic behavior of the total structure. This effect is limited if the bolted connection is designed conservatively in bearing on the bolts. Therefore, it is recommended that bolted connections, which are subjected to cyclic loadings, be designed for ultimate bearing stresses no larger than the yield stress of the material.

In addition to the above, there are several areas which are worthy of further study. These include:

1. The possibility of developing a new all-bolted beam-to-column connection for use in the eccentric bracing system. This connection

detail is not possible with the usual bolted web connection because of the high shear forces and bolt bearing problems noted earlier. This type of connection would have to be a hybrid connection which eliminates the bearing stress problem.

2. The effect of axial force on cyclic shear yielding of beams needs further study. The behavior of beams which yield in shear is excellent, if the axial force is low. However, no tests have been made on beams simultaneously loaded with axial and shear force. This type of condition occurs in systems such as the eccentric K brace, and it may also occur in other bracing systems under certain conditions.

3. Eccentric bracing creates a structure which utilizes the beam better and limits the magnitude of forces and moments in the members. The general eccentric bracing concept could be applied to other structural systems.

## References

1. Popov, E. P., Takanashi, K., and Roeder, C. W., "Structural Steel Bracing Systems: Behavior Under Cyclic Loading," EERC Report 76-17, University of California, Berkeley, June 1976.
2. Wakabayashi, et al, "Experiment on the Elastic-Plastic Behavior of Bars Subjected to Cyclic Axial Loads," Preprints of Annual Conference, AIJ, October 1972.
3. Kahn, L. F., and Hanson, R. D., "Inelastic Cycles of Axially Loaded Steel Members," ASCE Struct. Div. J., Vol. 102, May 1976.
4. Igarashi, S., and Inoue, I., "Memorandum on the Study of Braced Frames," Quarterly Column, No. 49, October, 1973.
5. Higginbotham, A. B., "The Inelastic Cyclic Behavior of Axially-Loaded Steel Members," Ph.D. Thesis, University of Michigan, 1973.
6. Nonaka, T., "An Elastic-Plastic Analysis of a Bar Under Repeated Axial Loading," J. Solids Structures, Vol. 9, 1973.
7. Igarashi, S., Inoue, I., Ogawa, K., and Asano, M., "Hysteretic Characteristics of Steel Braced Frames, Part I, The Behavior of Bracing Members Under Cyclic Axial Forces," Trans AIJ, No. 196, 1972.
8. Fujimoto, M., Wada, A., Shirakata, K., and Kosugi, R., "Nonlinear Analysis for K-Type Braced Steel Frames," Trans AIJ, No. 209, July 1973.
9. Tanabashi and Taneta, "On the Relation Between the Restoring Force Characteristics of Structures and the Patterns of Earthquake Ground Motion," Proceedings of Japan National Symposium Earthquake Engineering, Tokyo, Japan, 1962.
10. Veletsos, A. S., "Maximum Deformation of Certain Nonlinear Systems," Proceedings of 4th World Conference Earthquake Engineering, Santiago, Chile, 1969.
11. Workman, G. H., "The Inelastic Behavior of Multi-Story Braced Frame Structures Subjected to Earthquake Excitation," University of Michigan Research Report, September 1969.
12. Nilforoushan, R., "Seismic Behavior of Multi-Story K-Braced Frame Structures," University of Michigan Research Report UMEE 73R9, November 1973.
13. Wakabayashi, M., et al, "Experimental Study on the Elastic-Plastic Stability on Steel Frames and the Restoring Force Characteristics," JSSC, Vol. 6, No. 55, 1970, in Japanese.

14. Wakabayashi, M., Matsui, C., Minami, K., and Mitani, I., "Inelastic Behavior of Full-Scale Steel Frames with and without Bracing," Bulletin of Disaster Prevention Res. Inst., Kyoto University, Vol. 24, Part 1, No. 216, March 1974.
15. Krawinkler, H., Bertero, V. V., and Popov, E. P., "Inelastic Behavior of Steel Beam to Column Subassemblages," EERC Report 71-7, University of California, Berkeley, October 1971.
16. Bertero, V. V., Krawinkler, H., and Popov, E. P., "Further Studies on the Seismic Behavior of Steel Beam-Column Subassemblages," EERC Report 73-27, University of California, Berkeley, December, 1973.
17. Fujimoto, M., Aoyagi, T., Ukai, K., Wada, A., Saito, K., "Structural Characteristics of Eccentric K-Braced Frames," Trans AIJ, No. 195, May 1972.
18. Hisatoku, T., et al, "Experimental Study on the Static Behavior of the Y-Typed Bracings," Report of Takenaka Technical Institute, No. 12, August 1974.
19. Gupta, R. P., "Seismic Behavior of Staggered Truss Framing System," University of Michigan Report on AISI Project No. 175, December 1971.
20. Hanson, R., Goel, S., Berg, G., "Seismic Behavior of Staggered Truss Frame System Design Procedure for Earthquake Loading," University of Michigan Report on AISI Project No. 175, December 1971.
21. Teal, E. J., "Seismic Design Practice for Steel Buildings," Structural Steel Education Council, AISC, 1976.
22. Uniform Building Code, International Conference of Building Officials, Pasadena, 1973 edition.
23. Tsuji, B., "Behavior of Bracing," Quarterly Column, No. 49, October 1973.
24. Horne, M. R., "A Moment Distribution Method for the Analysis and Design of Structures by the Plastic Theory," Proceedings of Institute of Civil Engineers, Vol. 3, No. 1, April, 1954.
25. Gaylord, E. H., "Plastic Design by Moment Balancing," Steel Structures Symposium, University of Illinois, Urbana, October 1966.
26. "Plastic Design in Steel, A Guide and Commentary," ASCE Manual 41, 1971.
27. Petersson, H., "GENFEM - A Computer Program for Analysis of Three-Dimensional Building Structures by the Finite Element Method," to be published.
28. Petersson, H., and Popov, E. P., "Substructuring and Equation System Solutions in Finite Element Analysis," Computers and Structures, Vol. 7, Pergamon Press, Great Britain, 1977.

29. Newmark, N. M., and Hall, W. J., "Shear Deflection of Wide-Flange Steel Beams in the Plastic Range," Transactions ASCE, Vol. 122, Paper No. 2878, 1957.
30. Popov, E. P., Bertero, V. V., and Chandramouli, S., "Hysteretic Behavior of Steel Columns," EERC Report 75-11, University of California, Berkeley, September 1975.
31. Malvern, L. E., Introduction to the Mechanics of a Continuous Medium, Prentice-Hall, Englewood Cliffs, New Jersey, 1969.
32. Manual of Steel Construction, Seventh Edition, AISC, New York, 1969.
33. Iwan, W. D., "Distributed - Element Model for Hysteresis and Its Steady-State Dynamic Response," Journal of Applied Mechanics, Vol. 33, December, 1966.
34. Kanaan, A. E., and Powell, G. H., "DRAIN-2D - A General Purpose Computer Program for the Dynamic Analysis of Inelastic Plane Structures," EERC Report, University of California, Berkeley, April 1973.
35. Plantema, F. J., Sandwich Construction, The Bending and Buckling of Sandwich Beams, Plates, and Shells, John Wiley, and Sons, New York, 1966.
36. van der Neut, A., "The Three Point Bending Test of Wooden Box Beams," NLL Report S.72. (in Dutch).
37. Dafalias, Y. F., Ph.D. Thesis, Department of Civil Engineering, University of California, Berkeley, 1975.
38. Dafalias, Y. F., and Popov, E. P., "Plastic Internal Variable Formalism of Cyclic Plasticity," Journal of Applied Mechanics, Vol. 98, No. 4, December, 1976.
39. Petersson, H., and Popov, E. P., "Generalized Loading Constitutive Relations," ASCE Engineering Mechanics Specialty Conference, May 23-25, 1977.
40. Seely, F. B. and Smith, J. O., Advanced Mechanics of Materials, John Wiley and Sons, New York, 1932.
41. Timoshenko, S. P., and Goodier, J. N., Theory of Elasticity, McGraw-Hill, New York, 1956.
42. Biggs, J. M., Introduction to Structural Dynamics, McGraw-Hill, New York, 1964.
43. Goel, S. C., and Hanson, R. D., "Seismic Behavior of Multistory Braced Steel Frames," ASCE Journal of Structural Division, January 1974.
44. Plastic Design of Braced Multistory Steel Frames, AISI, New York, 1968.

45. Wang, T. Y., Bertero, V. V., and Popov, E. P., "Hysteretic Behavior of Reinforced Concrete Framed Walls," EERC Report 75-23, University of California, Berkeley, 1975.
46. Bertero, V. V., Popov, E. P., Endo, T., and Wang, T. Y., "Pseudo-Dynamic Testing of Wall Structural Systems," ASCE Engineering Mechanics Division Specialty Conference, UCLA, March, 1976.
47. Mondikar, D. P., and Powell, G. H., "ANSR-I, General Purpose Program for Analysis of Nonlinear Structural Reponse," EERC Report 75-37, University of California, Berkeley, 1975.
48. Timoshenko, S. P., and Wornowsky-Krieger, S., "Theory of Plates and Shells," McGraw-Hill, New York, 1959.

SPECIMEN NUMBER	DESIGN OPTION	SPAN DIMENSION B (IN.)	PRIMARY YIELD MECHANISM	SPECIAL NOTES
1	A	6.0	SHEAR	
2	A	6.0	SHEAR	
3	A	12.0	BENDING	
4	A	12.0	BENDING	3/16" DOUBLER PLATE TO WEB
5	A	6.0	COMBINED	3/16" DOUBLER PLATE TO WEB
6	A	6.0	SHEAR	
7	B	12.0	BENDING	STIFFENER PLATES (1/4") SPACED 2-1/2" O.C.
8	B	12.0	SHEAR	3/8" x 1 1/4" COVER PLATE ON ALL FOUR FLANGES
9	C	6.0	SHEAR	NO FLANGE OR WARPING RESTRAINT

TABLE 1 - DESIGN PARAMETERS OF BEAM SPECIMENS

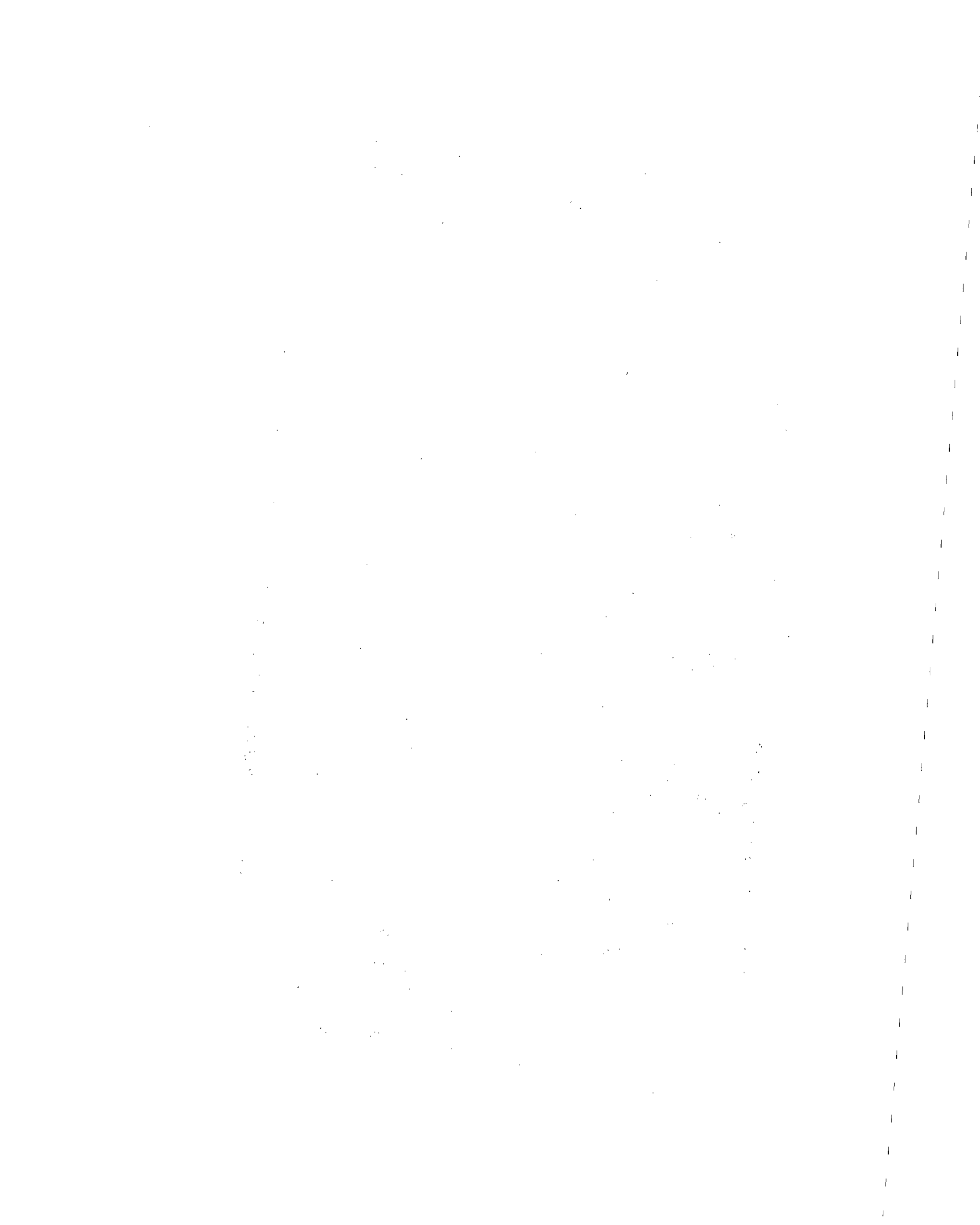
LOAD POINT	LATERAL FORCE		LATERAL DEFLECTION THIRD FLOOR		LATERAL DEFLECTION FIRST FLOOR		LATERAL DEFLECTION SECOND FLOOR		FLOOR DEFLECTION NORTH END FIRST FLOOR		FLOOR DEFLECTION SOUTH END FIRST FLOOR	
	TEST	ANSR	TEST	ANSR	TEST	ANSR	TEST	ANSR	TEST	ANSR	TEST	ANSR
LP 1	65.8	70.5	0.48	0.47	0.23	0.20	0.37	0.35	-.15	-.05	0.15	0.13
LP 7	85.6	83.0	.99	1.00	0.42	0.40	0.76	0.75	-.26	-.17	0.32	.33
LP 13	99.6	95.6	1.36	1.32	0.58	0.55	1.05	1.03	-.31	-.25	0.48	0.48
LP 19	112.9	108.4	2.78	2.76	1.17	1.37	2.15	2.29	-.61	-.59	1.07	1.32
LP 23	109.6	115.4	4.25	4.02	1.76	1.95	3.30	3.25	-.93	-.88	1.71	1.92

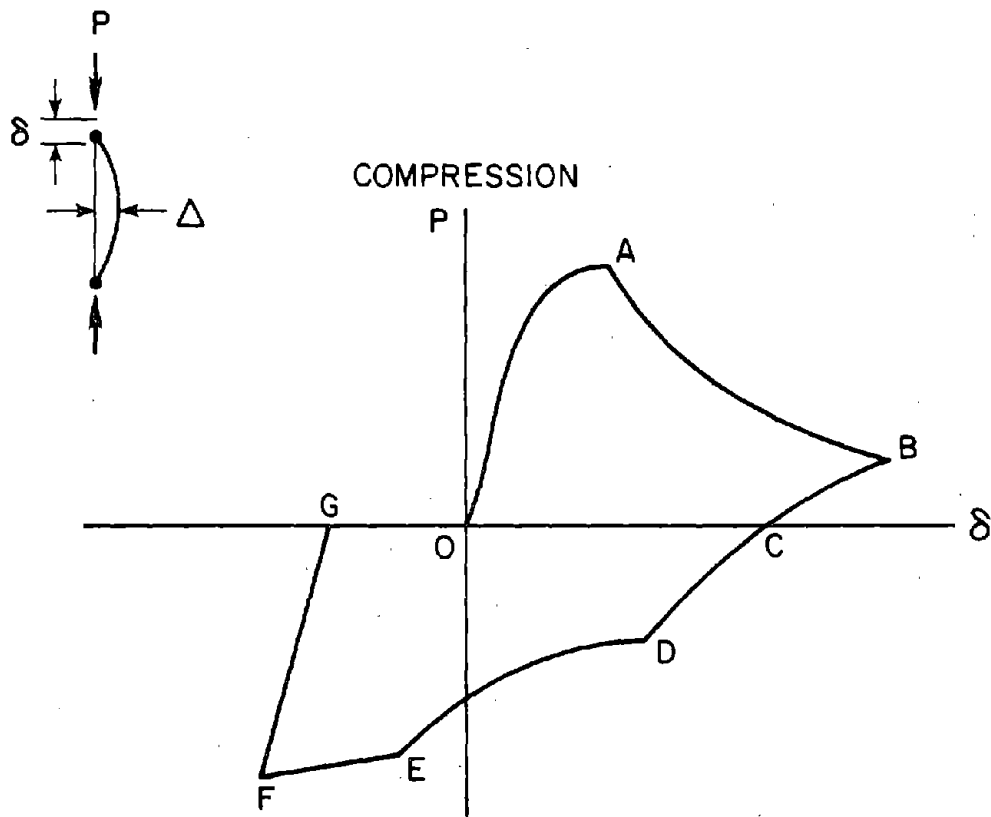
TABLE 2 - COMPARISON OF DATA POINTS BETWEEN ANSR-I AND TEST FRAME 1



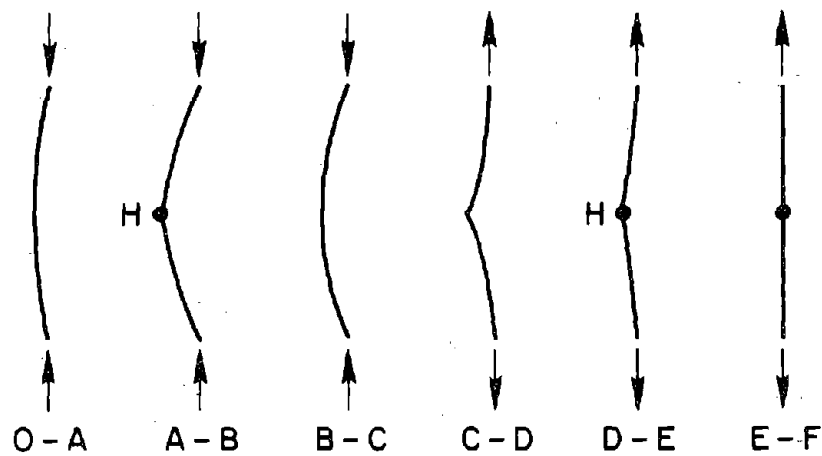
LOAD POINT	LATERAL FORCE		LATERAL DEFLECTION THIRD FLOOR		LATERAL DEFLECTION FIRST FLOOR		LATERAL DEFLECTION SECOND FLOOR		FLOOR DEFLECTION NORTH END FIRST FLOOR		FLOOR DEFLECTION SOUTH END FIRST FLOOR	
	TEST	ANSR	TEST	ANSR	TEST	ANSR	TEST	ANSR	TEST	ANSR	TEST	ANSR
LP 1	64.3	70.0	.50	.51	.22	.21	.39	.37	-0.06	-.05	0.14	0.11
LP 7	83.2	81.9	.99	1.00	.42	.39	.78	.75	-.17	-.18	.32	.29
LP 13	100.0	98.2	1.49	1.52	.65	.64	1.19	1.18	-.23	-.21	.53	.53
LP 19	113.6	107.1	3.00	2.98	1.31	1.38	2.38	2.39	-.52	-.16	1.16	1.30
LP 23	113.0	112.0	4.53	4.50	1.91	2.03	3.55	3.51	-.82	-.38	1.79	1.97

TABLE 3 - COMPARISON OF DATA POINTS BETWEEN ANSR-I AND TEST FRAME 2





A) HYSTERETIC BEHAVIOR



B) ZONES OF BEHAVIOR

FIGURE 1 - TYPICAL LOAD DEFORMATION RELATIONSHIP OF A SLENDER BAR

Preceding Page Blank

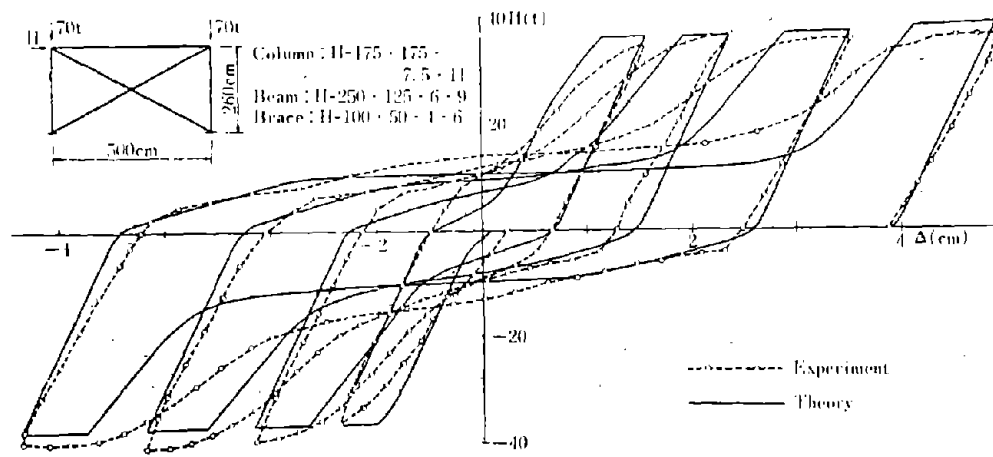
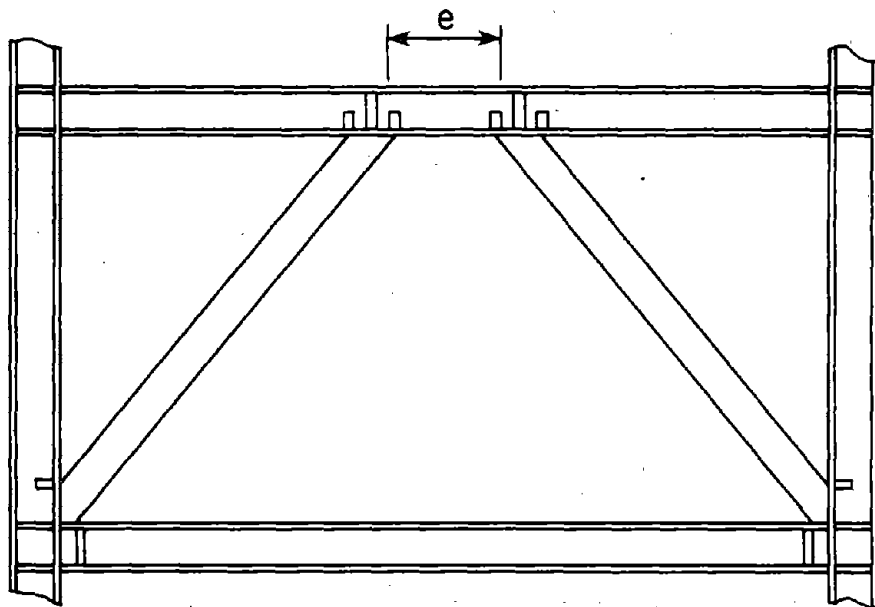
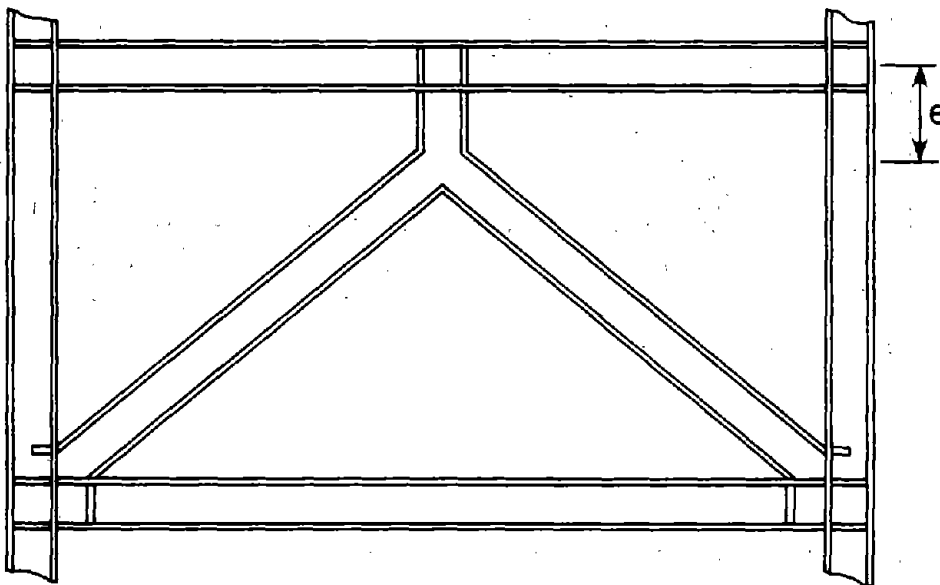


FIGURE 2 - TYPICAL PINCHED HYSTERESIS LOOPS FOR A CONCENTRICALLY BRACED FRAME [4]



(a) ECCENTRIC K-BRACE



(b) INVERTED Y-BRACE

FIGURE 3 - ALTERNATE ECCENTRICALLY BRACED ELEMENTS

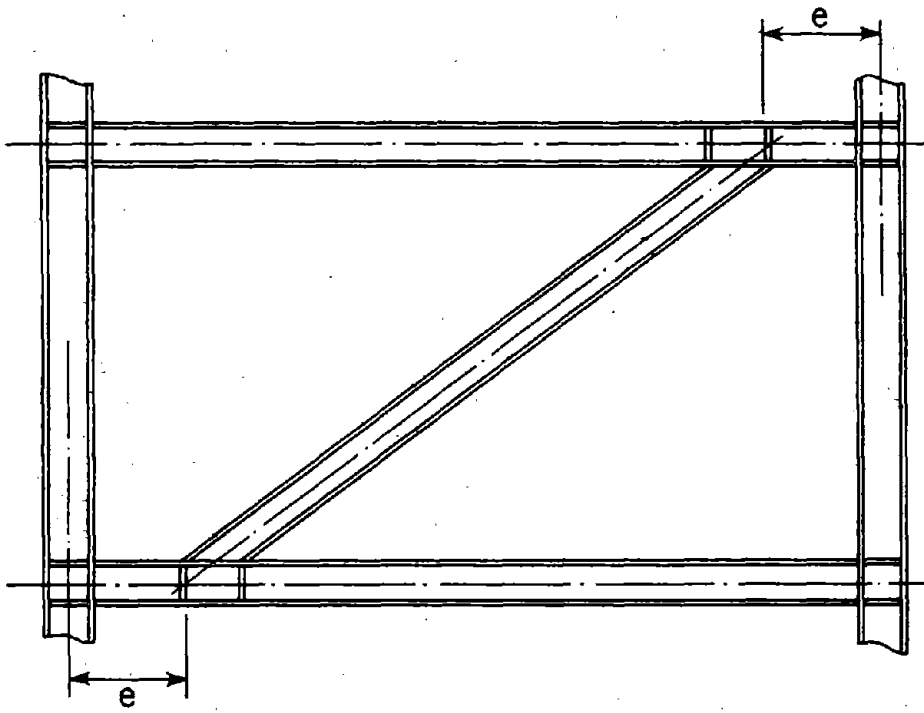
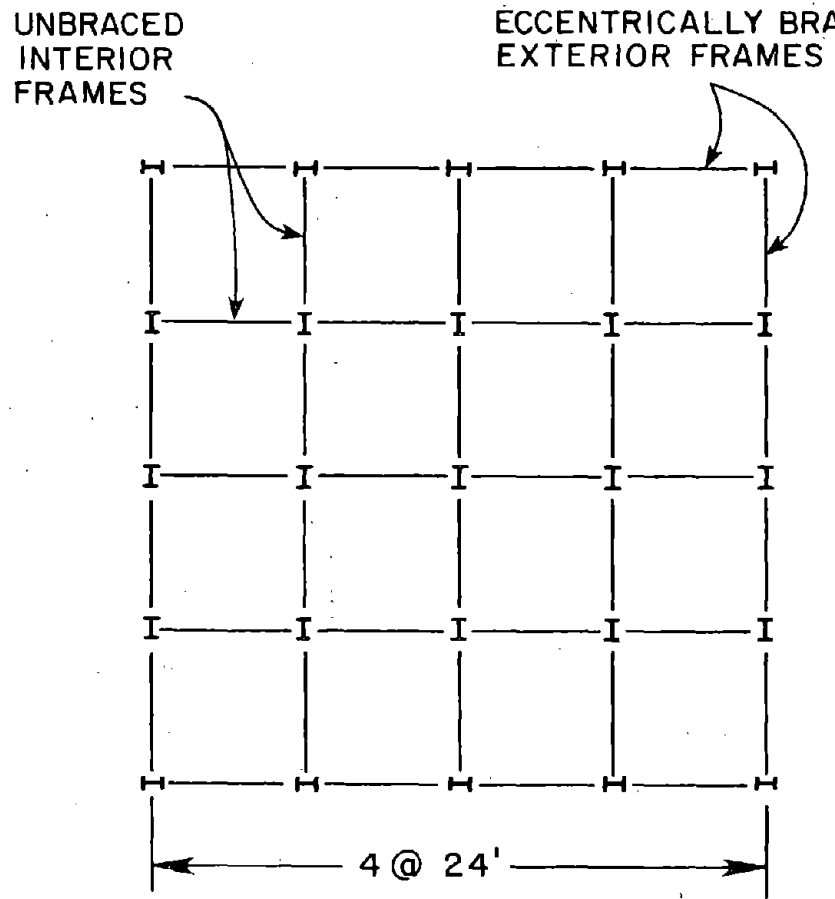
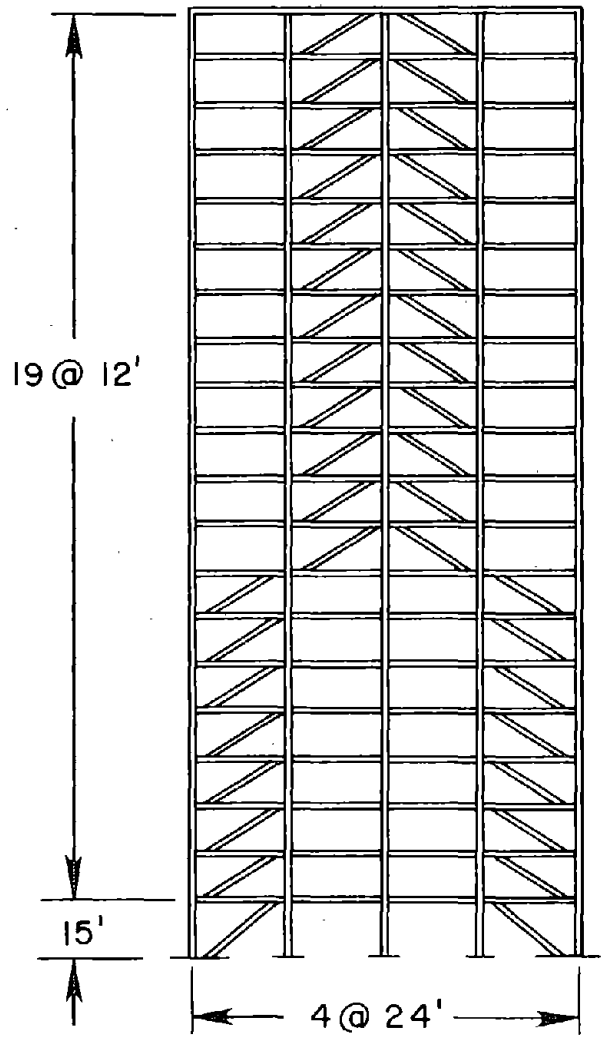


FIGURE 4 - ECCENTRIC BRACING SYSTEM OF THIS STUDY



(a) LAYOUT OF PROTOTYPE STRUCTURE



(b) ELEVATION OF ECCENTRICALLY BRACED EXTERIOR FRAME

FIGURE 5 - PROTOTYPE STRUCTURE

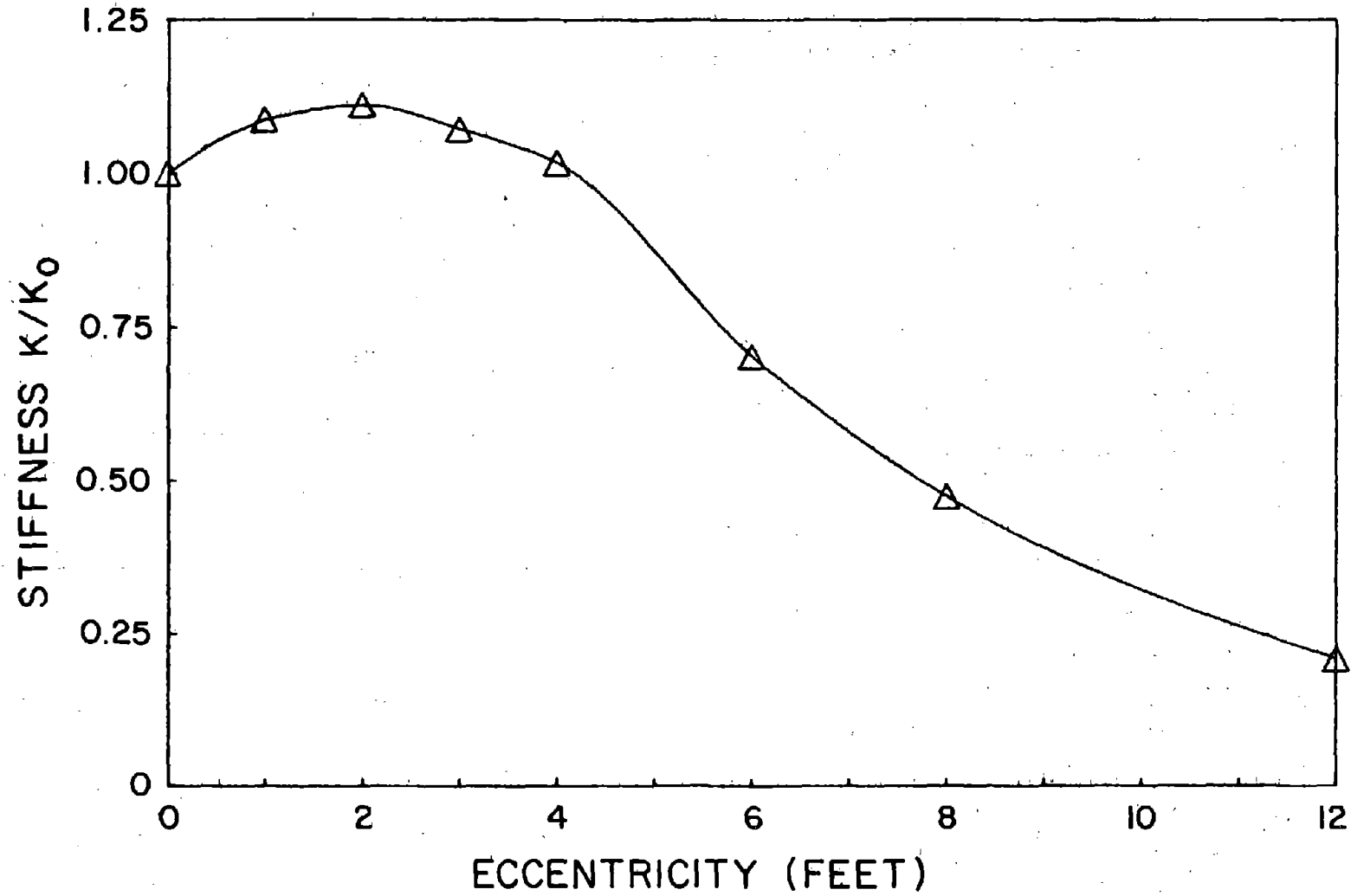
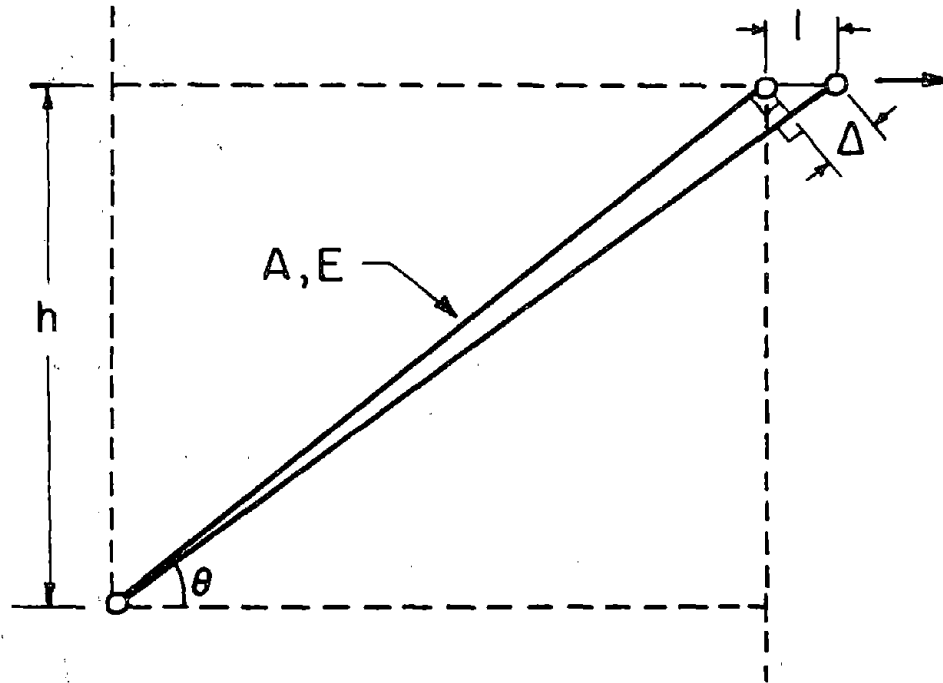


FIGURE 6 - NORMALIZED STIFFNESS OF THE PROTOTYPE STRUCTURE AS A FUNCTION OF ITS ECCENTRICITY





$$\text{AXIAL LOAD IN BRACE} = P = \frac{\Delta AE}{l}$$

$$\text{LENGTH OF BRACE (UNDEFORMED)} = l = \frac{h}{\sin \theta}$$

$$\text{LATERAL STIFFNESS OF BRACE} = K = P \cos \theta$$

SMALL ANGLE GEOMETRY IMPLIES THAT

$$\Delta = l (\cos \theta) = h \cos \theta$$

$$K = \frac{AE}{h} (\cos^2 \theta) (h \sin \theta)$$

FIGURE 7 - COMPUTATION OF THE LATERAL STIFFNESS PROVIDED BY THE BRACE

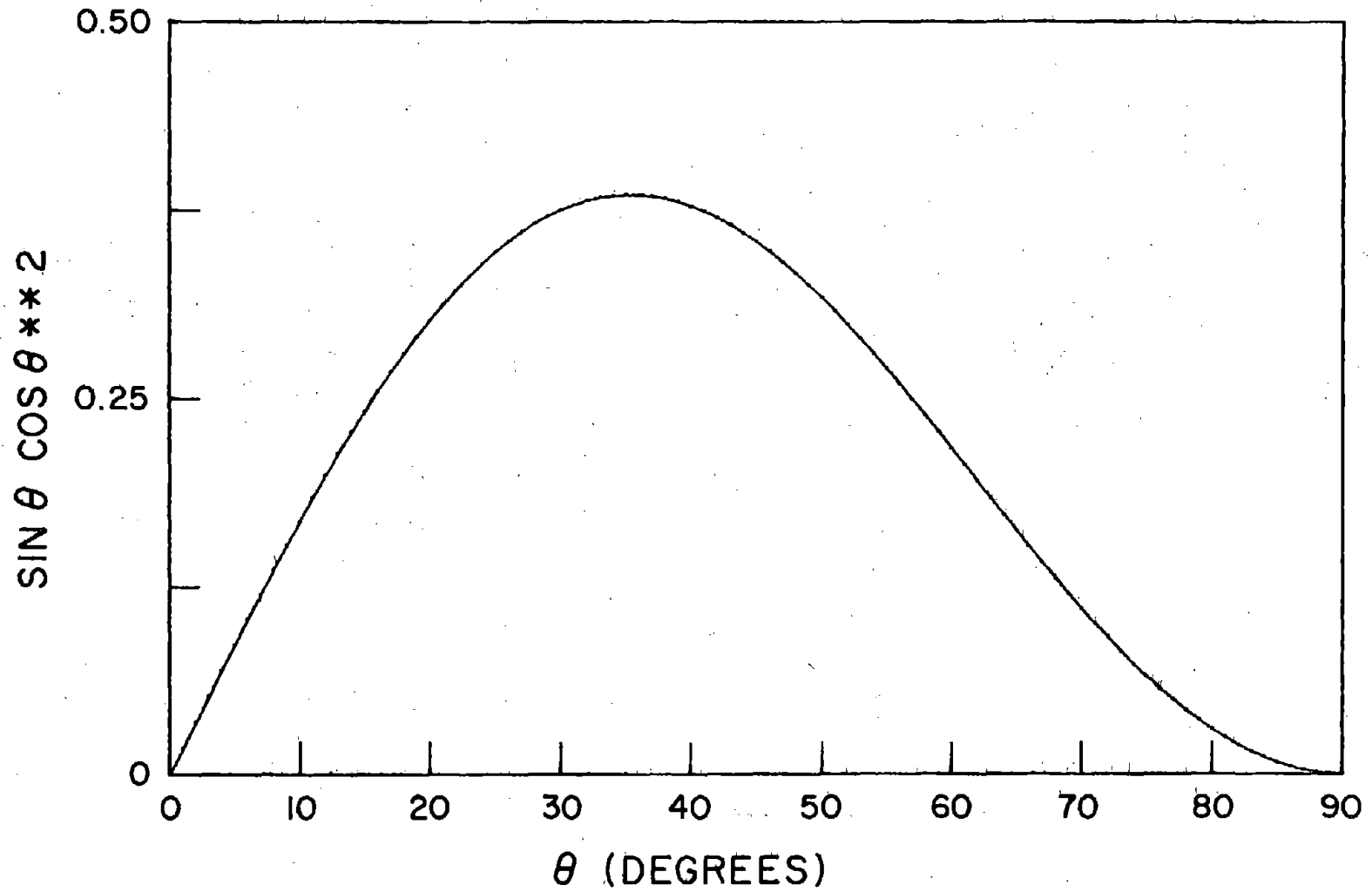
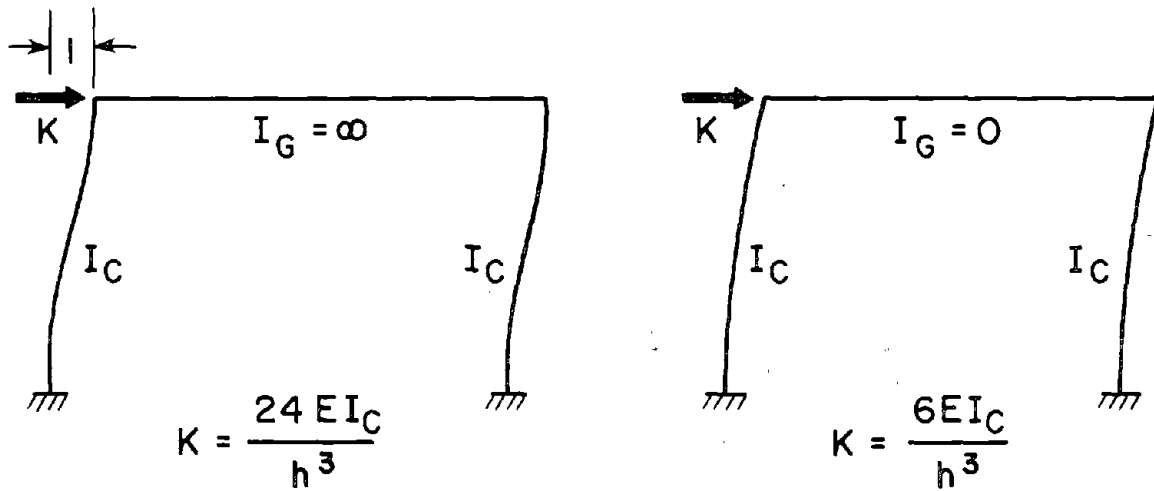
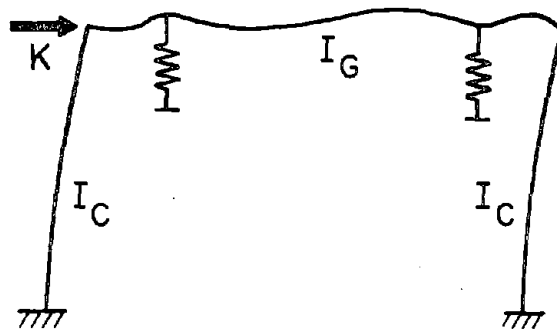


FIGURE 8 - VARIATION IN THE LATERAL STIFFNESS PROVIDED BY THE BRACE



(a) SINGLE STORY MOMENT-RESISTING FRAMES



THIS GIRDER IS RESTRAINED BY THE ECCENTRIC BRACE AND THUS ITS BENDING STIFFNESS IS GREATLY INCREASED. THUS:  $K \rightarrow \frac{24 EI_C}{h^3}$

(b) SINGLE STORY ECCENTRIC BRACED FRAME BENDING STIFFNESS

FIGURE 9 - LATERAL STIFFNESS OF A SINGLE STORY FRAME

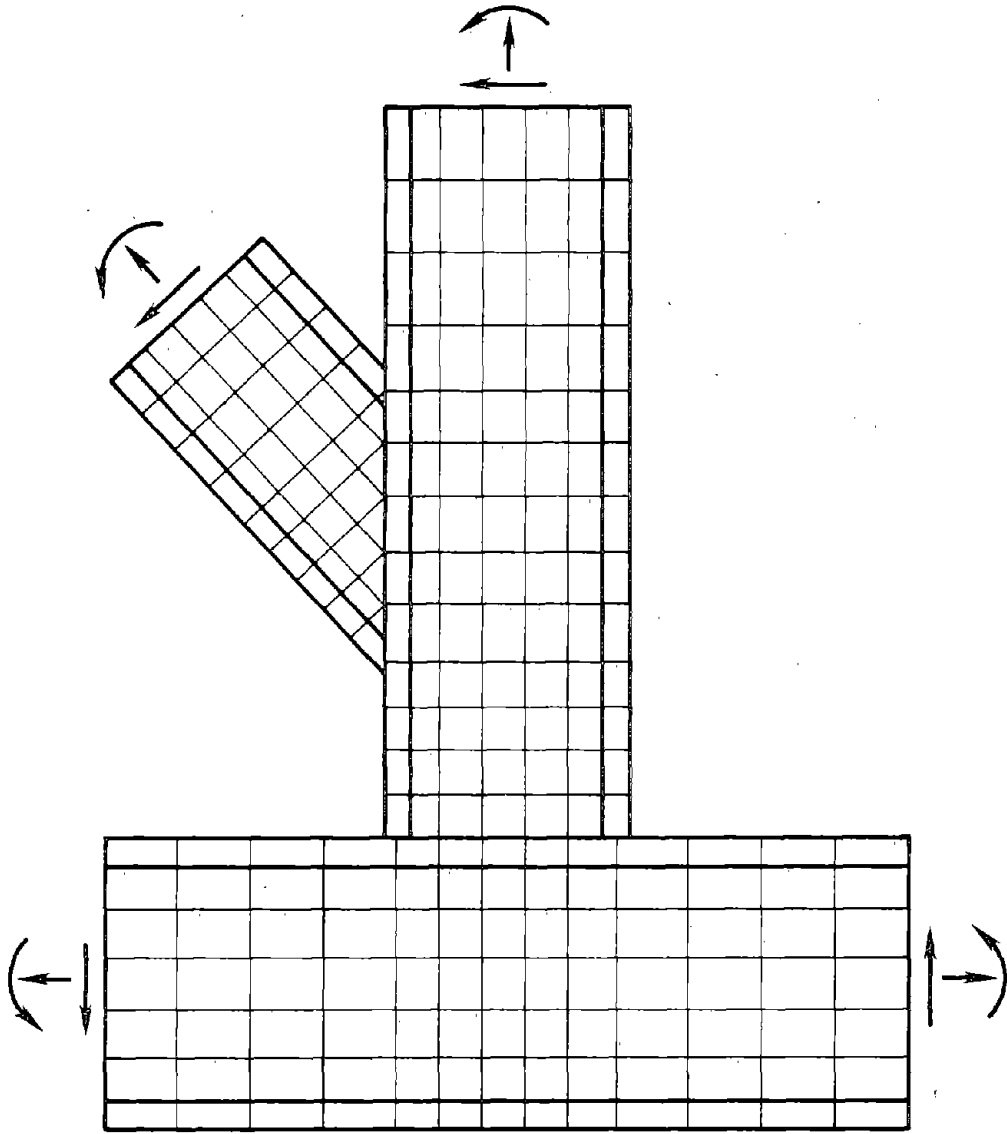
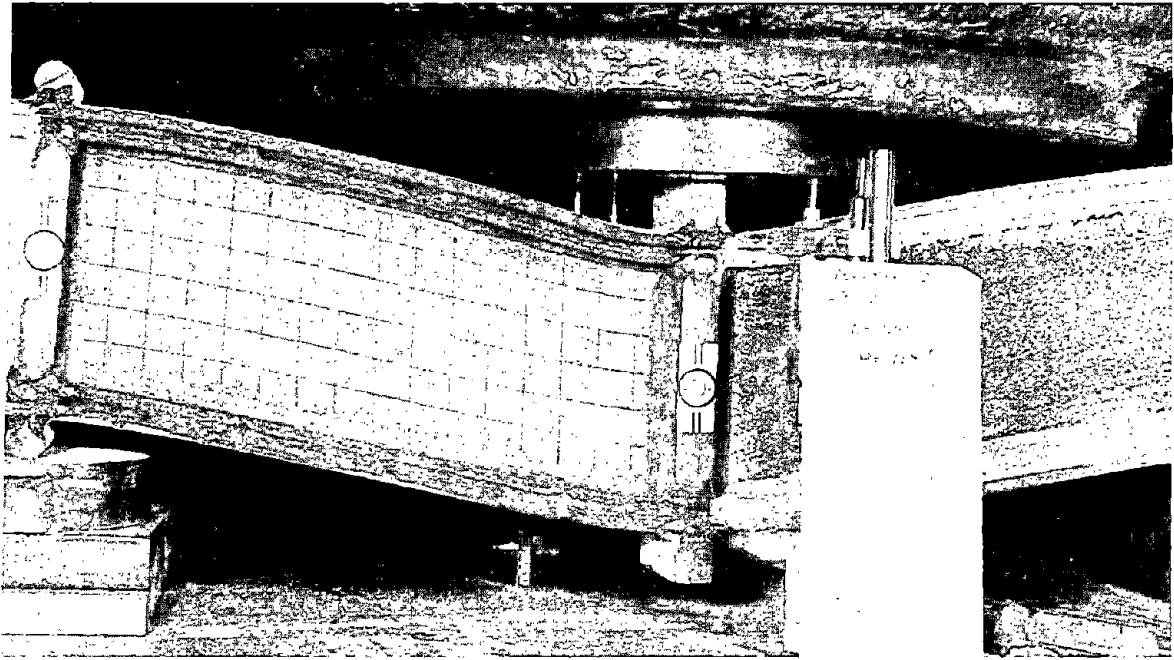
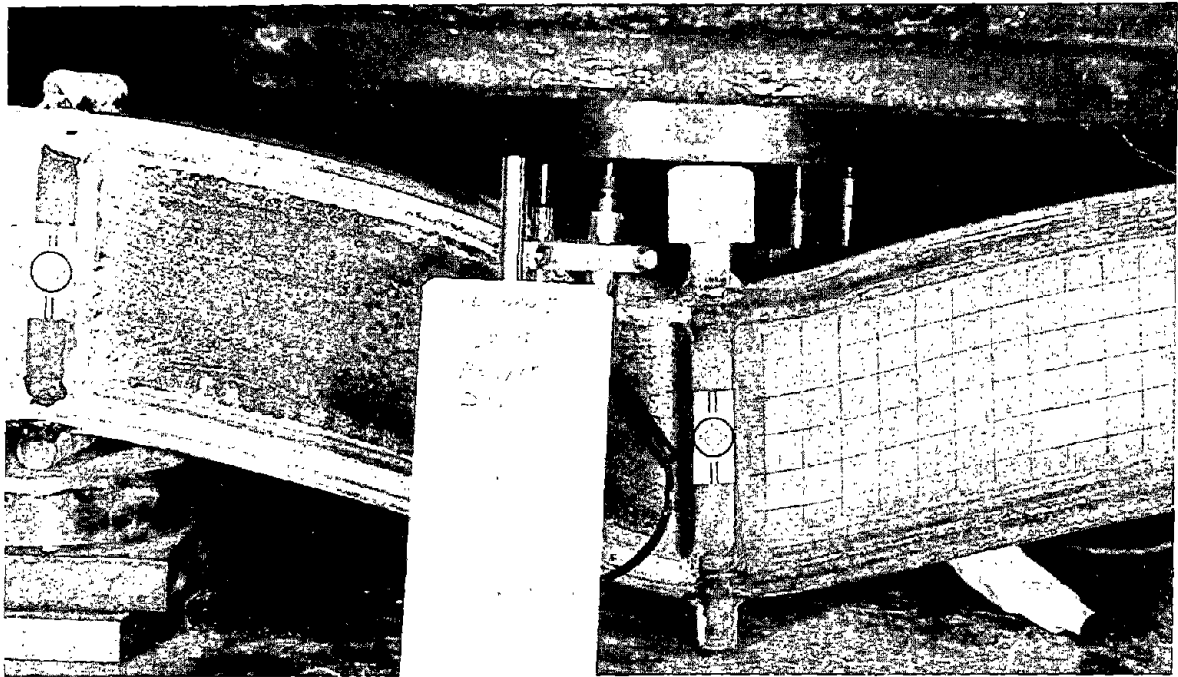


FIGURE 10 - SUBASSEMBLAGE USED IN THE DETAILED LINEAR ELASTIC ANALYSIS

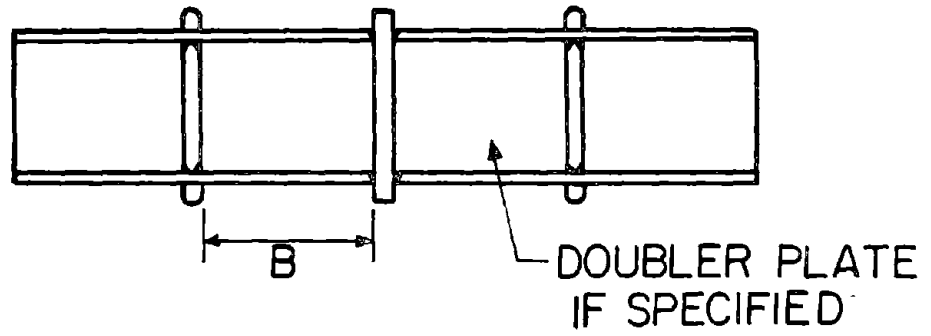


A) PHOTOGRAPH AT THE END OF A GIVEN HALF CYCLE

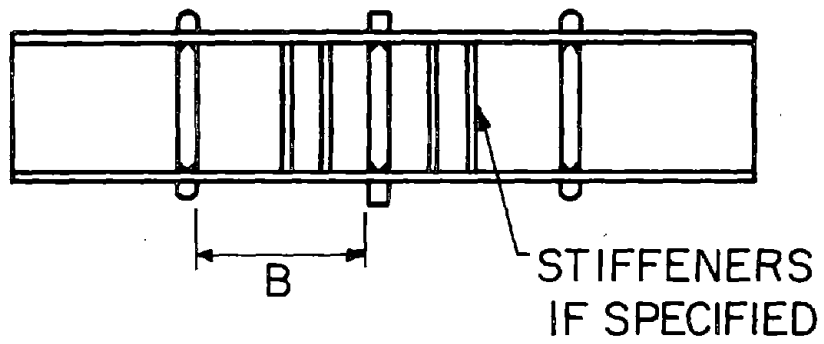


B) PHOTOGRAPH AT THE END OF THE NEXT HALF CYCLE

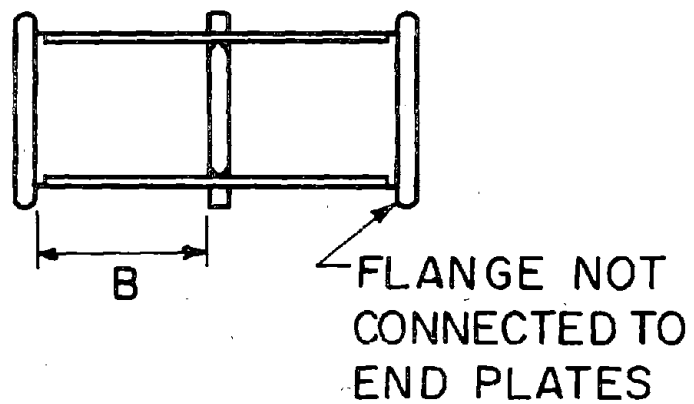
FIGURE 11 - PHOTOGRAPH OF THE TEST APPARATUS AND CYCLING PROCEDURE



a) OPTION A



b) OPTION B



c) OPTION C

FIGURE 12 - DESIGN OPTIONS OF THE TEST SPECIMENS

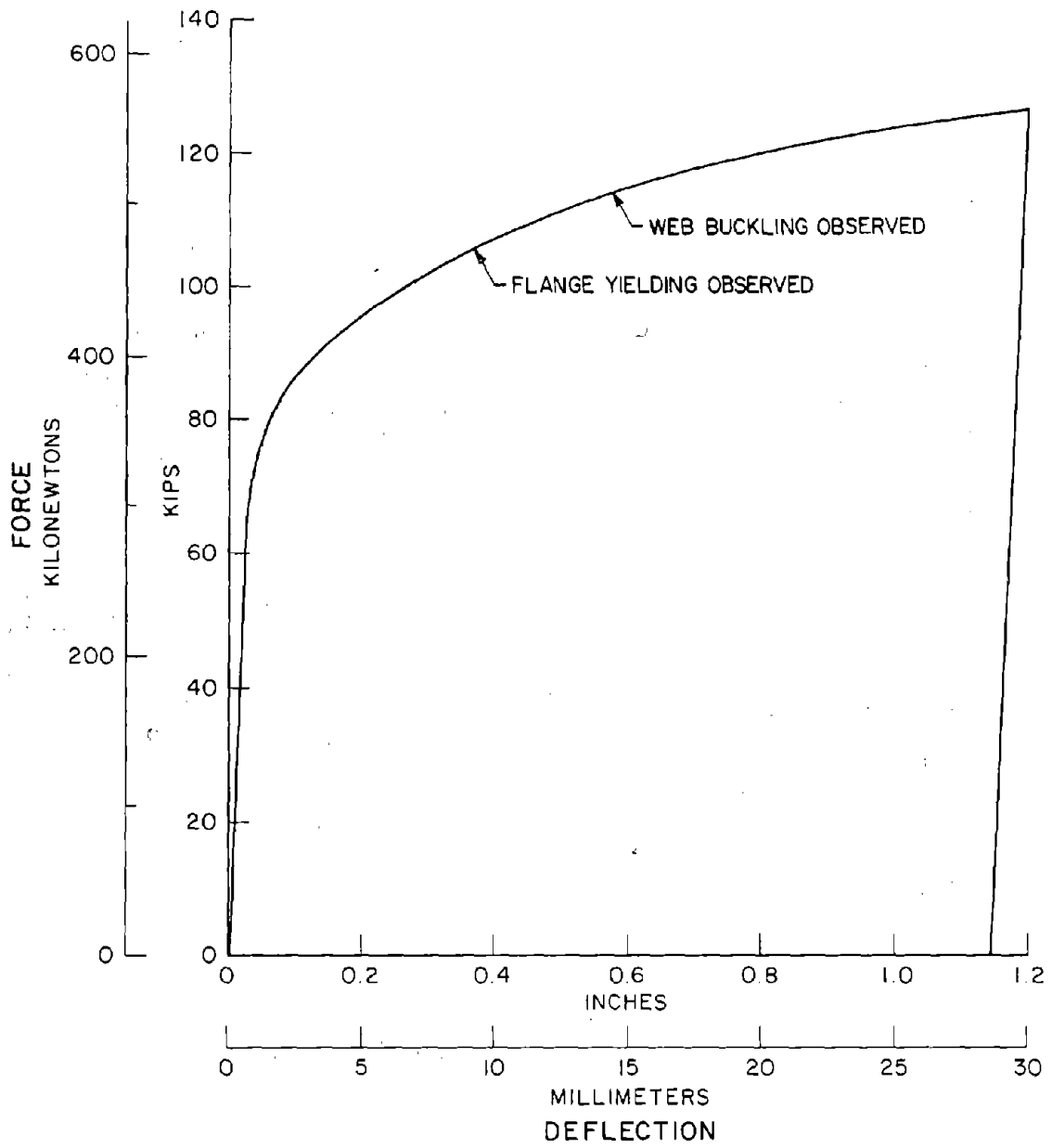


FIGURE 13 - FORCE-DISPLACEMENT RELATIONSHIP FOR MONOTONIC TEST

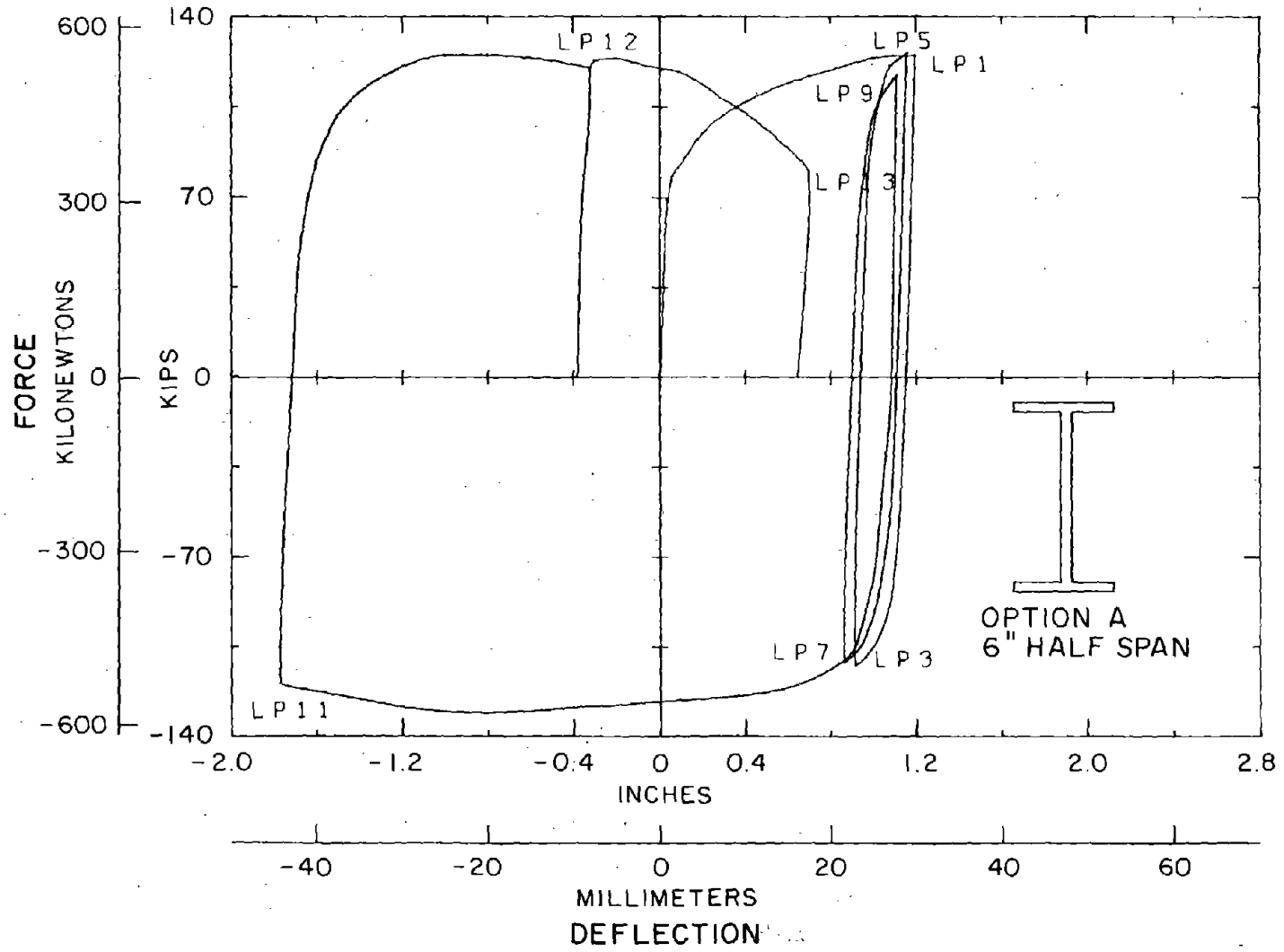


FIGURE 14 - CYCLIC FORCE - DEFLECTION BEHAVIOR OF SPECIMEN 1



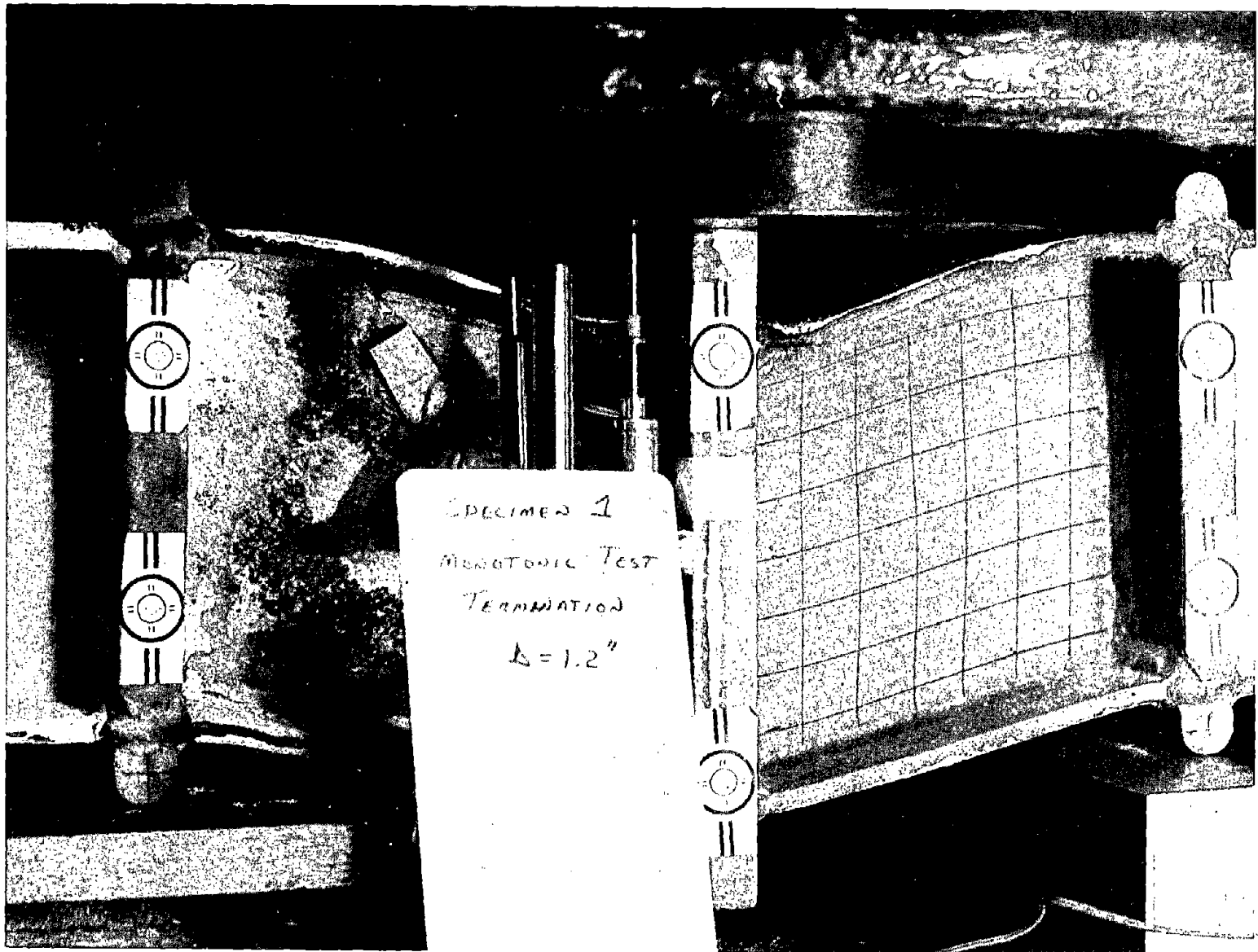


FIGURE 15 - PHOTOGRAPH OF THE PHOTOGRAMMETRIC GRID FOR SPECIMEN 1

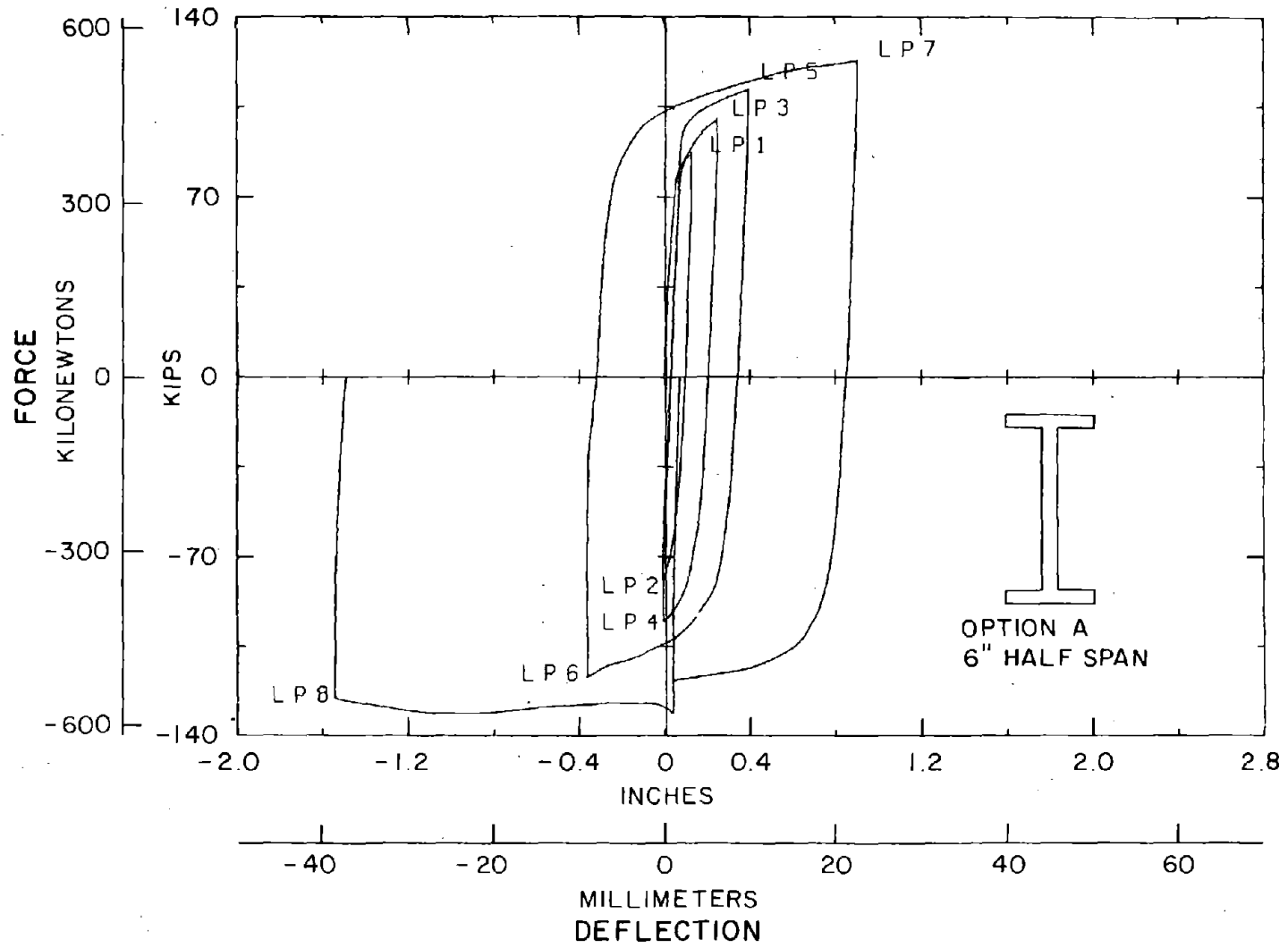


FIGURE 16 - CYCLIC FORCE - DEFLECTION BEHAVIOR OF SPECIMEN 2

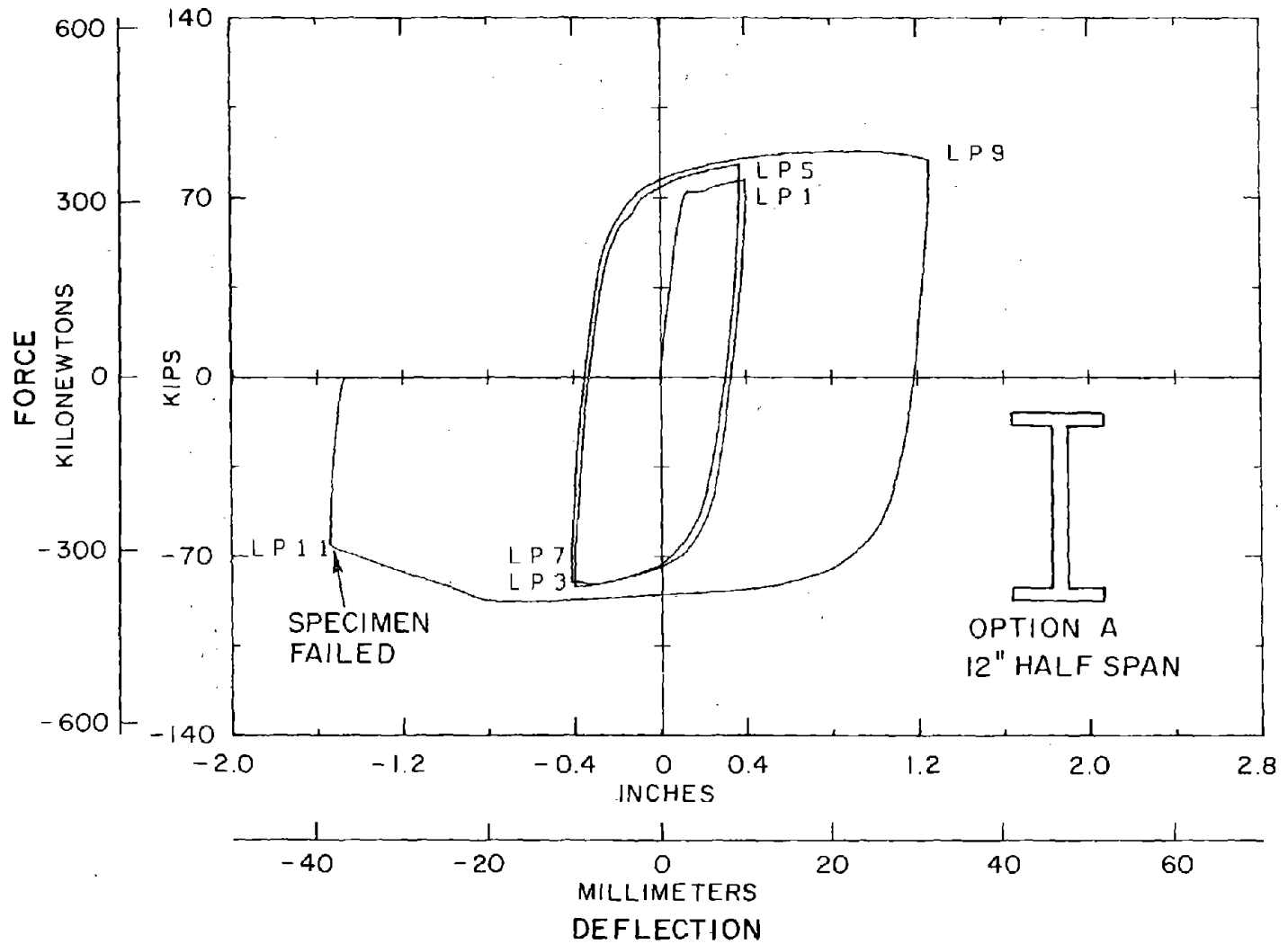


FIGURE 17 - CYCLIC FORCE - DEFLECTION BEHAVIOR OF SPECIMEN 3

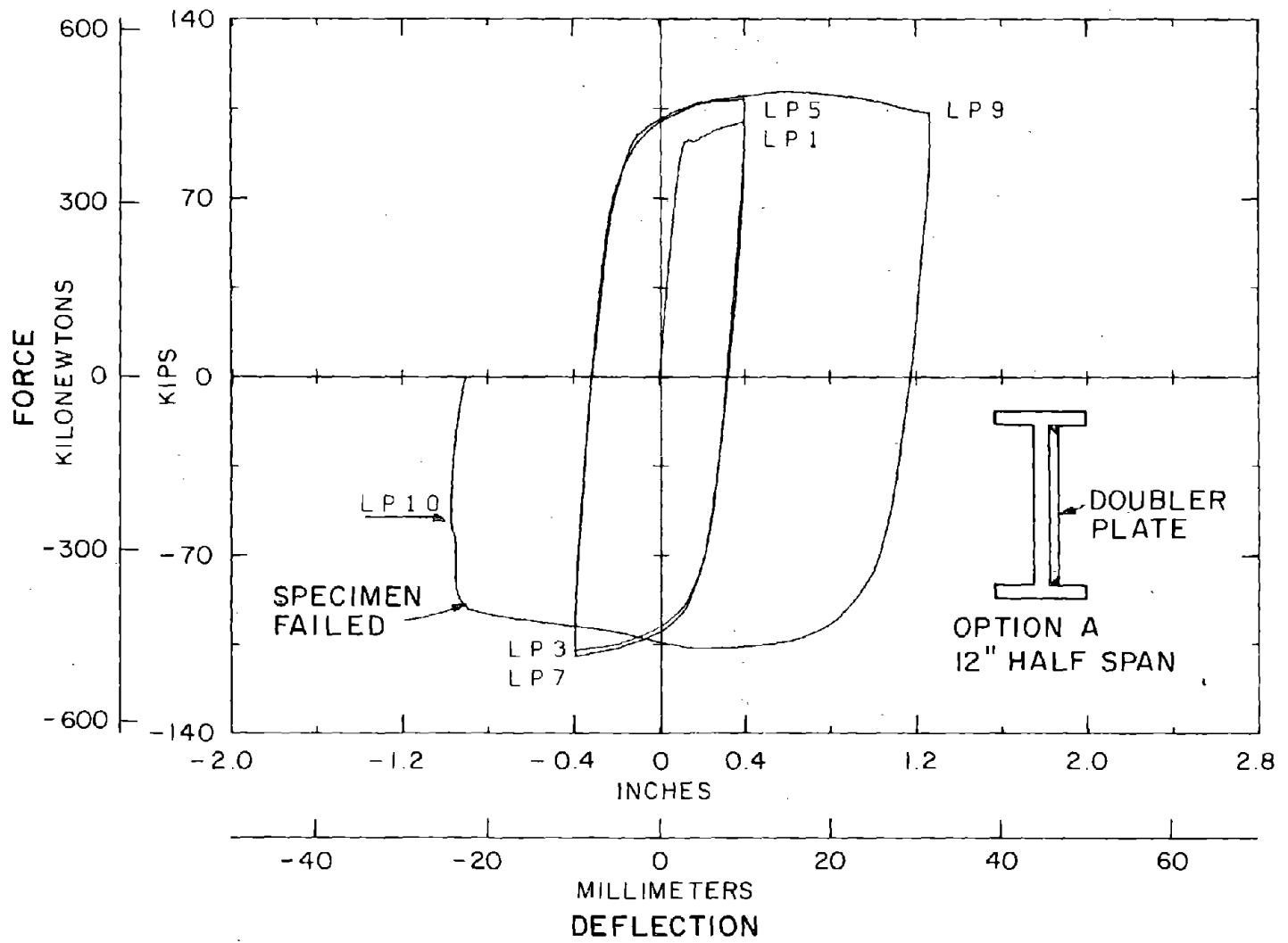


FIGURE 18 - CYCLIC FORCE - DEFLECTION BEHAVIOR OF SPECIMEN 4

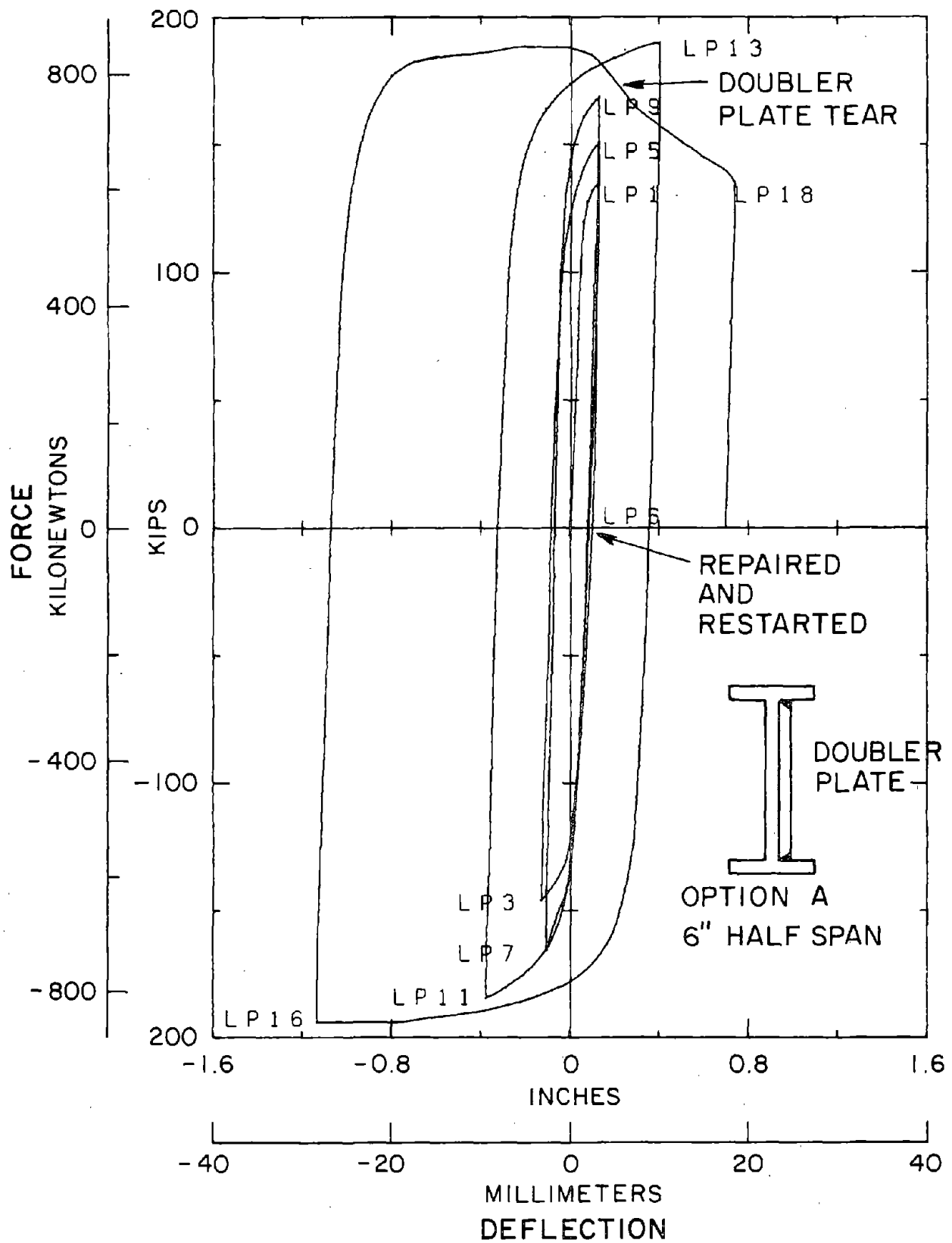
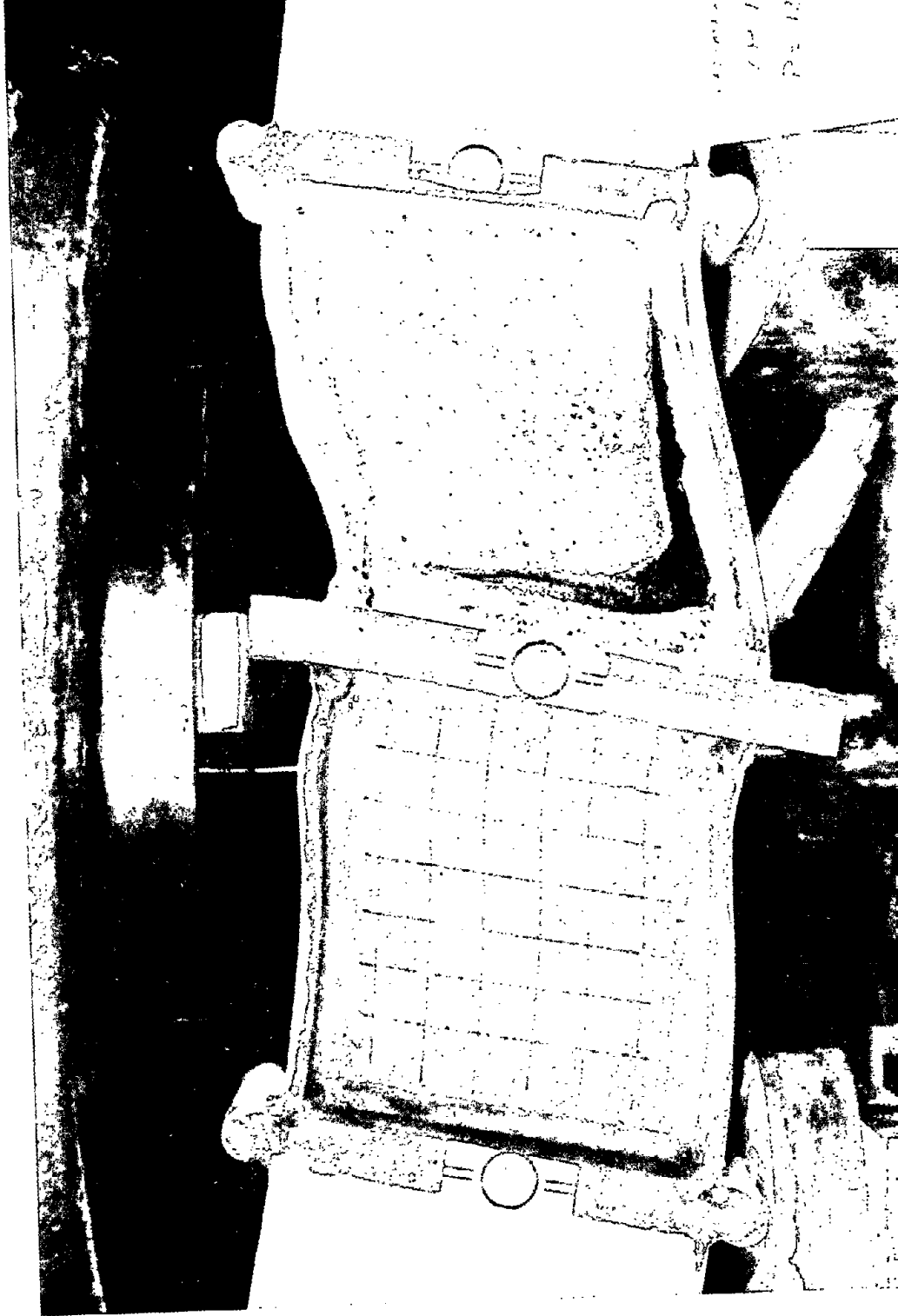


FIGURE 19 - CYCLIC FORCE - DEFLECTION BEHAVIOR OF SPECIMEN 5



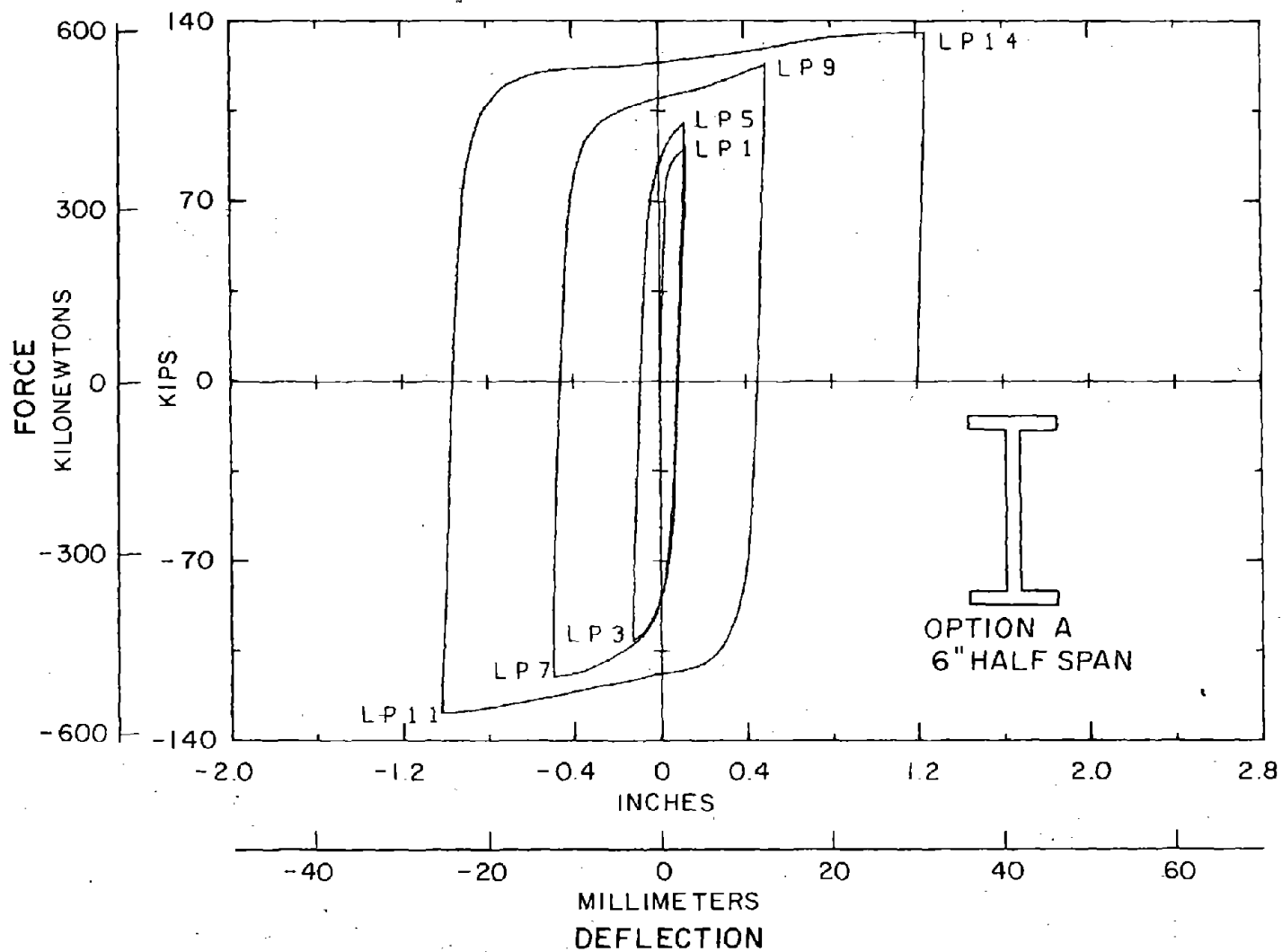


FIGURE 21 - CYCLIC FORCE - DEFLECTION BEHAVIOR IN SPECIMEN 6

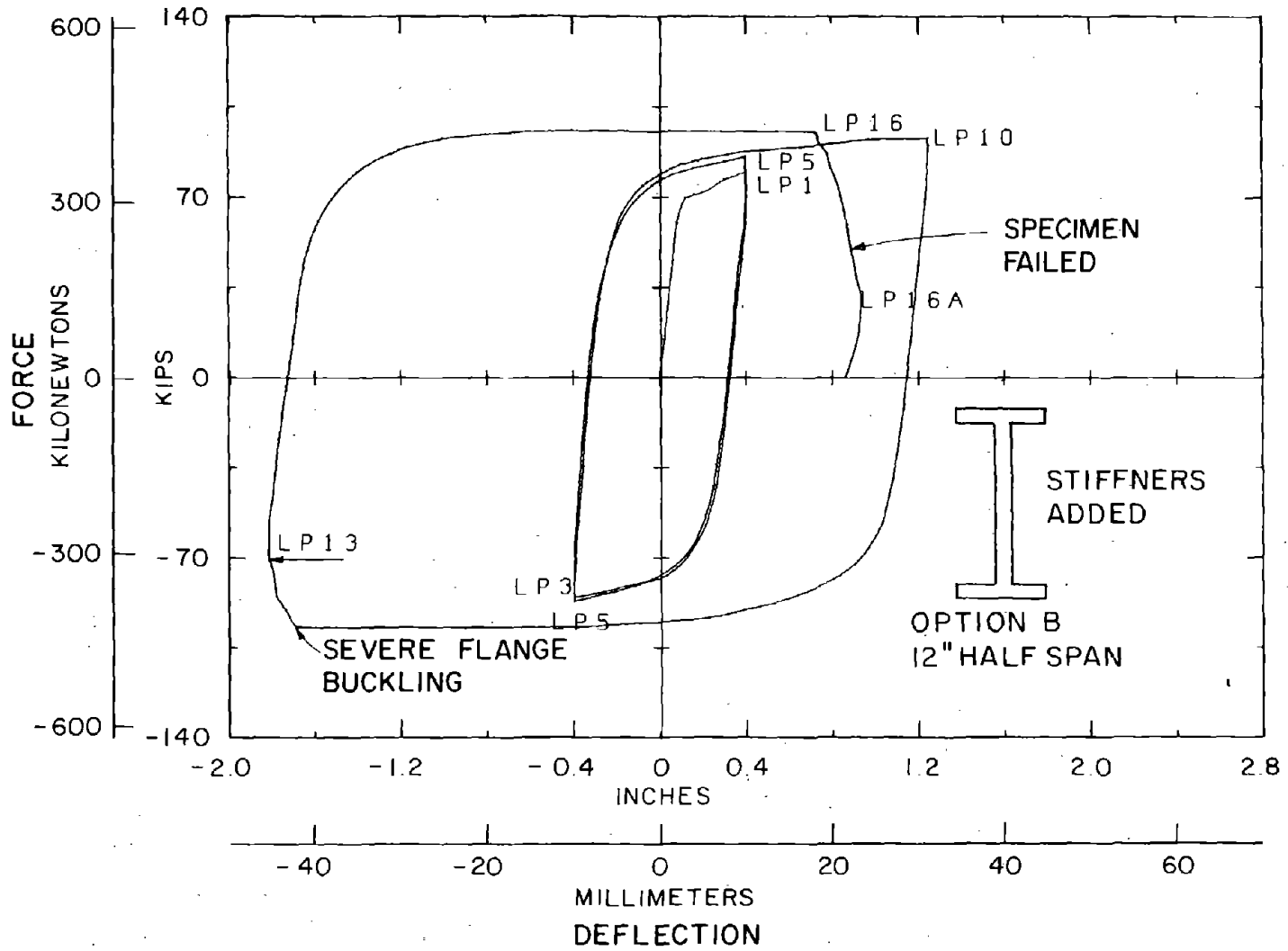


FIGURE 22 - CYCLIC FORCE - DEFLECTION BEHAVIOR OF SPECIMEN 7



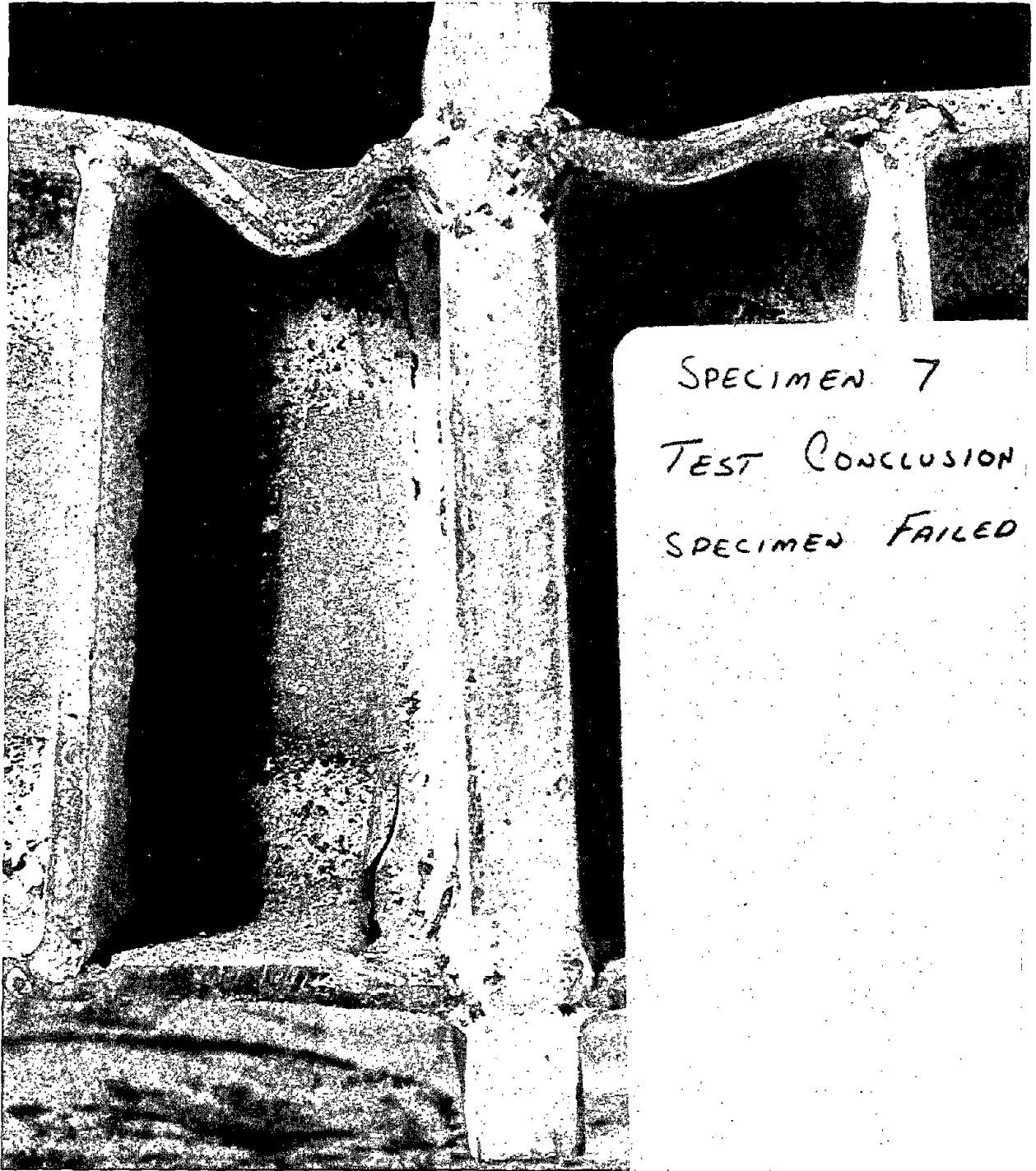


FIGURE 23 - PHOTOGRAPH OF THE FAILURE IN SPECIMEN 7

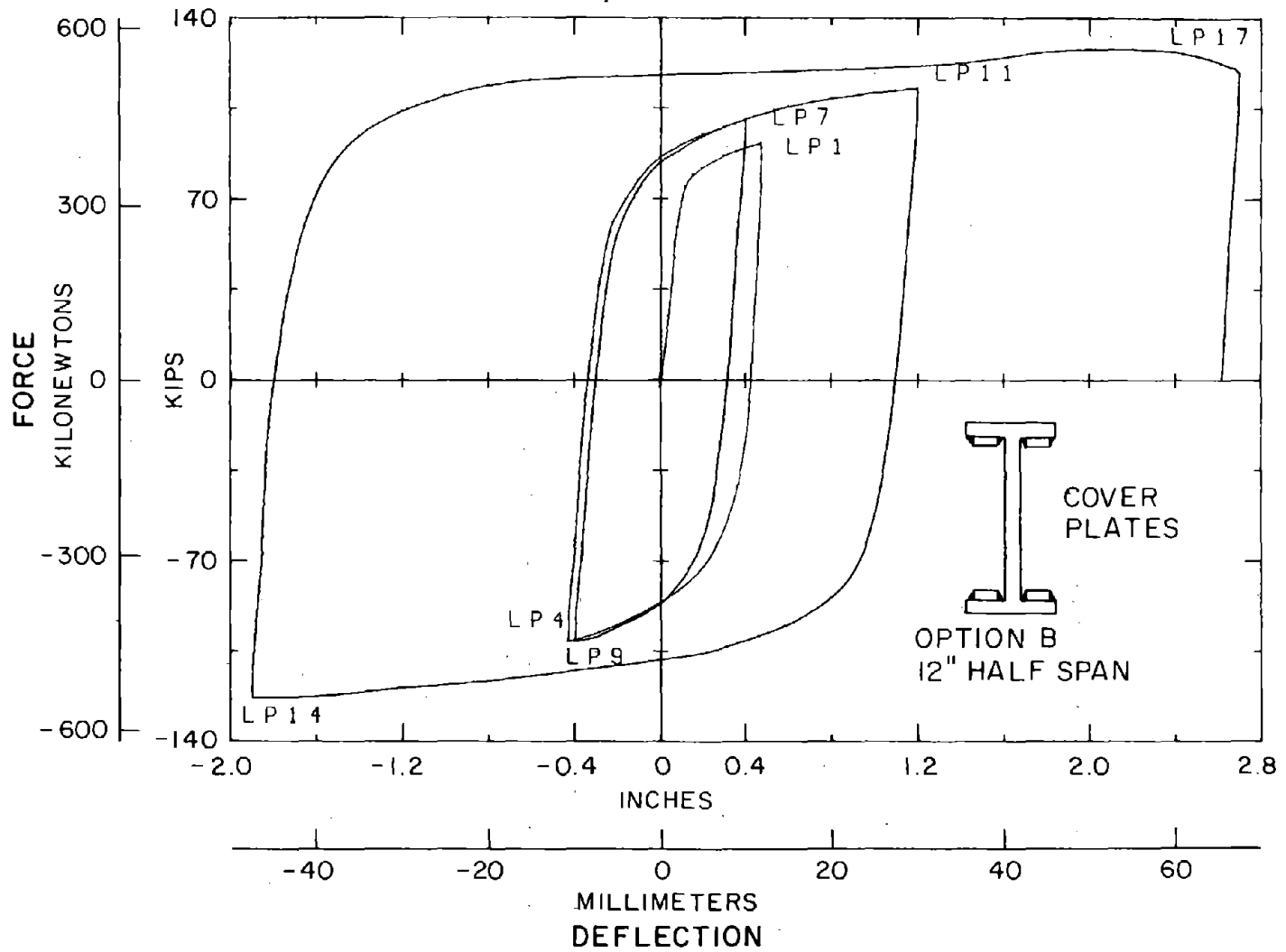


FIGURE 24 - CYCLIC FORCE - DEFLECTION BEHAVIOR IN SPECIMEN 8

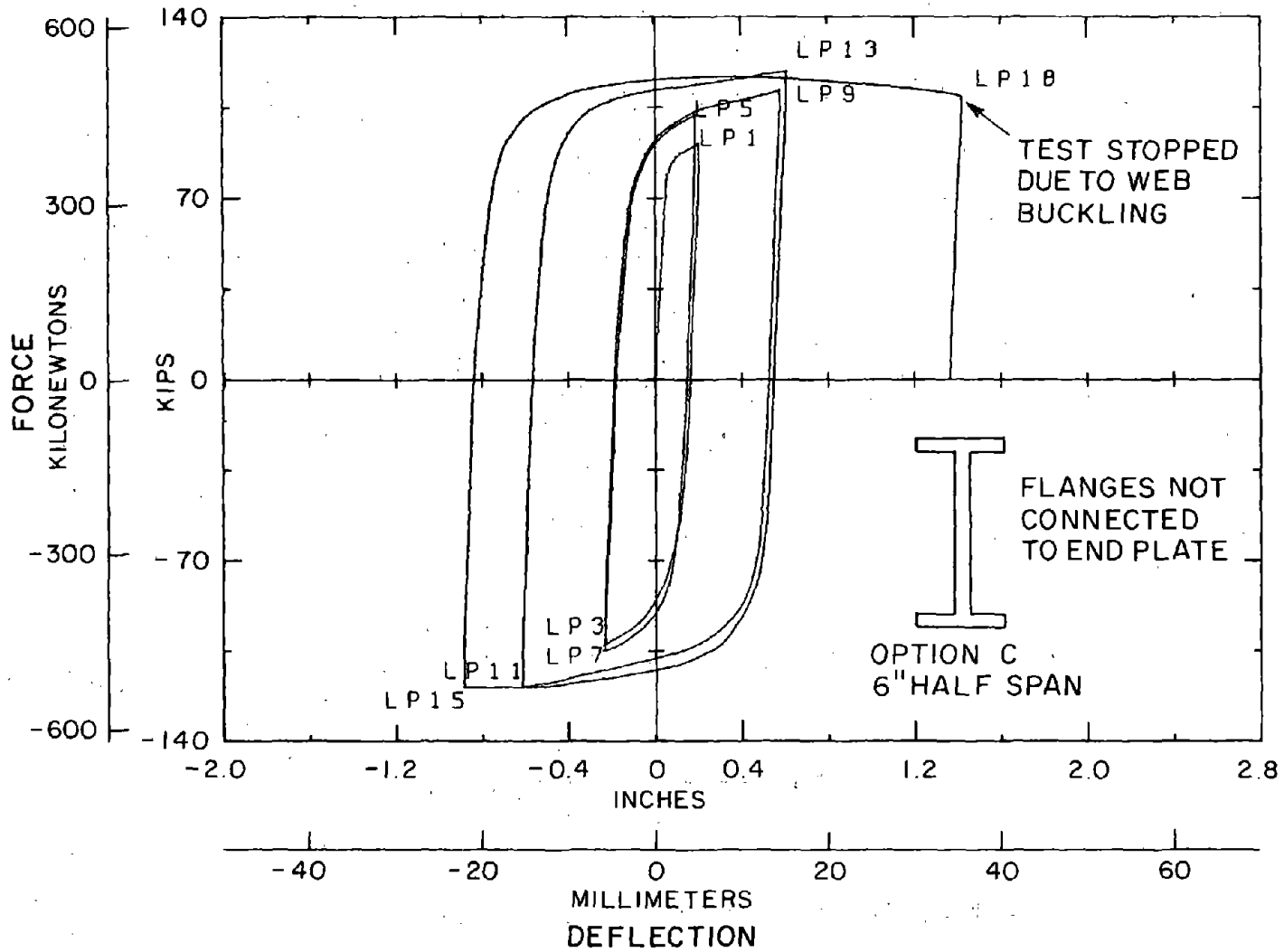


FIGURE 25 - CYCLIC FORCE - DEFLECTION BEHAVIOR OF SPECIMEN 9

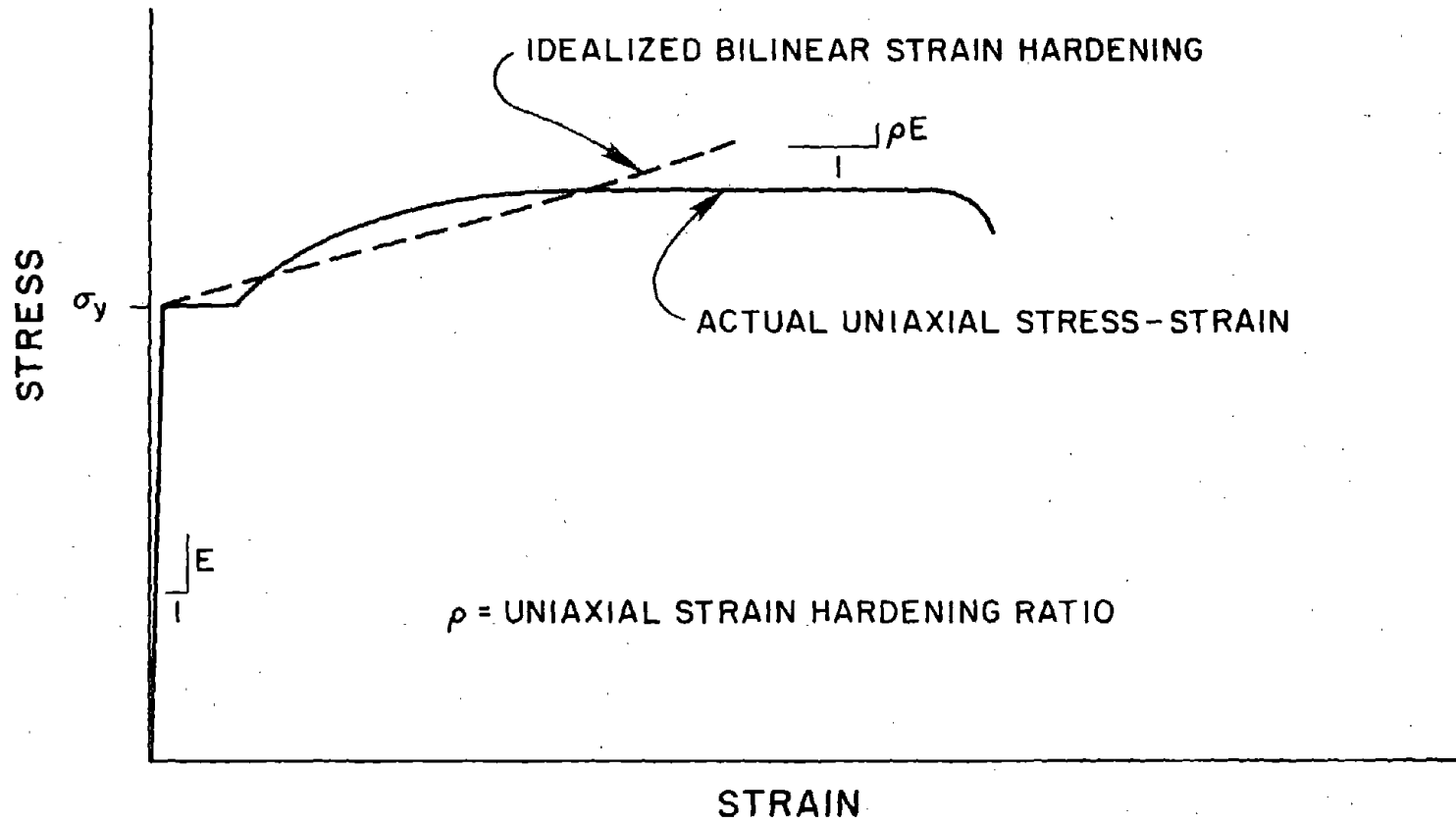
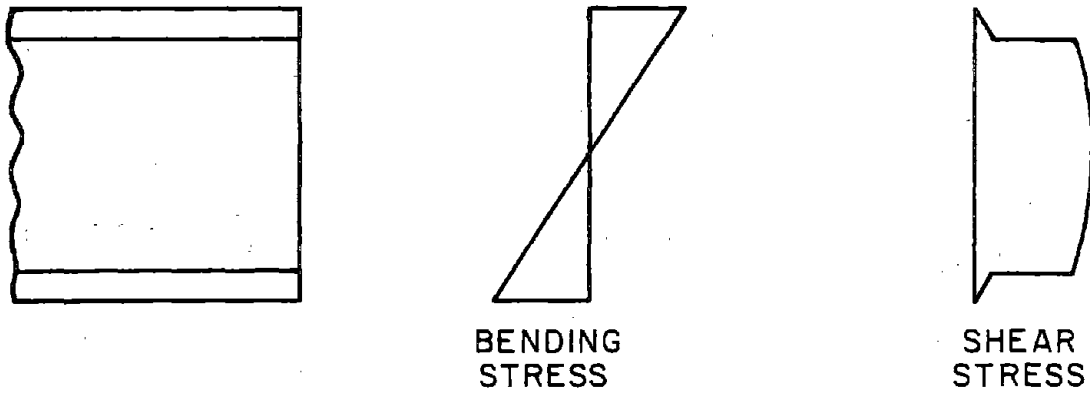
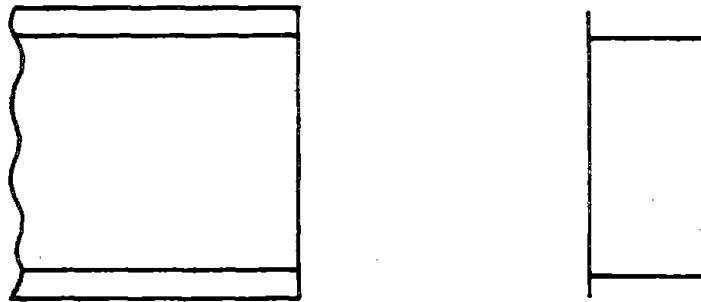


FIGURE 26 - IDEALIZED BI-LINEAR STRESS - STRAIN DIAGRAM FOR STEEL



(a) ELASTIC STRESS DISTRIBUTION FOR WF BEAM WITH PLANE SECTIONS REMAINING PLANE



(b) APPROXIMATE SHEAR STRESS DISTRIBUTION



(c) CROSSSECTIONAL WARPING DUE TO HIGH SHEAR STRESS IN WEB

FIGURE 27 - SHEAR STRESS DISTRIBUTION AND CROSS-SECTIONAL WARPING DUE TO SHEAR DEFORMATION IN A WIDE FLANGE SECTION

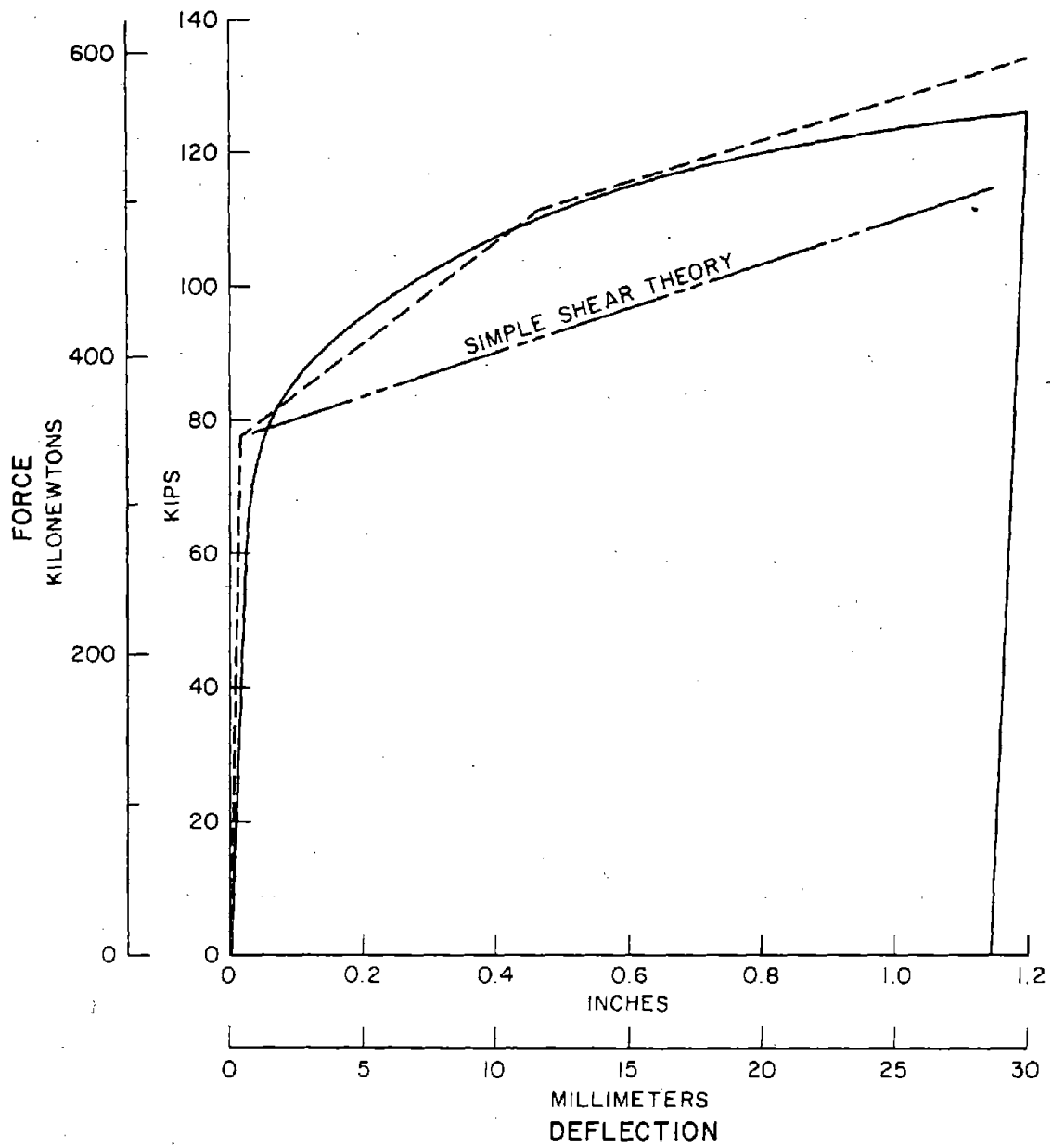
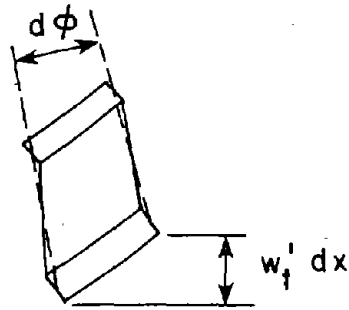
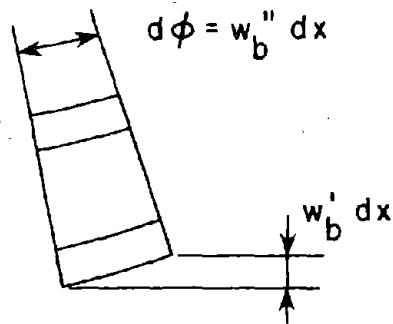


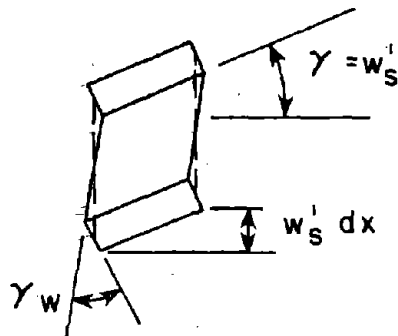
FIGURE 28 - COMPARISON OF THE SHEAR YIELD THEORIES WITH EXPERIMENTAL DATA



(a) TOTAL DEFORMATION



(b) BENDING DEFORMATION



(c) SHEAR DEFORMATION

FIGURE 29 - COMPONENTS OF DEFLECTION OF A SANDWICH BEAM ELEMENT

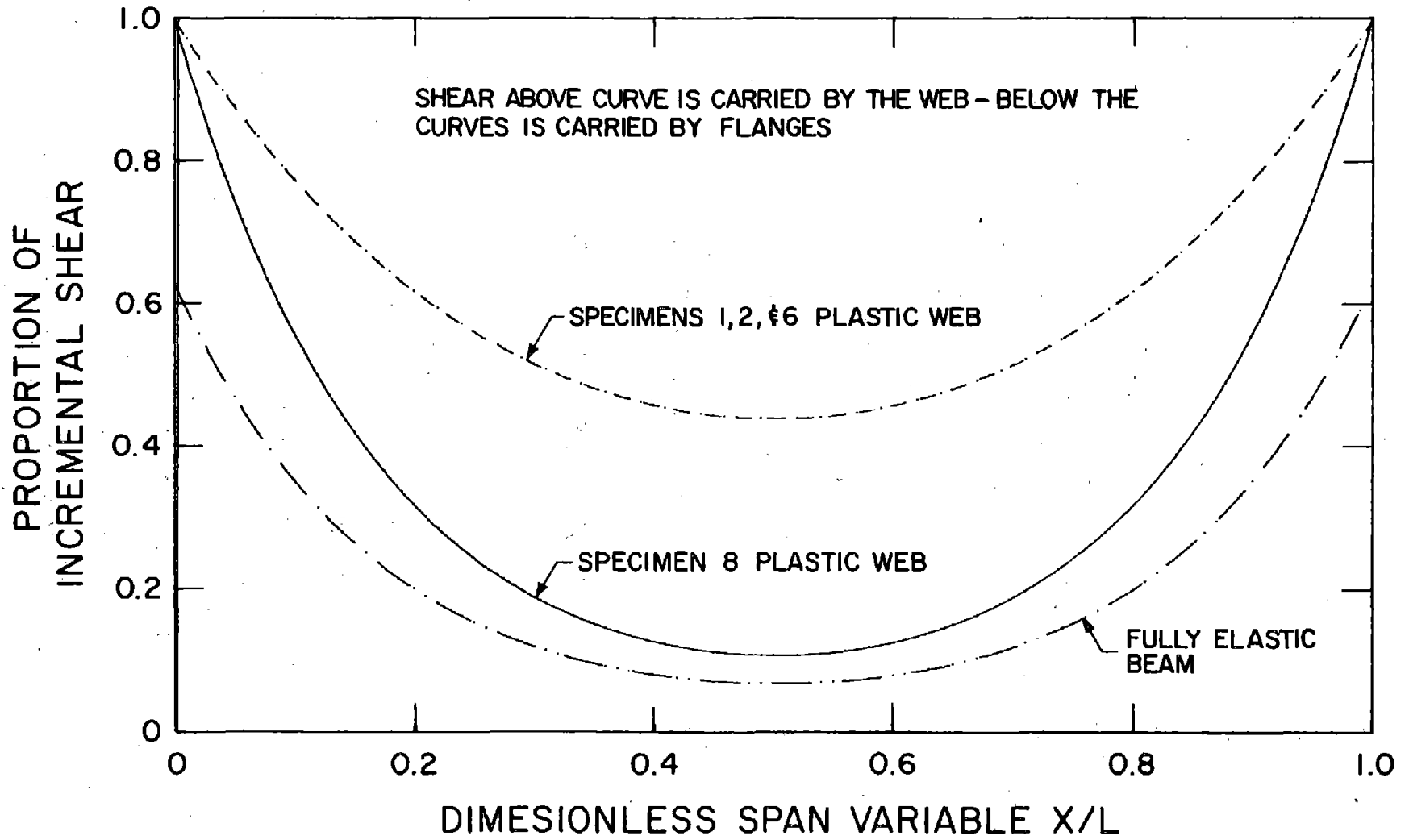


FIGURE 30 - PROPORTION OF INCREMENTAL SHEAR CARRIED BY THE WEB AND FLANGES



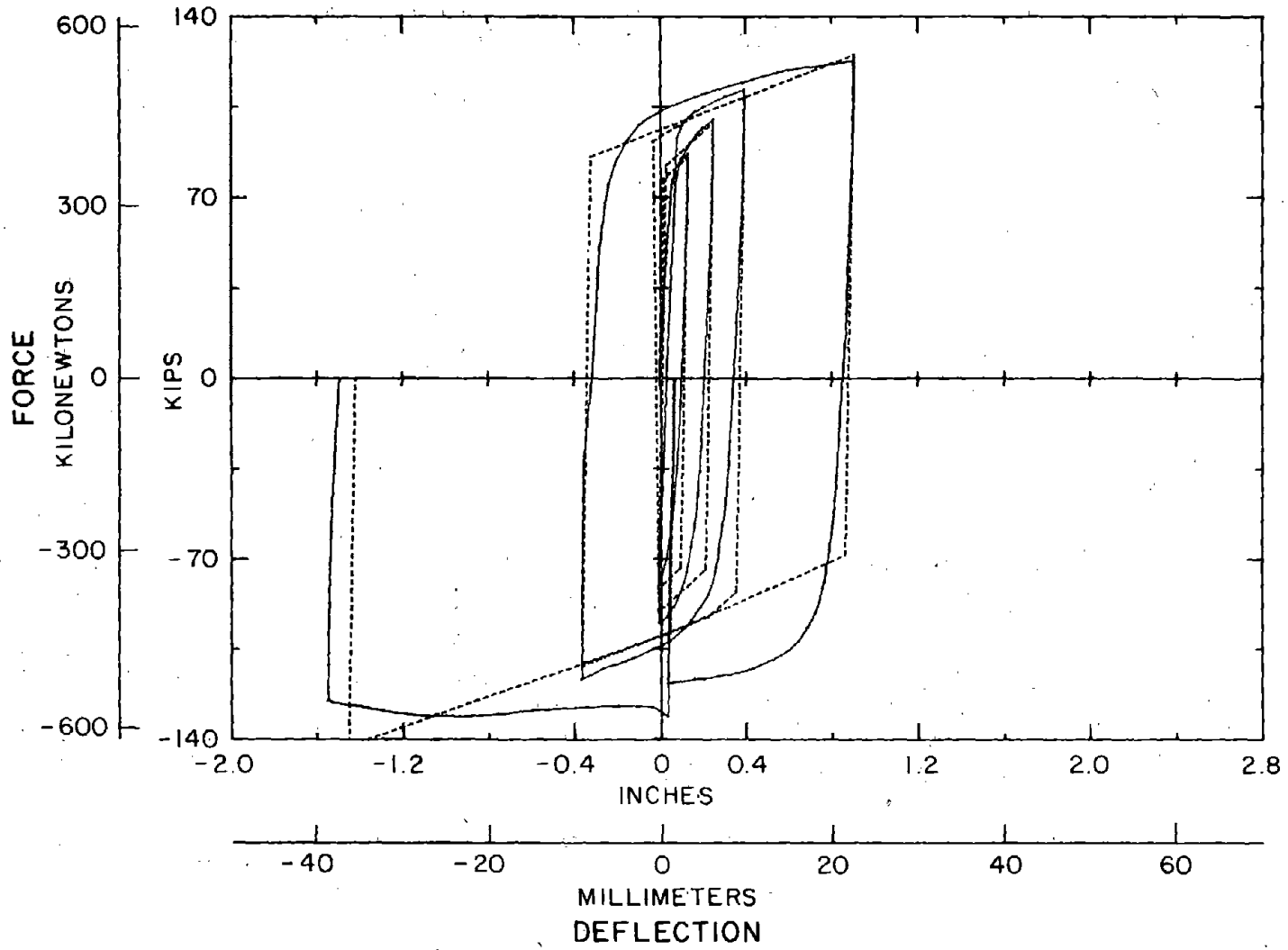


FIGURE 31 - COMPARISON OF THE CYCLIC SHEAR YIELD MODEL WITH TEST SPECIMEN 2

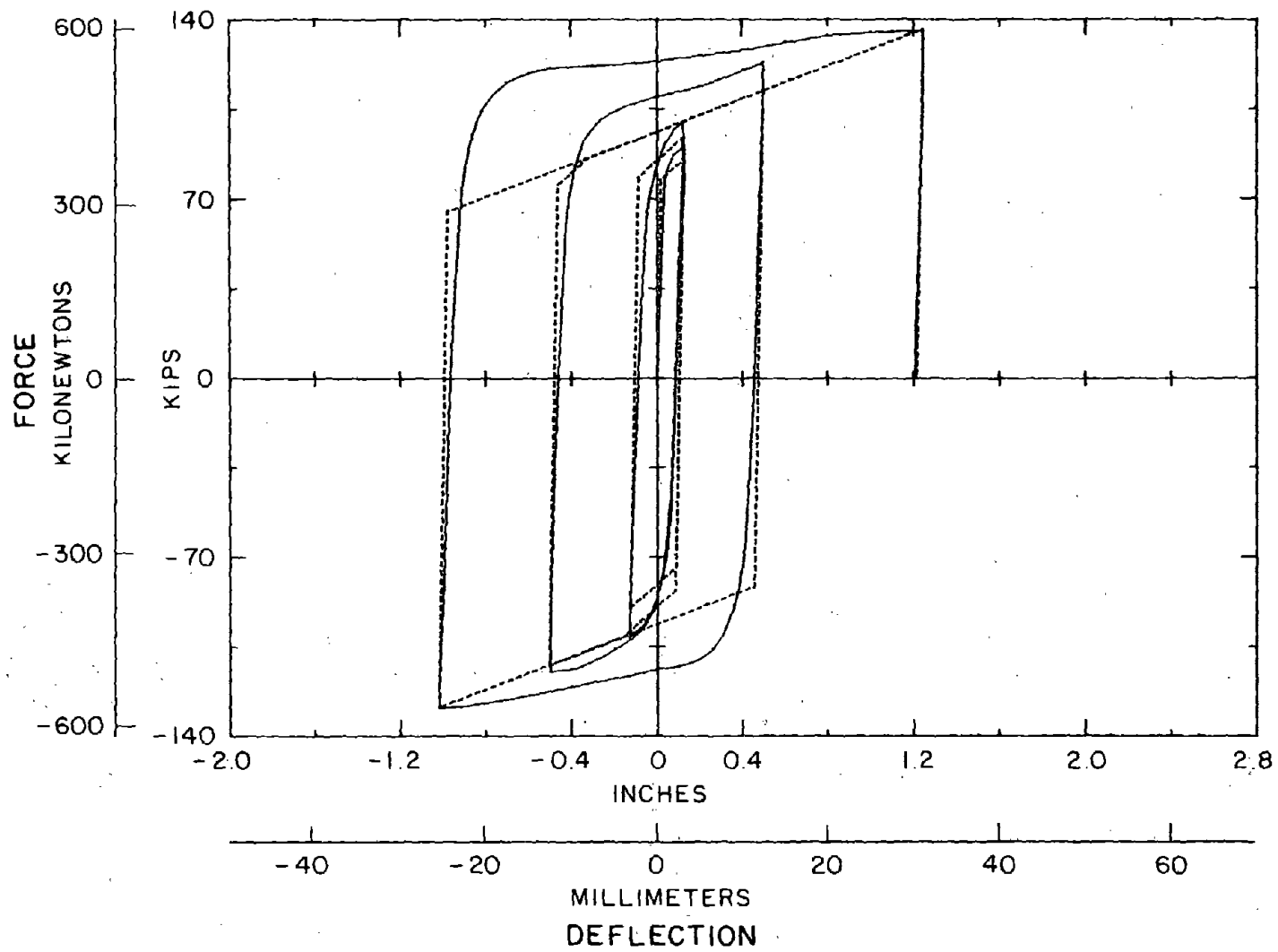


FIGURE 32 - COMPARISON OF THE CYCLIC SHEAR YIELD MODEL WITH TEST SPECIMEN 6

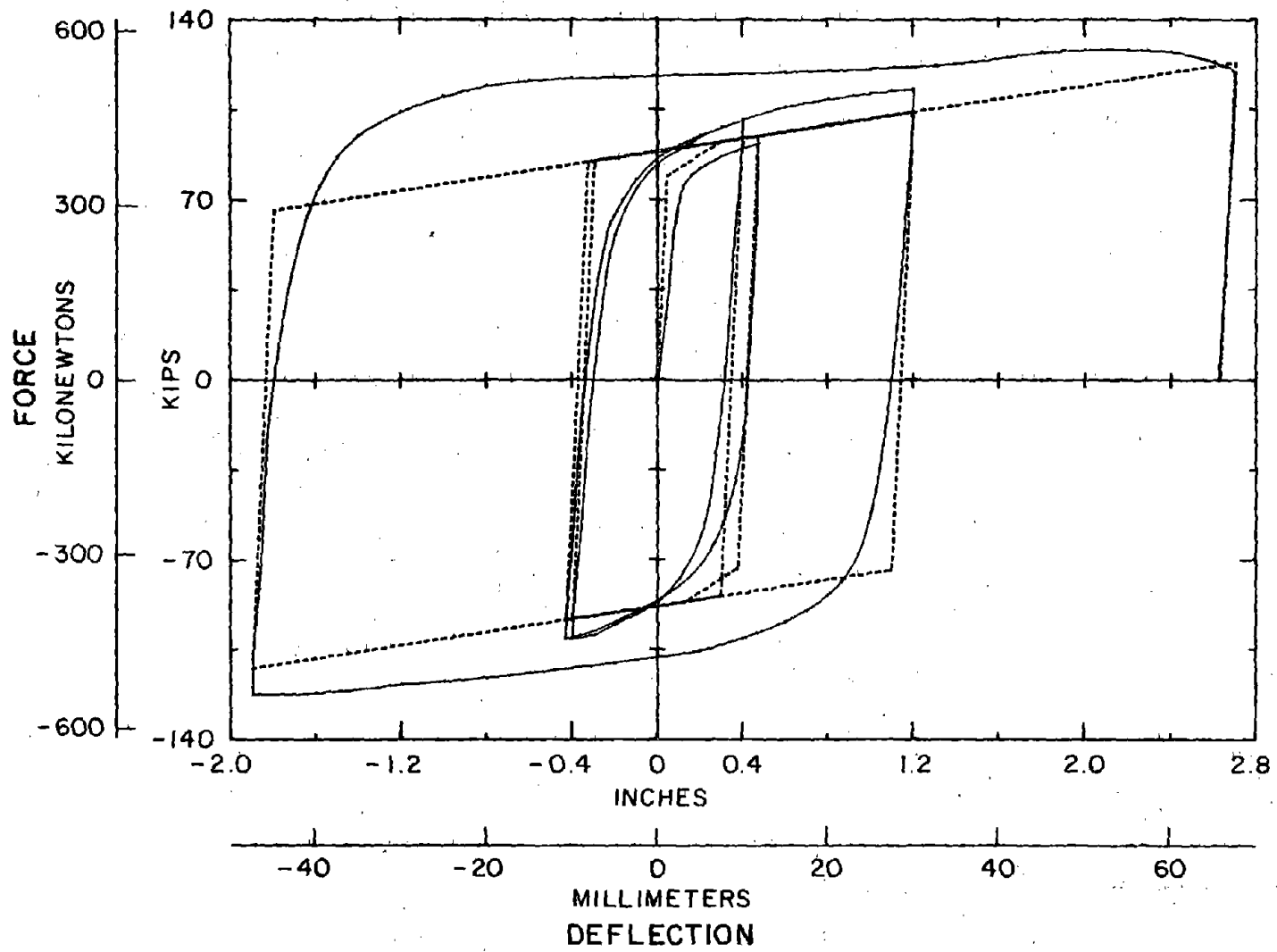


FIGURE 33 - COMPARISON OF THE CYCLIC SHEAR YIELD MODEL WITH TEST SPECIMEN 8

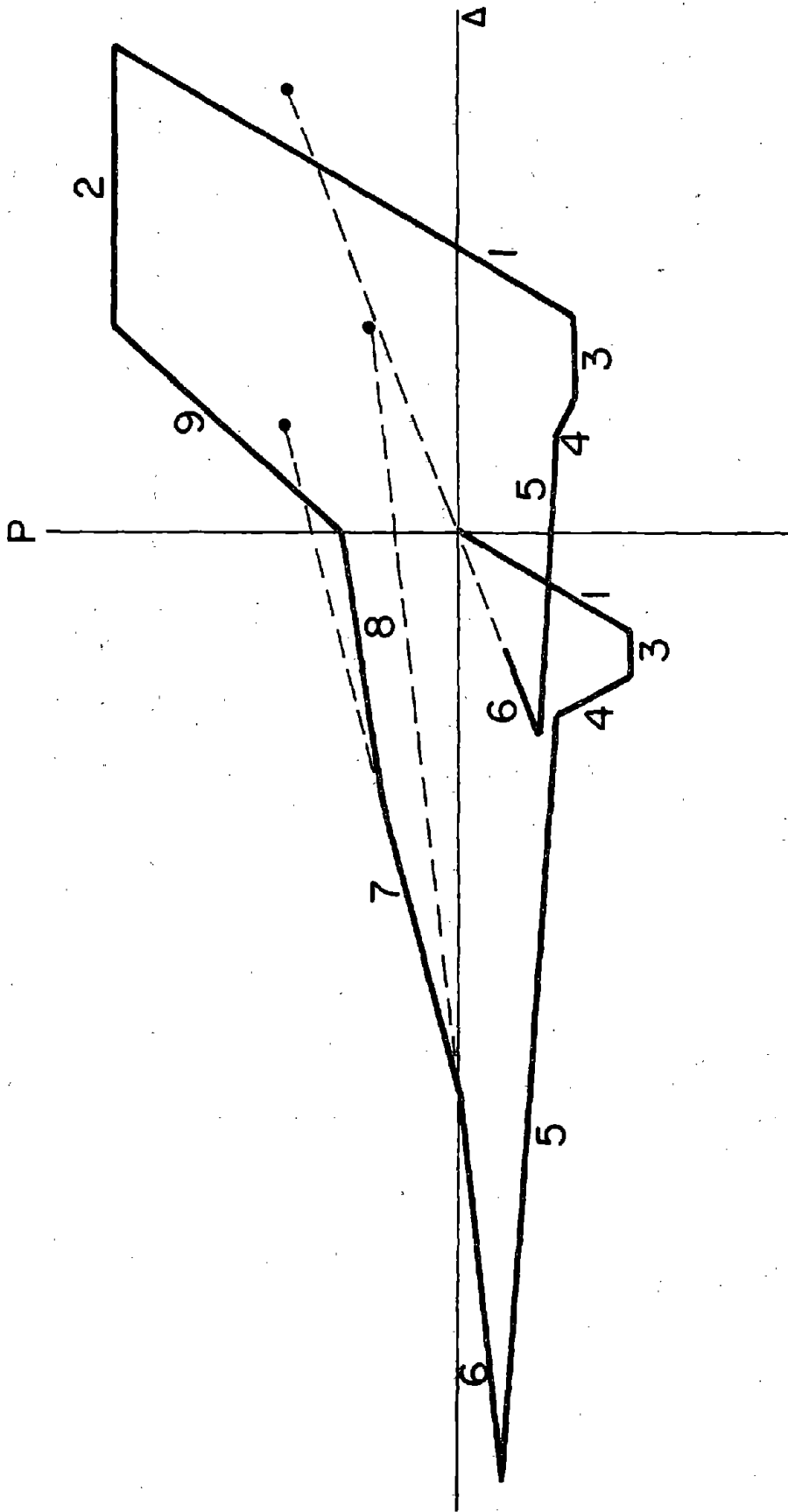


FIGURE 34 - LINEAR APPROXIMATION OF THE POST-BUCKLING BRACE BEHAVIOR

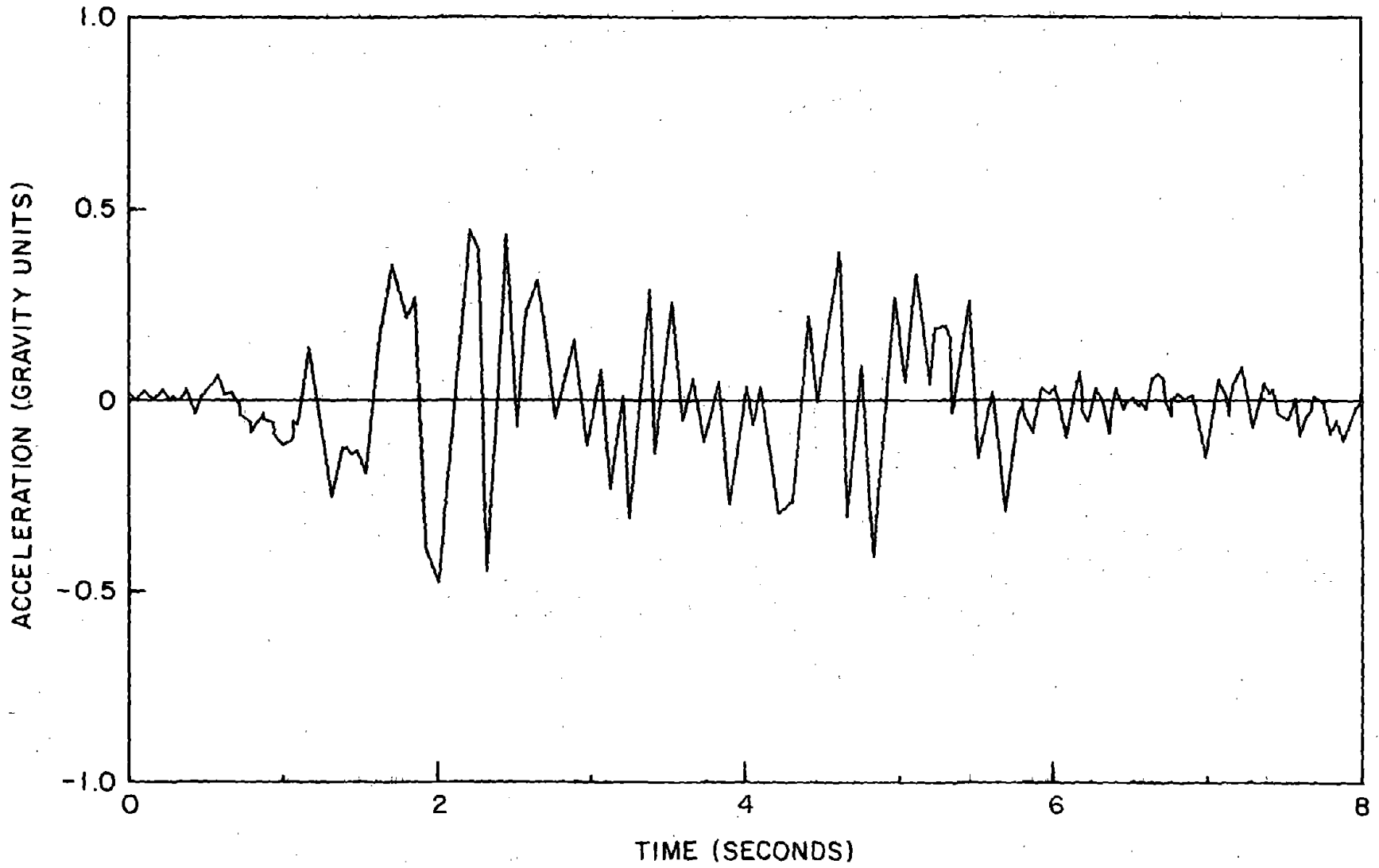


FIGURE 35 - ACCELERATION RECORD FOR 1.5 TIMES EL CENTRO N-S COMPONENT 1940

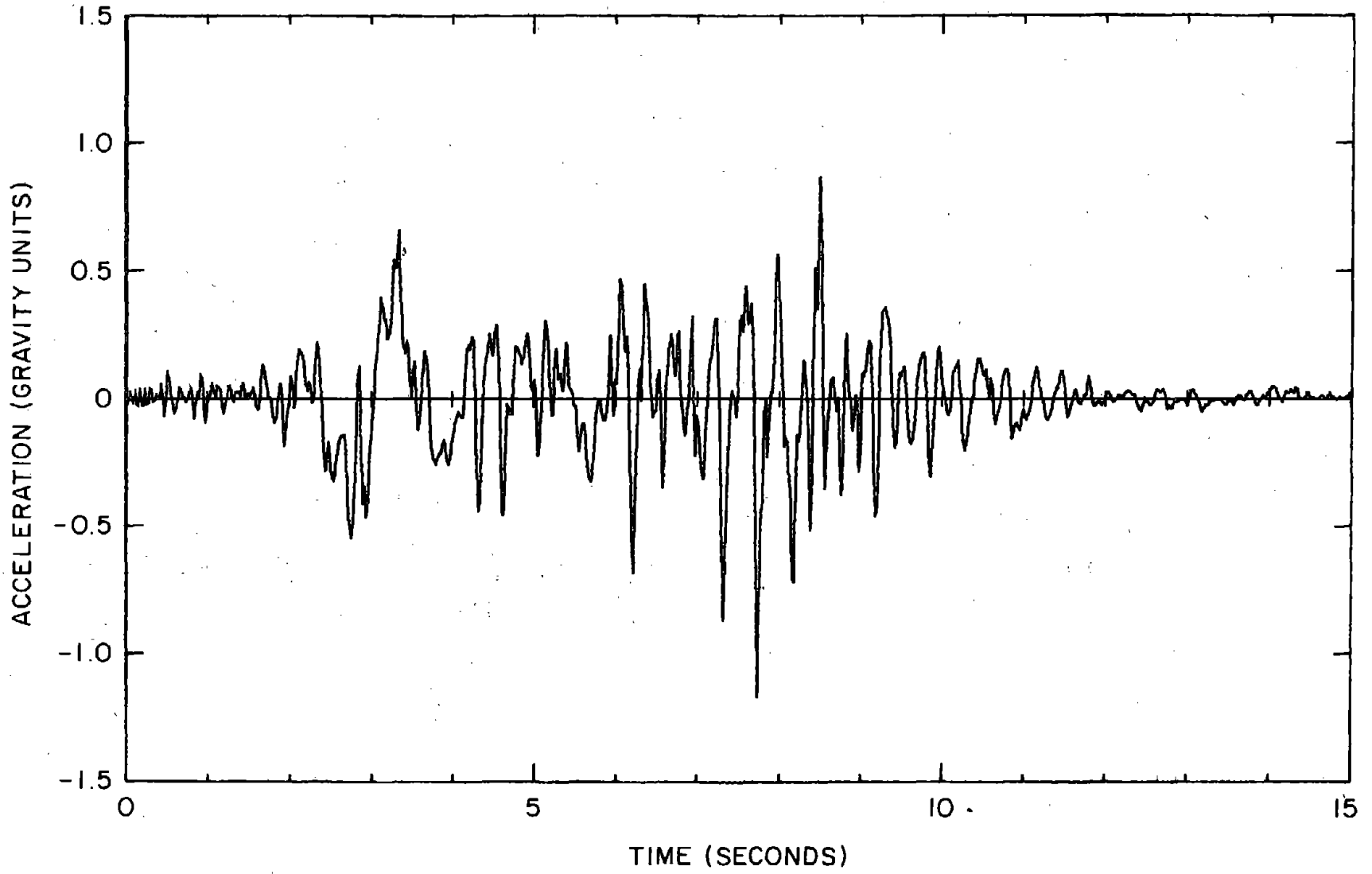


FIGURE 36 - ACCELERATION RECORD FOR PACOIMA DAM 1971

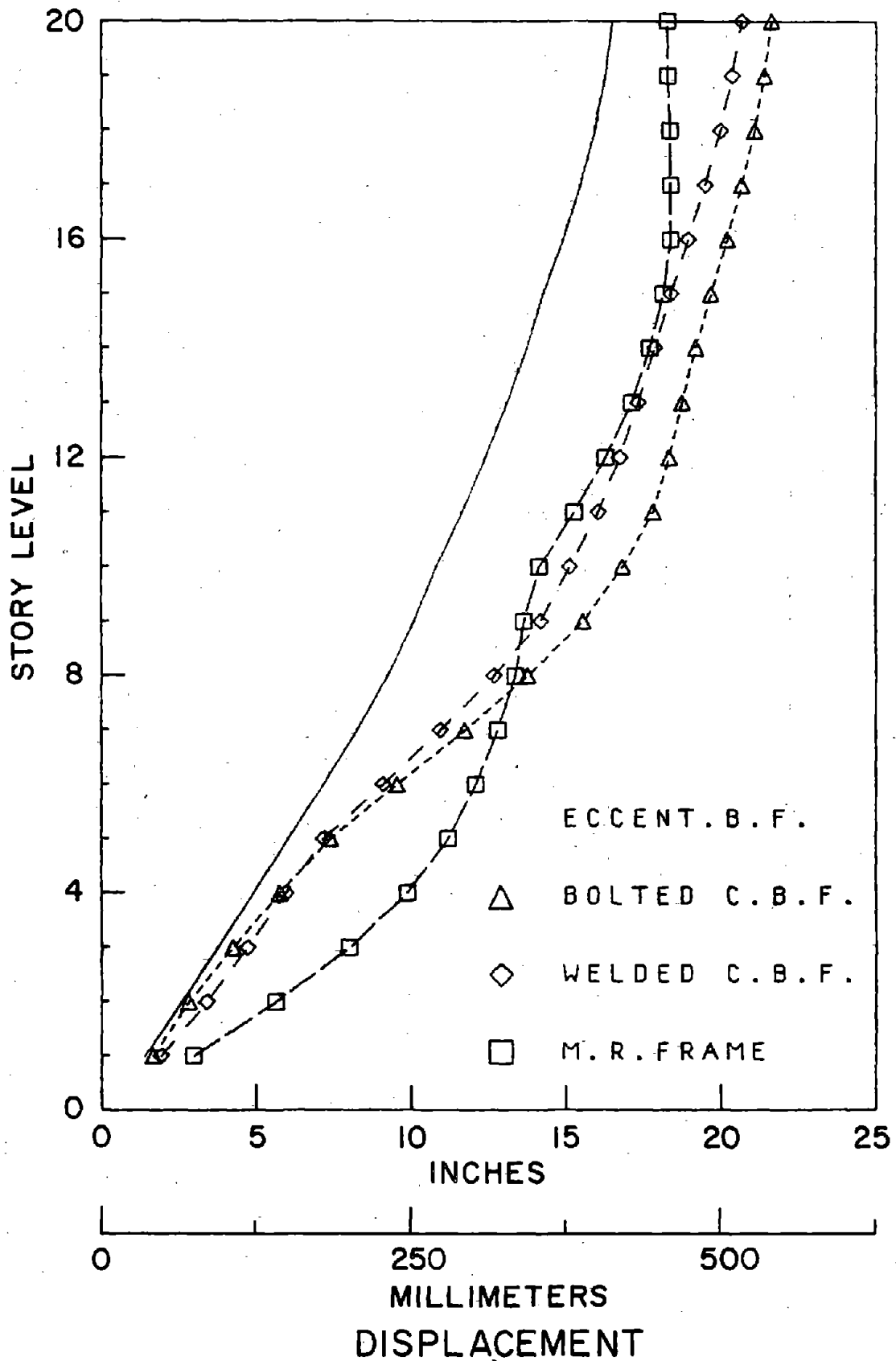


FIGURE 37 - MAXIMUM RELATIVE DISPLACEMENT DUE TO THE 1.5 TIMES EL CENTRO BASE EXCITATION

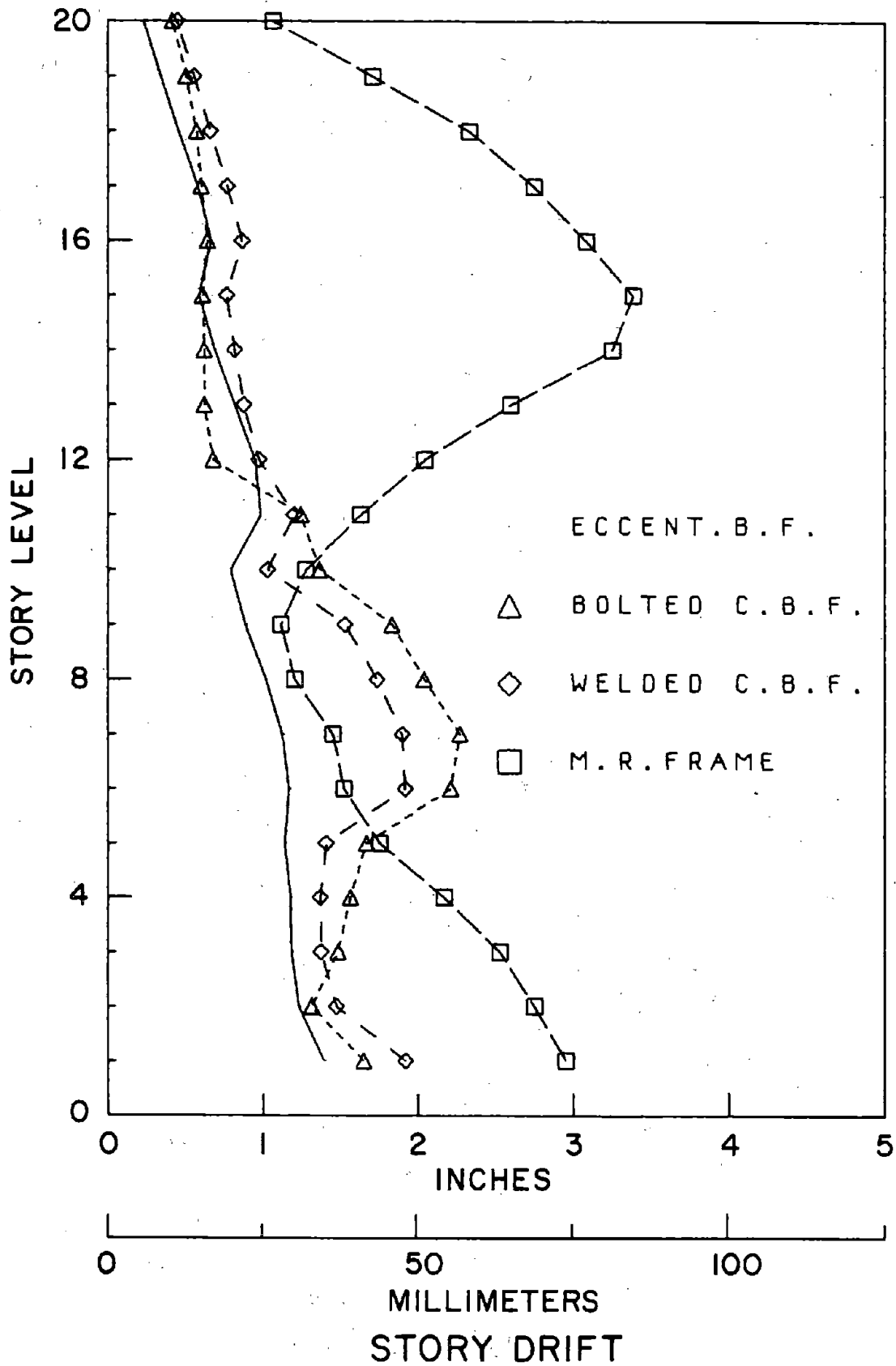


FIGURE 38 - MAXIMUM STORY DRIFT DUE TO 1.5 TIMES EL CENTRO EXCITATION



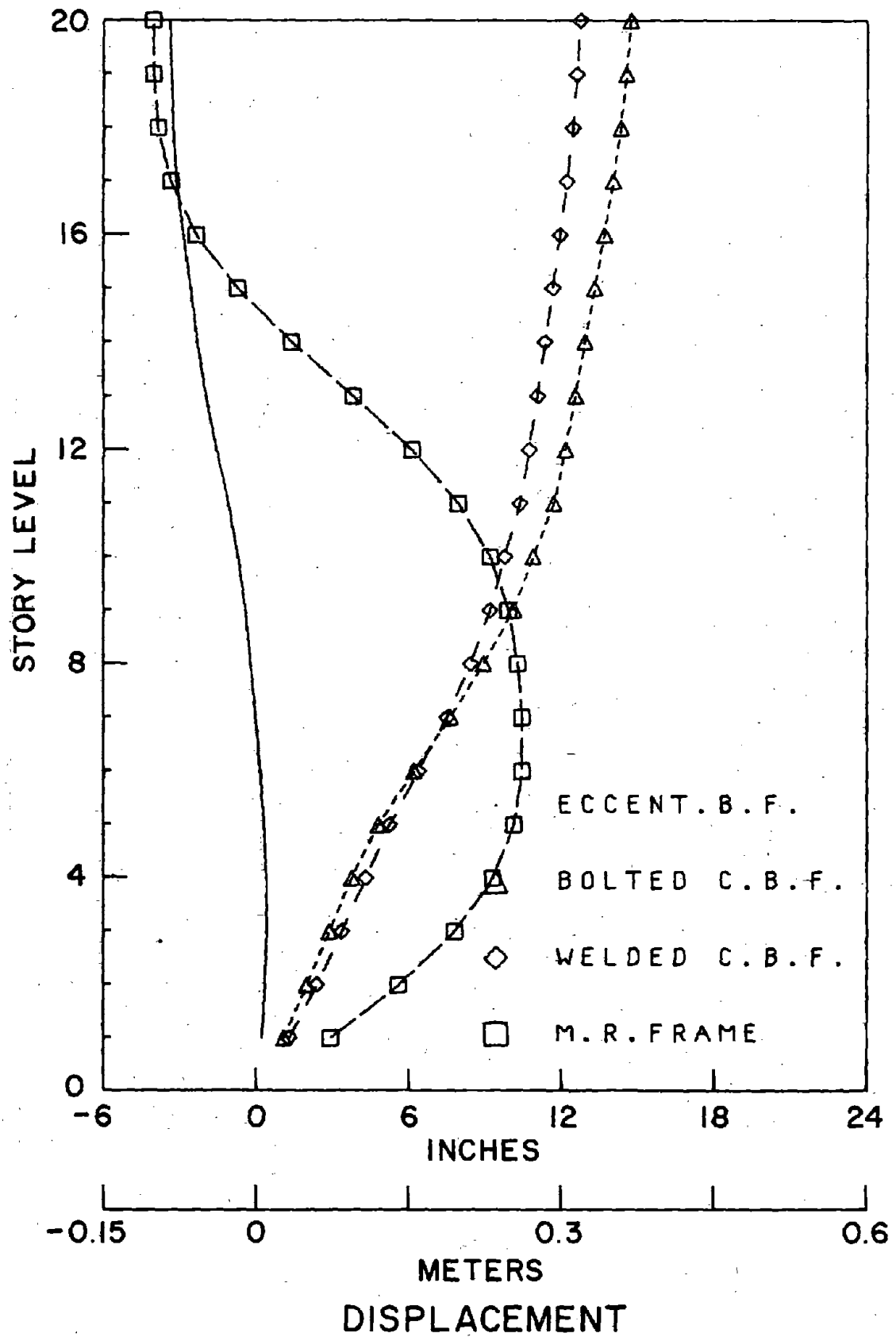


FIGURE 39 - DEFLECTED SHAPE AT THE END OF 8.0 SECONDS OF THE 1.5 TIMES EL CENTRO EXCITATION

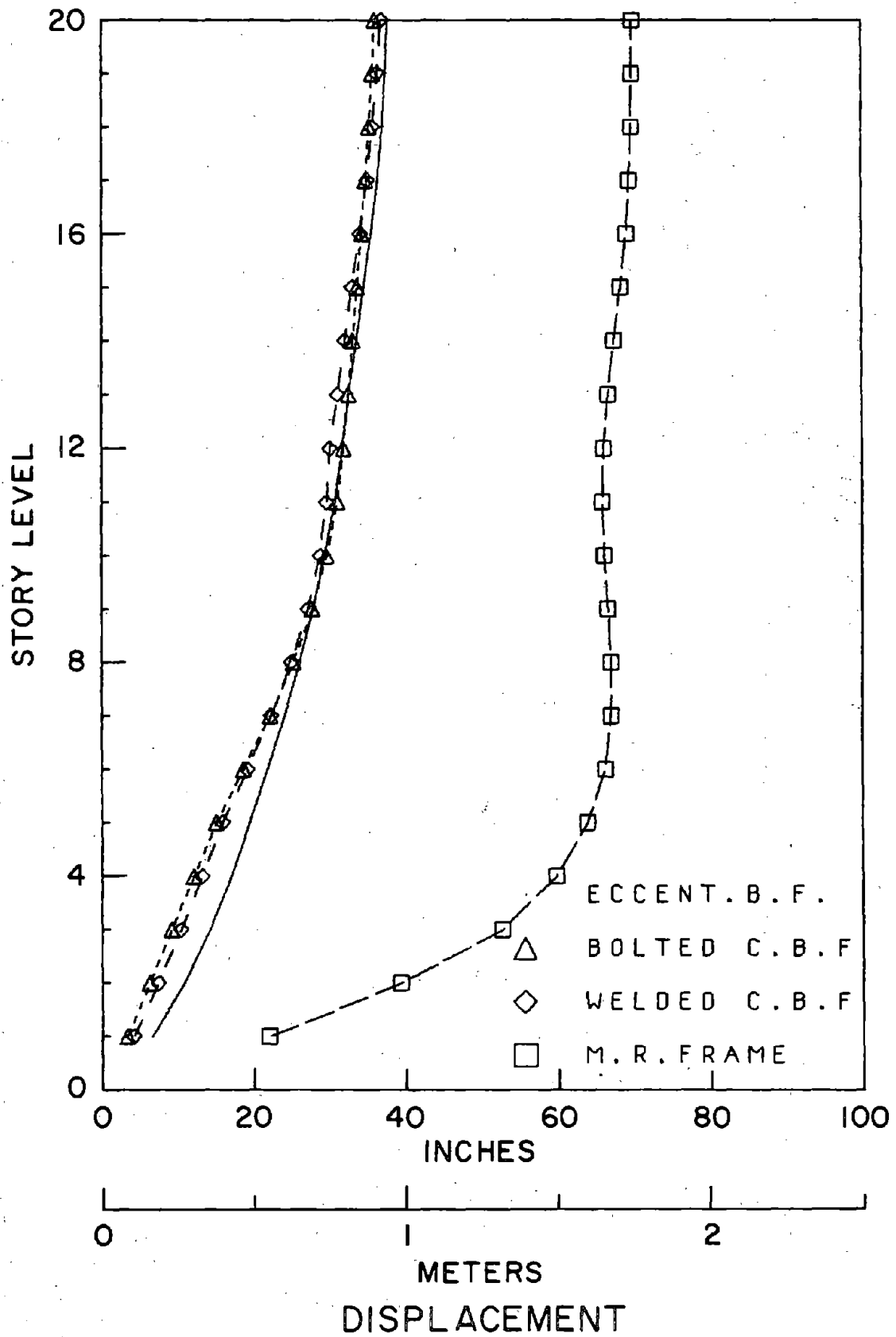


FIGURE 40 - MAXIMUM RELATIVE DISPLACEMENT DUE TO THE PACOIMA DAM EXCITATION

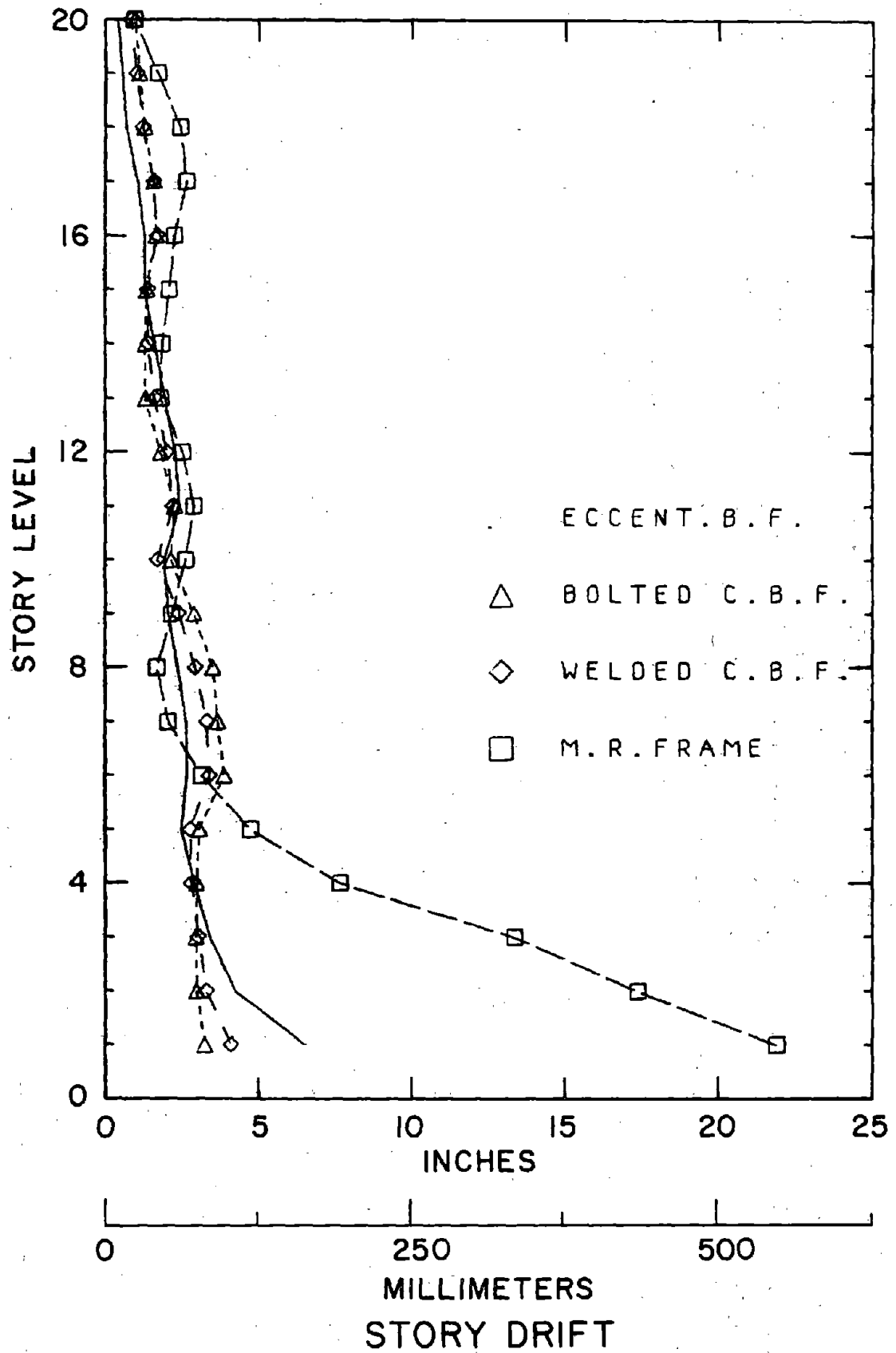


FIGURE 41 - MAXIMUM STORY DRIFT DUE TO THE PACOIMA DAM EXCITATION

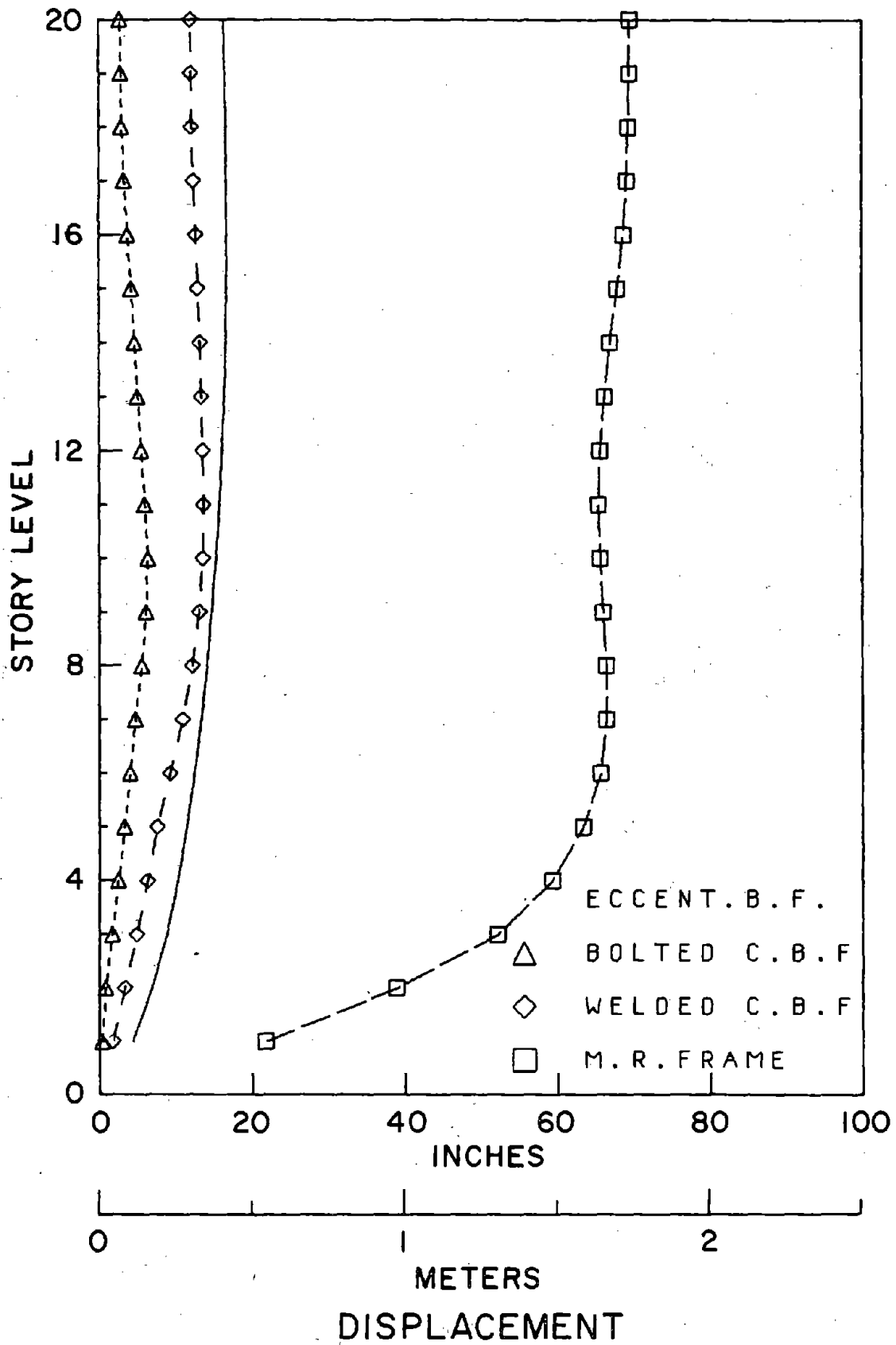


FIGURE 42 - DEFLECTED SHAPE AT THE END OF 15.0 SECONDS OF THE PACOIMA DAM EXCITATION

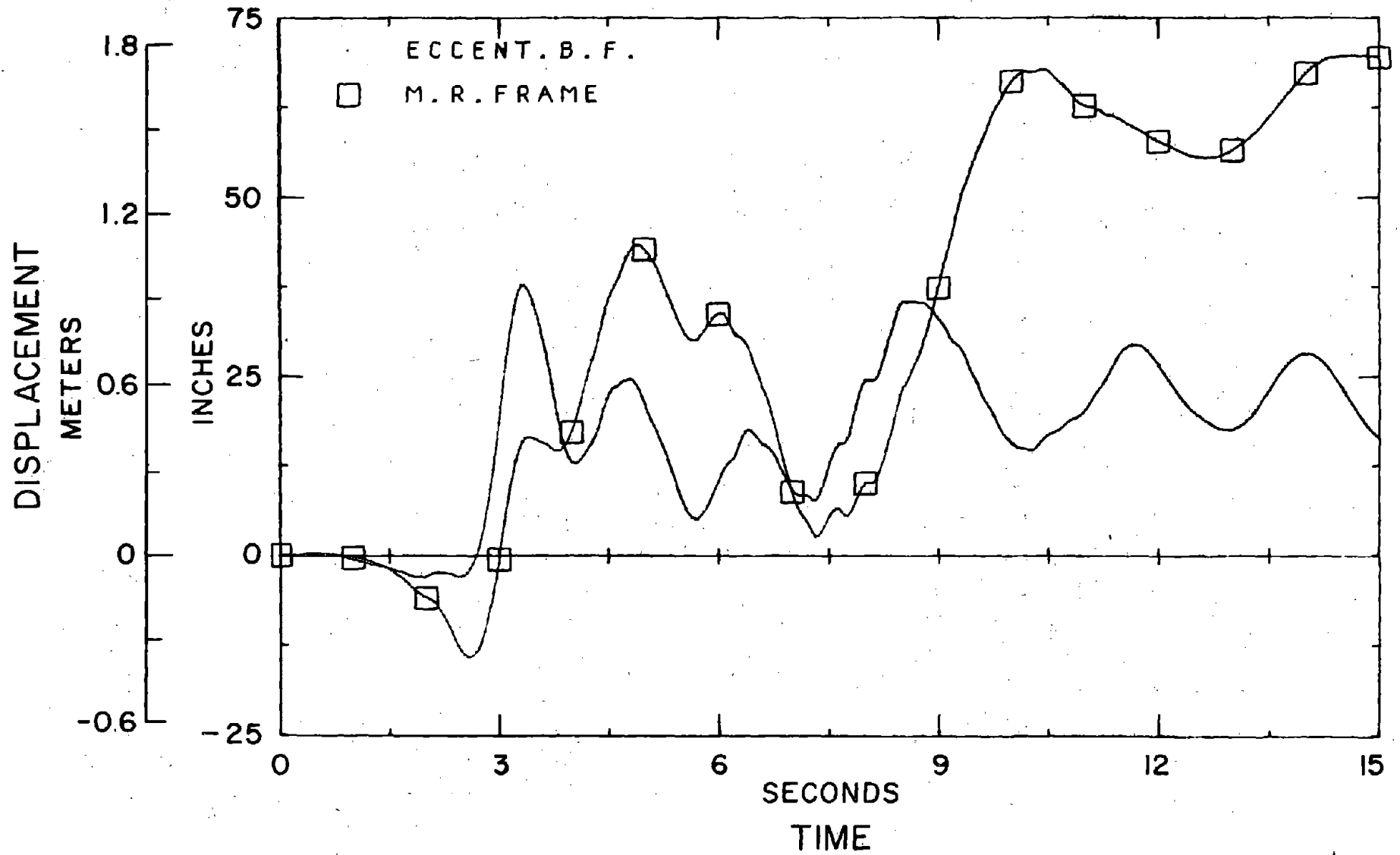
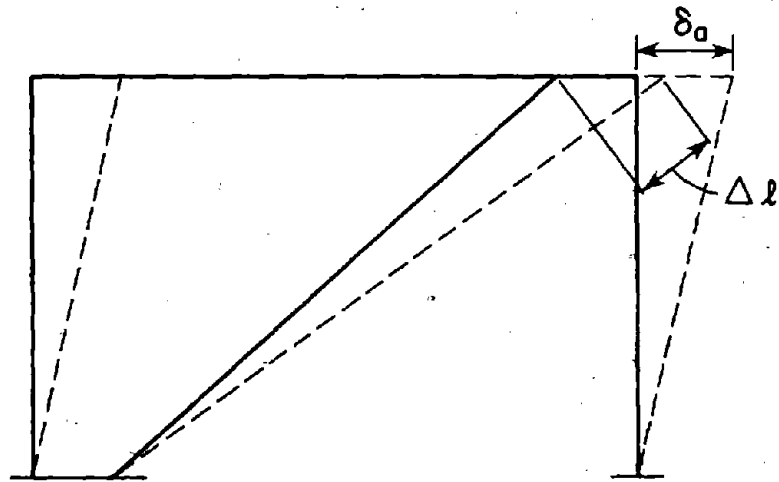
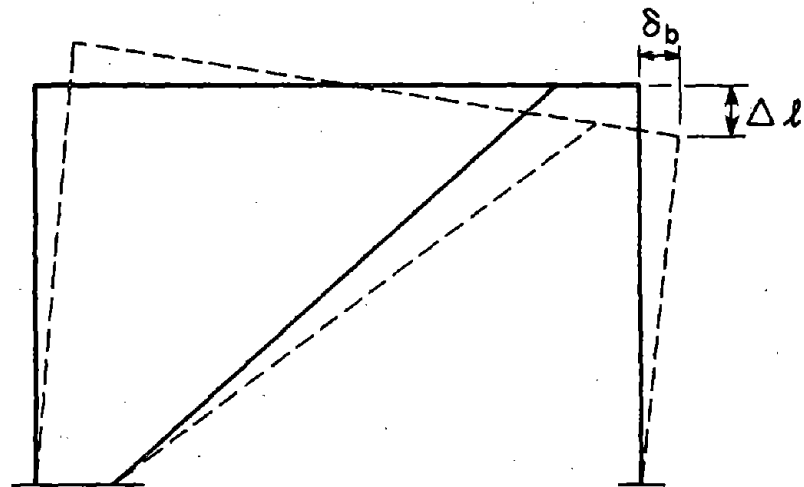


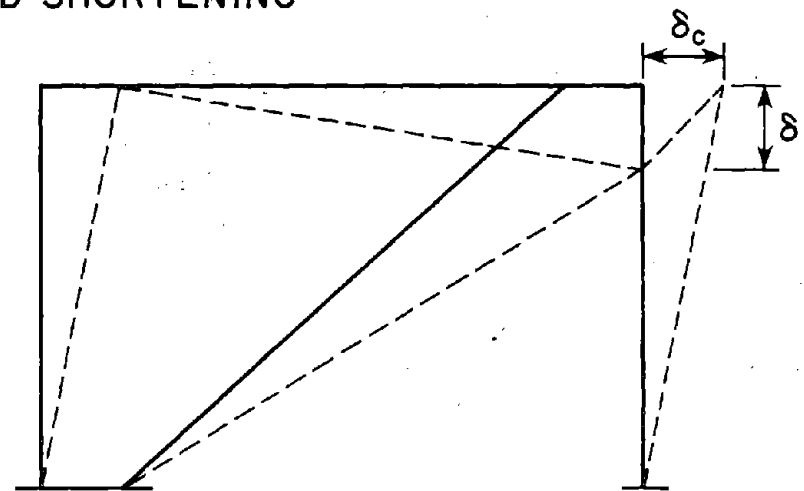
FIGURE 43 - TIME-HISTORY OF THE ROOF DISPLACEMENT OF THE MOMENT-RESISTING AND ECCENTRICALLY BRACED FRAMES DUE TO THE PACOIMA DAM EXCITATION



(a) DEFLECTION DUE TO ELONGATION OF BRACE



(b) DEFLECTION DUE TO COLUMN ELONGATION AND SHORTENING



(c) DEFLECTION DUE TO ECCENTRIC ELEMENTS DEFORMATION

FIGURE 44 - COMPONENTS OF BRACED FRAME DEFLECTION

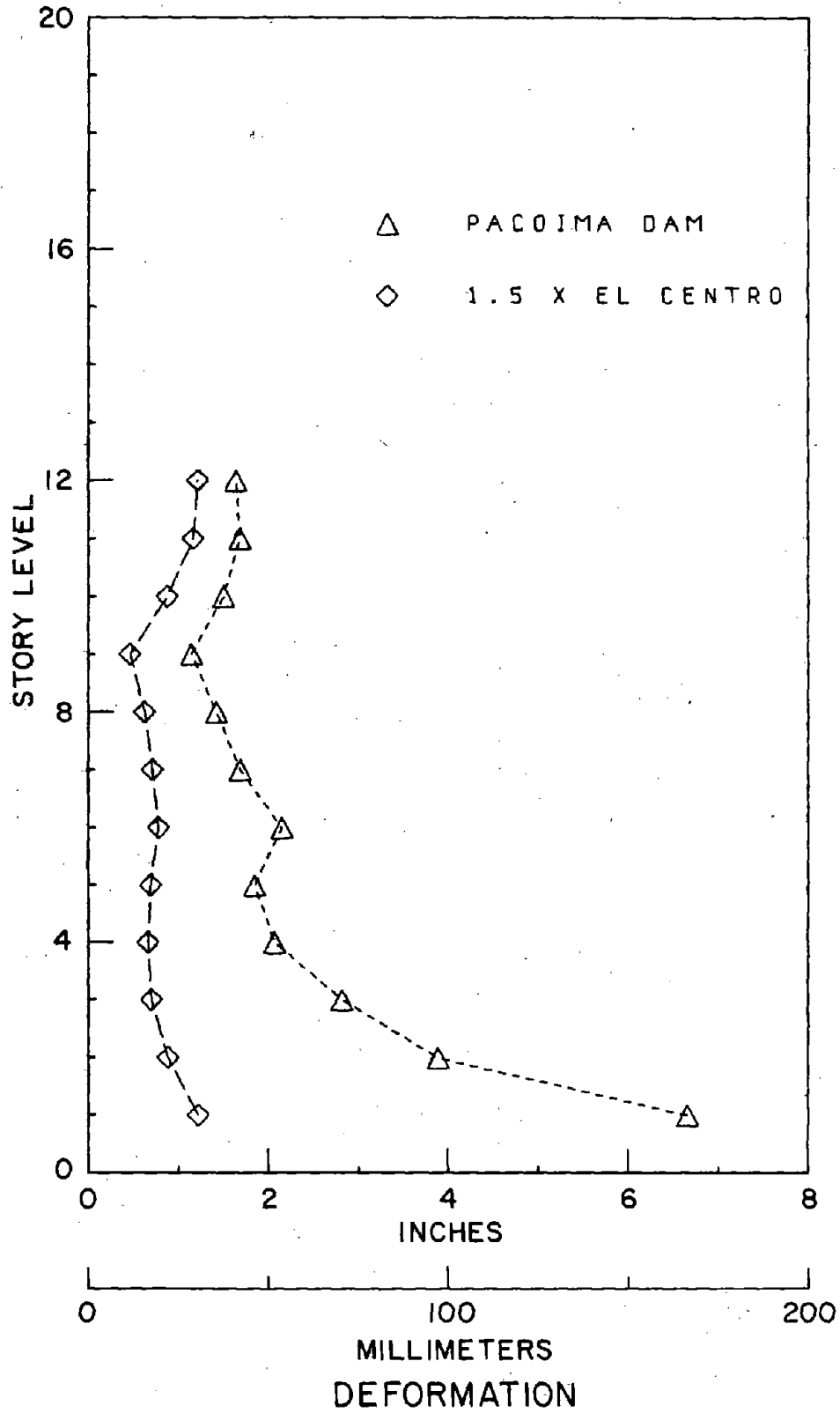


FIGURE 45 - MAXIMUM FLOOR DEFORMATIONS OF THE ECCENTRIC ELEMENTS

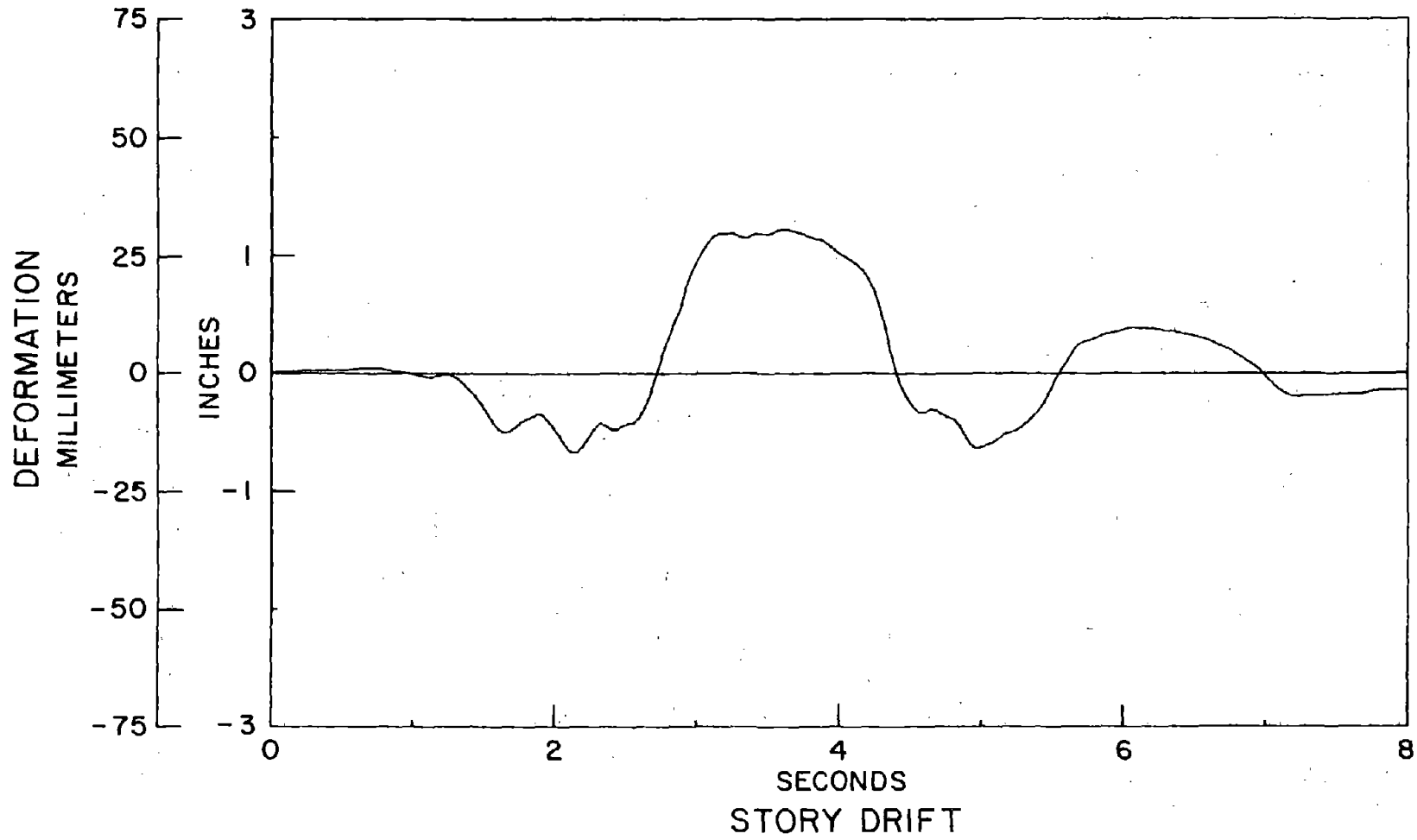


FIGURE 46 - TIME-HISTORY PLOT OF THE ECCENTRIC ELEMENT DURING 1.5 TIMES EL CENTRO EXCITATION



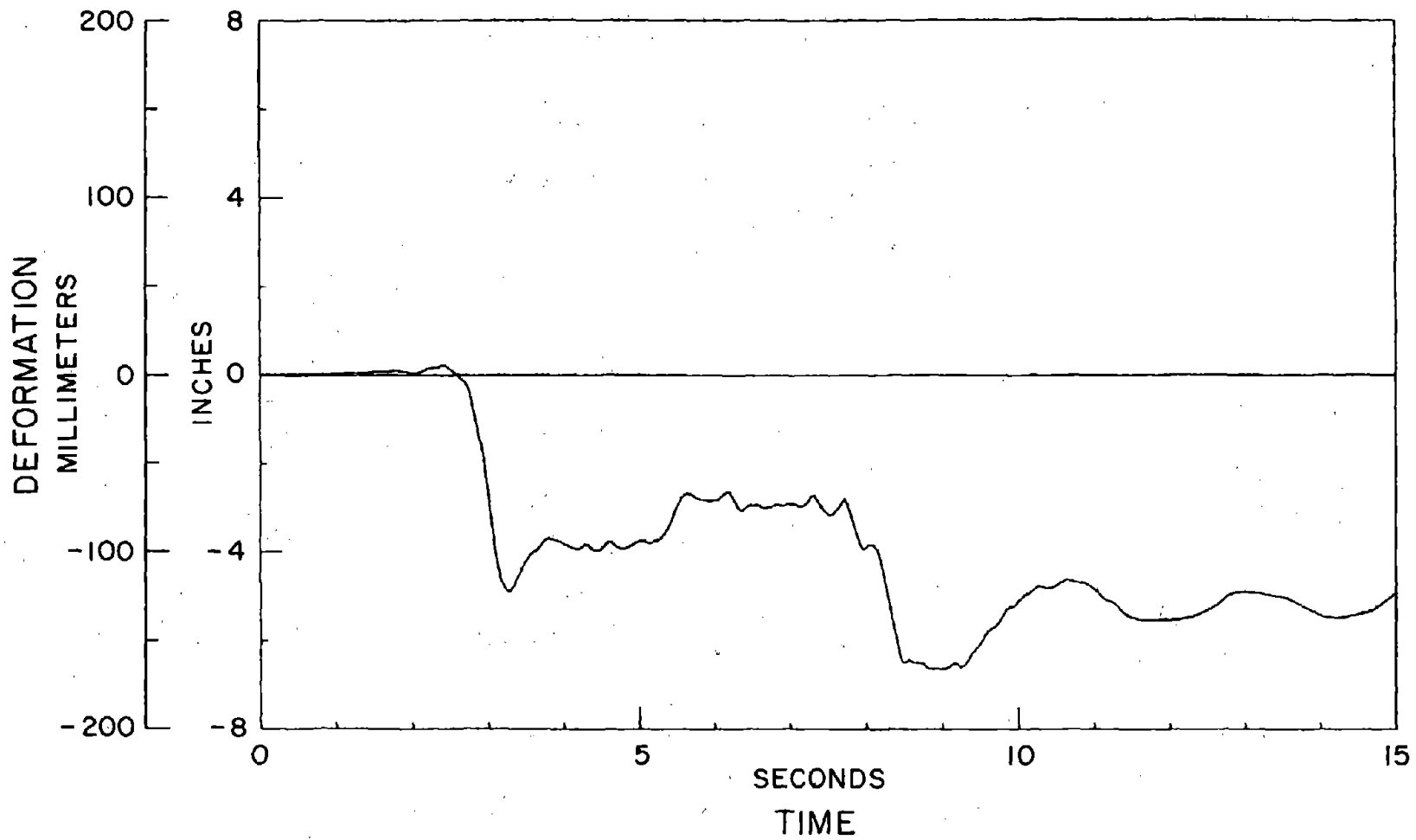


FIGURE 47 - TIME-HISTORY OF THE ECCENTRIC ELEMENT DURING PACOIMA DAM EXCITATION

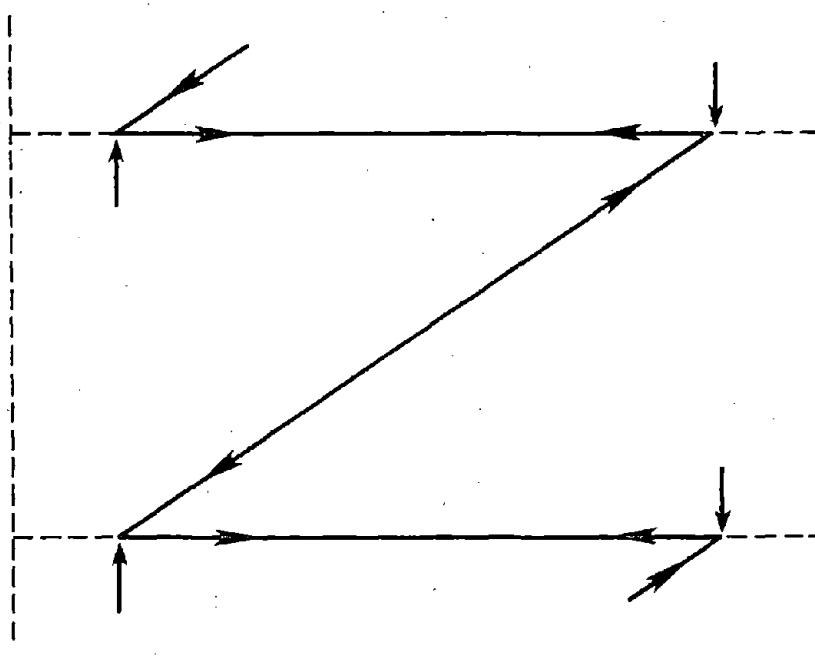
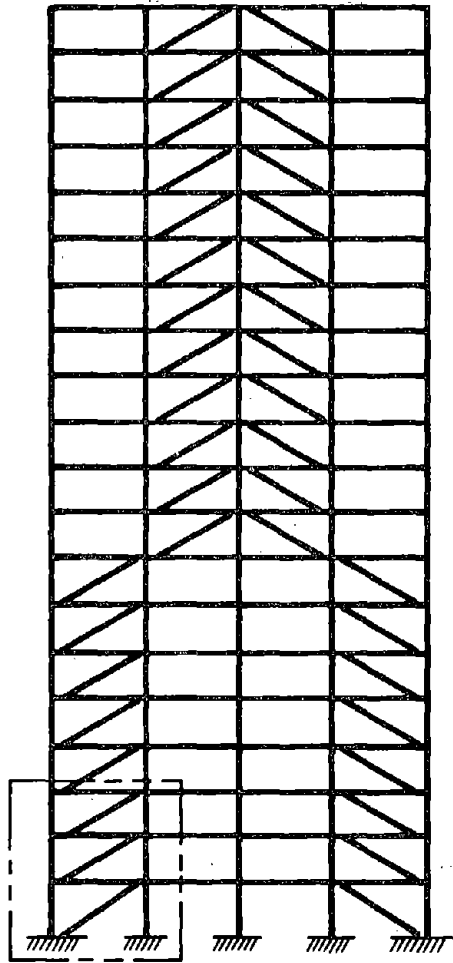
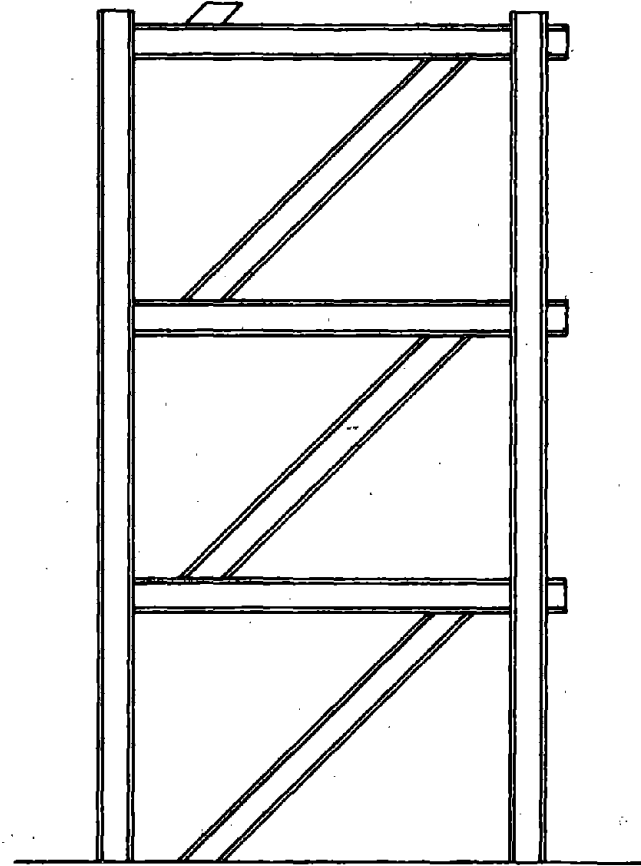


FIGURE 48 - DAMPING FORCES ON THE ELASTIC CENTRAL BRACING SYSTEM

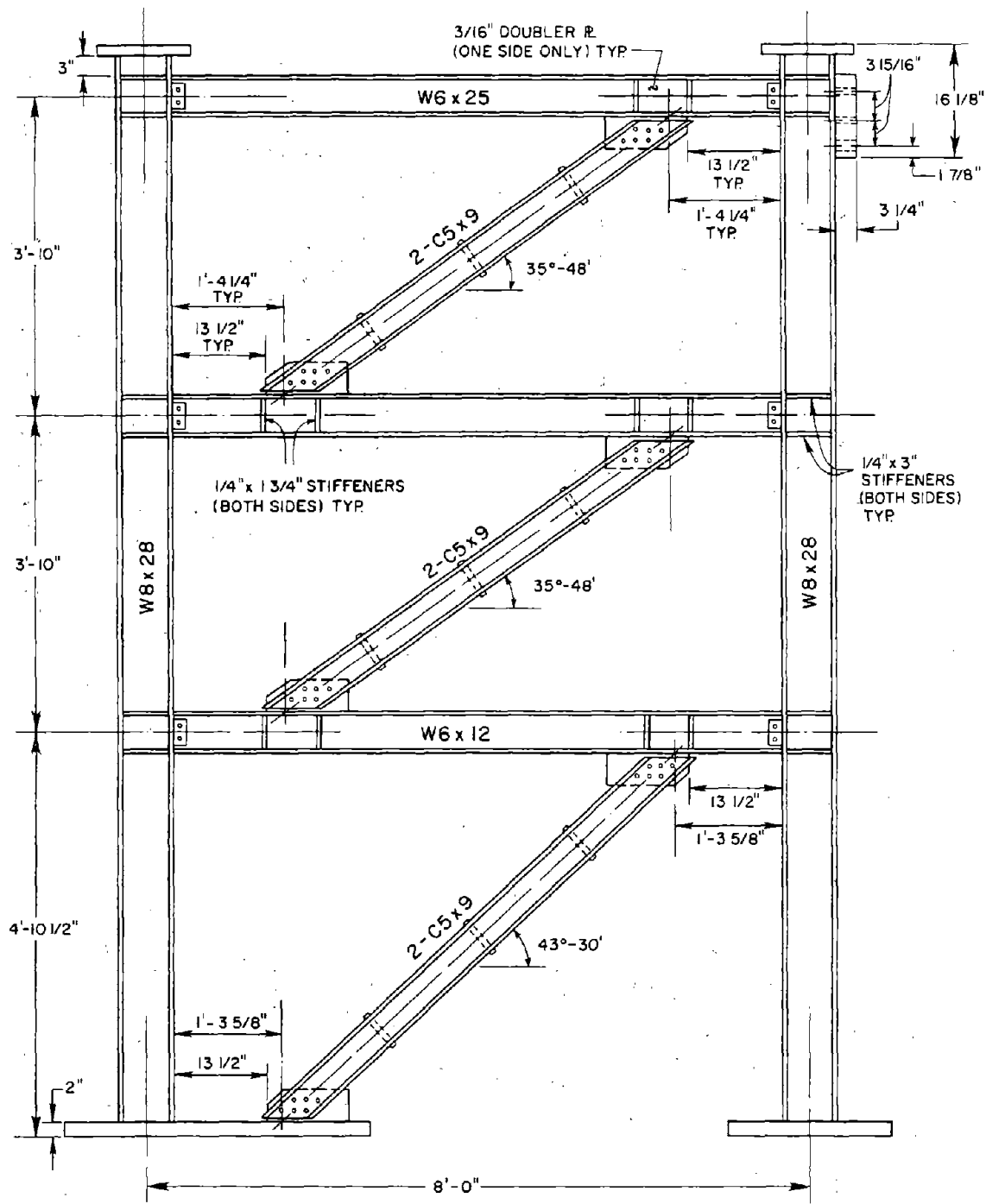


(a) LOCATION OF TEST FRAME



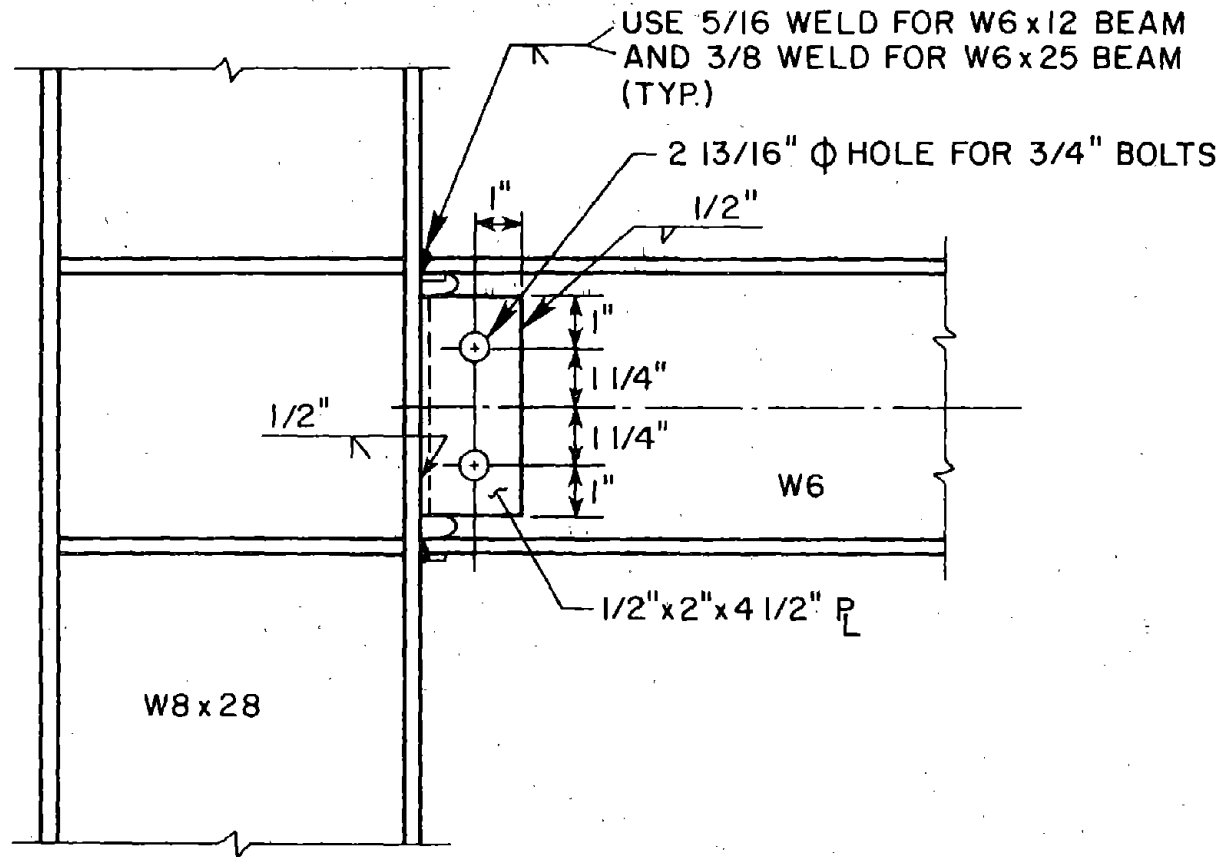
(b) FREEBODY OF TEST FRAME

FIGURE 49 - LOCATION AND FREE BODY OF THE TEST FRAME



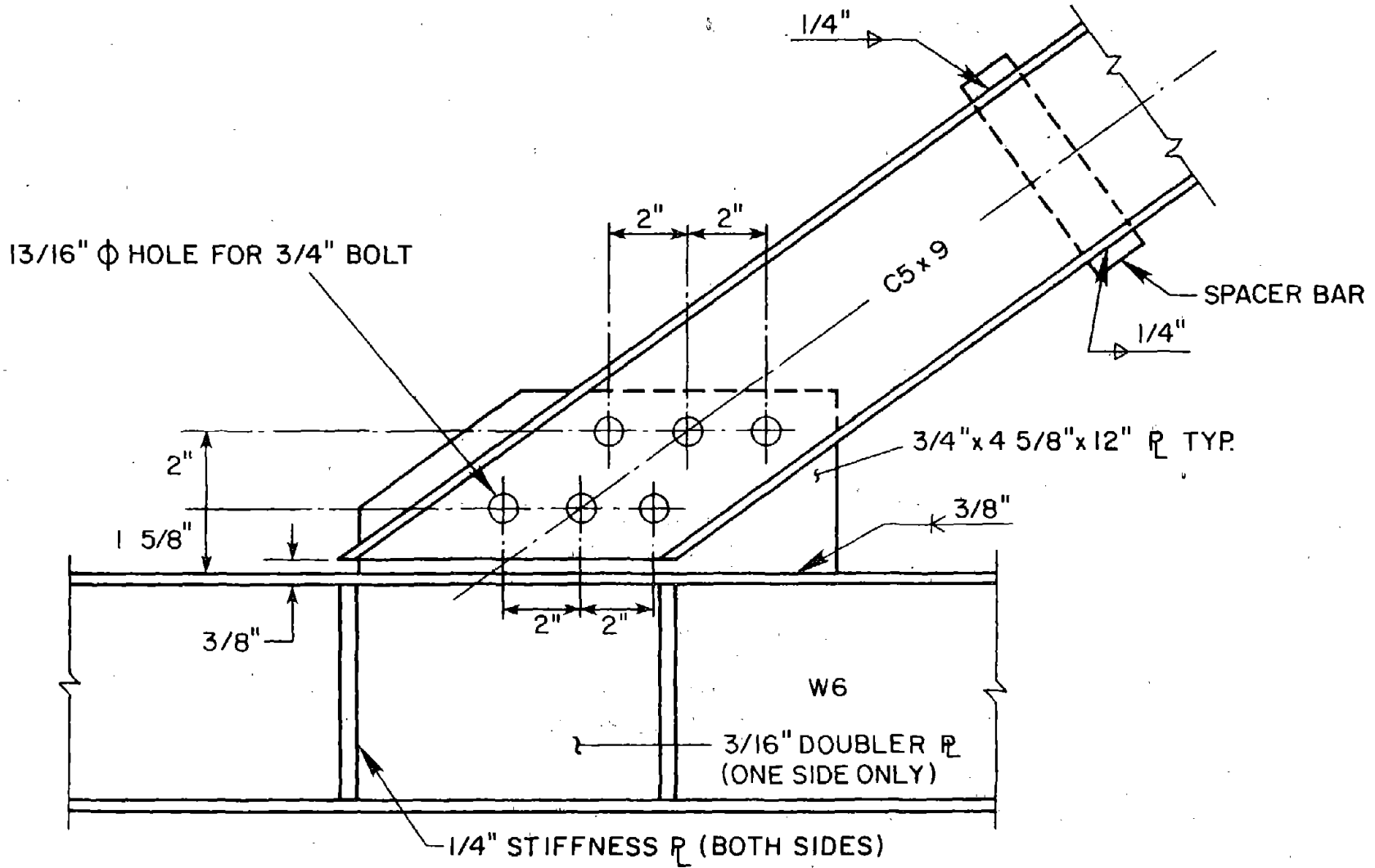
ELEVATION

FIGURE 50 - GENERAL DESIGN OF TEST FRAME 1



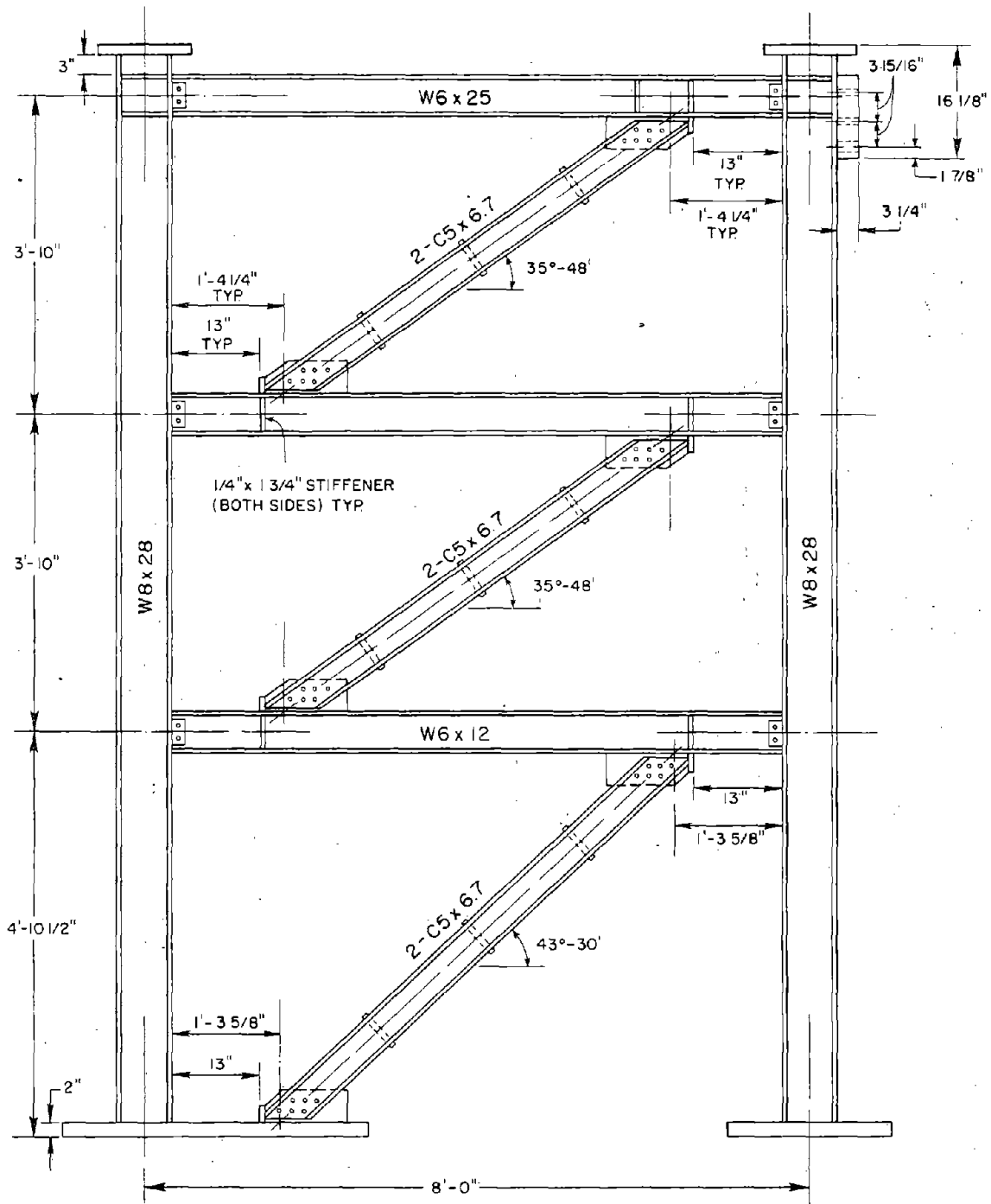
### COLUMN - BEAM CONNECTION

FIGURE 51 - BEAM-TO-COLUMN CONNECTION USED ON TEST FRAME 1



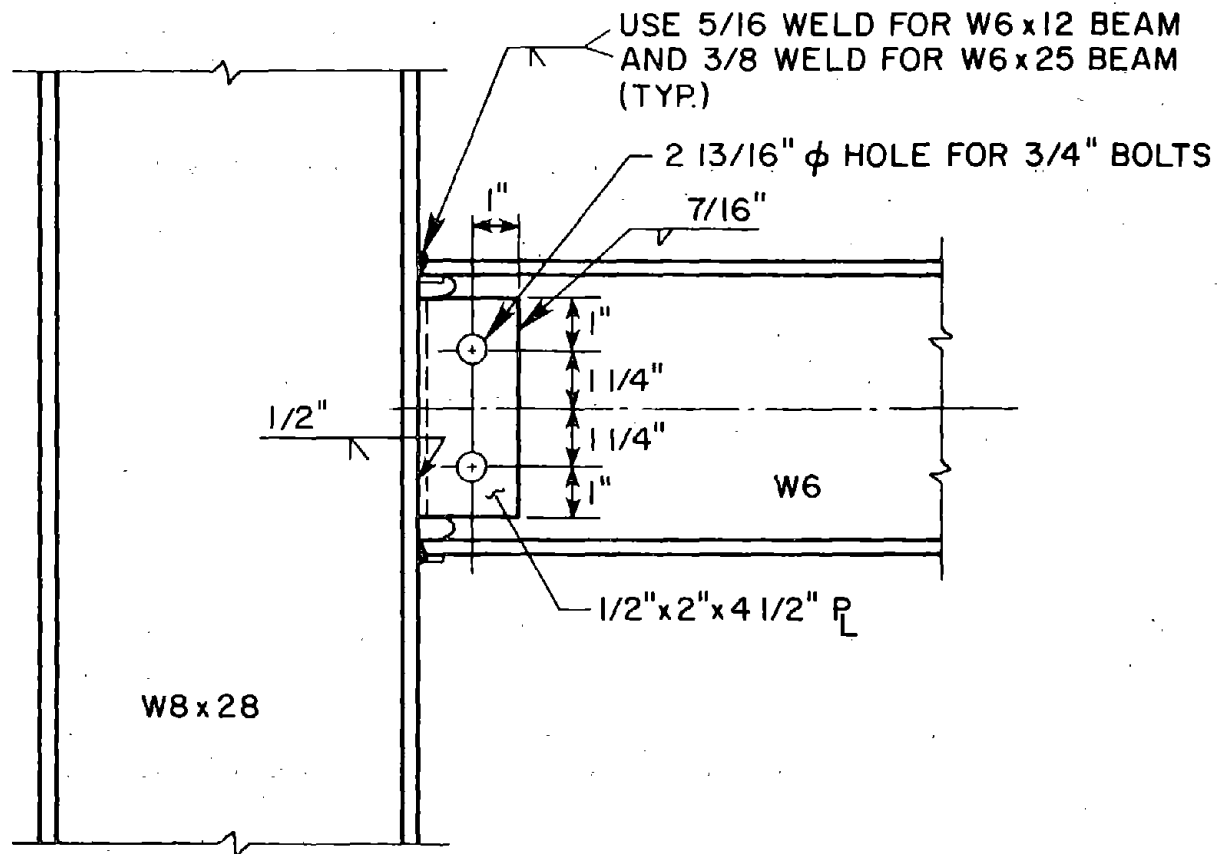
### BRACE - BEAM CONNECTION

FIGURE 52 - BRACE-TO-BEAM CONNECTION USED ON TEST FRAME 1



ELEVATION

FIGURE 53 - GENERAL DESIGN OF TEST FRAME 2

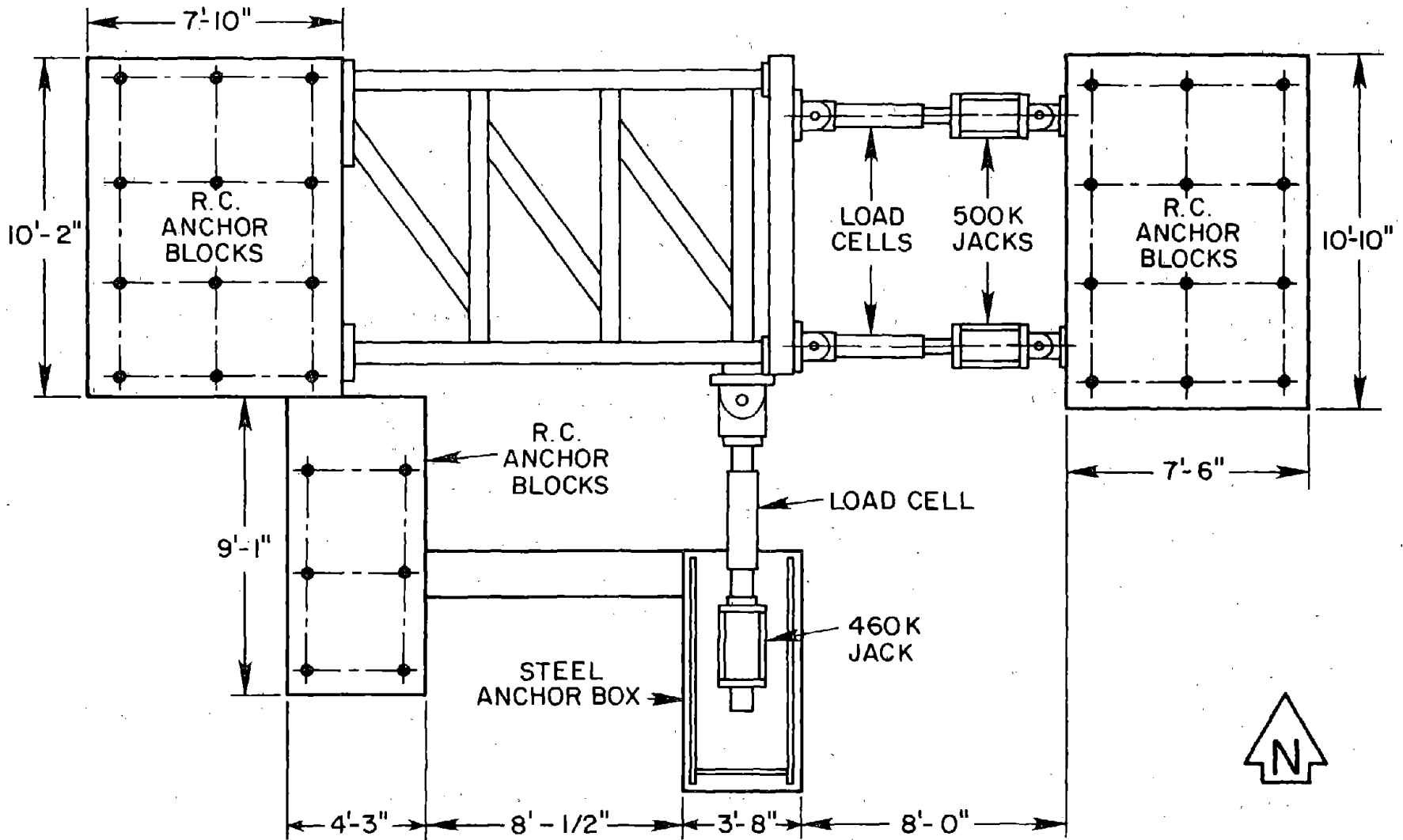


### COLUMN - BEAM CONNECTION

FIGURE 54 - BEAM-TO-COLUMN CONNECTION USED ON TEST FRAME 2







**SPECIMEN IN TEST FIXTURE**

FIGURE 56 - LAYOUT OF THE TEST APPARATUS

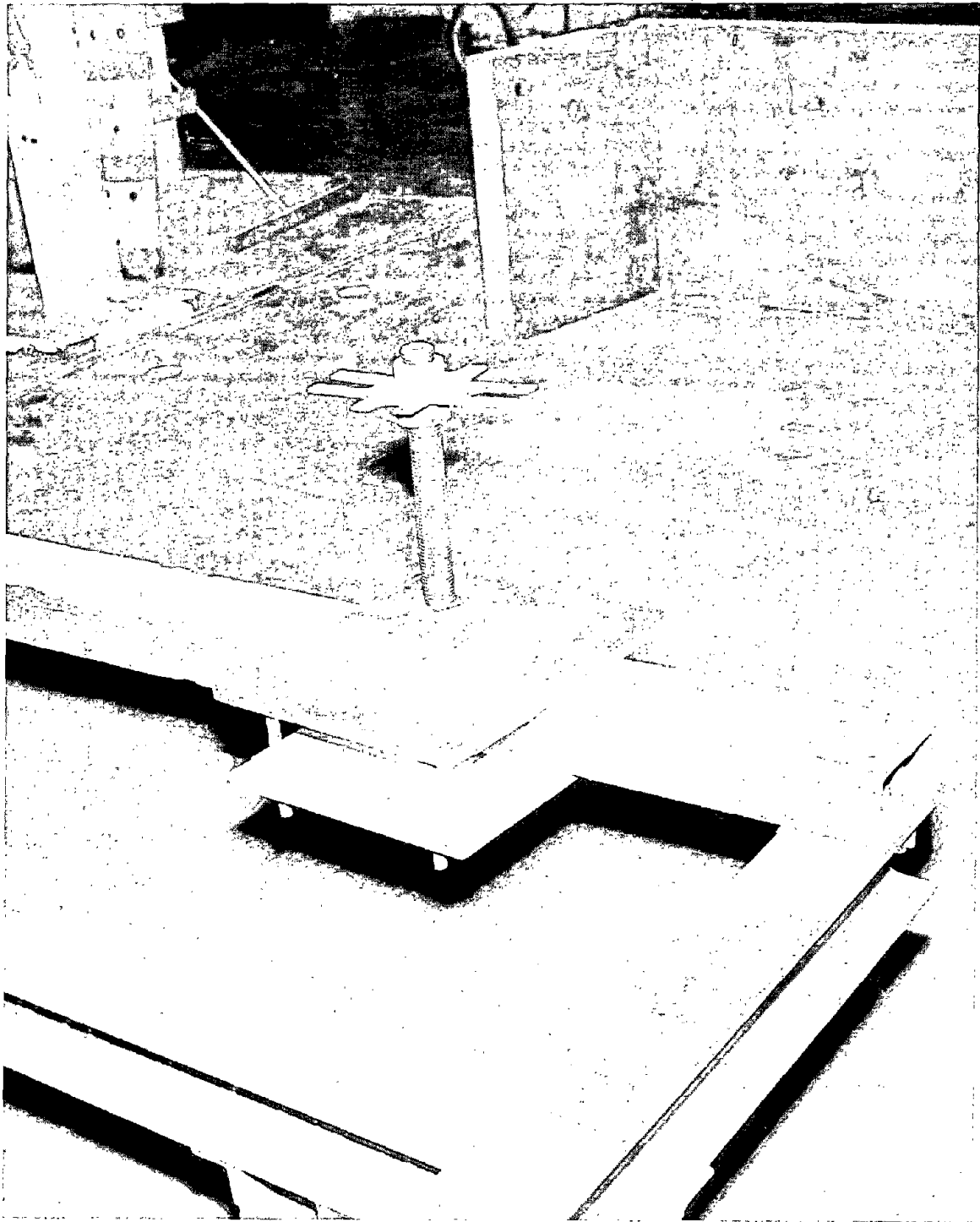
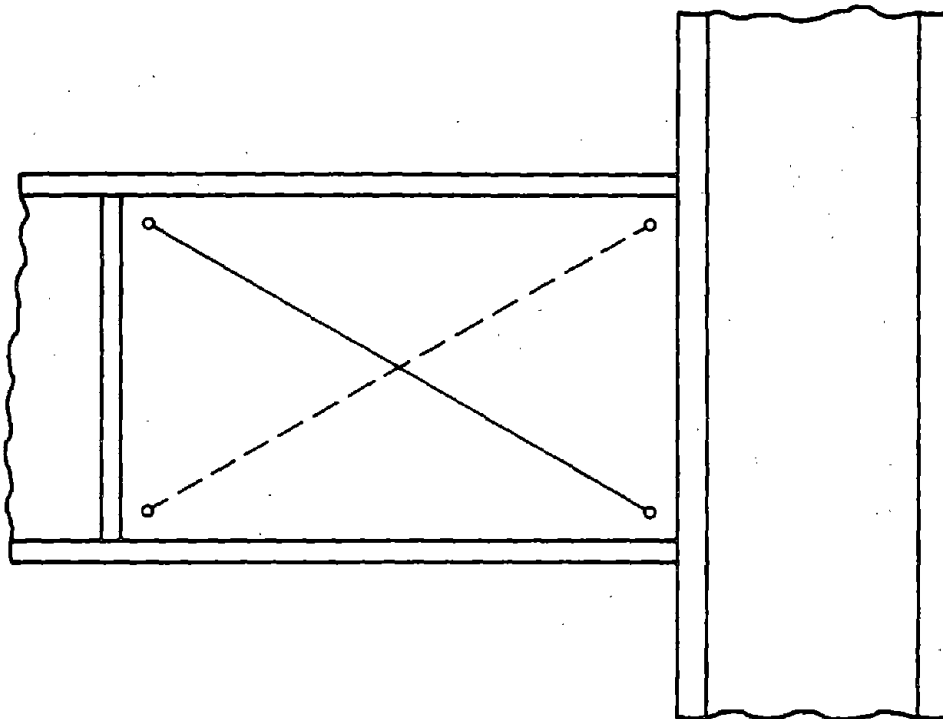
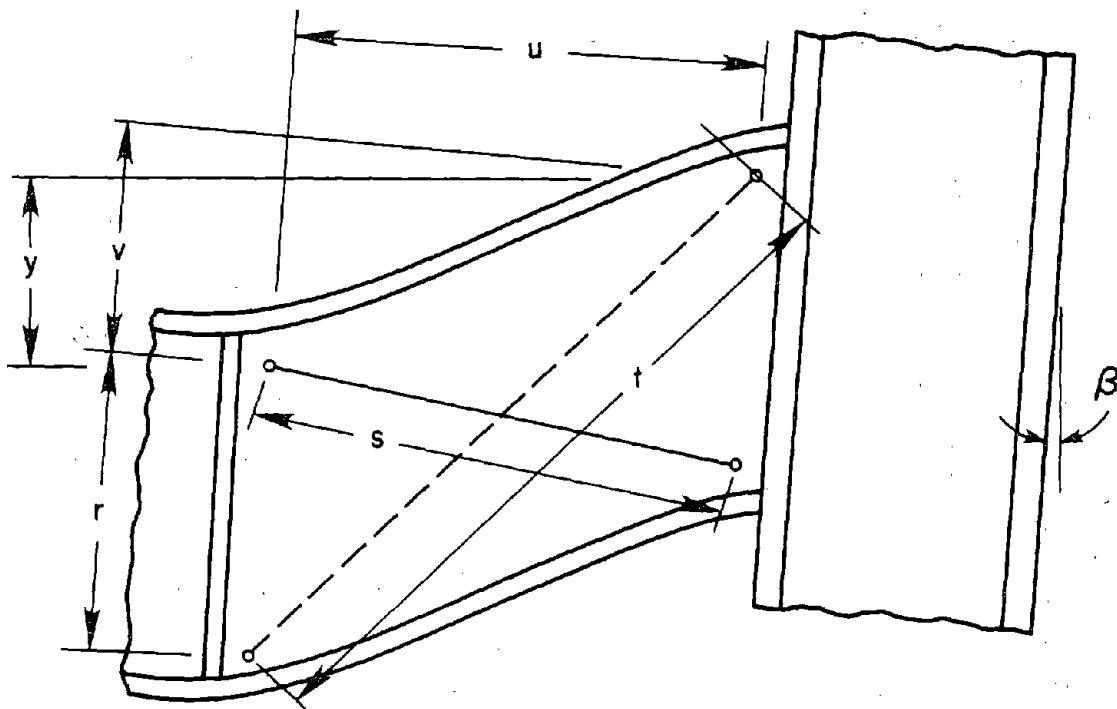


FIGURE 57 - PHOTOGRAPH OF THE KEY COMPONENTS OF THE LATERAL SUPPORT SYSTEM



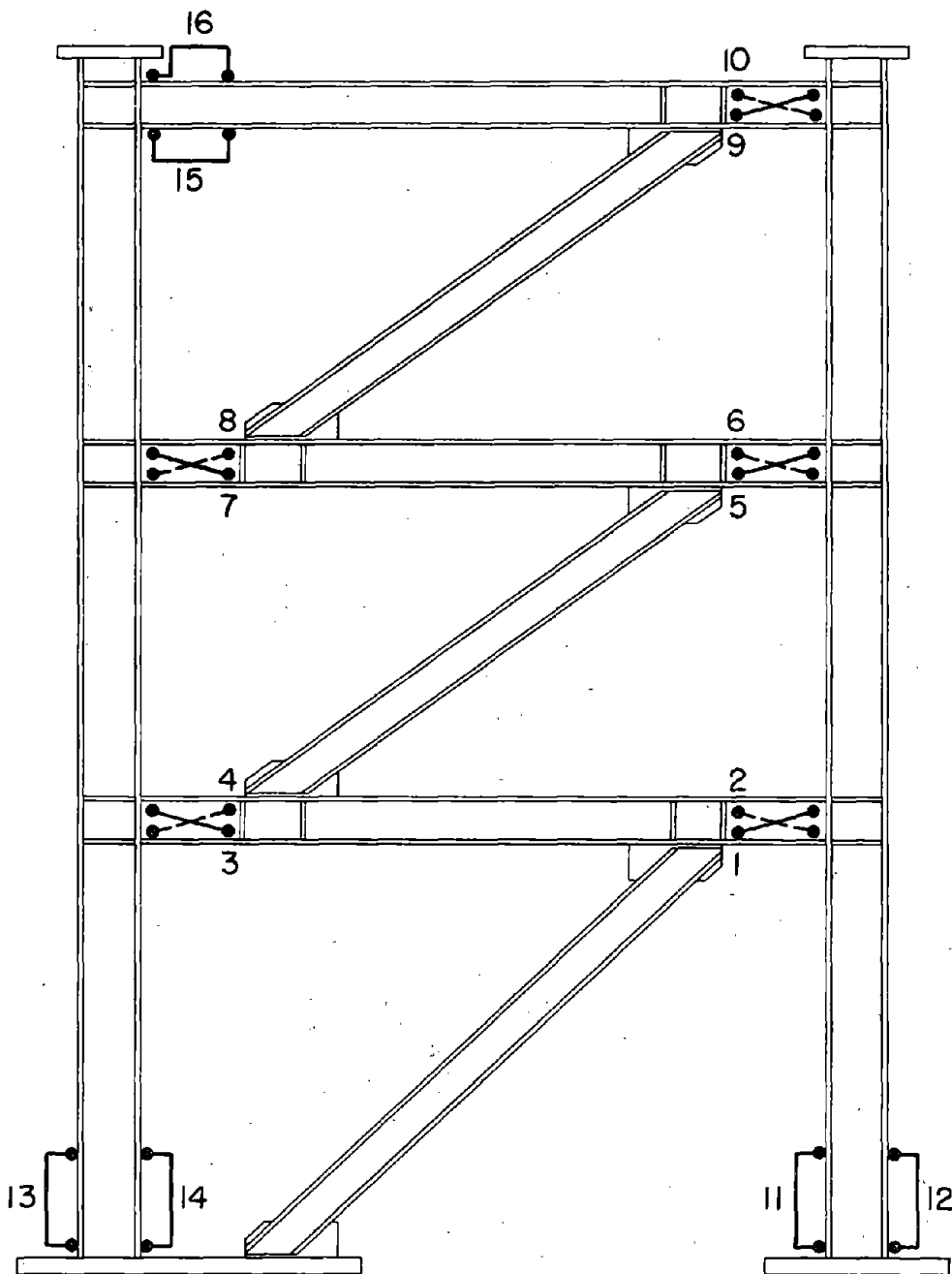


(a) CLIP GAGE PLACEMENT



(b) GEOMETRY OF ECCENTRIC ELEMENT DEFORMATION

FIGURE 59 - PLACEMENT AND DEFORMATION GEOMETRY OF CLIP GAGES IN ECCENTRIC ELEMENTS






- 
 9" CLIP GAGE MOUNTED ON FRONT SIDE OF WEB
- 
 9" CLIP GAGE MOUNTED ON BACK SIDE OF WEB
- 
 12" CLIP GAGE MOUNTED TO FLANGE

FIGURE 60 - PLACEMENT OF CLIP GAGES ON THE TEST FRAMES



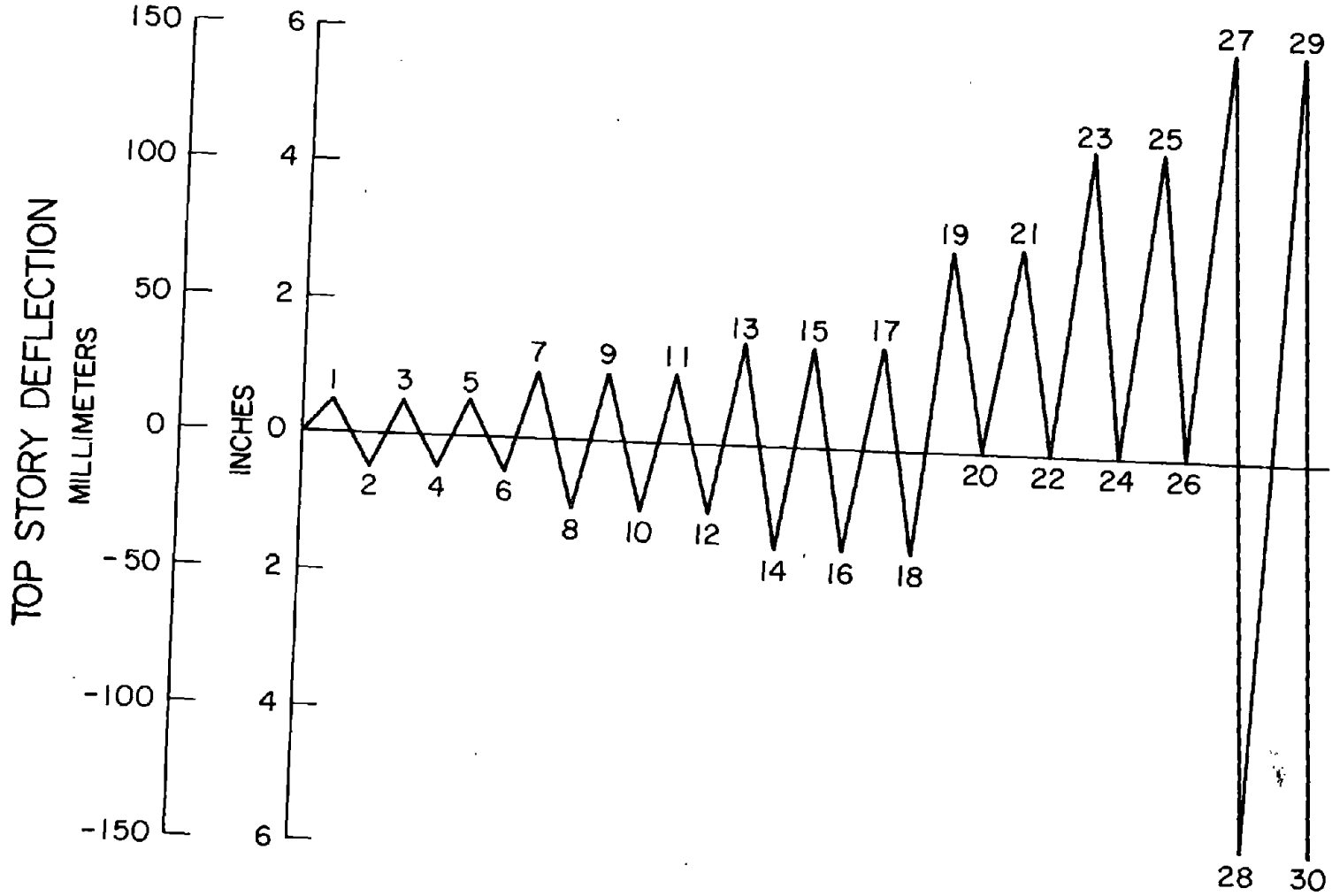


FIGURE 62 - LOAD PROGRAM FOR THE INELASTIC CYCLES OF TESTING



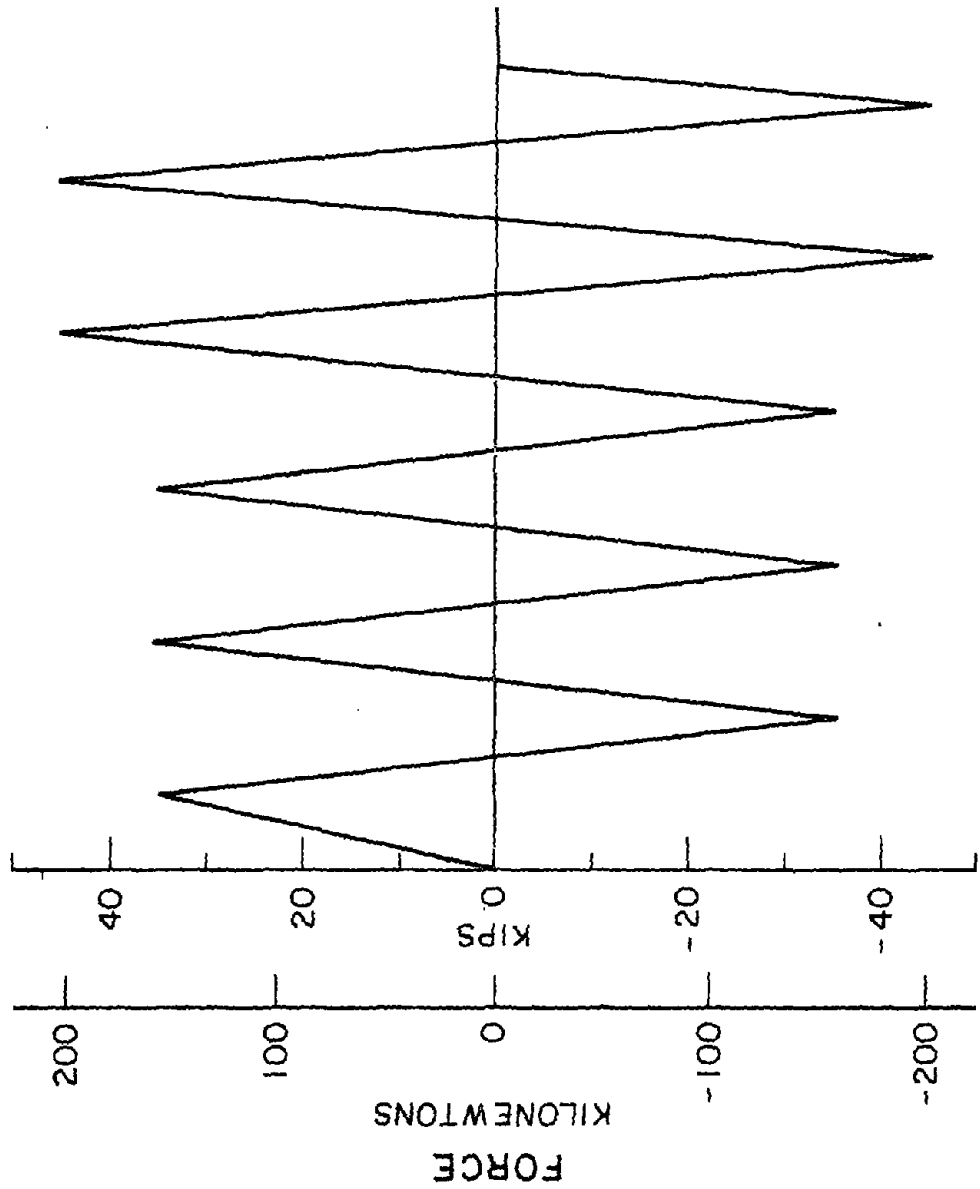


FIGURE 63 - LOAD PROGRAM FOR THE ELASTIC CYCLES OF TESTING

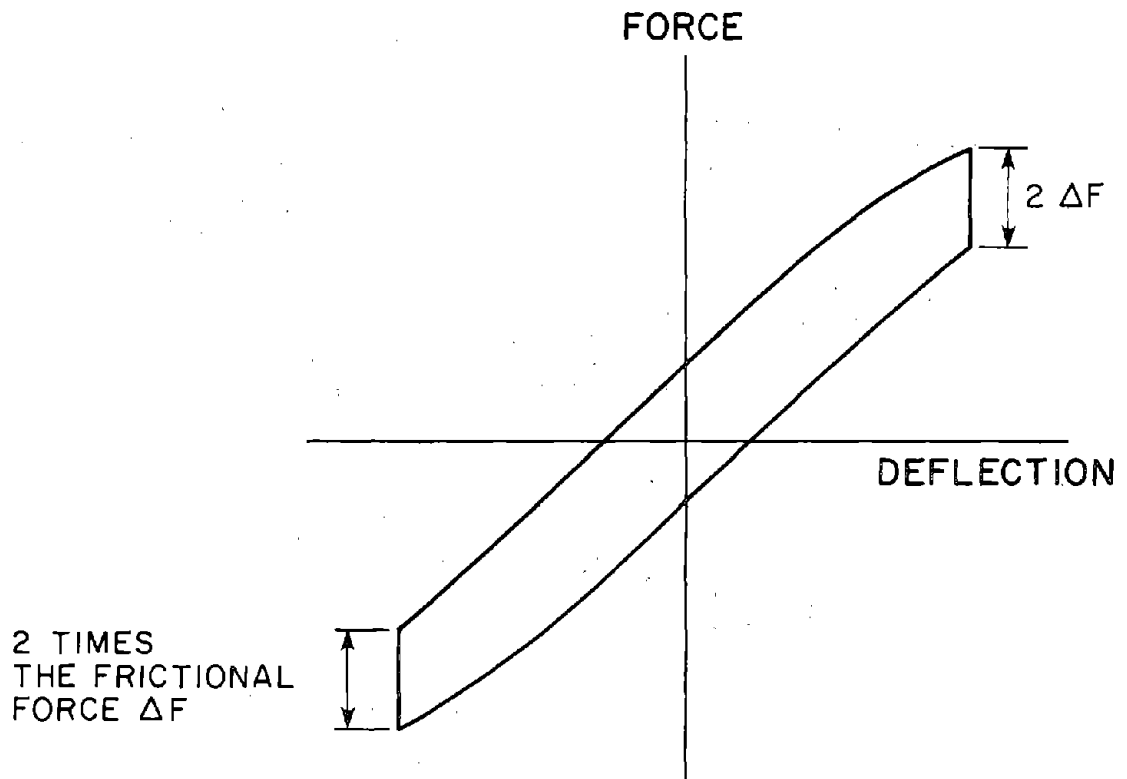


FIGURE 64 - EFFECT OF THE FRICTIONAL FORCE ON THE FORCE-DEFLECTION HYSTERETIC CURVES

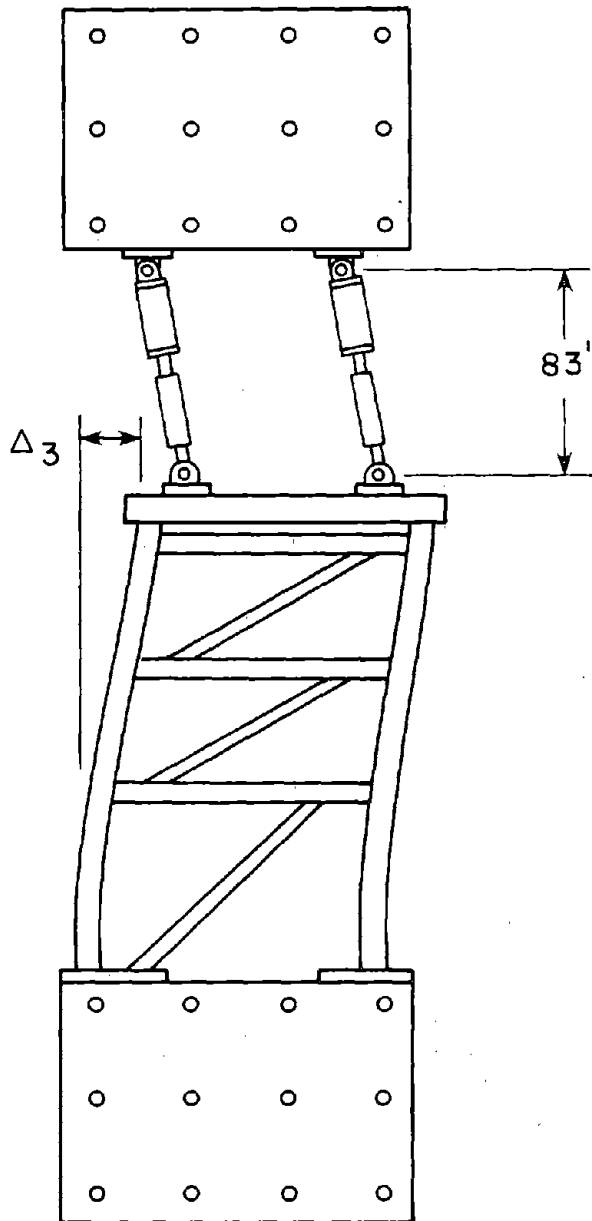


FIGURE 65 - COMPONENT OF LATERAL FORCE INDUCED BY VERTICAL LOAD CELLS



FIGURE 66 - PHOTOGRAPH OF THE TEST FRAME AND TEST FACILITY

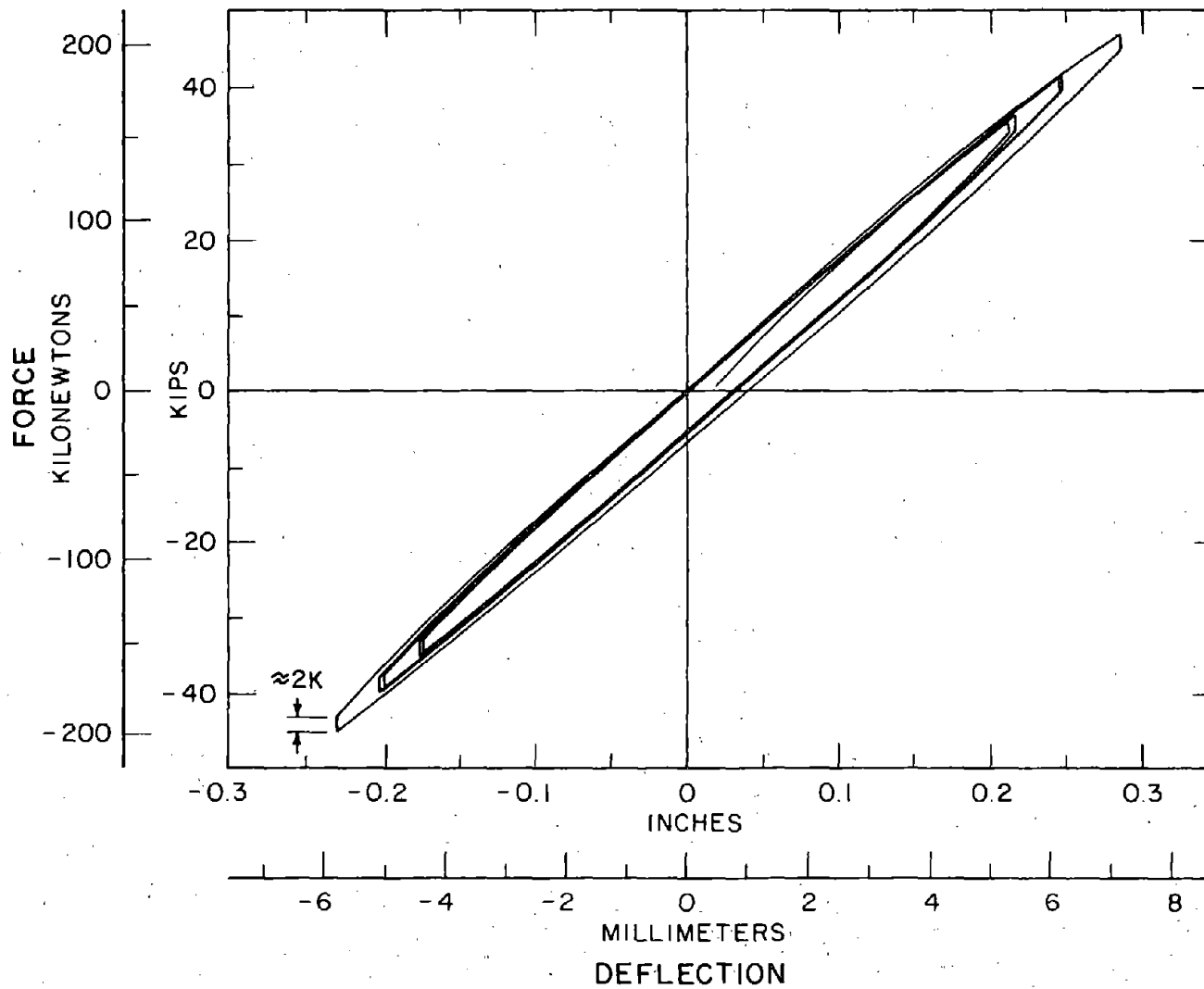


FIGURE 67 - LATERAL FORCE - THIRD FLOOR DEFLECTION HYSTERETIC BEHAVIOR FOR THE ELASTIC CYCLES AT THE START OF TEST 1

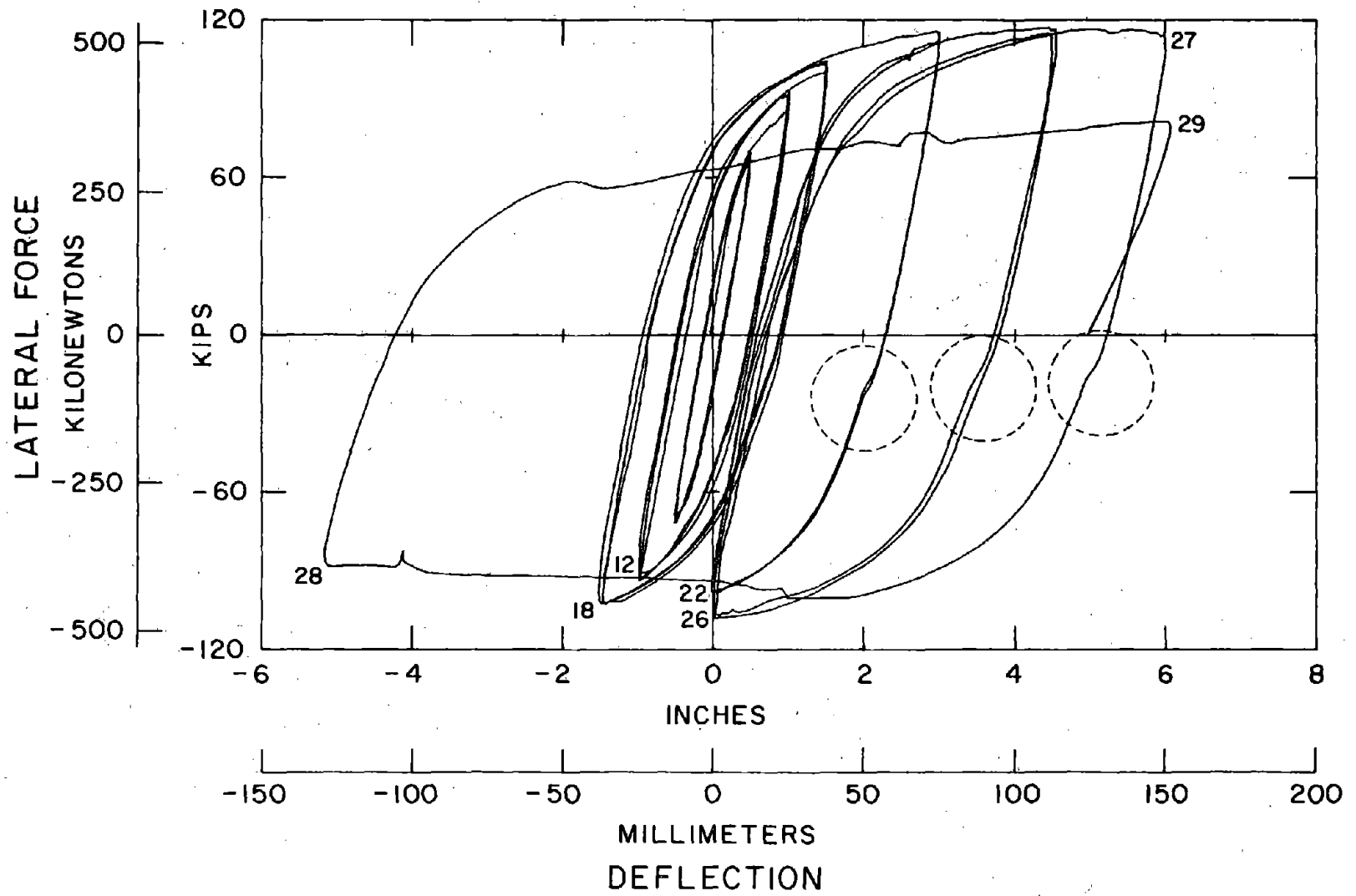


FIGURE 68 - LATERAL FORCE - THIRD FLOOR DEFLECTION HYSTERETIC BEHAVIOR FOR THE INELASTIC CYCLES OF TEST FRAME 1

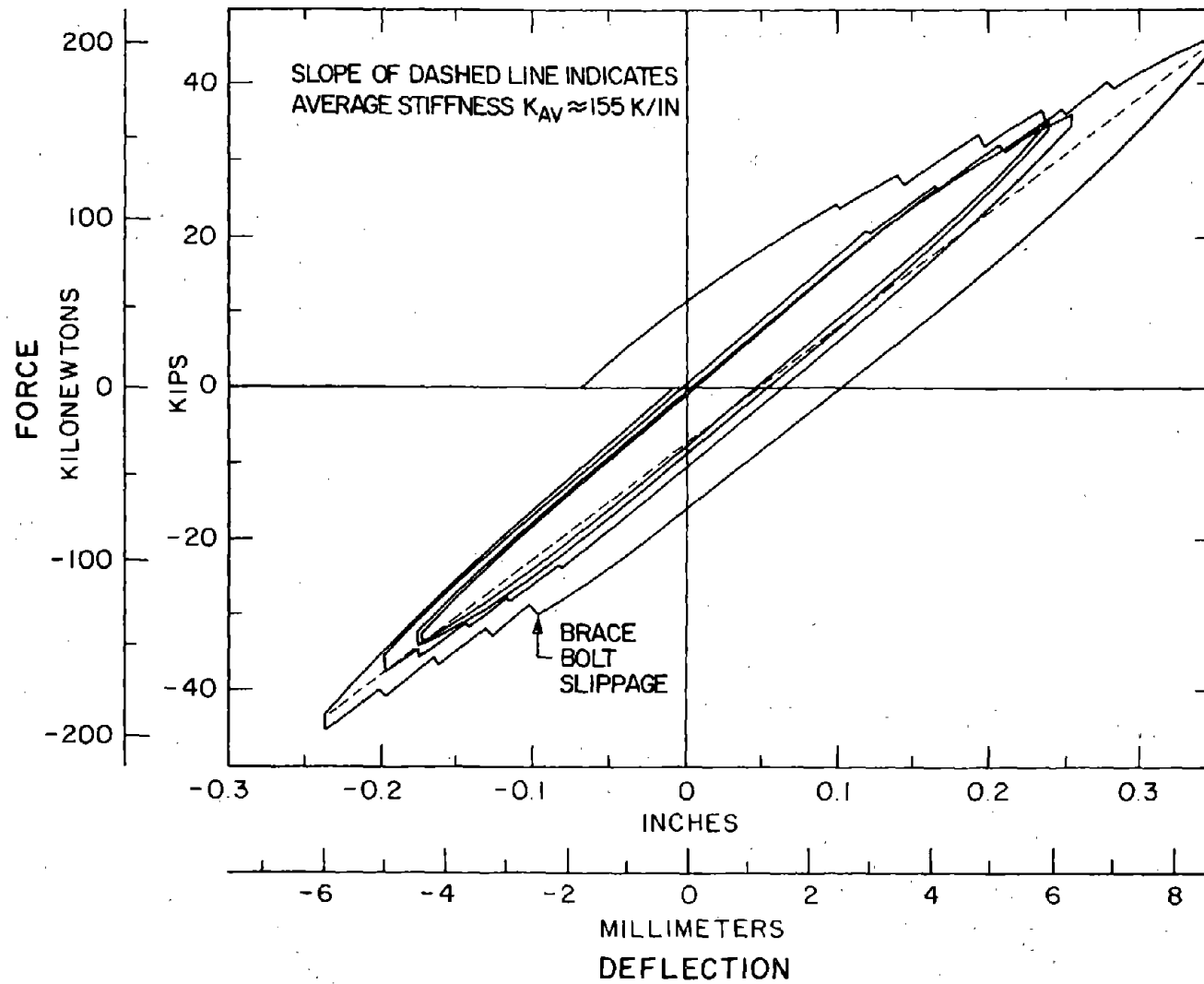


FIGURE 69 - LATERAL FORCE - THIRD FLOOR DEFLECTION HYSTERETIC BEHAVIOR FOR THE ELASTIC CYCLES AFTER LP 12

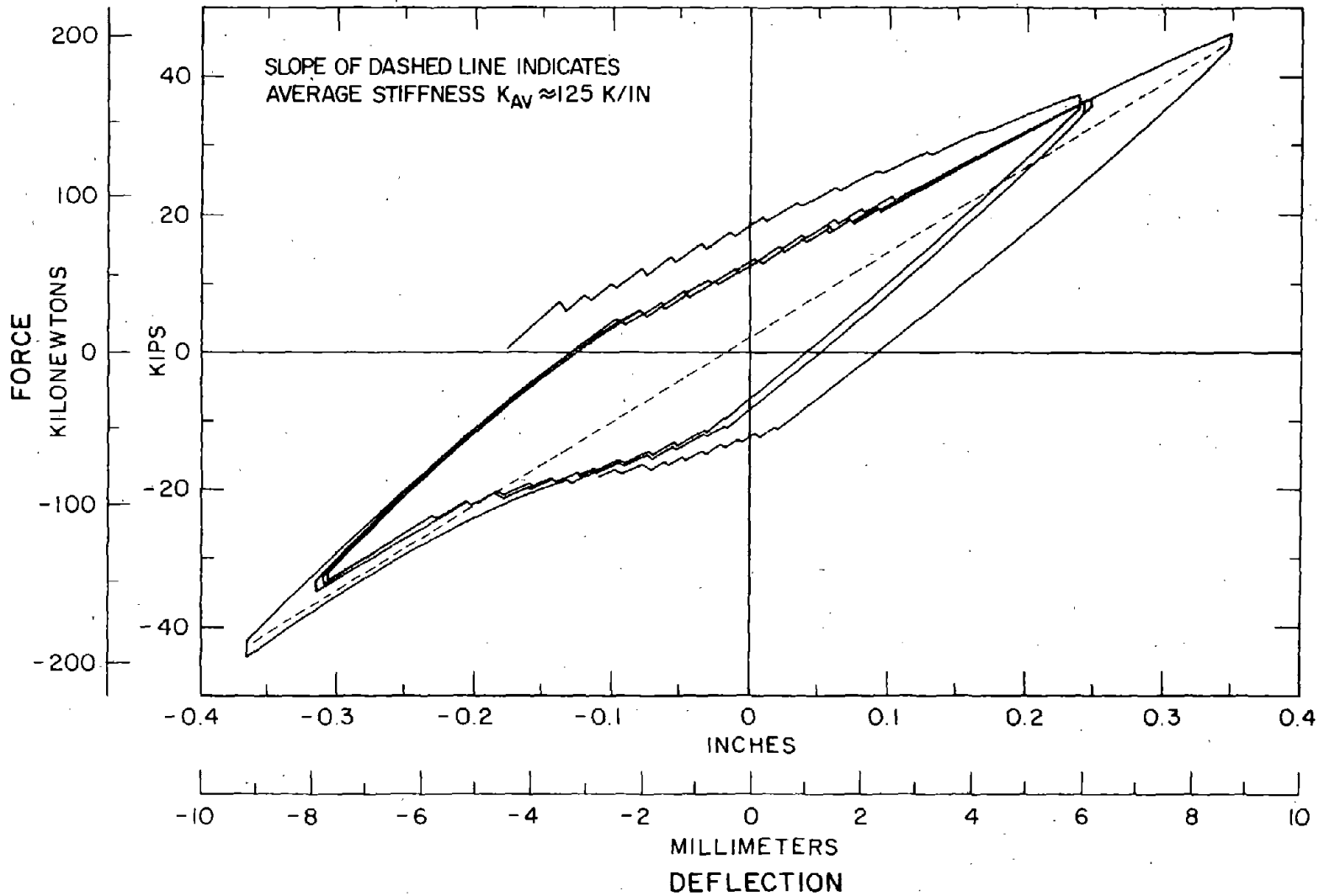


FIGURE 70 - LATERAL FORCE - THIRD FLOOR DEFLECTION HYSTERETIC BEHAVIOR FOR THE ELASTIC CYCLES AFTER LP 22



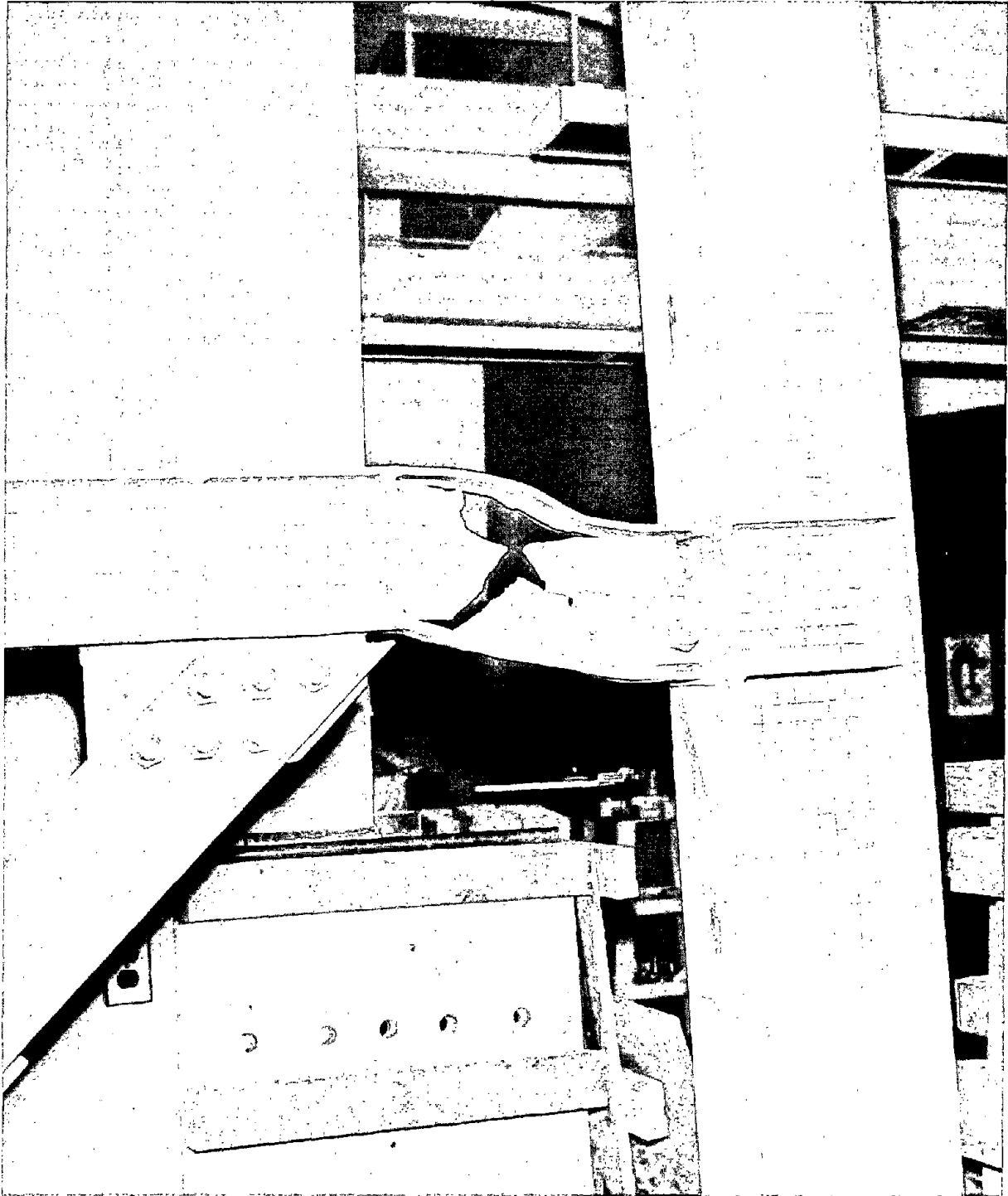


FIGURE 71 - PHOTOGRAPH OF THE TORN SOUTH ECCENTRIC ELEMENT OF TEST FRAME 1

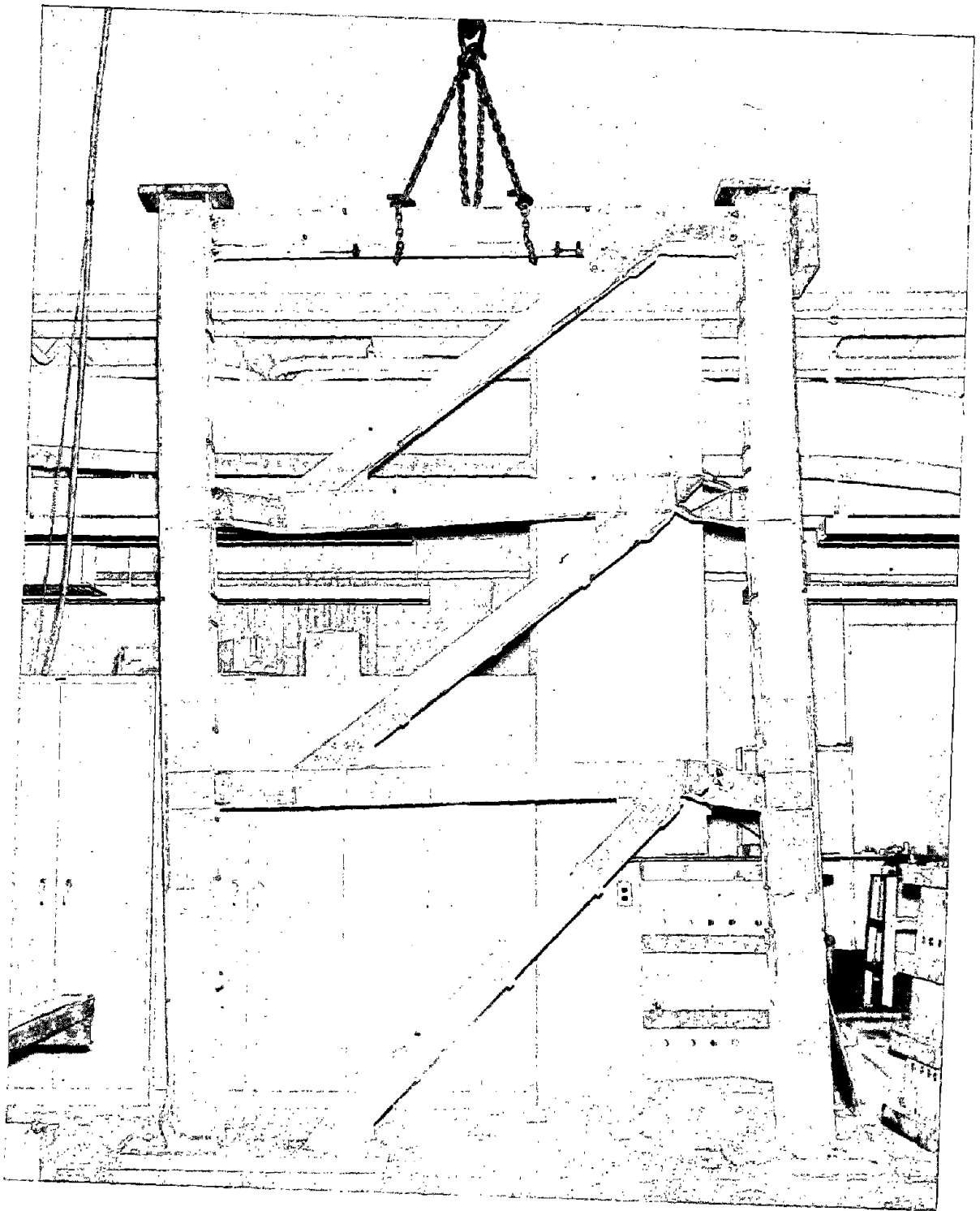


FIGURE 72 - PHOTOGRAPH OF TEST FRAME 1 AFTER COMPLETION OF THE TEST

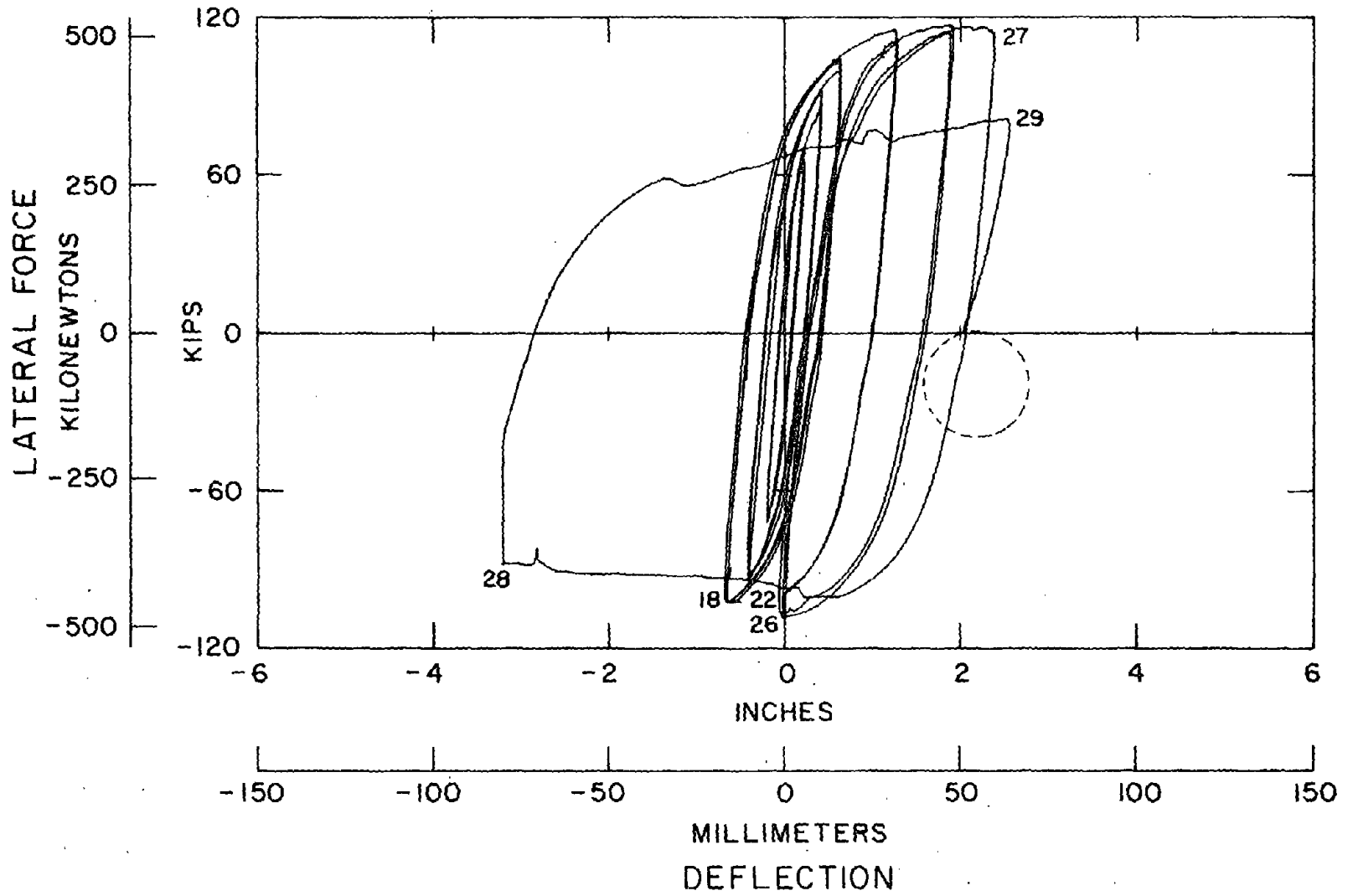


FIGURE 73 - LATERAL FORCE - FIRST FLOOR DEFLECTION HYSTERETIC BEHAVIOR FOR THE INELASTIC CYCLES OF TEST FRAME 1

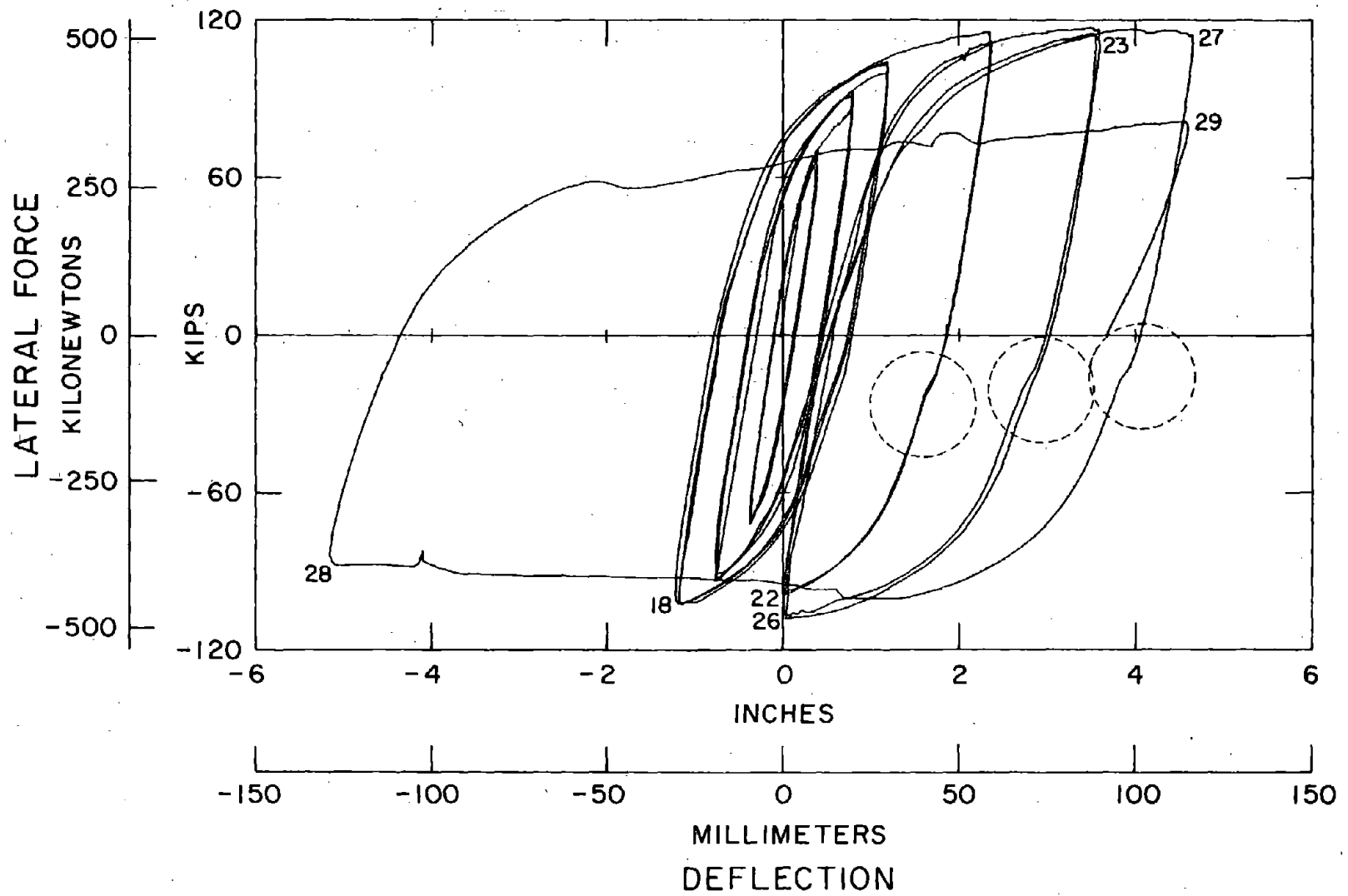


FIGURE 74 - LATERAL FORCE - SECOND FLOOR DEFLECTION HYSTERETIC BEHAVIOR FOR THE INELASTIC CYCLES OF TEST FRAME 1

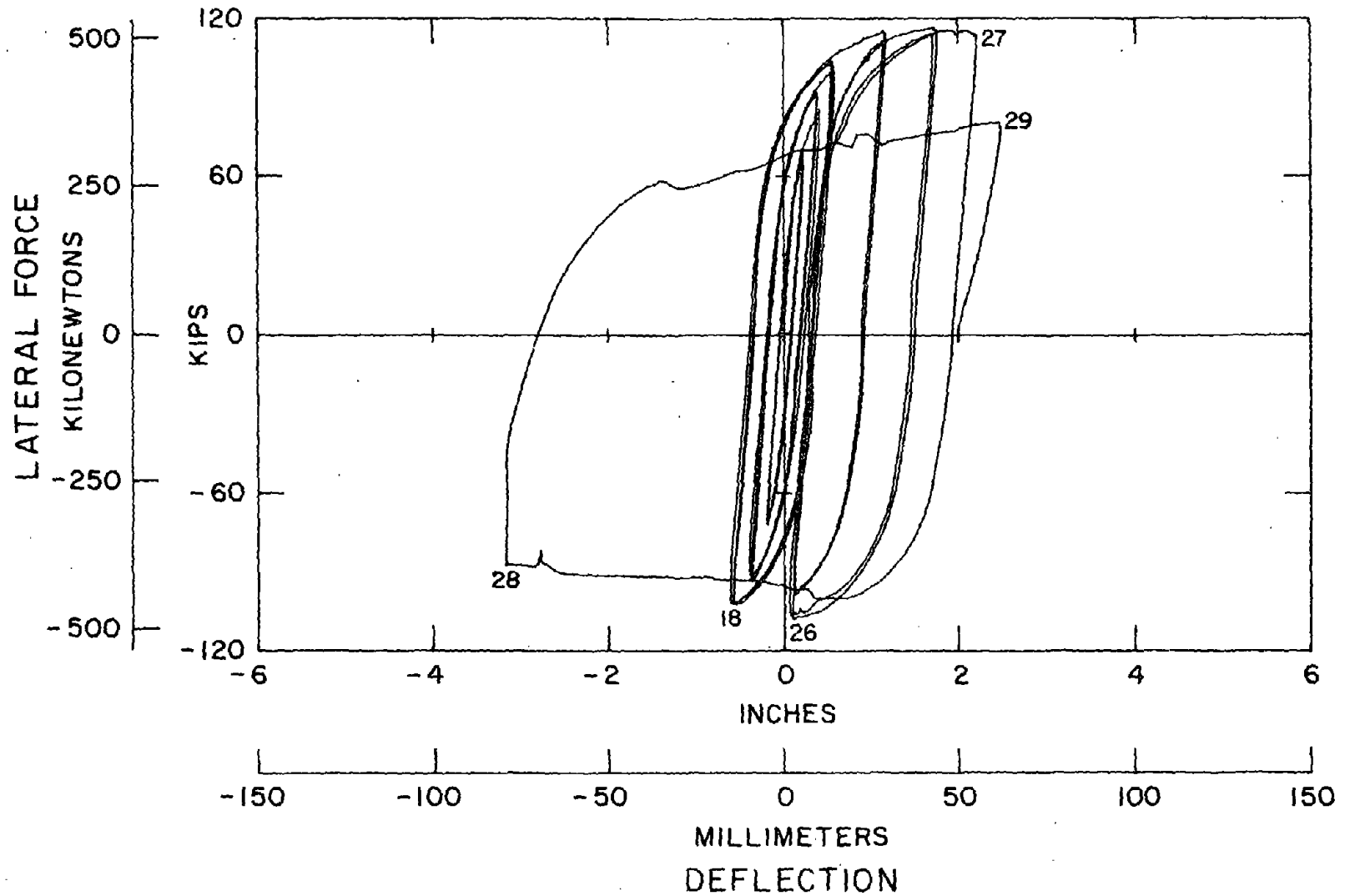


FIGURE 75 - LATERAL FORCE - FIRST FLOOR DEFLECTION HYSTERESIS LOOPS FOR INELASTIC CYCLES OF TEST FRAME 1 AFTER CORRECTION FOR BRACE CONNECTION SLIPPAGE

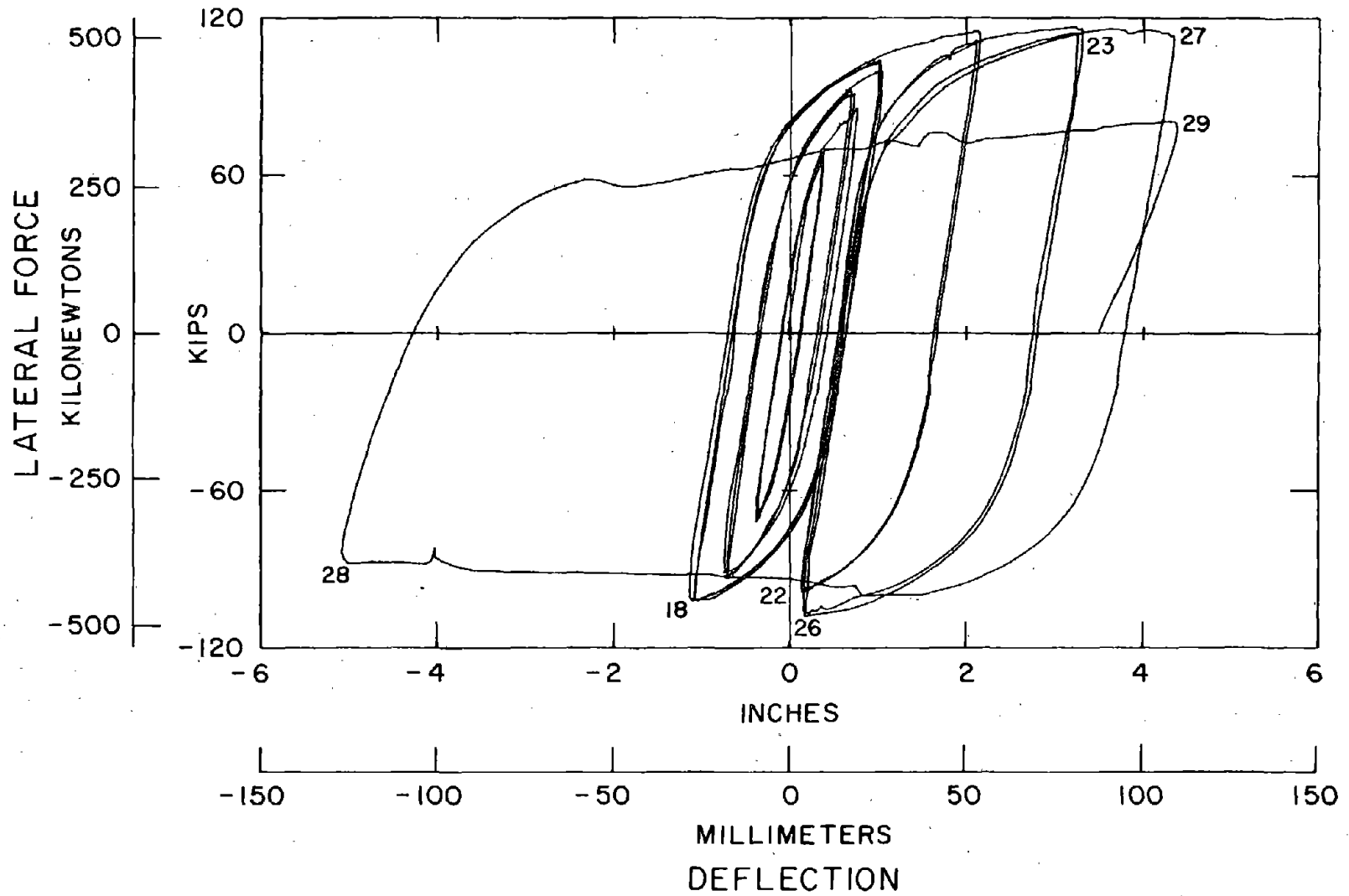


FIGURE 76 - LATERAL FORCE - SECOND FLOOR DEFLECTION HYSTERESIS LOOPS FOR THE INELASTIC CYCLES OF TEST FRAME 1 AFTER CORRECTION FOR BRACE CONNECTION SLIPPAGE

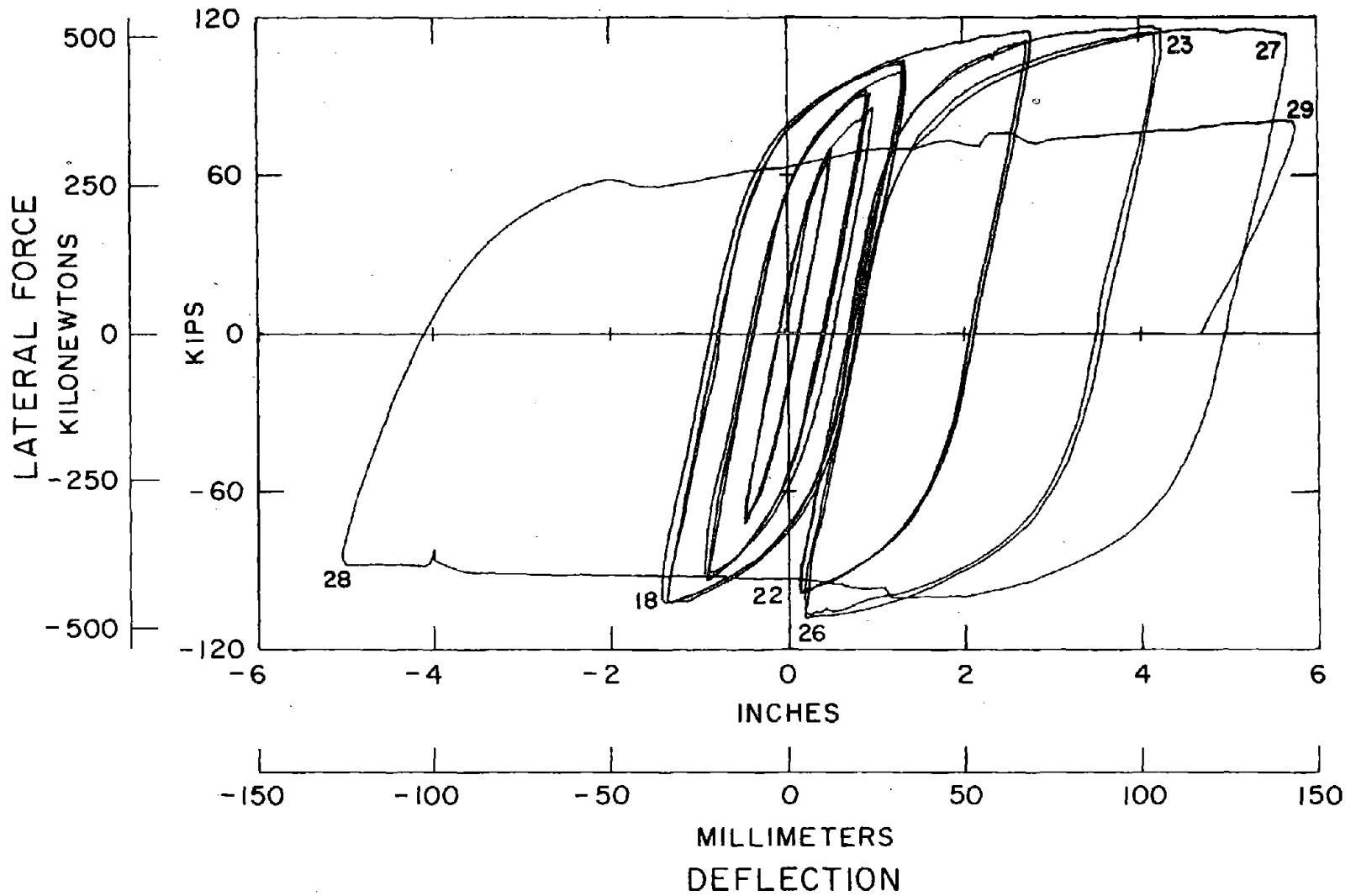


FIGURE 77 - LATERAL FORCE - THIRD FLOOR DEFLECTION HYSTERESIS LOOPS FOR THE INELASTIC CYCLES OF TEST FRAME 1 AFTER CORRECTION FOR BRACE CONNECTION SLIPPAGE

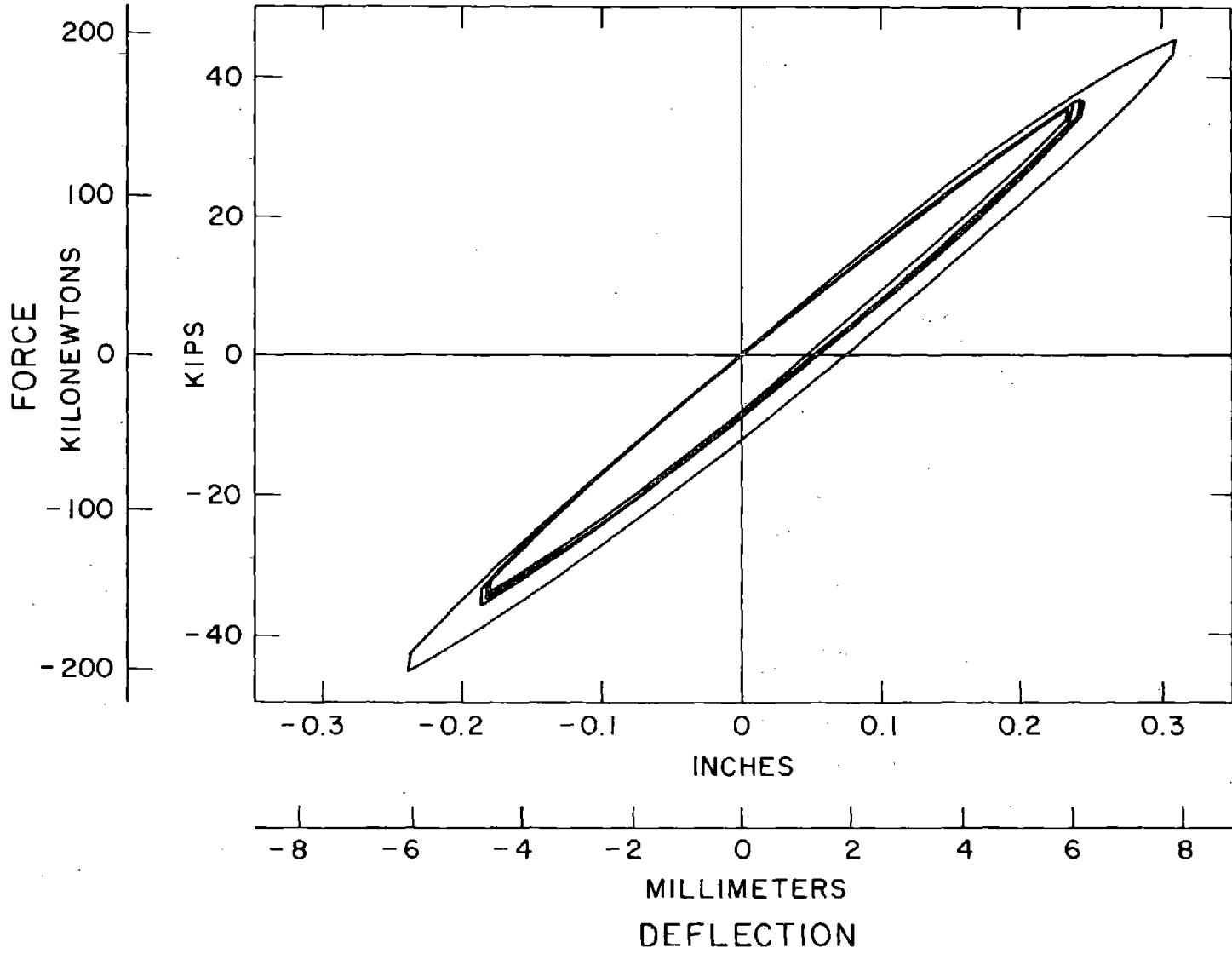


FIGURE 78 - LATERAL FORCE - THIRD FLOOR DEFLECTION FOR THE ELASTIC CYCLES AFTER LP 22 AFTER CORRECTION FOR BRACE CONNECTION SLIPPAGE



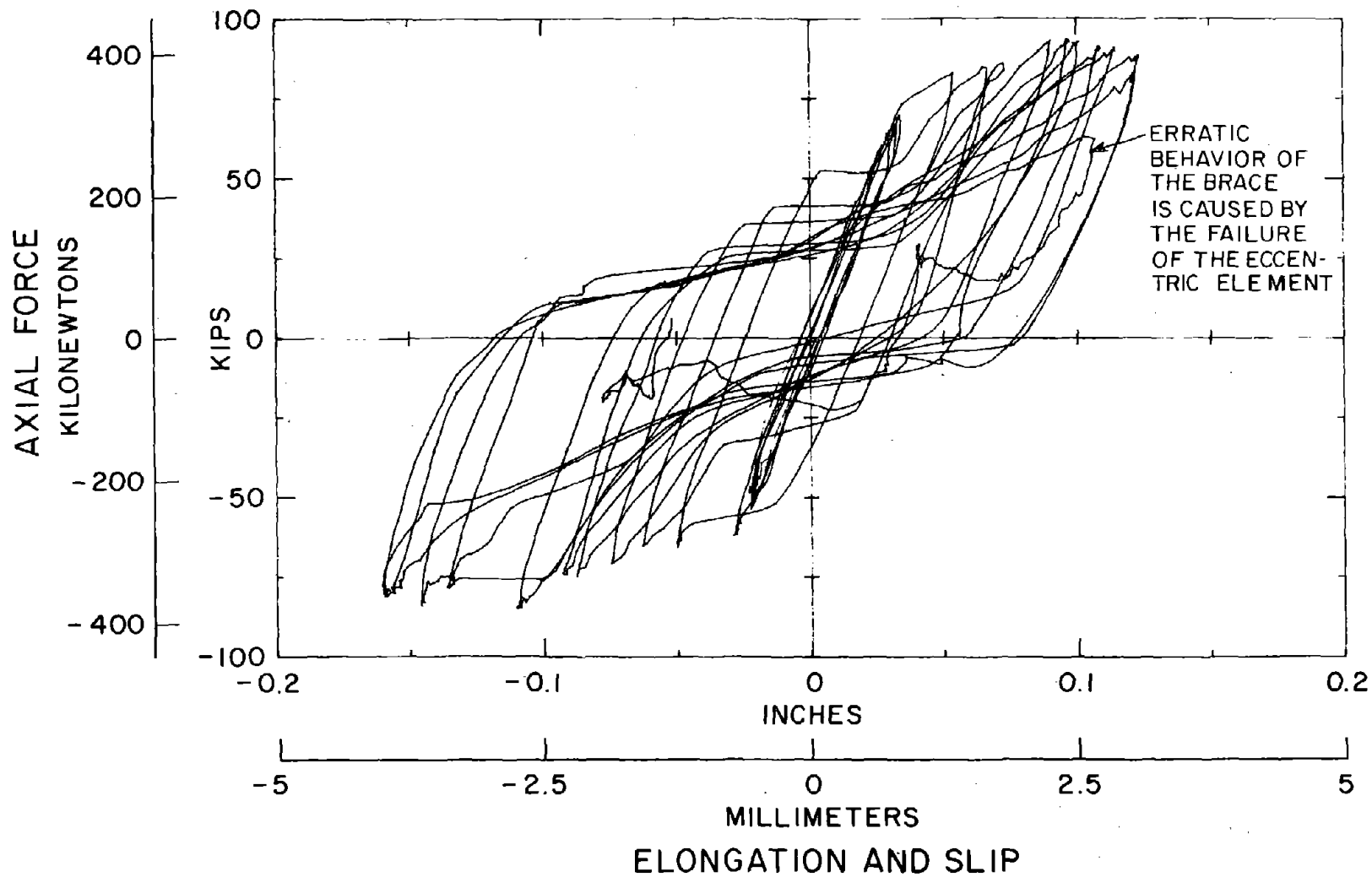


FIGURE 79 - AXIAL FORCE - BRACE SLIPPAGE HYSTERESIS LOOPS FOR THE FIRST FLOOR BRACE OF TEST FRAME 1

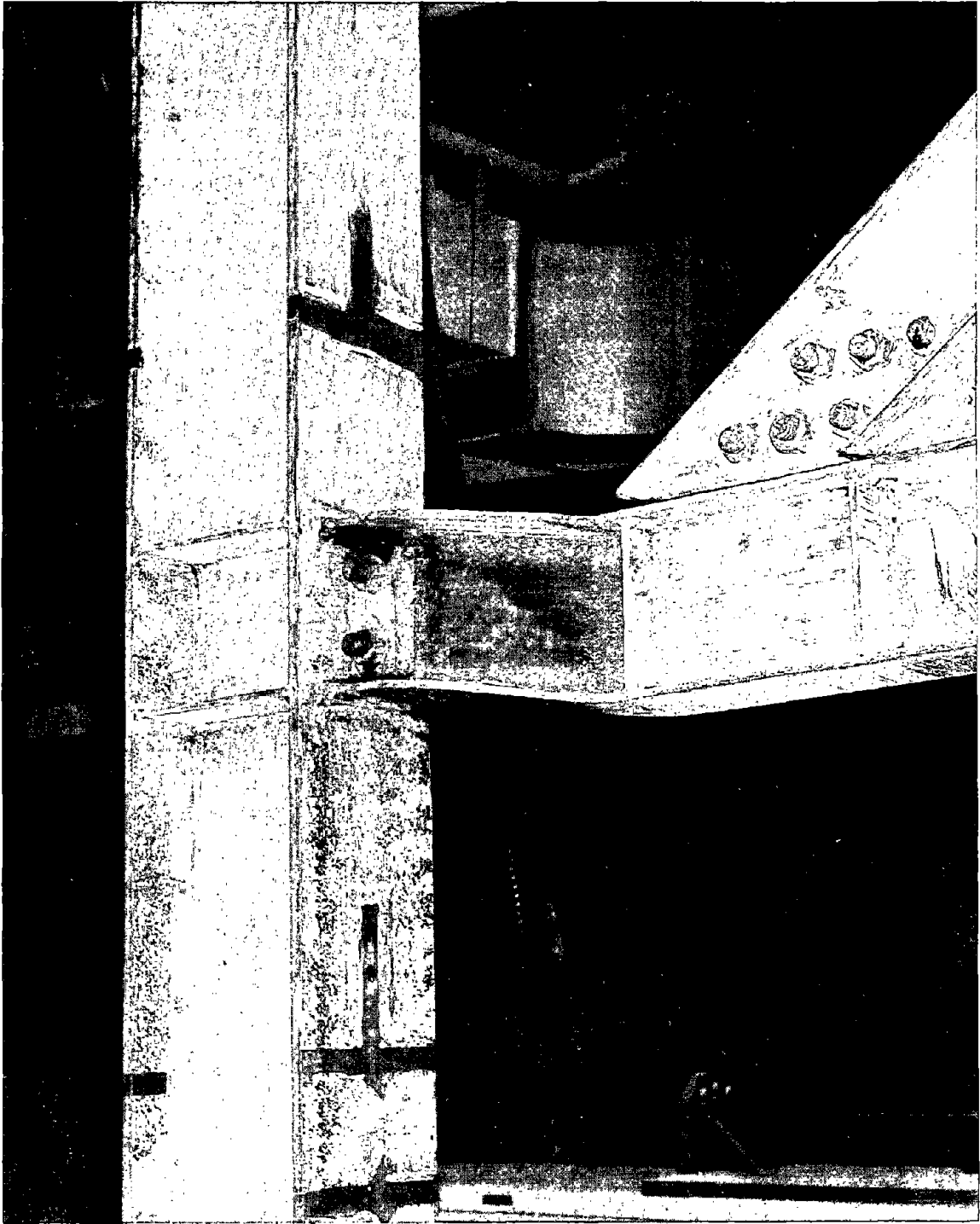


FIGURE 80 - PHOTOGRAPH OF A TYPICAL YIELDED ECCENTRIC ELEMENT

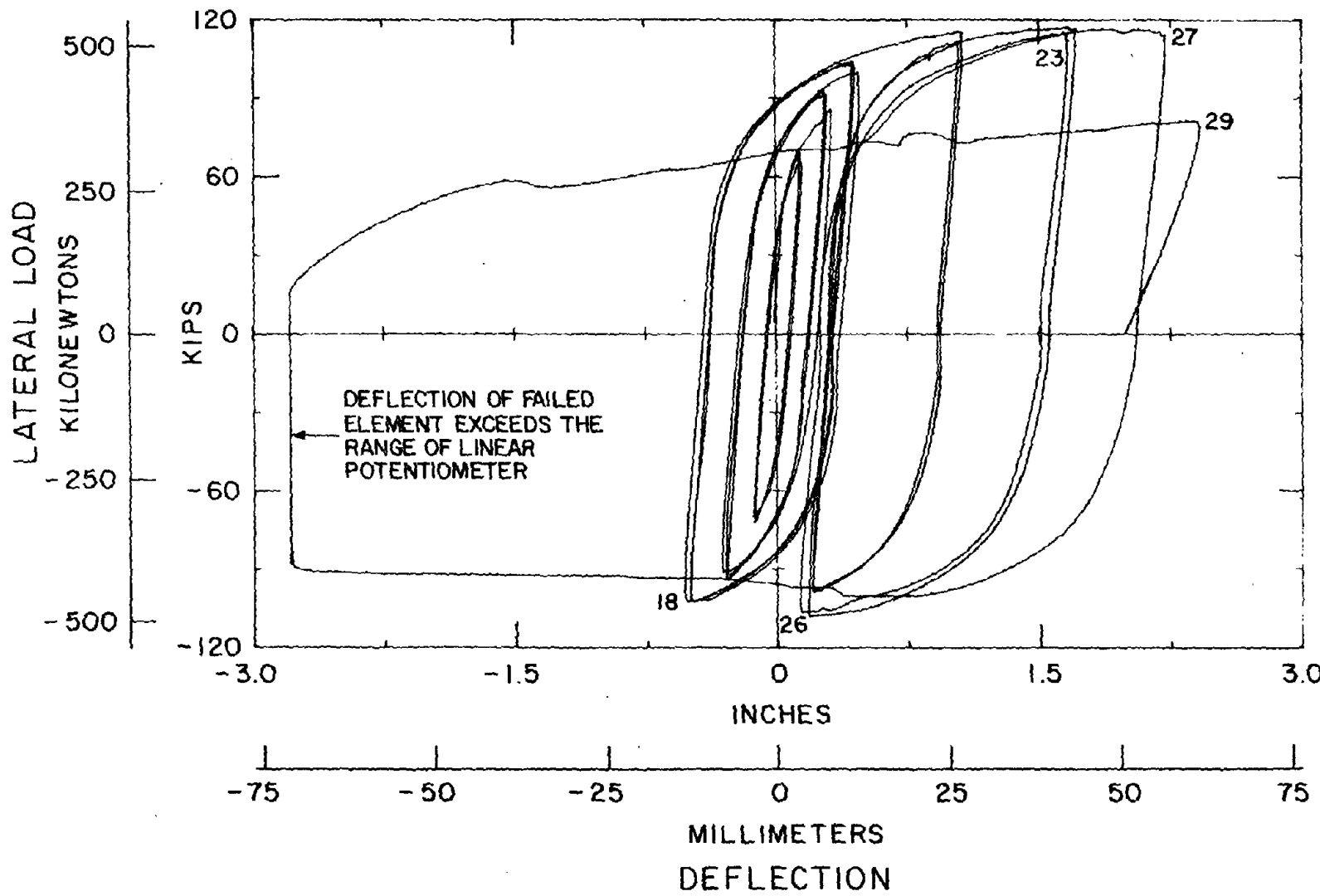


FIGURE 81 - LATERAL FORCE - FLOOR DEFLECTION OF THE FIRST FLOOR SOUTH ECCENTRIC ELEMENT OF TEST FRAME 1

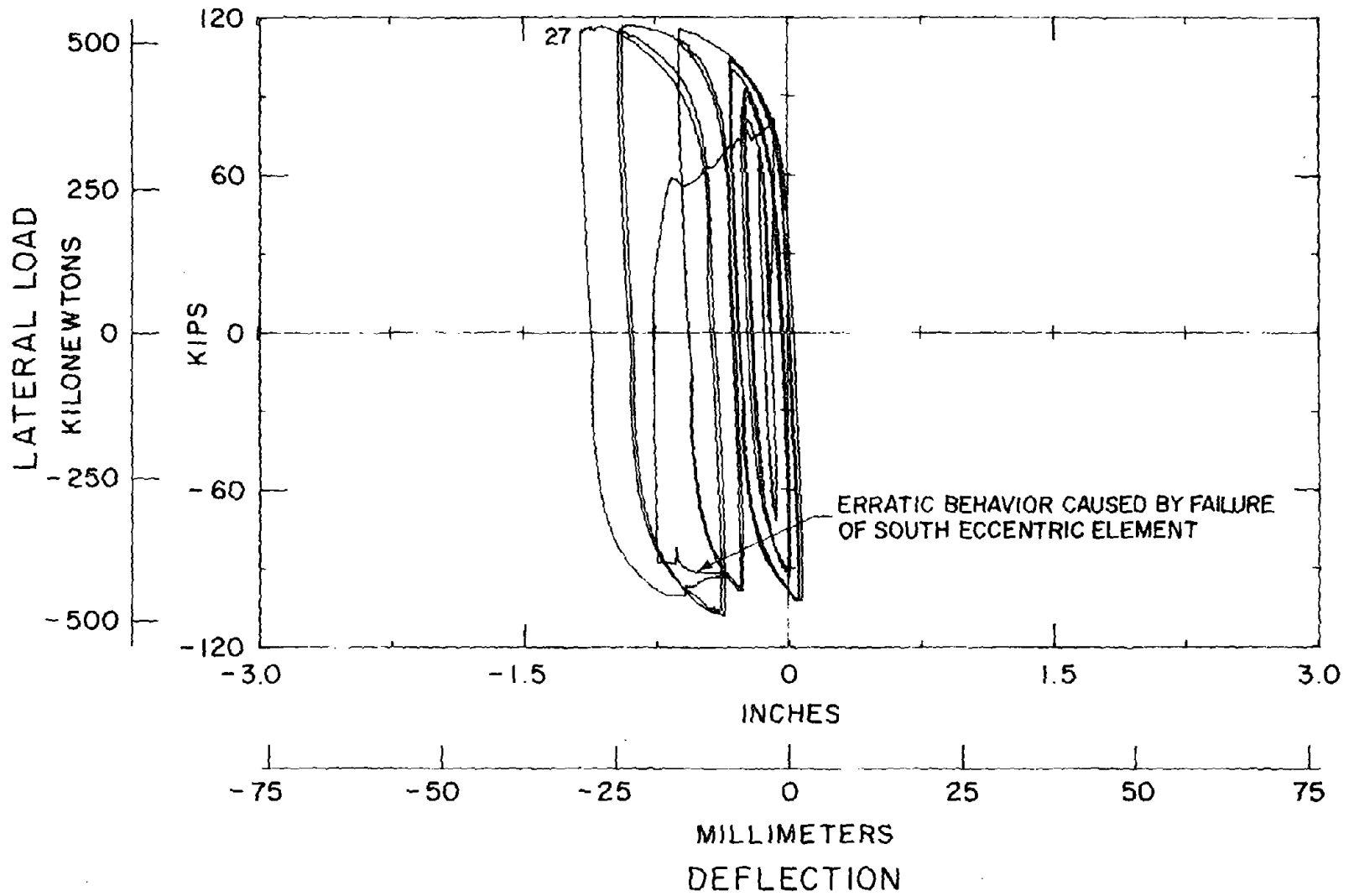


FIGURE 82 - LATERAL FORCE - FLOOR DEFLECTION OF THE FIRST FLOOR NORTH ECCENTRIC ELEMENT OF TEST FRAME 1

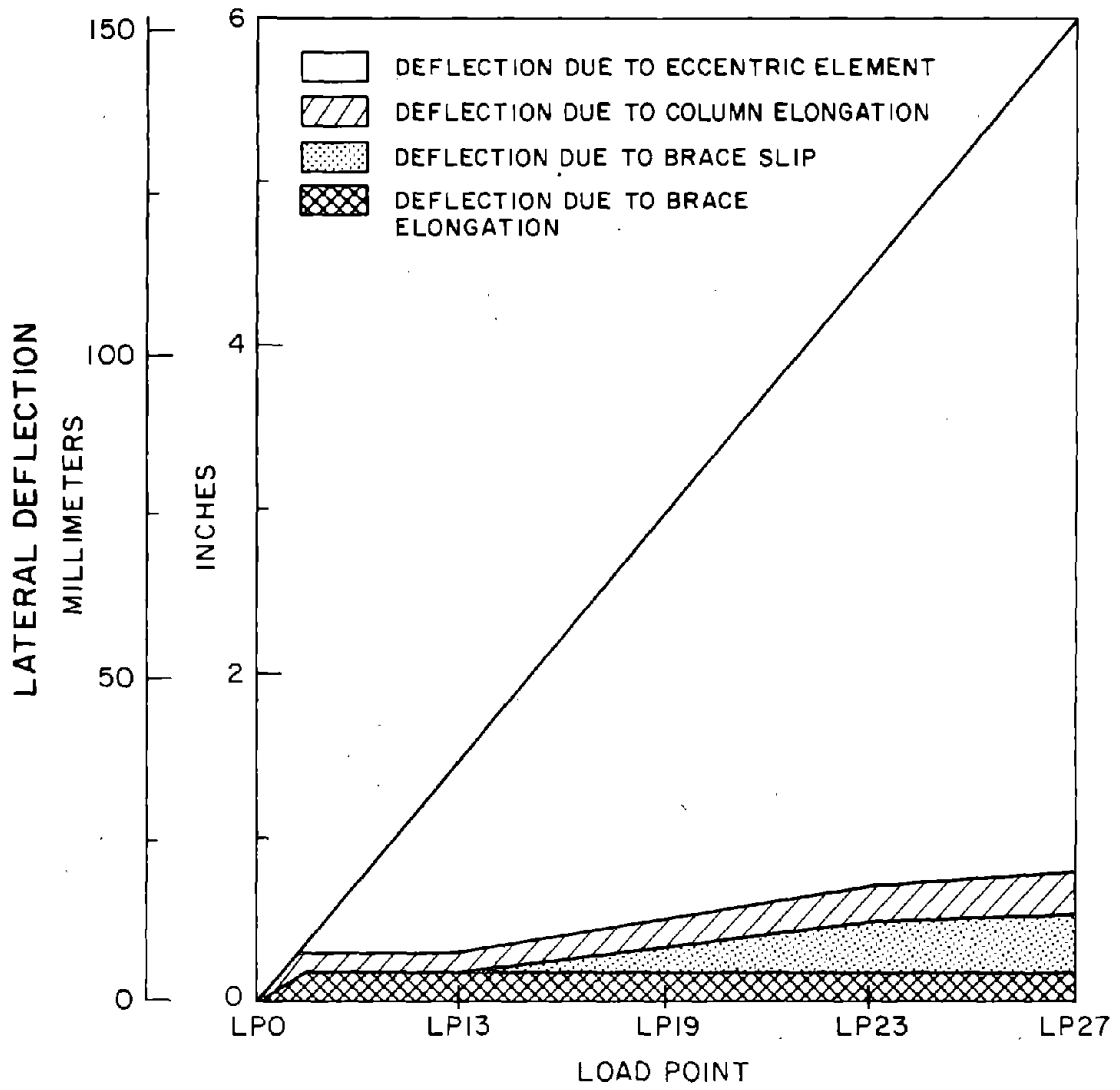


FIGURE 83 - COMPONENTS OF LATERAL DEFLECTION FOR TEST FRAME 1

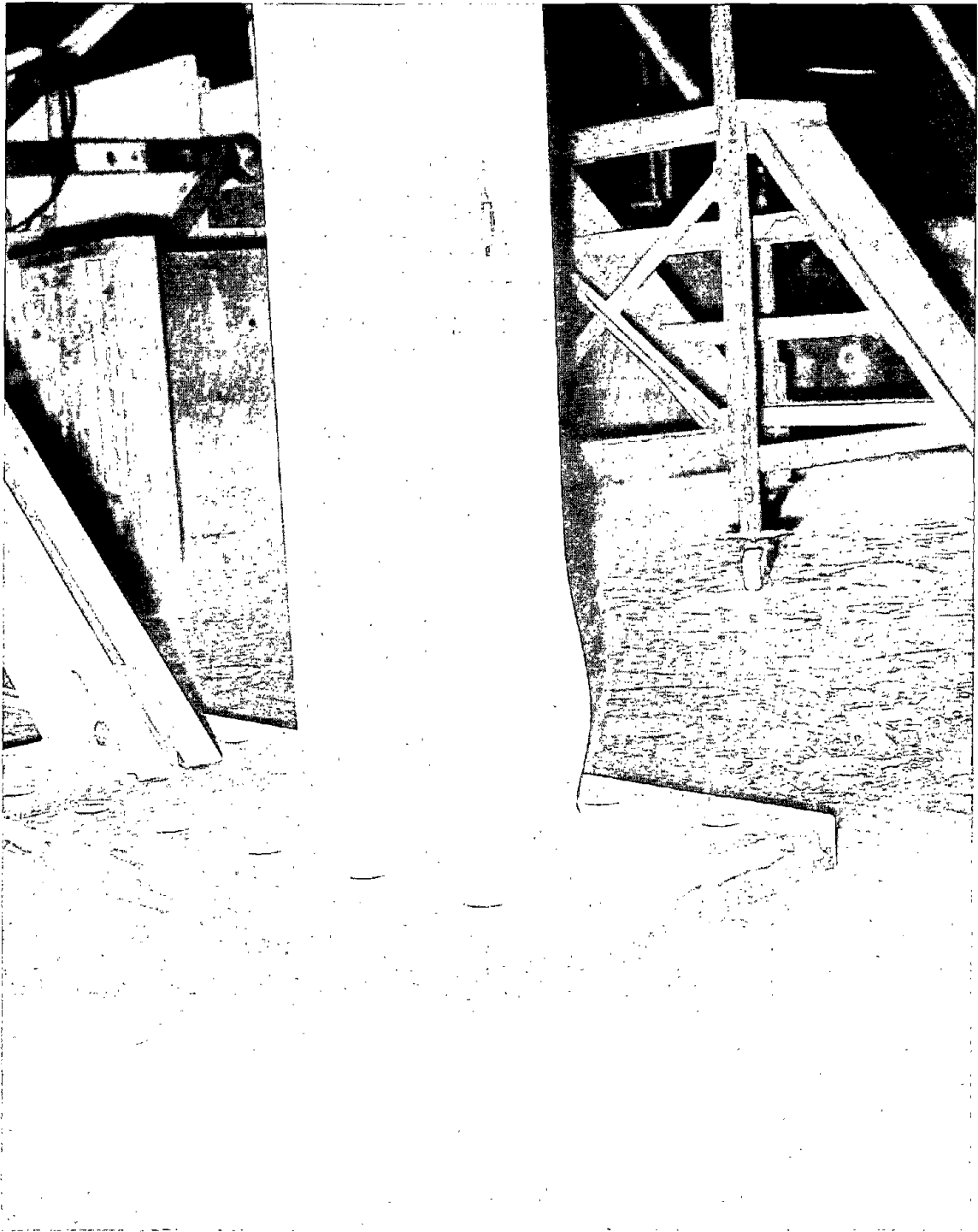


FIGURE 84 - TEST FRAME 1 - COLUMN FLANGE BUCKLING

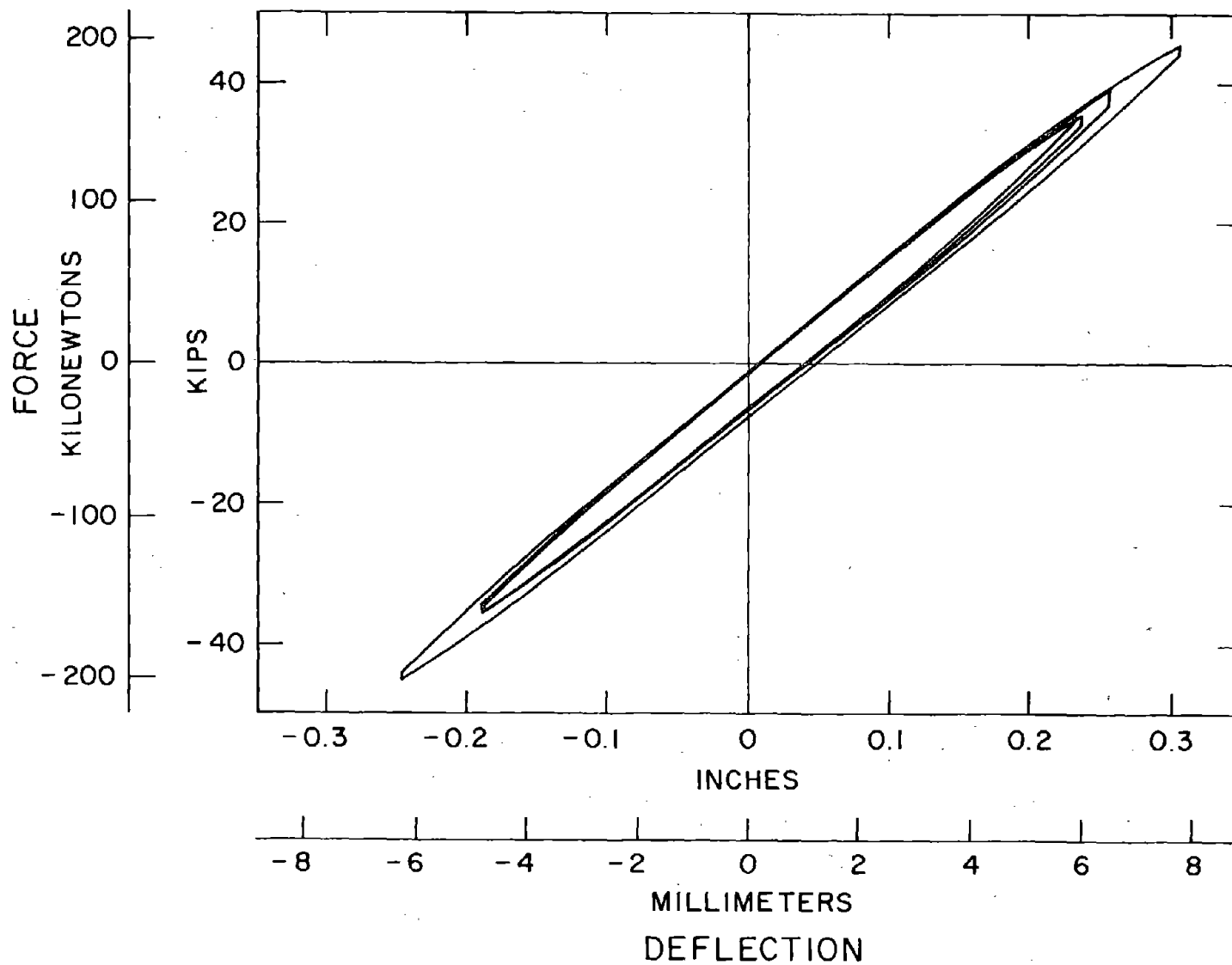


FIGURE 85 - LATERAL FORCE - THIRD FLOOR DEFLECTION HYSTERETIC BEHAVIOR FOR THE ELASTIC CYCLES AT THE START OF TEST 2

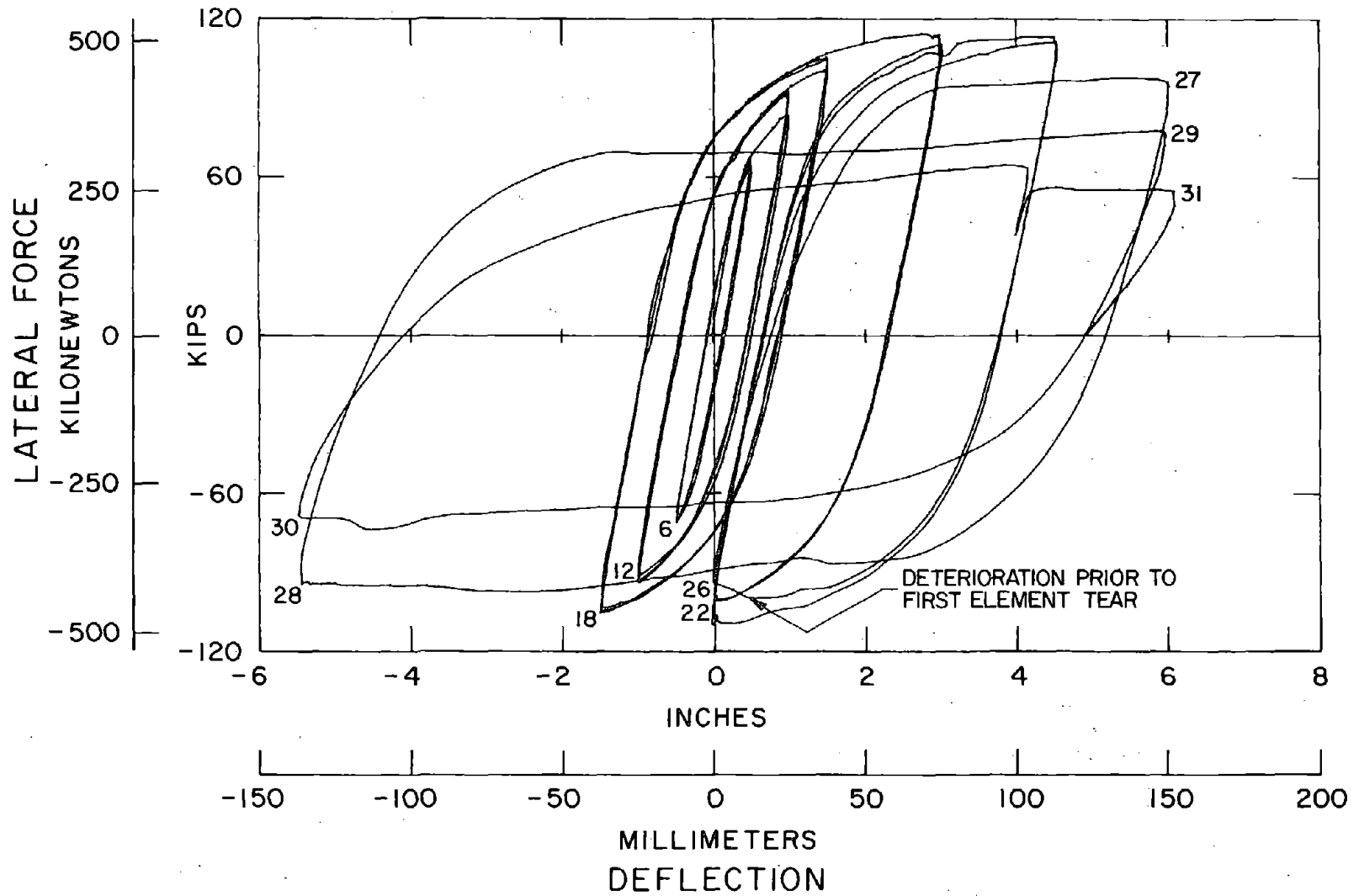


FIGURE 86 - LATERAL FORCE - THIRD FLOOR DEFLECTION HYSTERETIC BEHAVIOR FOR THE INELASTIC CYCLES OF TEST FRAME 2



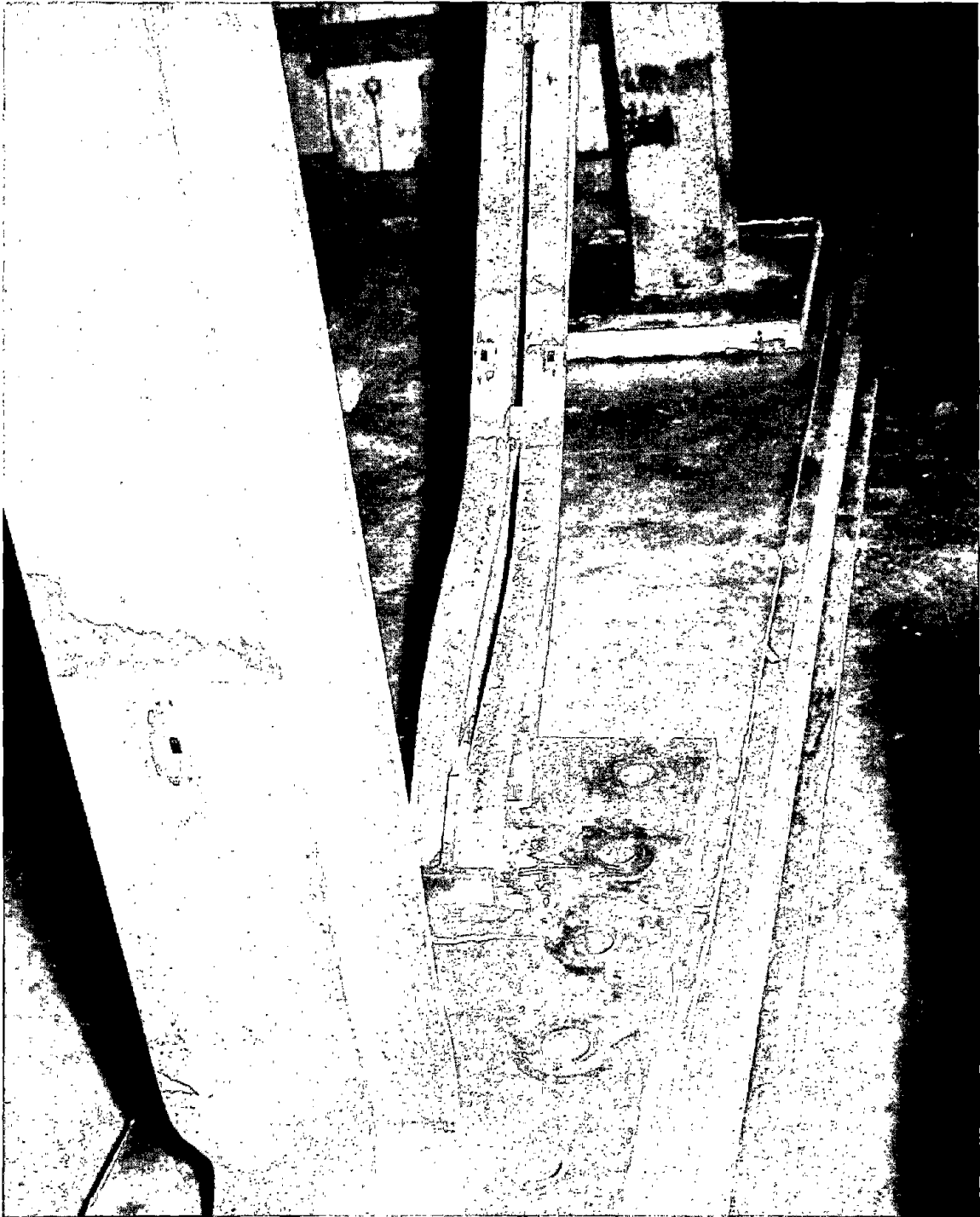


FIGURE 87 - LATERAL TORSIONAL BUCKLING IN TEST FRAME 2

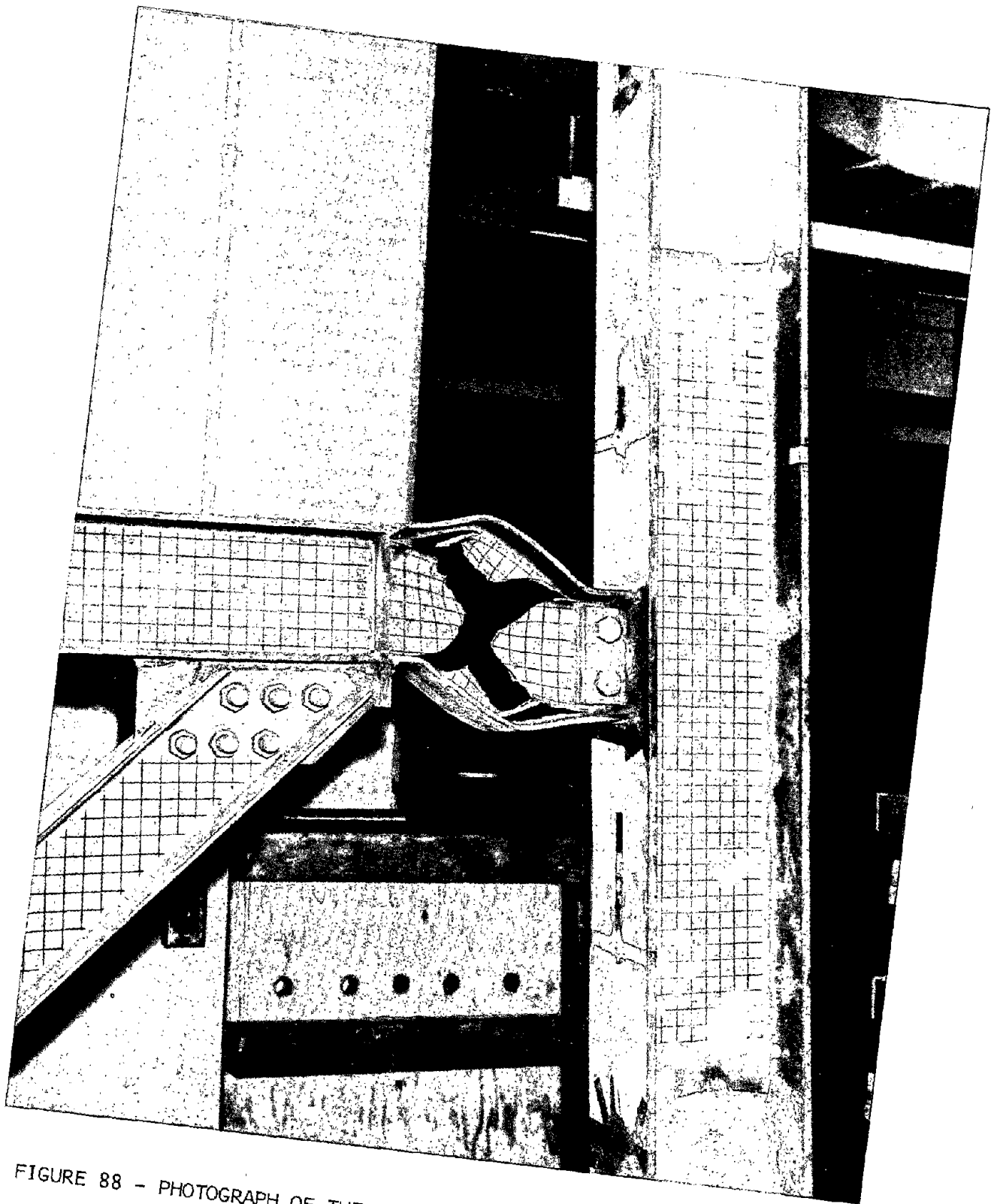


FIGURE 88 - PHOTOGRAPH OF THE TORN ECCENTRIC ELEMENT OF TEST FRAME 2

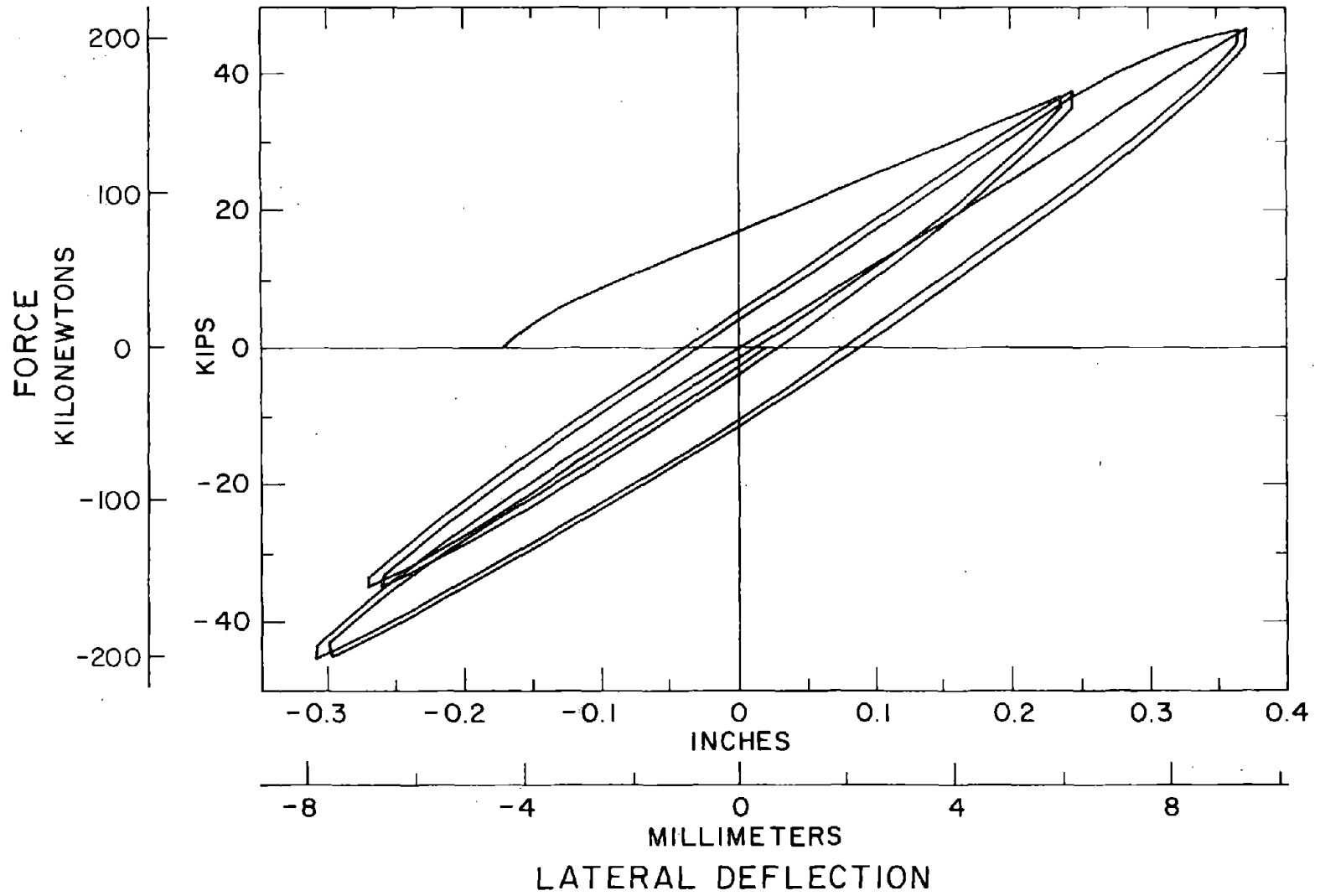


FIGURE 89 - LATERAL FORCE - THIRD FLOOR DEFLECTION HYSTERETIC BEHAVIOR FOR THE ELASTIC CYCLES AFTER LP 26 OF TEST 2

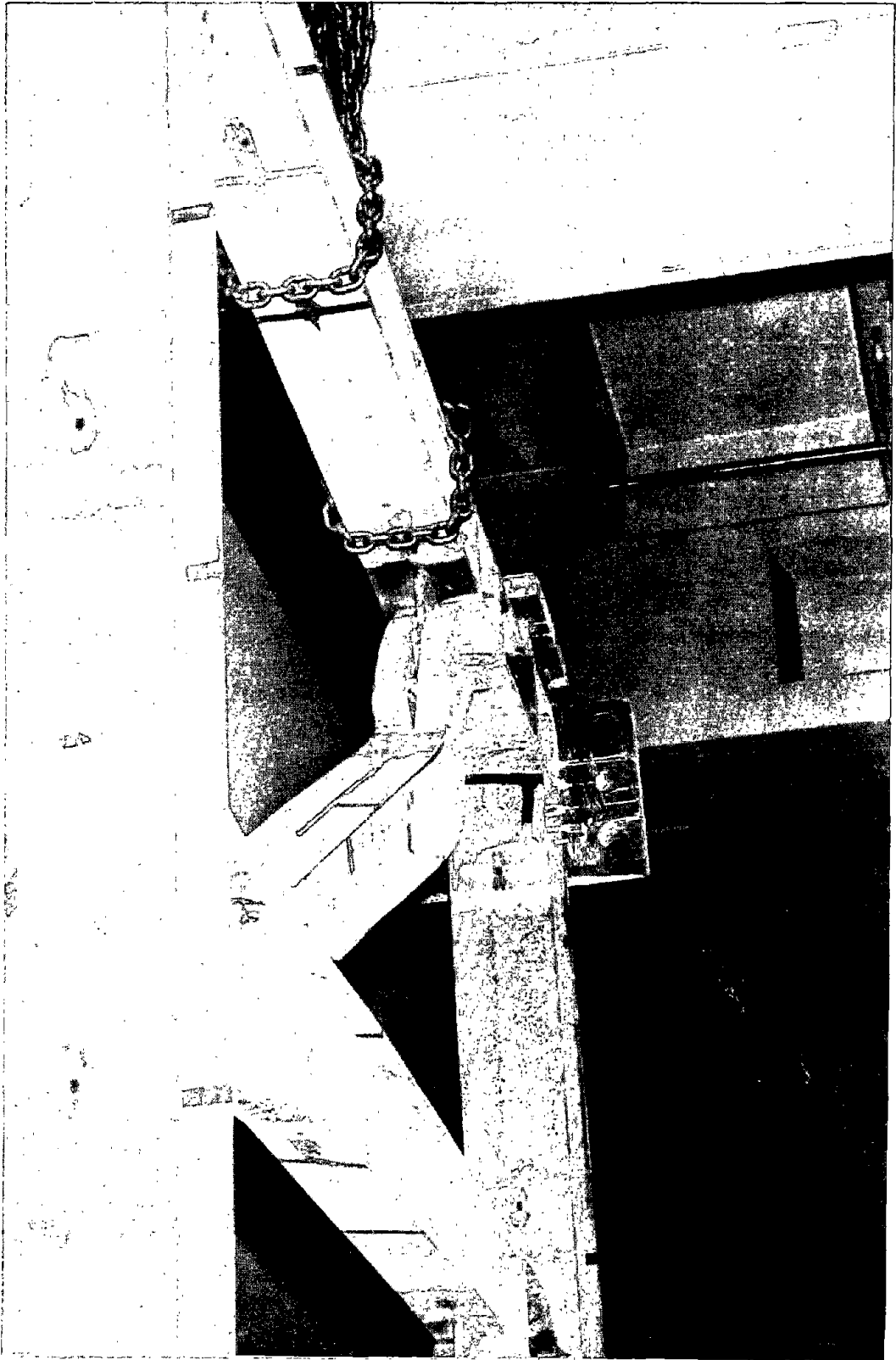


FIGURE 90 - BUCKLED THIRD FLOOR BRACE IN TEST FRAME 2

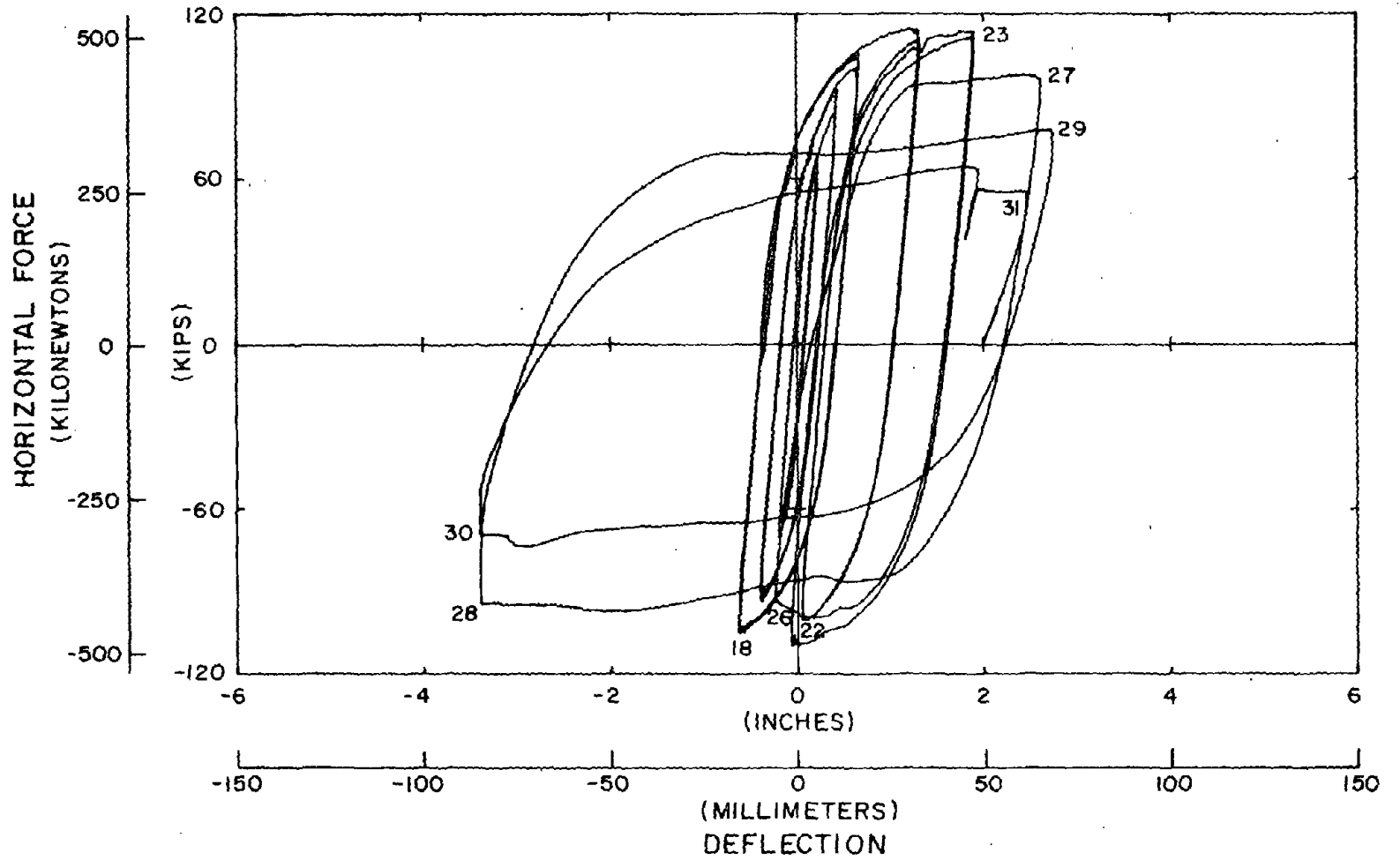


FIGURE 91 - LATERAL FORCE - FIRST FLOOR DEFLECTION HYSTERETIC BEHAVIOR FOR THE INELASTIC CYCLES OF TEST FRAME 2

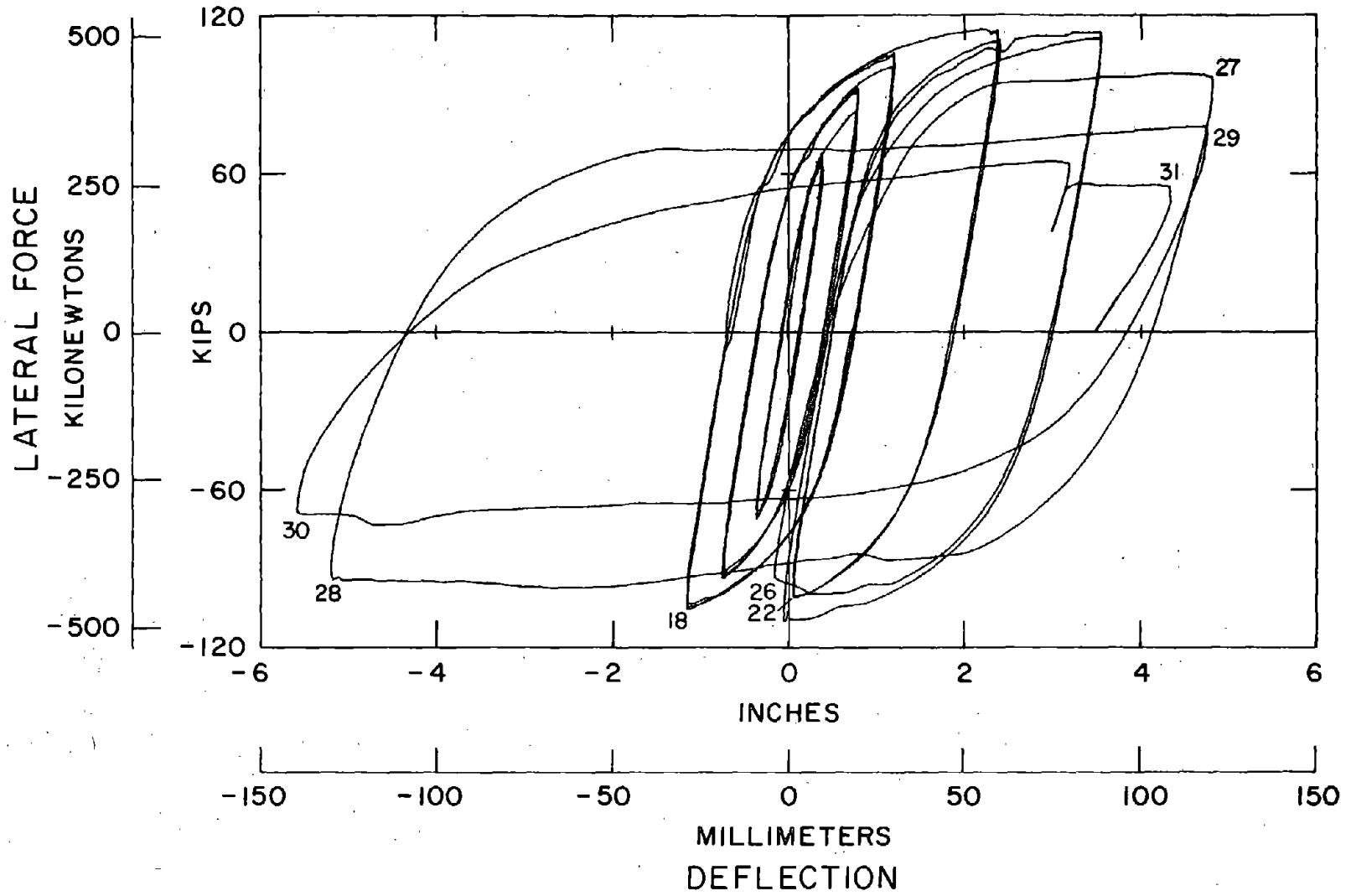
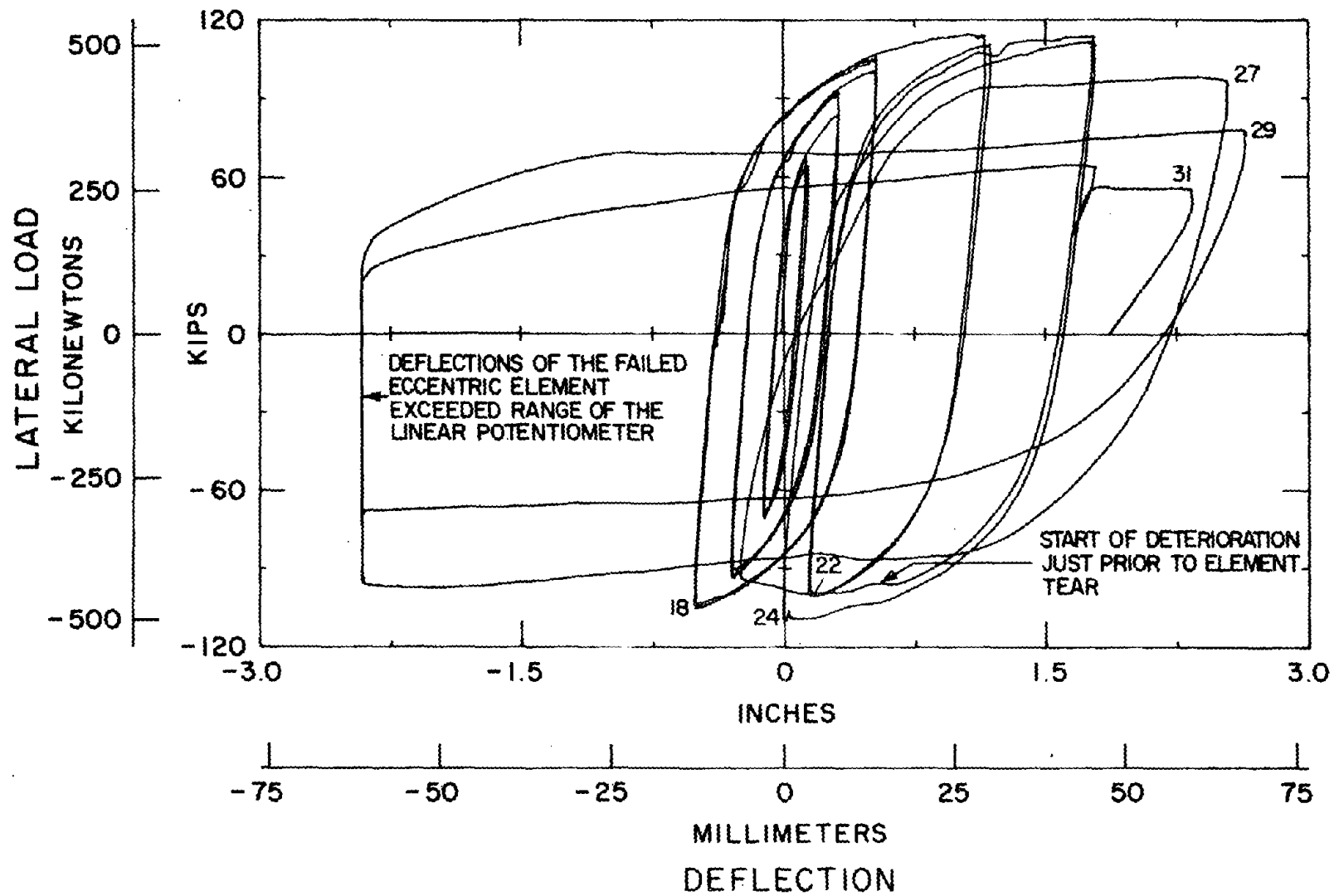


FIGURE 92 - LATERAL FORCE - SECOND FLOOR DEFLECTION HYSTERETIC BEHAVIOR FOR THE INELASTIC CYCLES OF TEST FRAME 2



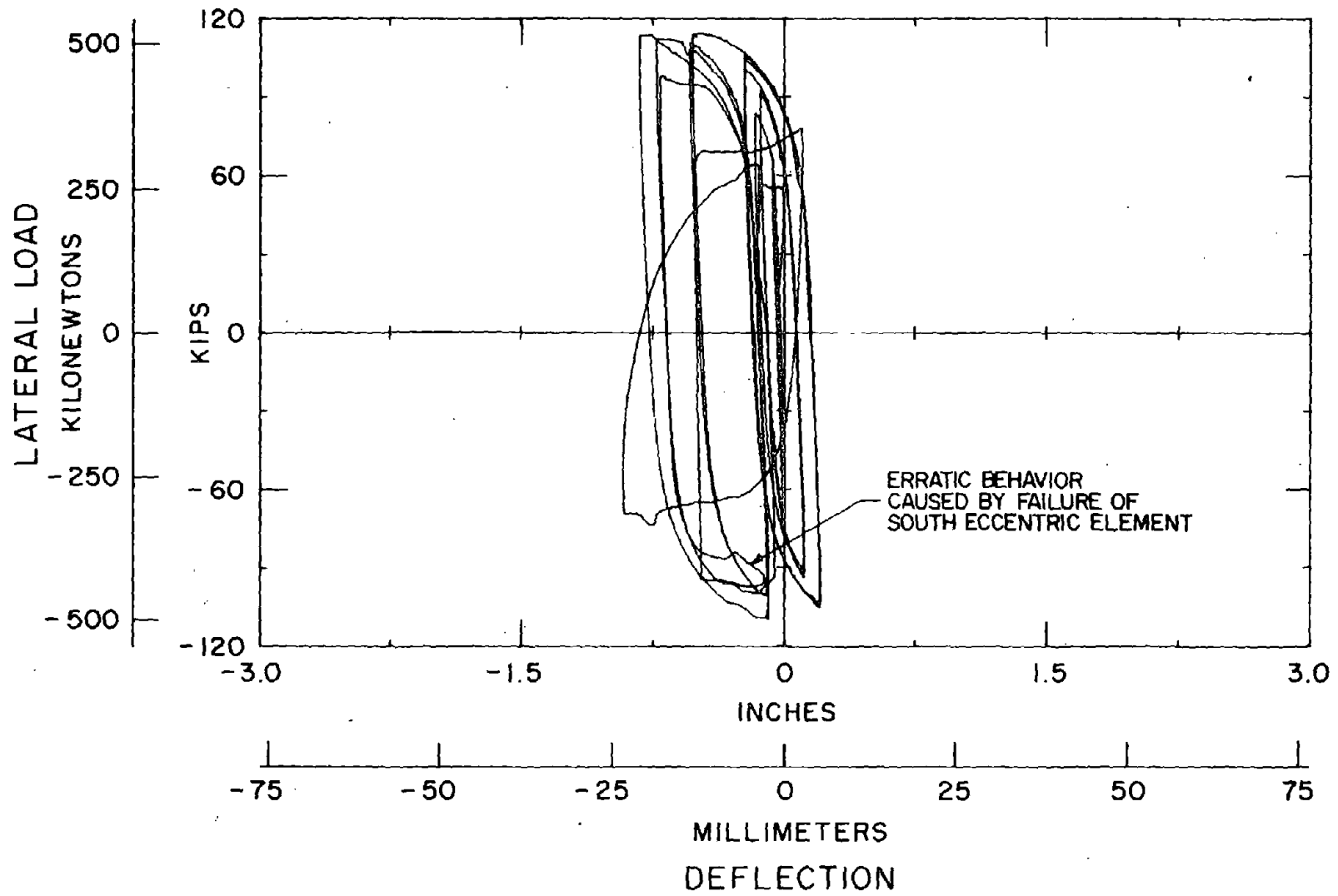


FIGURE 94 - LATERAL FORCE - FLOOR DEFLECTION OF THE FIRST FLOOR NORTH ECCENTRIC ELEMENT OF TEST FRAME 2



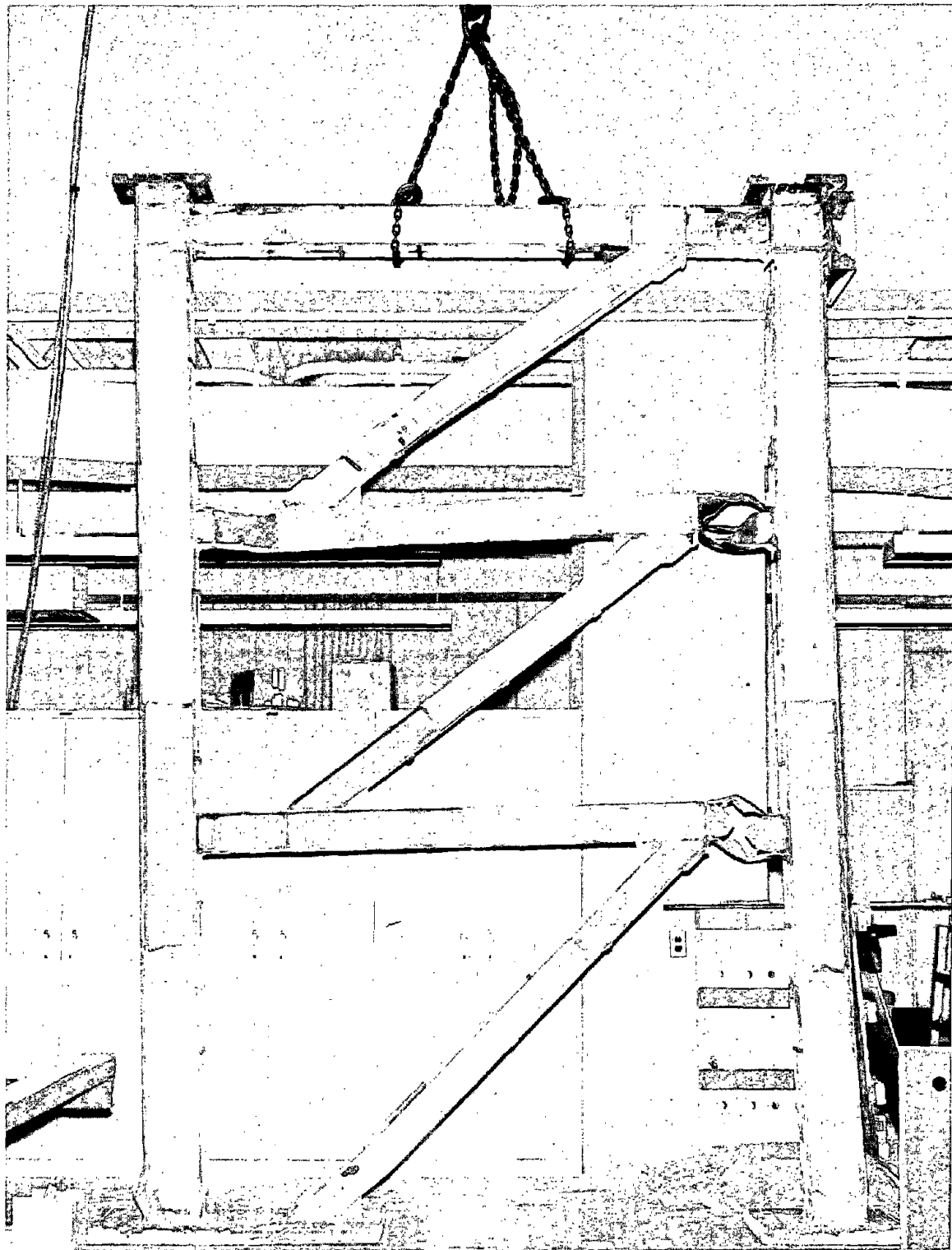


FIGURE 95 - PHOTOGRAPH OF TEST FRAME 2 AFTER COMPLETION OF THE TEST

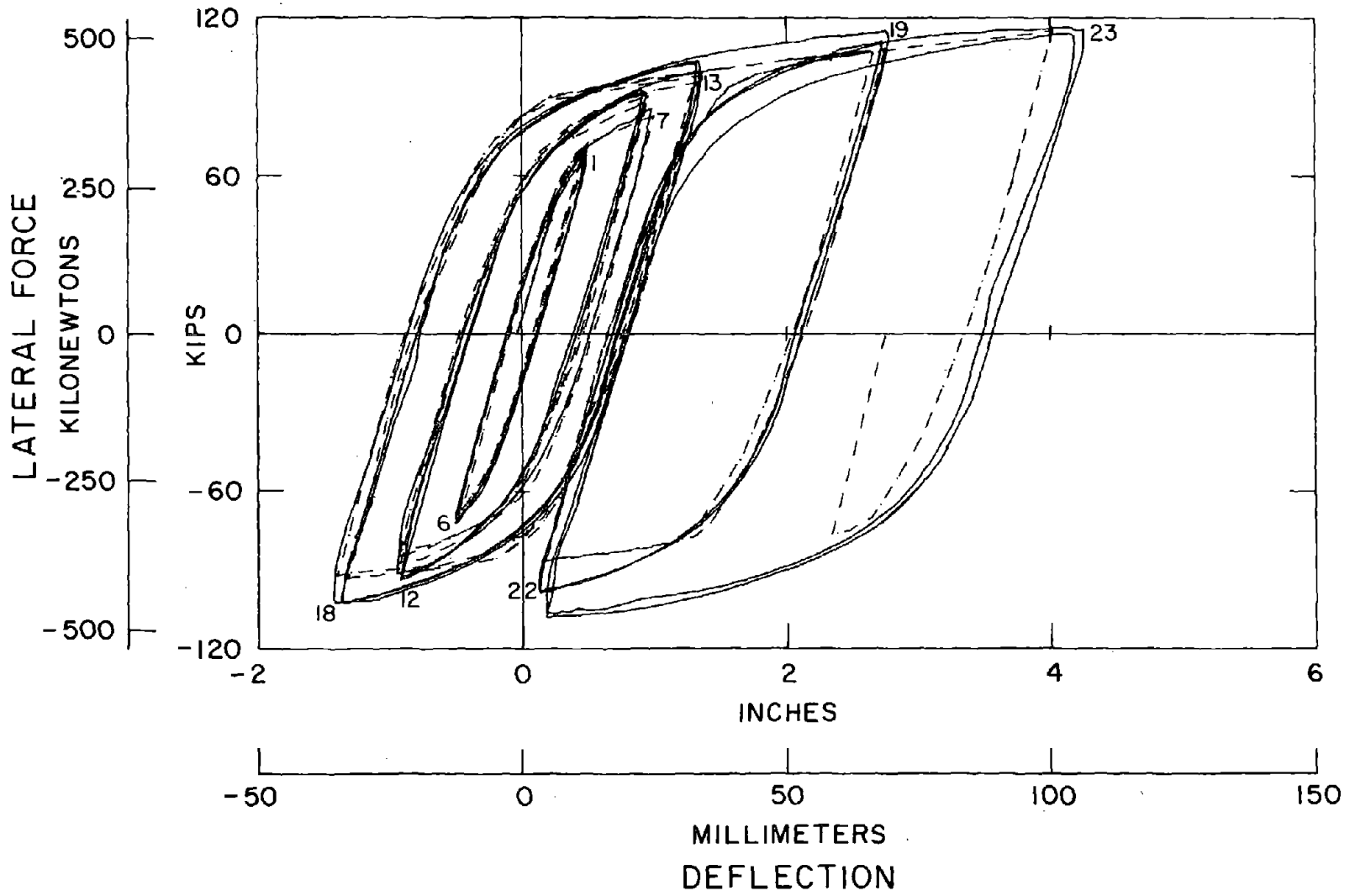


FIGURE 96 - COMPARISON OF THE ANALYTICAL MODEL WITH THE THIRD FLOOR TEST RESULTS OF TEST FRAME 1

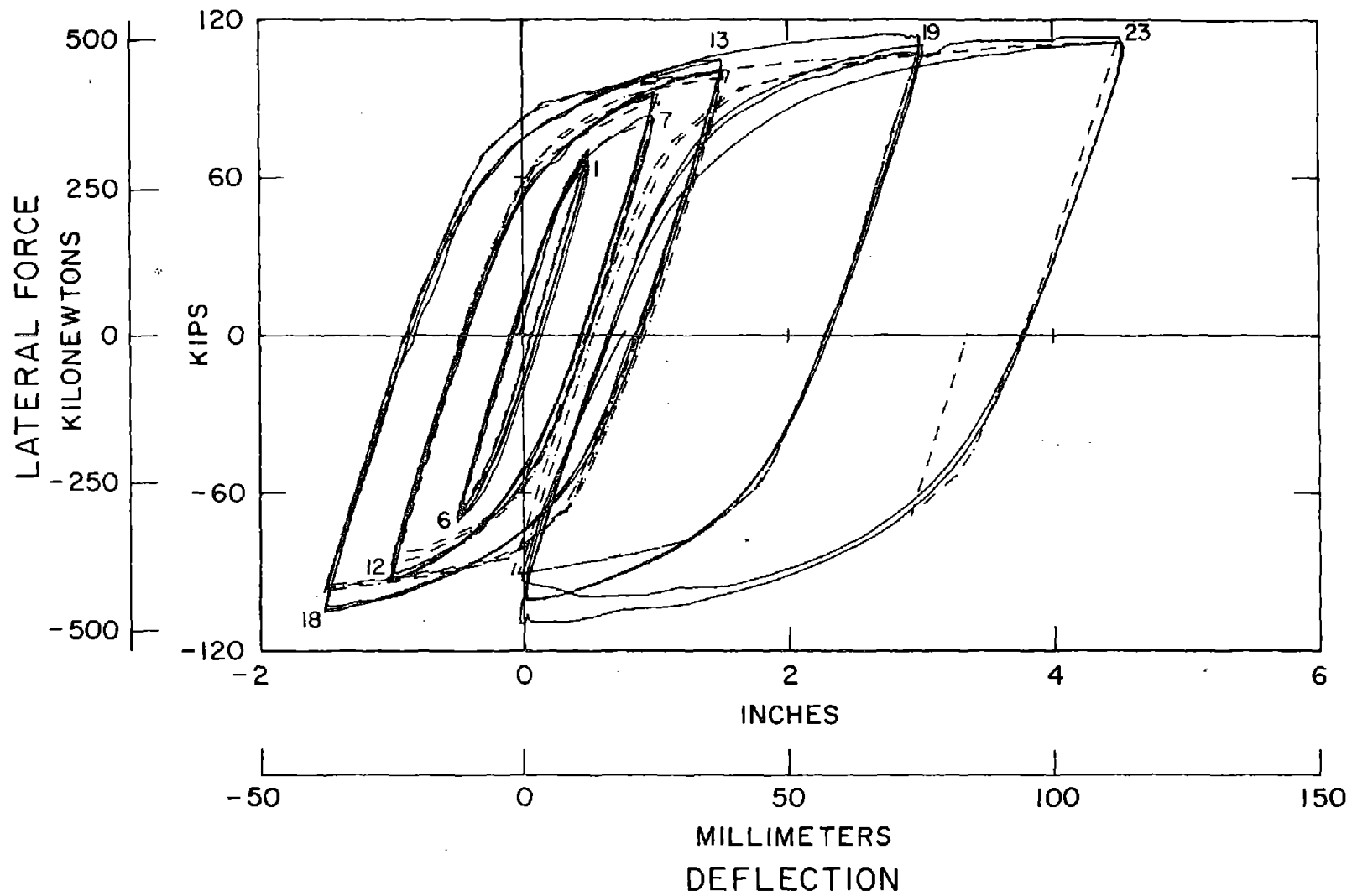
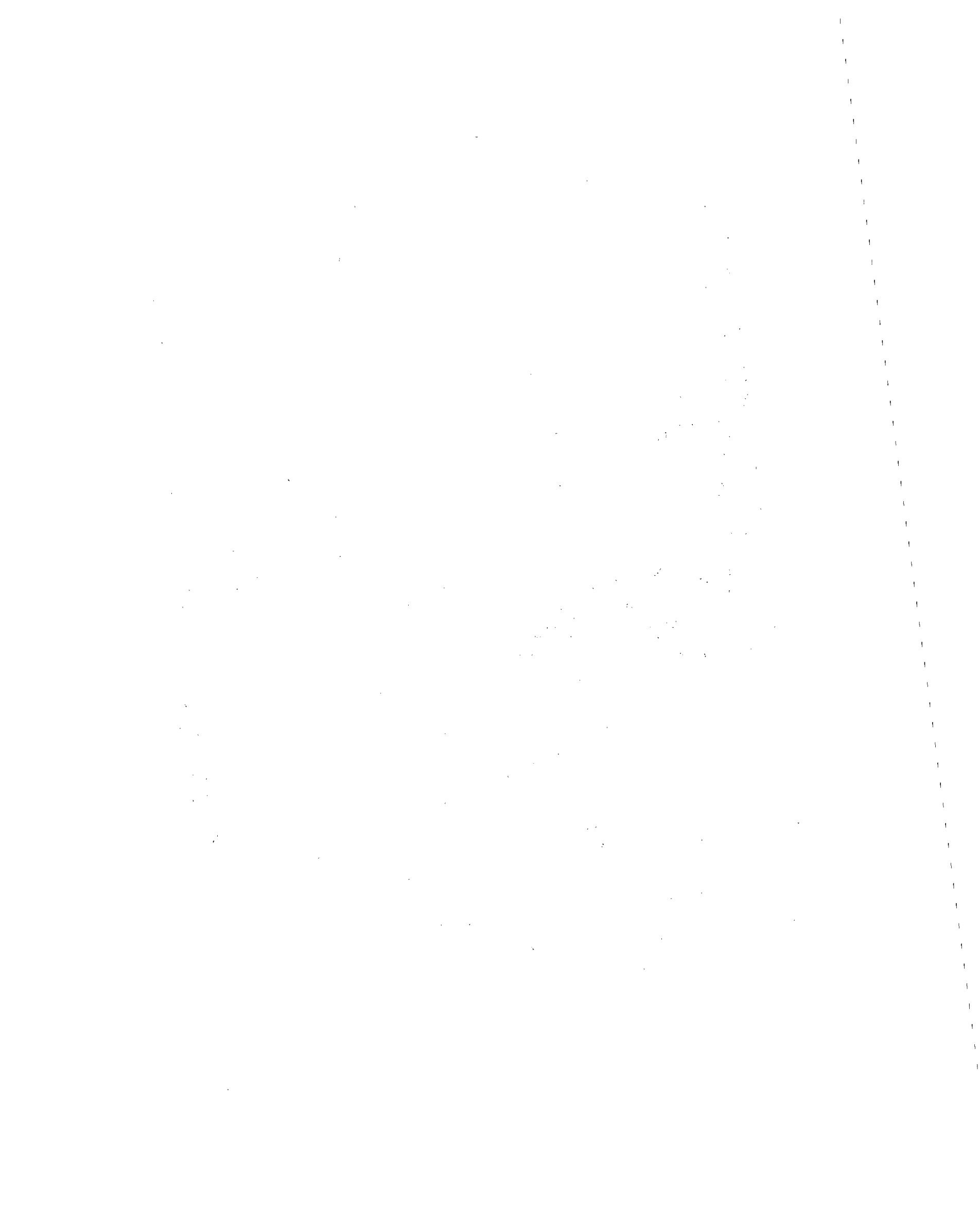


FIGURE 97 - COMPARISON OF THE ANALYTICAL MODEL WITH THE THIRD FLOOR TEST RESULTS OF TEST FRAME 2

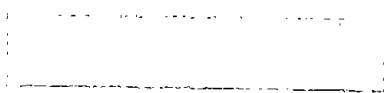


APPENDIX A  
AN EXAMPLE OF MOMENT BALANCING

The basic design of the eccentric bracing system must consider the inelastic behavior of the frame. Moment balancing (24,25) is a very versatile procedure for considering this behavior. This technique is based on the concept that, if a structure is designed to any moment diagram which satisfies statics, the loadings will be a lower bound of the true strength of the structure. If the design is also performed to attain a specific mechanism, the lower and upper bound theories are simultaneously satisfied. It is immaterial how the distribution of forces and moments was attained in moment balancing. The distribution can be obtained by a good guess or by any of a number of rational procedures. This appendix will give an example of one possible way of finding an acceptable moment distribution. The example frame and its factored loadings are shown in Fig. A1. The brace is assumed to be pin-connected, but all other connections are moment-resisting connections.

It is also very necessary to consider the desired collapse mechanism of the frame when performing moment balancing on an eccentrically braced frame. The eccentric system should be designed so that essentially all of the plastic action is concentrated in the eccentric beam elements. Therefore, the mechanism shown in Fig. A2 is appropriate.

The first step in the balancing procedure is to obtain an initial estimate of member forces and bending moments for the brace, the beam, and the column. In arriving at these estimates, it is required that each individual member be in equilibrium even though the nodes may not be in equilibrium.



The balancing then proceeds by arbitrarily assigning approximately 80% of the lateral load to the brace since it provides approximately 80% of the lateral stiffness. This assumption is applied to the brace in the example shown in Fig. A3. Once the original estimate of the brace force has been agreed upon, this force can then be used to compute the moments and forces in the beam. This is done by assuring that the eccentric node is in equilibrium, and the final moment diagram is consistent with the collapse mechanism (see Figure A2). Figure A4 indicates a typical loading diagram for the top beam. End moments  $M_1$  and  $M_2$  of this figure should be chosen so that the moment diagram of the beam is compatible with the collapse mechanism shown in Fig. A2. It should be borne in mind that the plastic hinges of the beam form at the face of the column; they do not form at the center line intersection. Because of the steep moment gradient in the eccentric beam element, this distinction makes a considerable difference. The initial estimates of the force and moment diagram is found for the other beams just as they were for the top beam.

The forces and moments in the columns are found by recalling that the remaining 20% of the lateral forces which are not carried by the brace must be carried by the columns. This is assumed to be equally distributed between both columns as is shown in Fig. A5. Figure A5 shows that the two end moments,  $M_1$  and  $M_2$ , are coupled by the known shear force. However, one of these end moments must be determined by an arbitrary estimate. Figures A6(a) and A6(b) represent typical initial distributions of forces and bending moments which could be obtained by the above procedure. The forces in Fig. A6(a) were chosen so that all of the nodes are in equilibrium with respect to force. Further Fig. A6(b)

was chosen so that the bending moments are in equilibrium at the eccentric nodes. However, the bending moments are not in equilibrium at the beam-to-column joints. The next step in the moment balancing procedure is to eliminate these imbalances. There are several methods of eliminating these imbalances, but the easiest is to note that the moment diagram of the column can be shifted, without affecting the balanced shear and axial forces, by adding a constant bending moment over the length of the column as shown in Fig. A7. This technique first must be used to balance the top nodes, and the constant moment is passed down the column to the next node. Each successive node is balanced down the column until all nodes are in equilibrium. This correction procedure produces the final moment diagram shown in Fig. A8. All forces and moments are in equilibrium with this moment diagram.

It should be recalled that the initial distribution of moments shown in Fig. A6(b) was obtained by arbitrarily assigning one of the end moments for each column segment. The correction procedure used to obtain Fig. A8 is modifying this initial assignment, and so if the arbitrarily selected end moment had been chosen with enough foresight, there would have been no imbalance.

Since the distribution shown in Fig. A8 is in equilibrium, moment balancing permits the use of this distribution of forces to perform a plastic design. However, a better, more economical design will result if the distributed forces are examined carefully. The above distribution produced columns which are under single curvature. Single curvature results in larger column sizes than double curvature. This problem is not too severe in this particular example, but in other cases it could produce unrealistically high design moments in the columns. When this

happens, the balancing should be corrected by slightly increasing or decreasing the proportion of lateral force which is carried by the brace and rebalancing. Thus, the final step in this balancing procedure is to examine the resulting moment diagram, and, if necessary, revising the initial estimate of the percentage of lateral force carried by the brace and repeating the first two steps.

This has been an example of one way of handling moment balancing. The method, which is used to obtain the final force distribution, is not important. It is important to assure that the final force and moment be consistent with the desired collapse mechanism (see Fig. A2). The procedure used above does this by making a judicious selection of end moments for the beam and holding these end moments constant throughout the balancing. This same procedure could also be applied to very large or tall structures. However, it is recommended, that the balancing be done in parts for these structures. That is, the very top story or stories should be completely checked and balanced before starting on the next lower level. The balancing then proceeds down the structure, and the analysis is simplified, because it is always concerned with only a small part of the total structure.



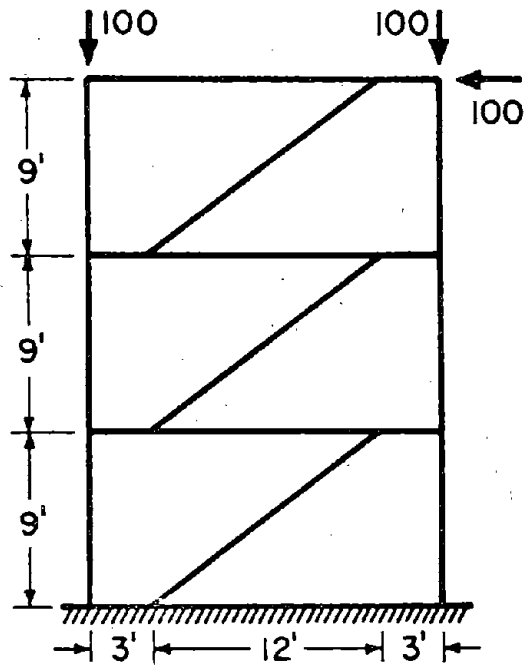


FIGURE A1 - EXAMPLE PROBLEM

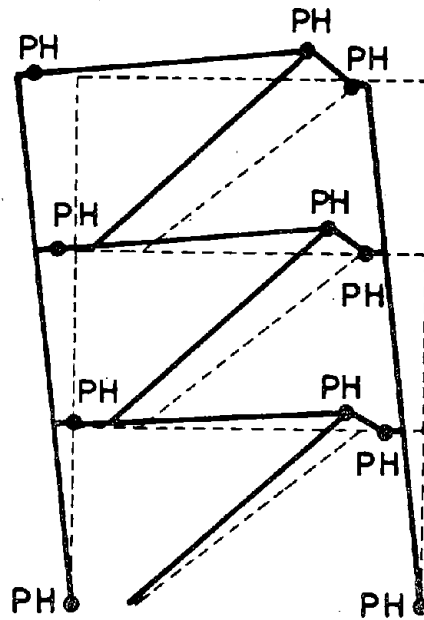


FIGURE A2 - COLLAPSE MECHANISM

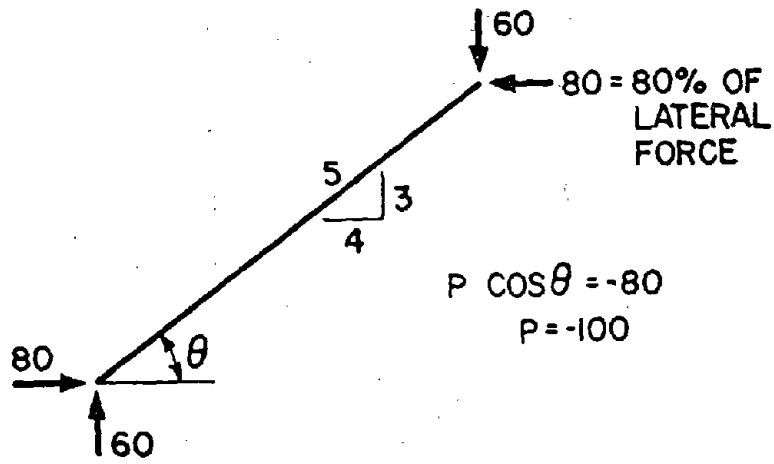


FIGURE A3 - INITIAL ESTIMATE OF THE BRACE FORCE

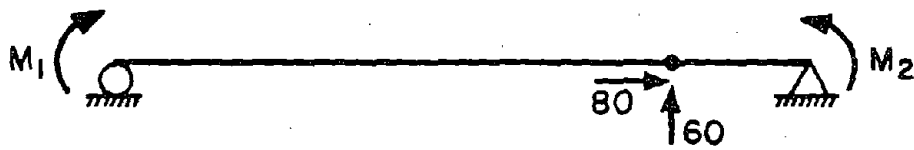


FIGURE A4 - INITIAL ESTIMATE OF THE BEAM MOMENT DIAGRAM

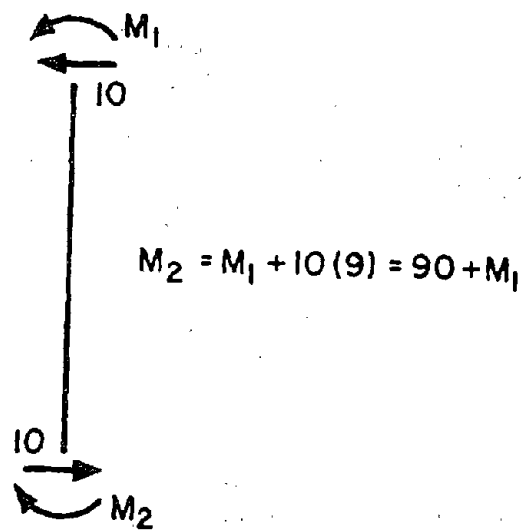
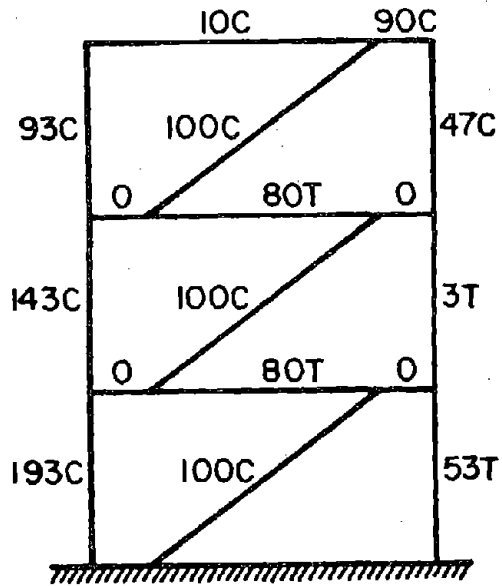
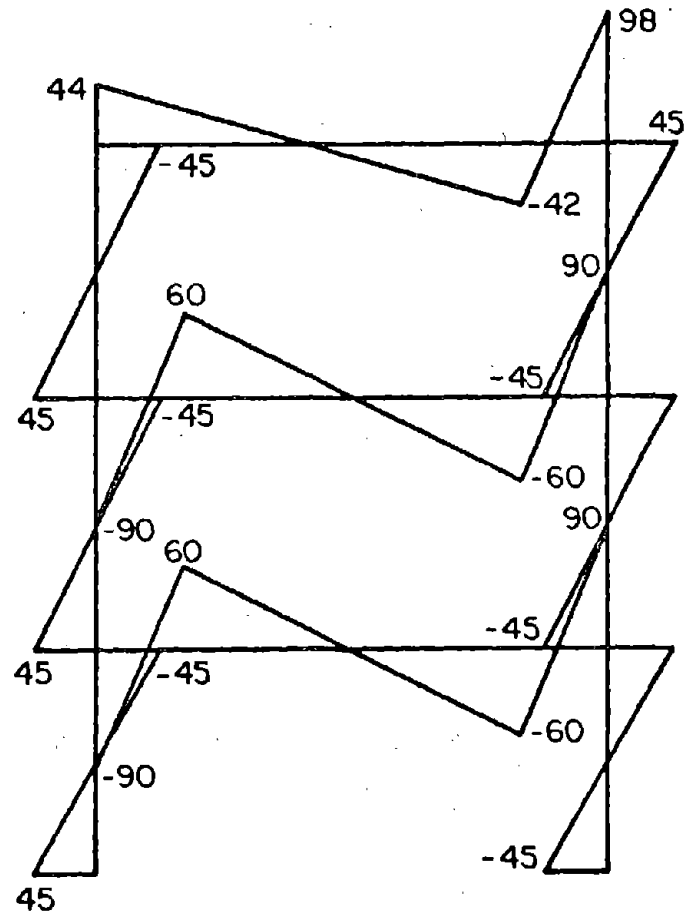


FIGURE A5 - INITIAL ESTIMATE OF THE COLUMN MOMENT DIAGRAM

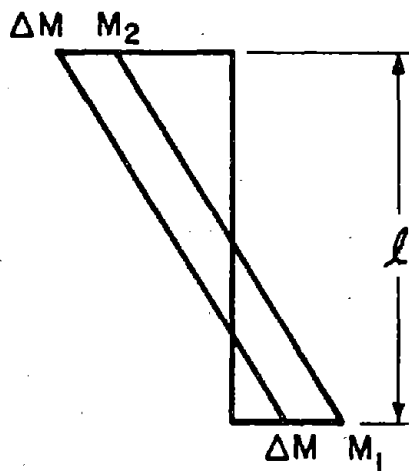


(A) AXIAL FORCES



(B) BENDING MOMENTS

FIGURE A6 - INITIAL ESTIMATE OF THE MEMBER FORCES AND MOMENTS



$$\begin{aligned} \text{SHEAR} &= \frac{M_1 + M_2}{l} \\ &= \frac{(M_1 + \Delta M) + (M_2 + \Delta M)}{l} \end{aligned}$$

FIGURE A7 - CONSTANT MOMENT CORRECTION FOR COLUMN MOMENT DIAGRAM

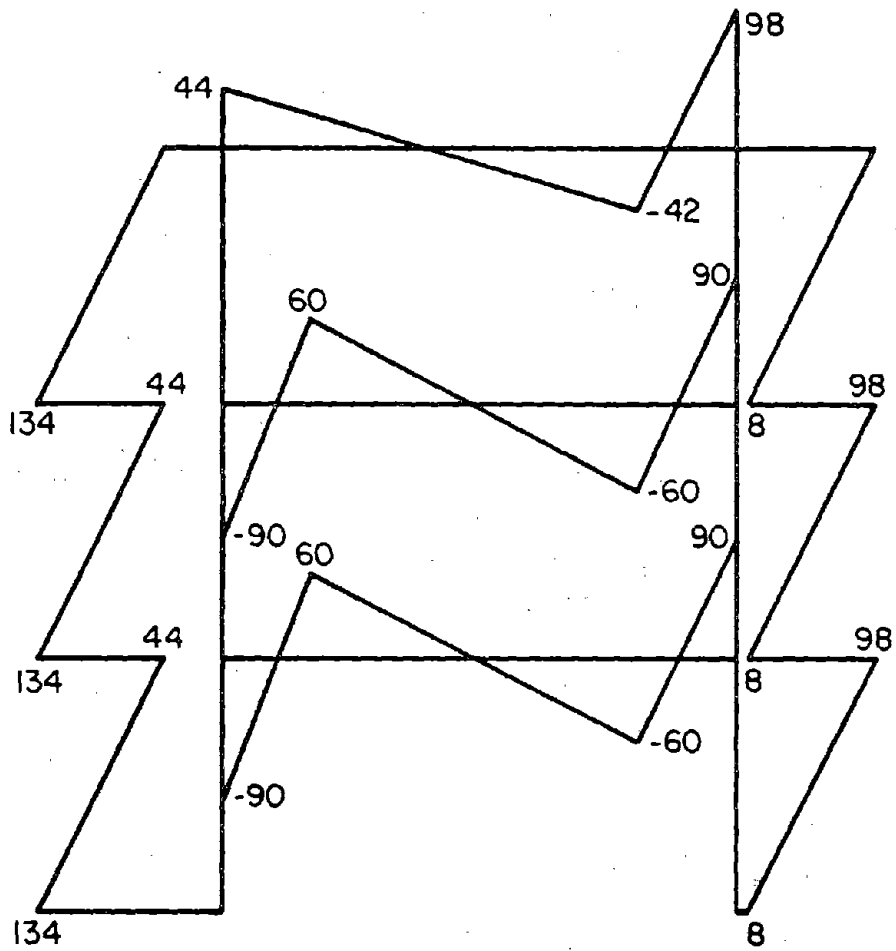
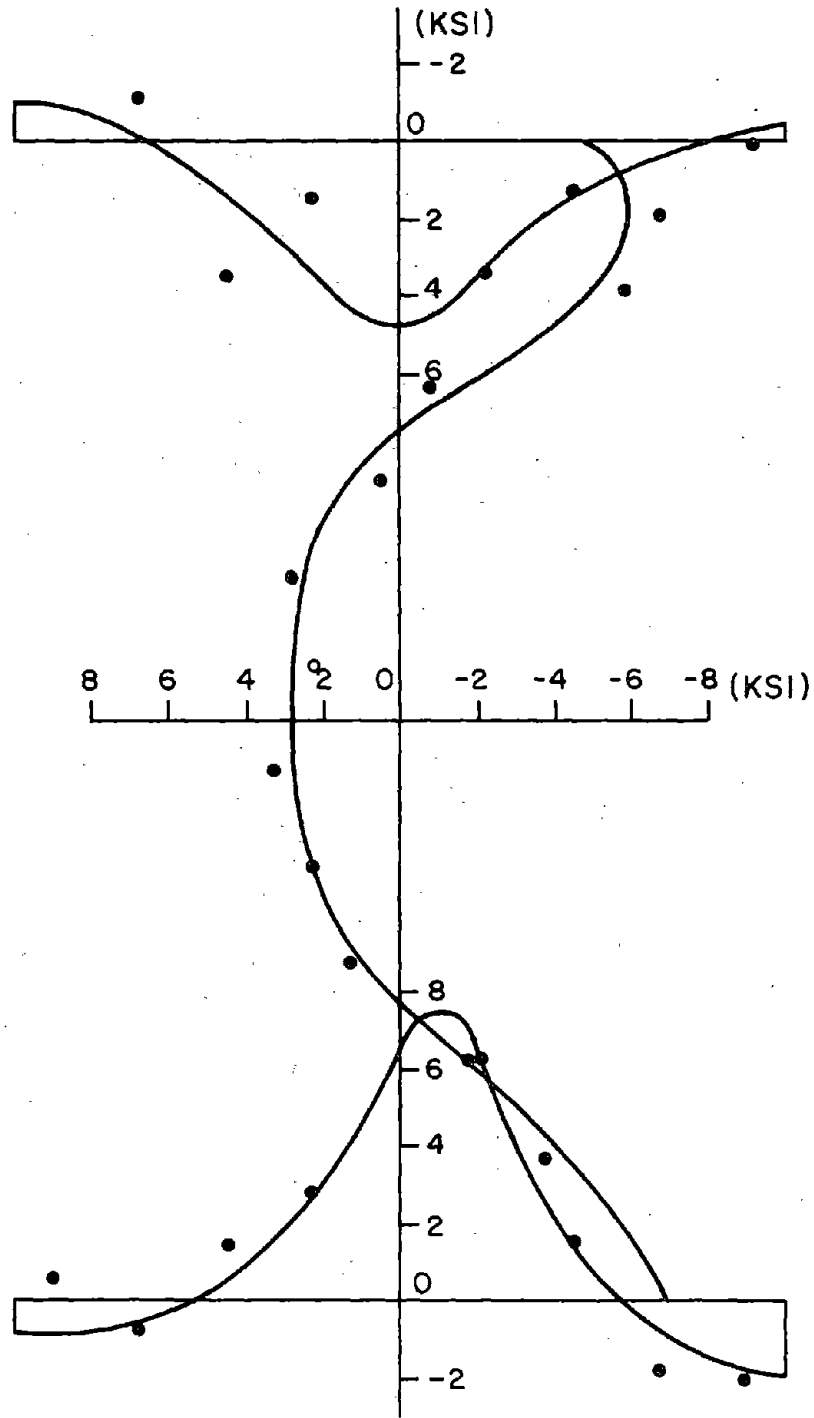


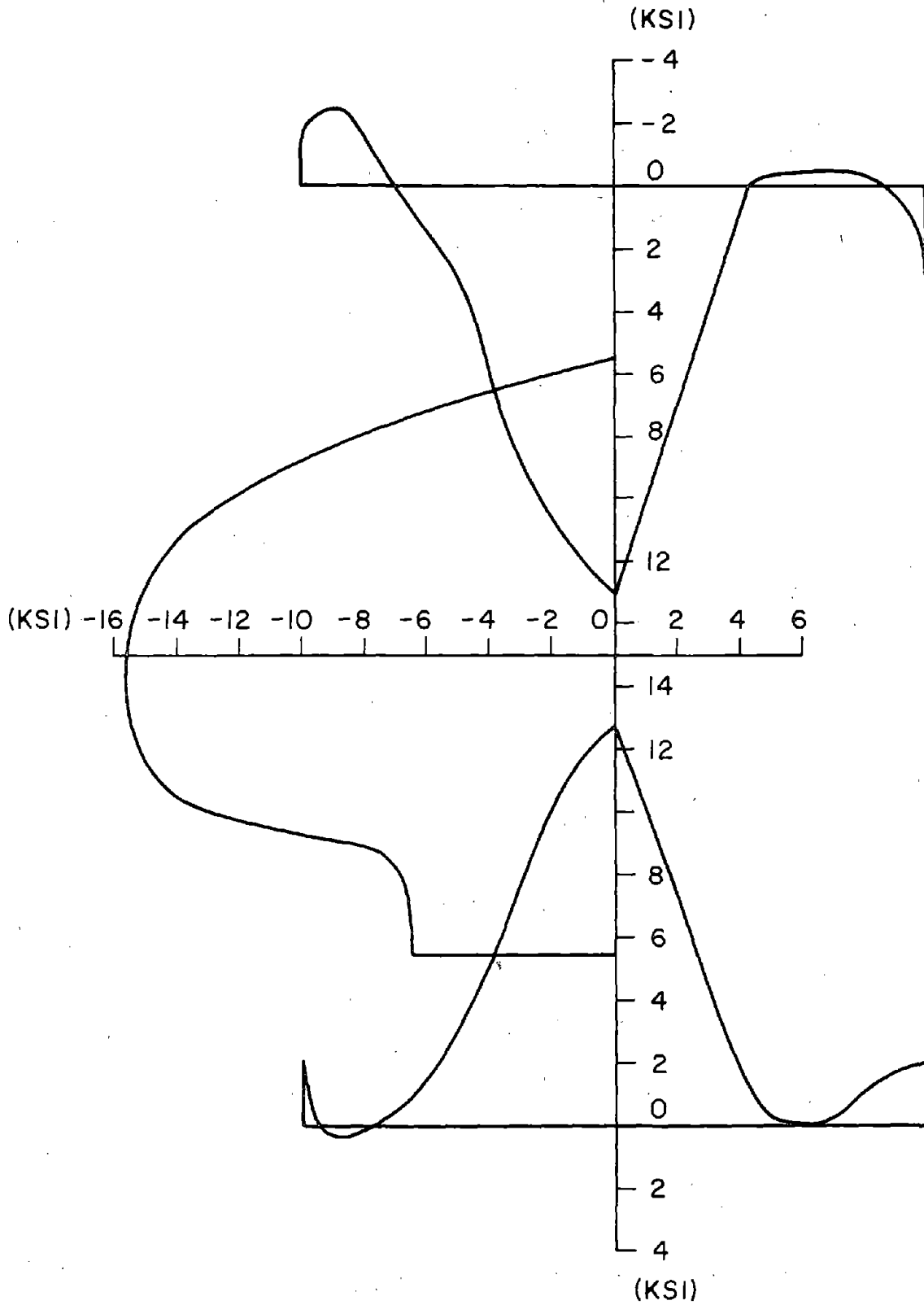
FIGURE A8 - BALANCED MOMENT DIAGRAM



W6 x 12

RESIDUAL STRESS DISTRIBUTION  
USED IN BEAM TEST SPECIMEN

FIGURE B1 - RESIDUAL STRESS DISTRIBUTION FOR W6X12 USED IN THE BEAM SPECIMENS

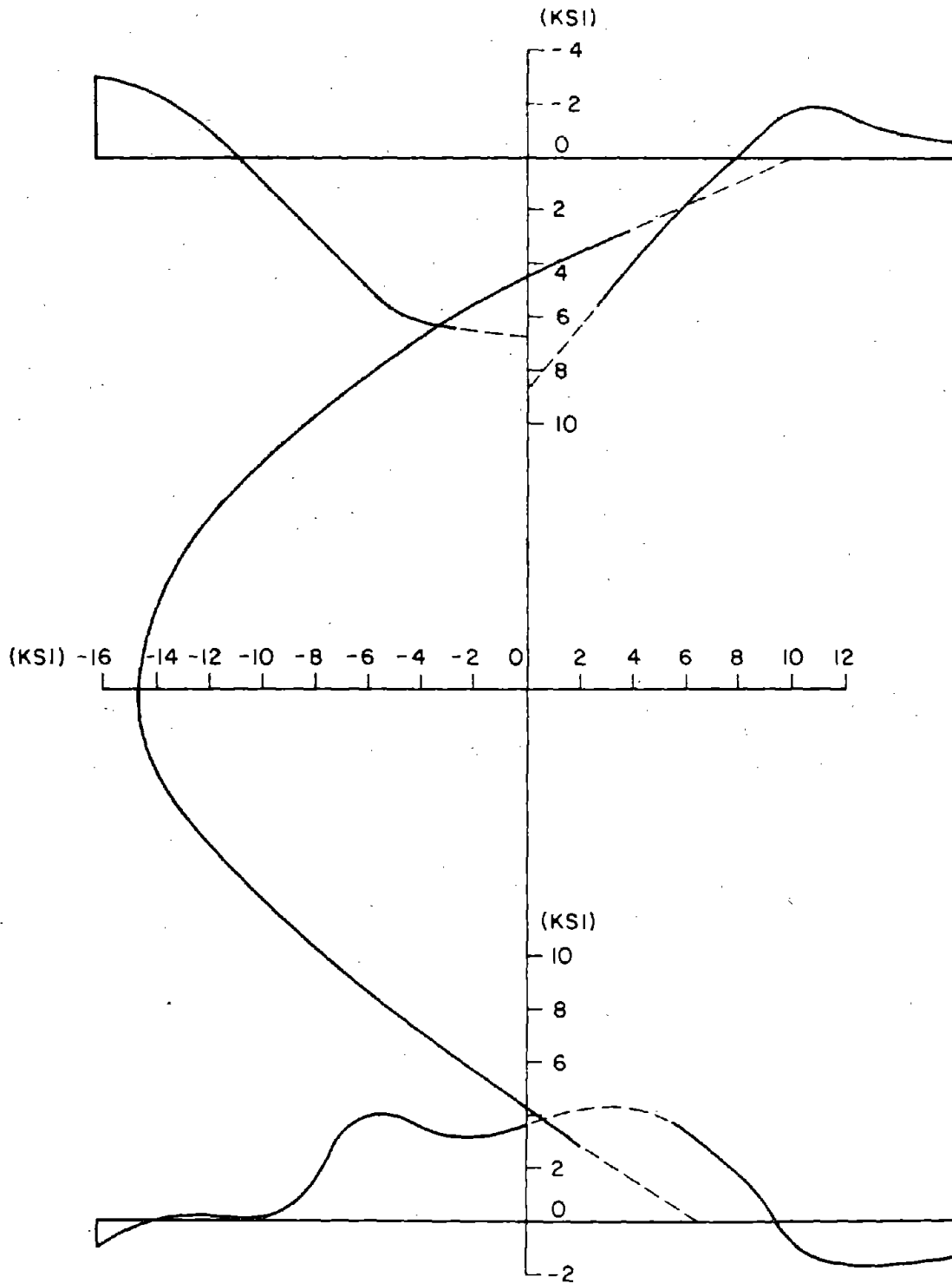


W6x12

**AVERAGE RESIDUAL STRESSES**

FIGURE B2 - RESIDUAL STRESS DISTRIBUTION FOR W6X12 USED IN THE TEST FRAMES

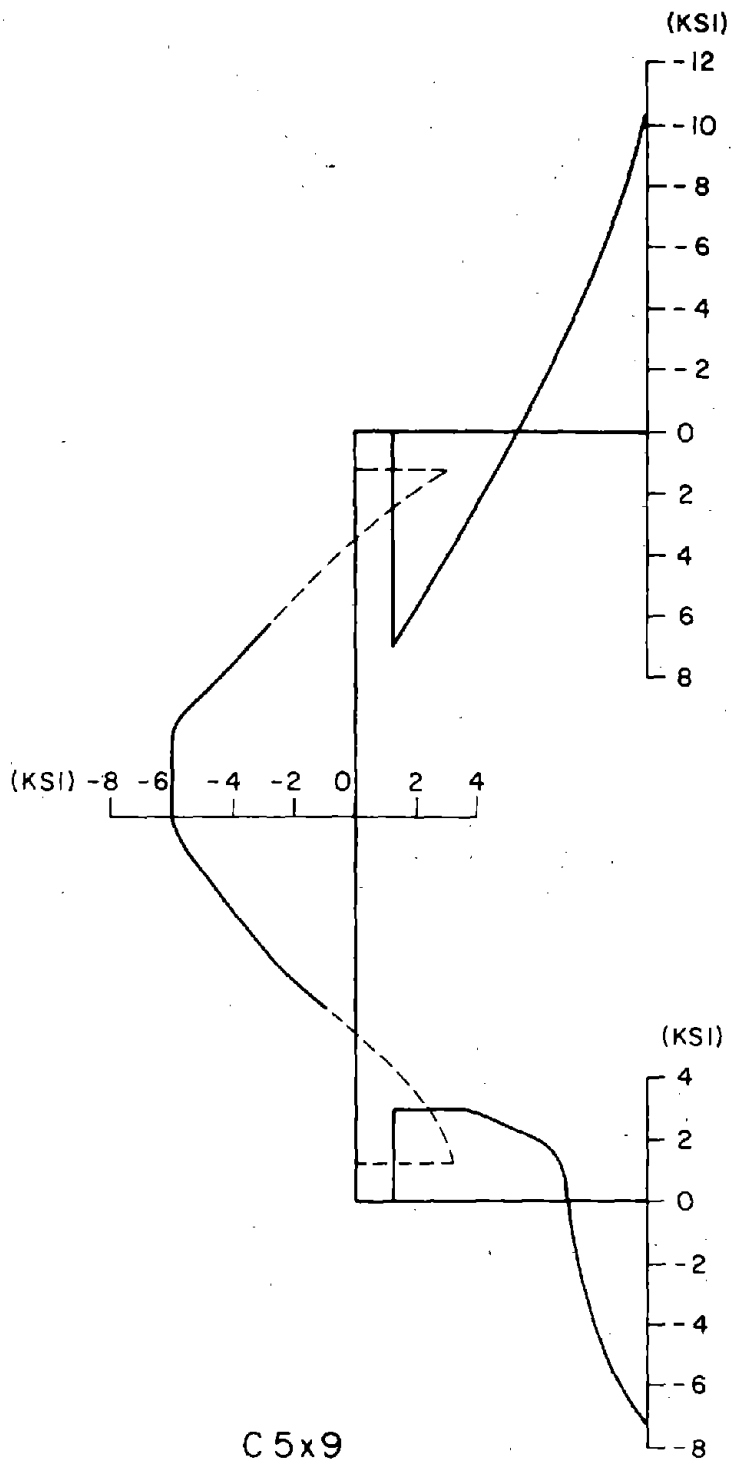




W8x28

AVERAGED RESIDUAL STRESSES

FIGURE B3 - RESIDUAL STRESS DISTRIBUTION FOR W8X28



AVERAGED RESIDUAL STRESSES

FIGURE B4 - RESIDUAL STRESS DISTRIBUTION FOR C5X9

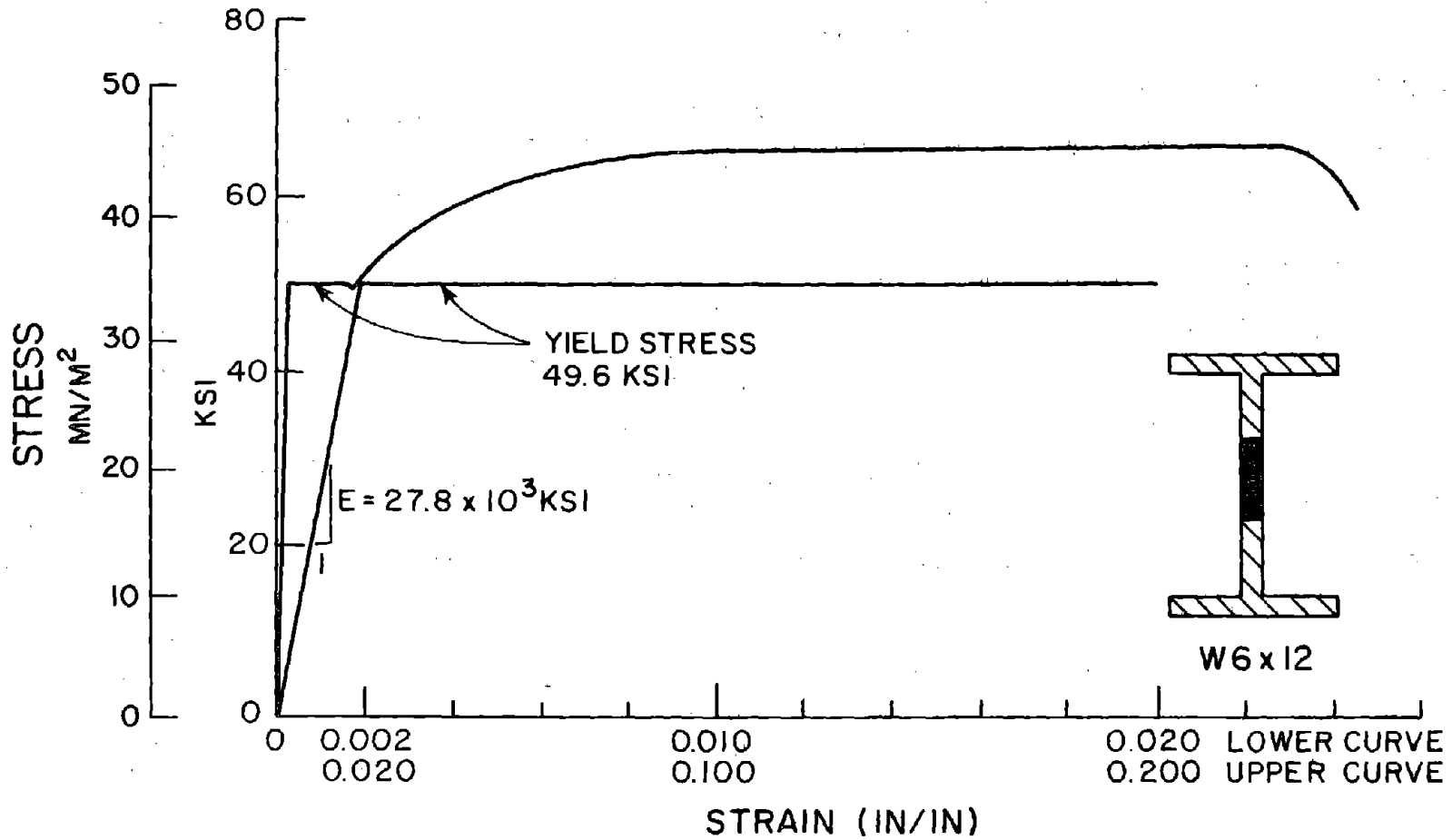


FIGURE B5 - STRESS-STRAIN CURVE FOR THE WEB OF THE W6X12 USED IN THE BEAM SPECIMENS

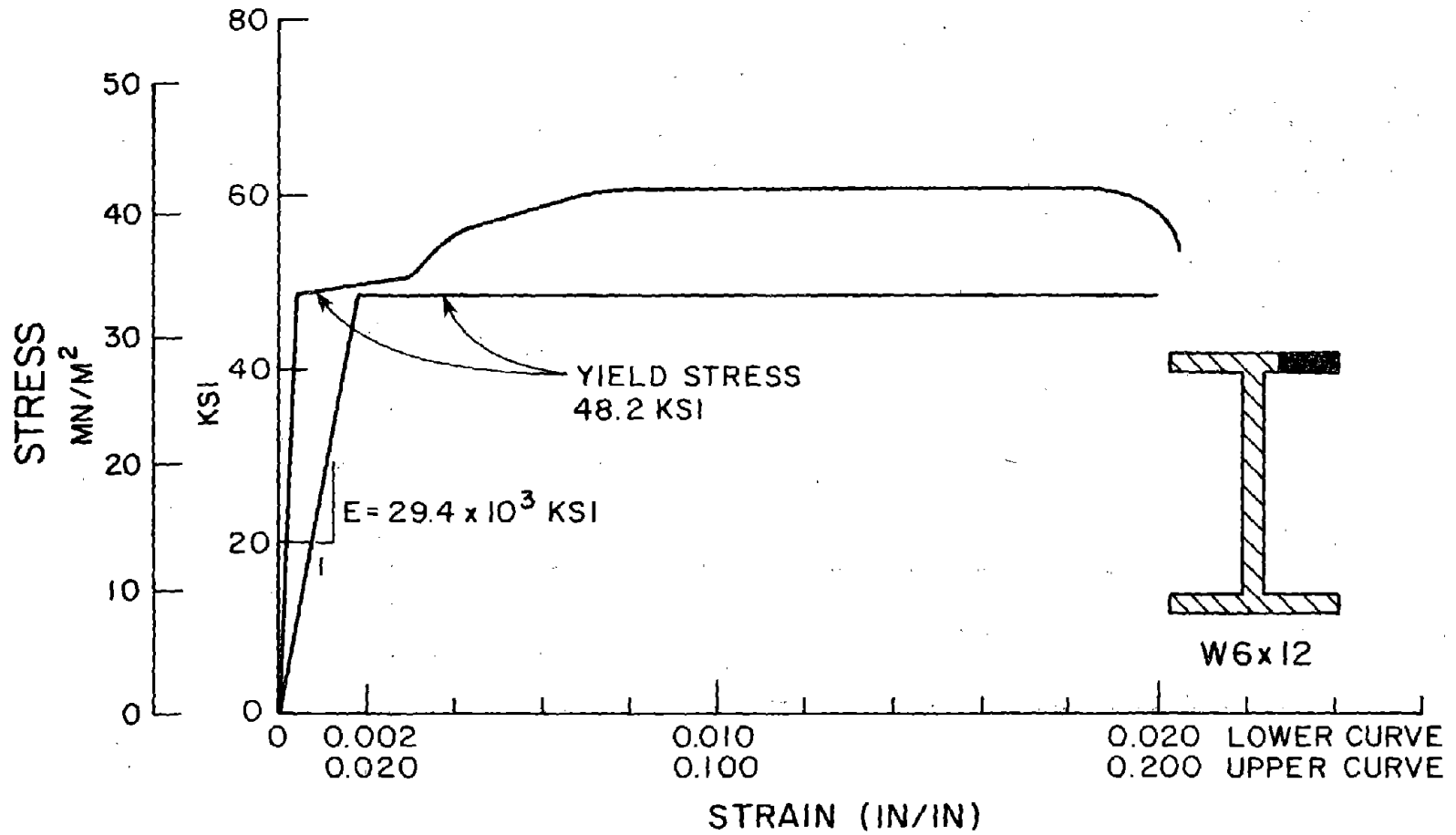


FIGURE B6 - STRESS-STRAIN CURVE FOR THE FLANGE OF THE W6X12 USED IN THE BEAM SPECIMENS

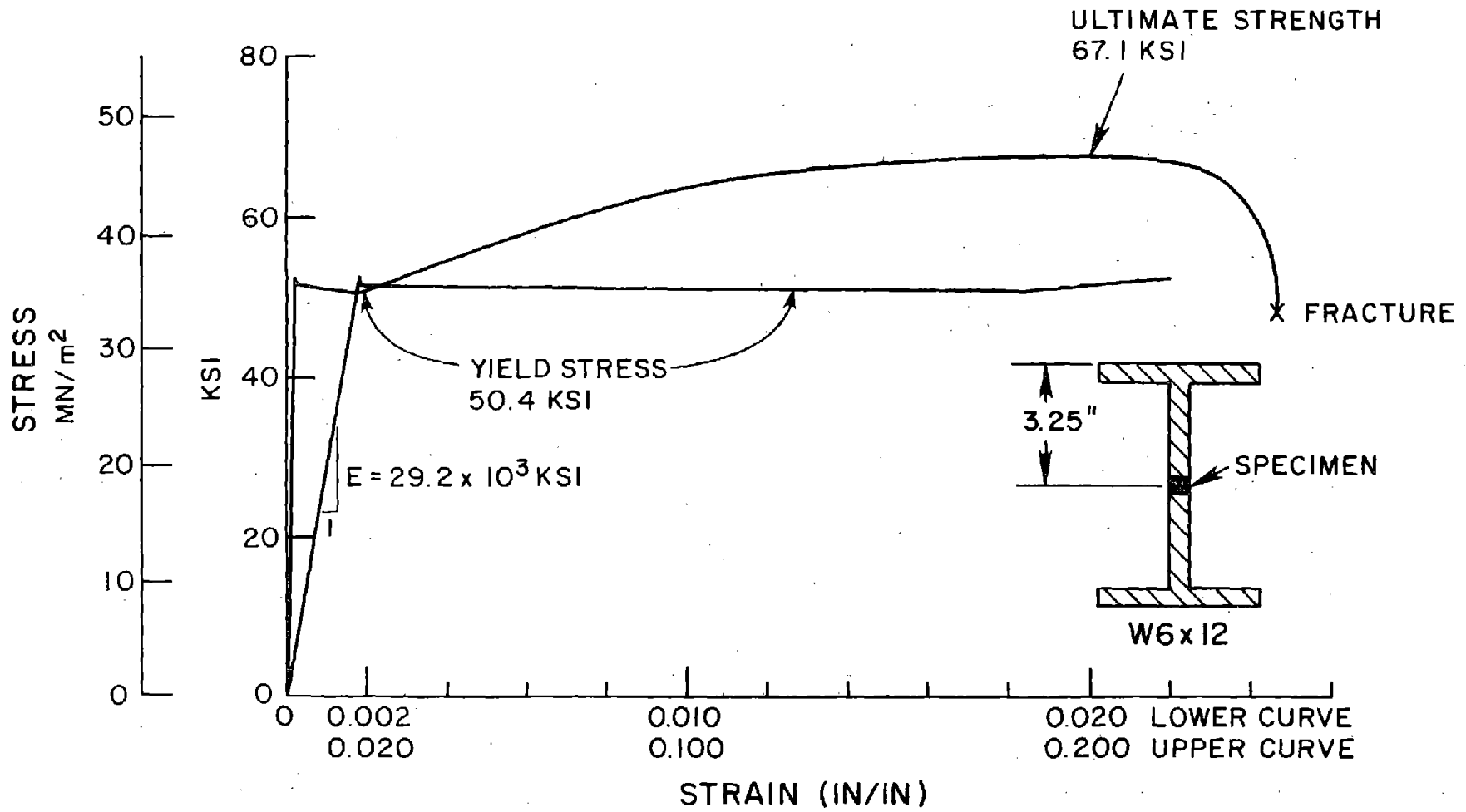


FIGURE B7 - STRESS-STRAIN CURVE FOR THE WEB OF THE W6x12 USED IN THE TEST FRAME

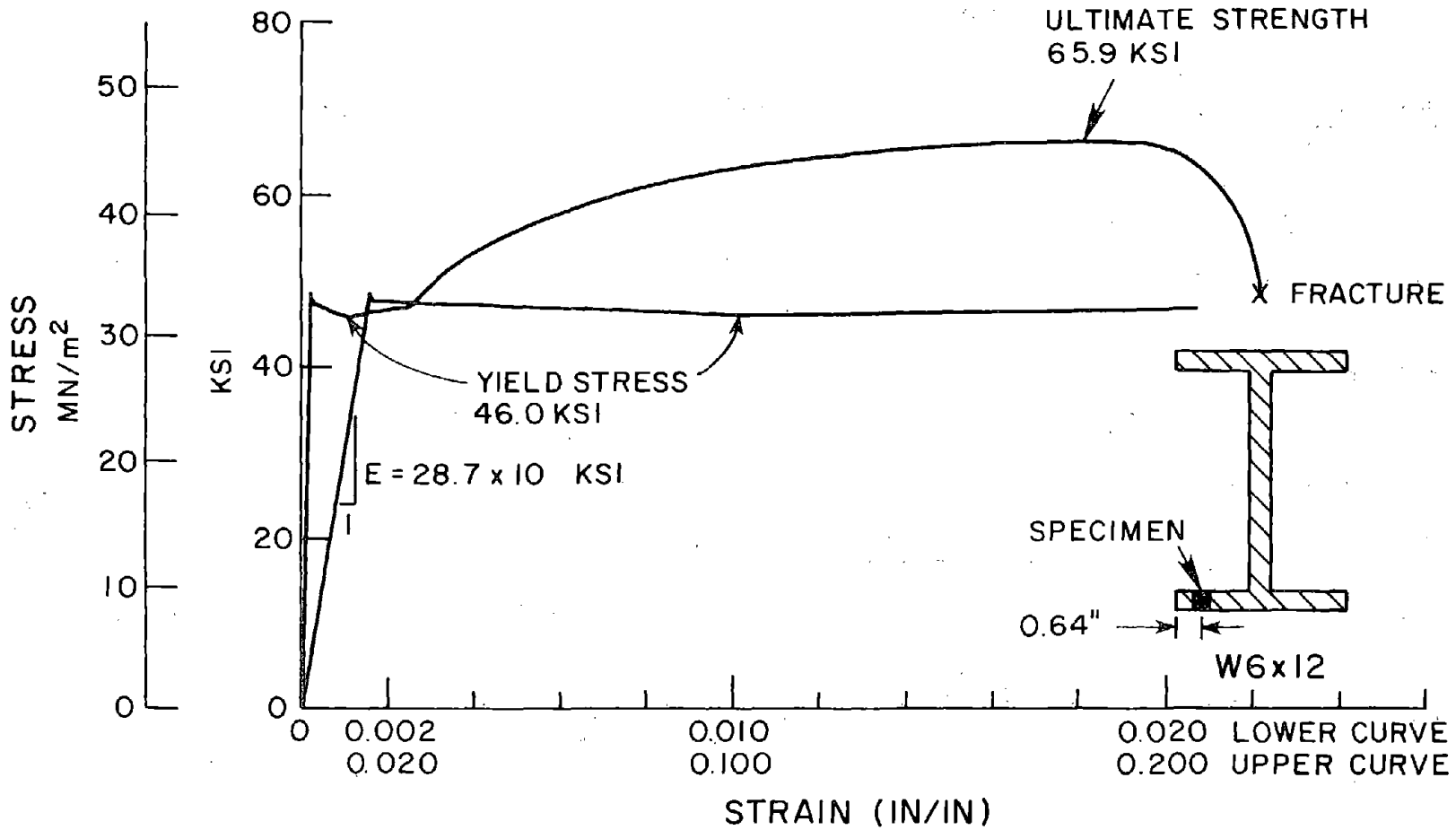


FIGURE B8 - STRESS-STRAIN CURVE FOR THE FLANGE OF THE W6X12 USED IN THE TEST FRAMES

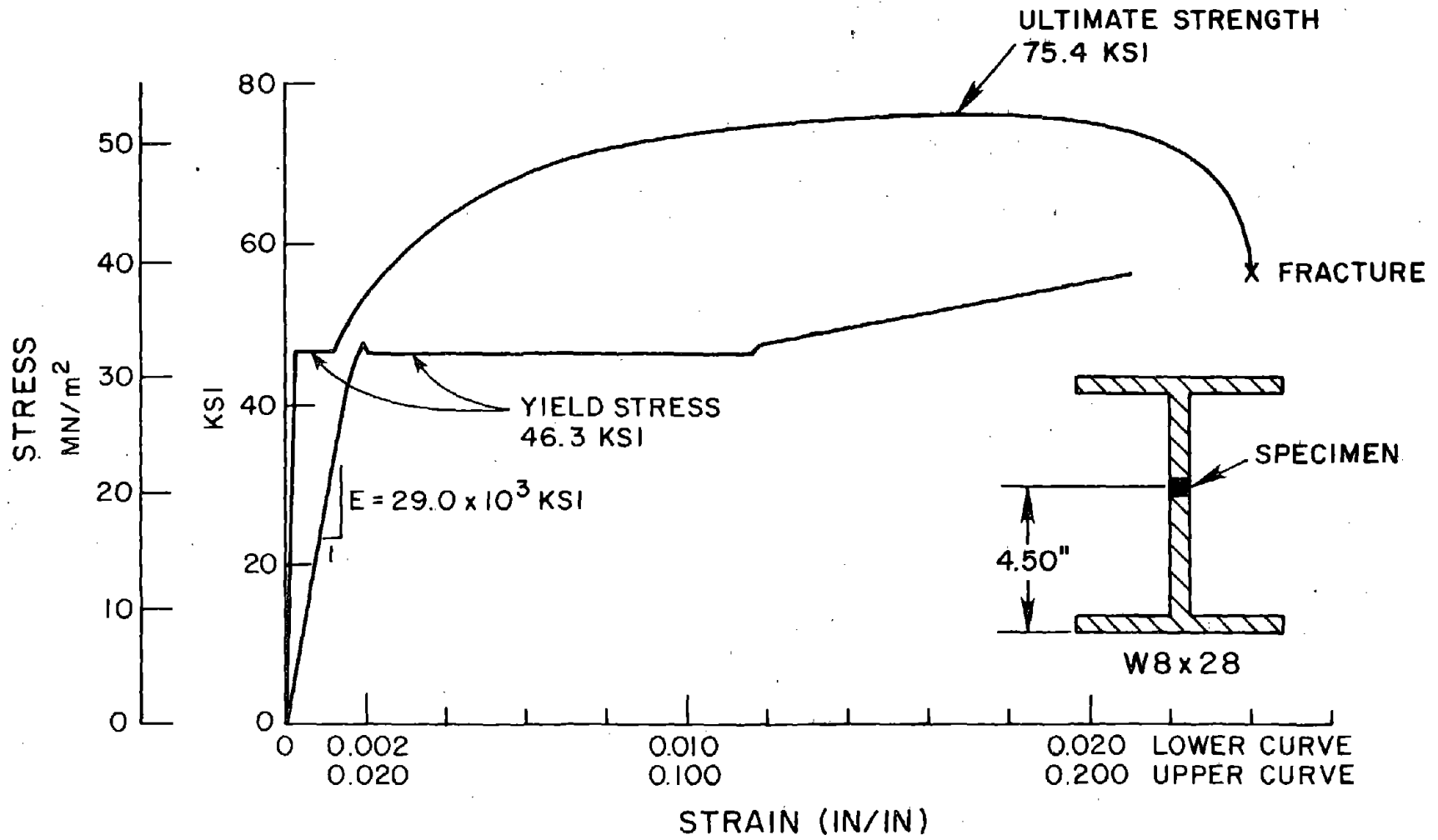


FIGURE B9 - STRESS-STRAIN CURVES FOR THE WEB OF THE W8X28

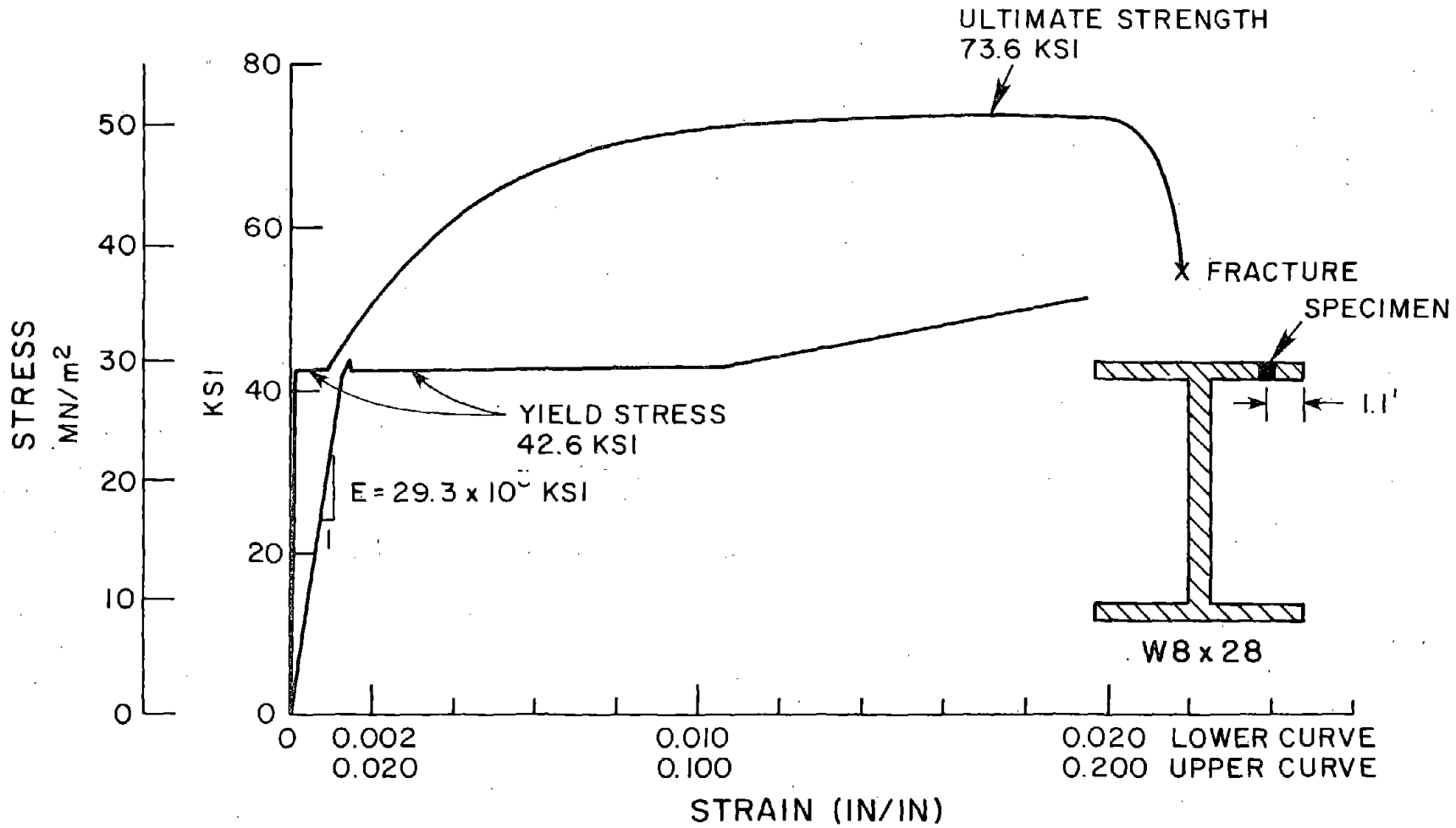


FIGURE B10 - STRESS-STRAIN CURVES FOR THE FLANGE OF THE W8X28



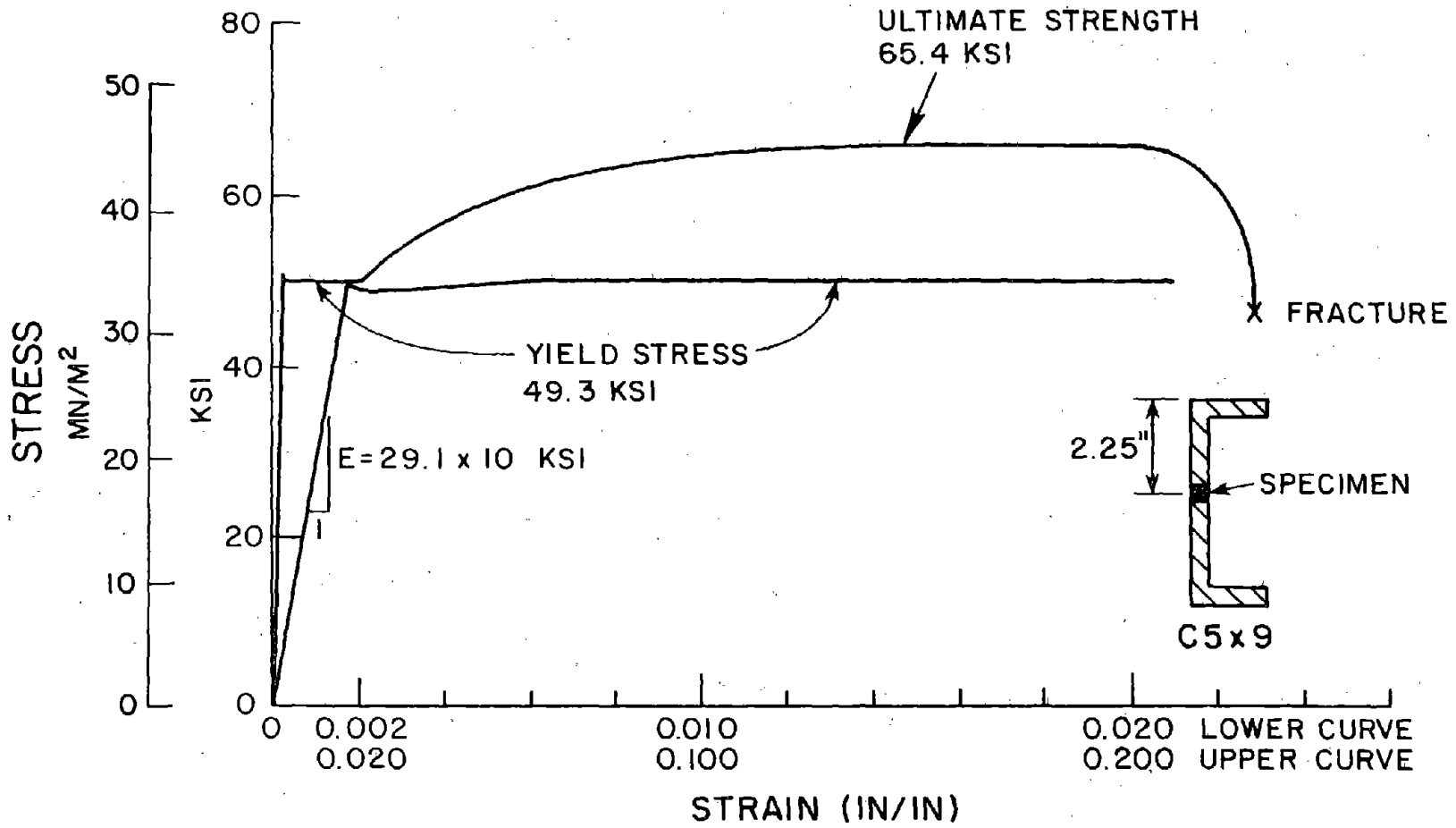


FIGURE B11 - STRESS-STRAIN CURVE FOR THE WEB OF THE C5X9

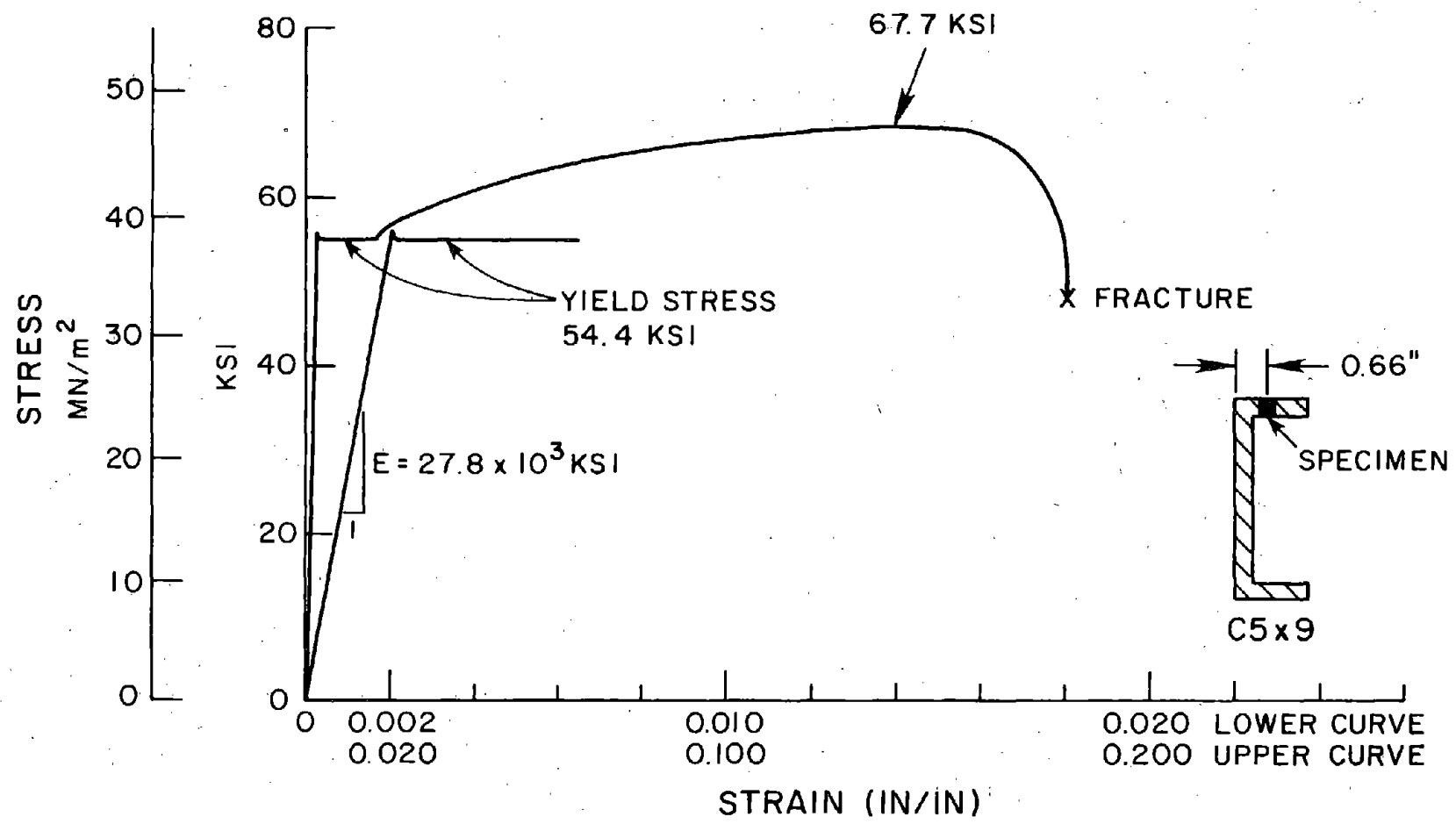


FIGURE B12 - STRESS-STRAIN CURVE FOR THE FLANGE OF THE C5X9

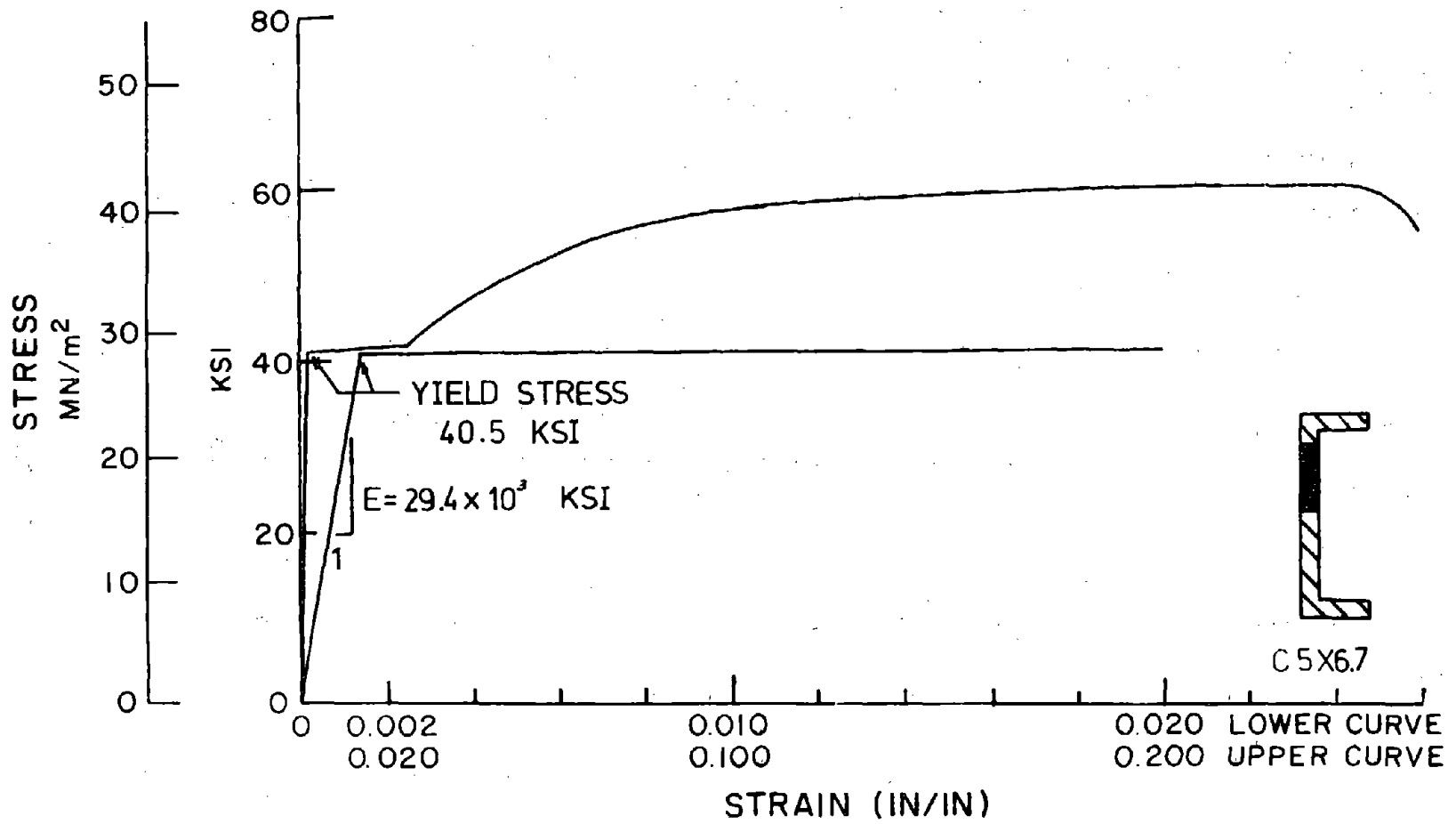


FIGURE B13 - STRESS-STRAIN CURVE FOR THE WEB OF THE C5X6.7

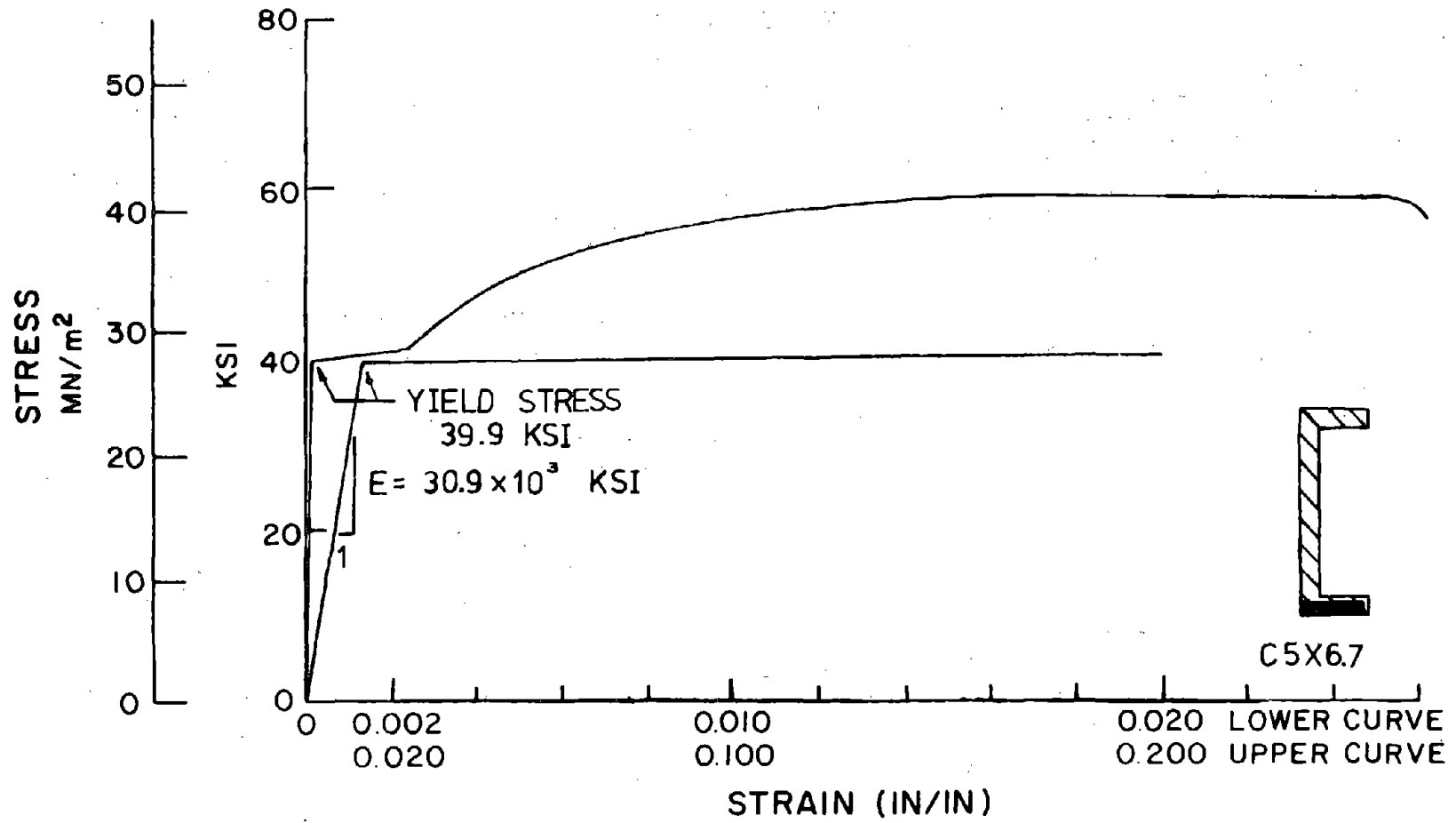


FIGURE B14 - STRESS-STRAIN CURVE FOR THE FLANGE OF THE C5X6.7

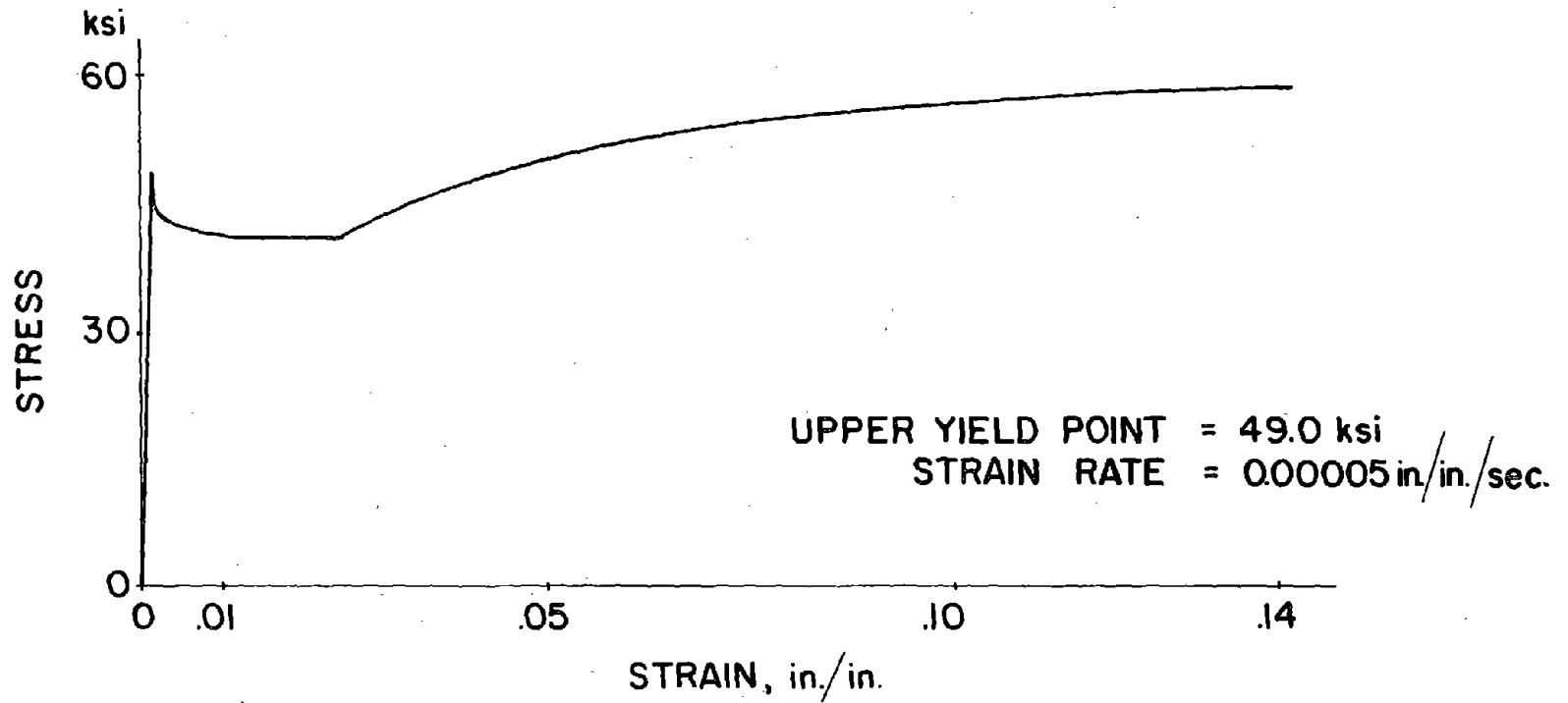


FIGURE B15 - MONOTONIC TENSILE TEST OF W6X12

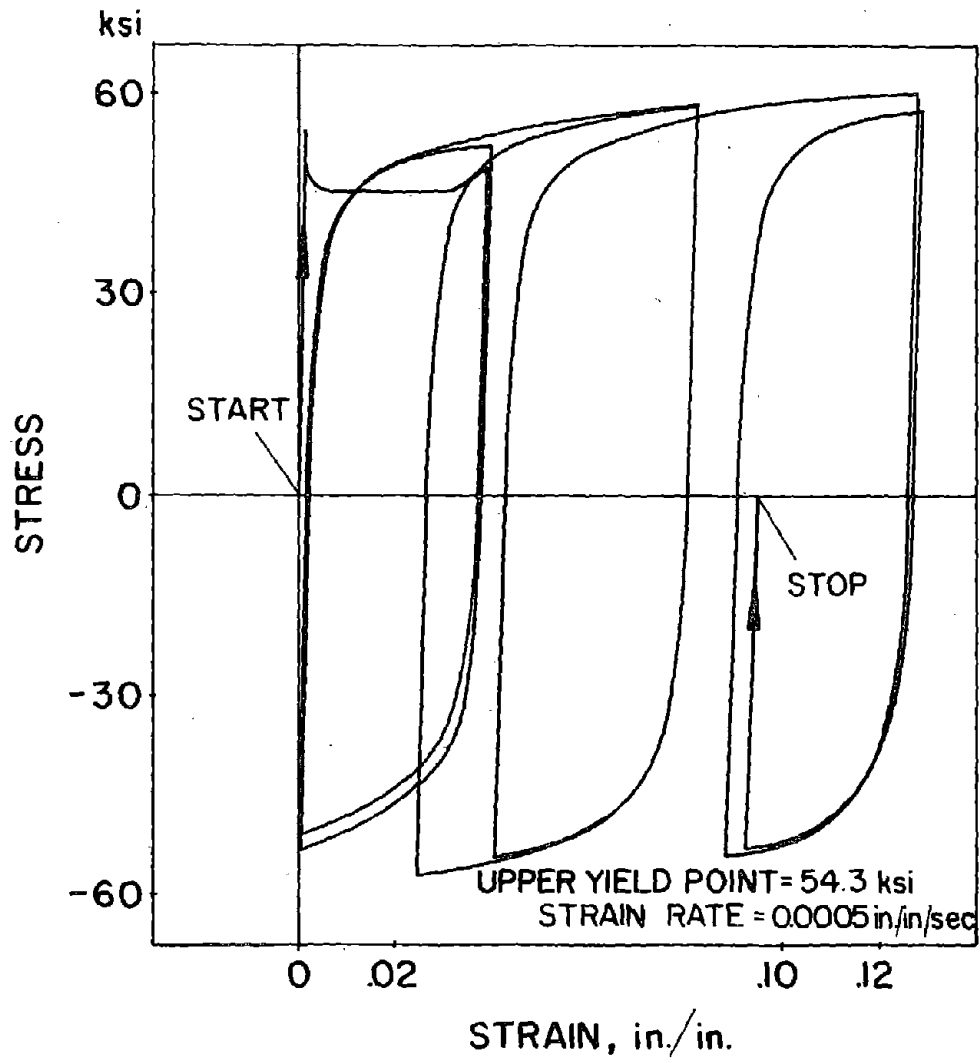


FIGURE BT6 - AVERAGE CYCLIC STRESS-STRAIN CURVE OF W6X12

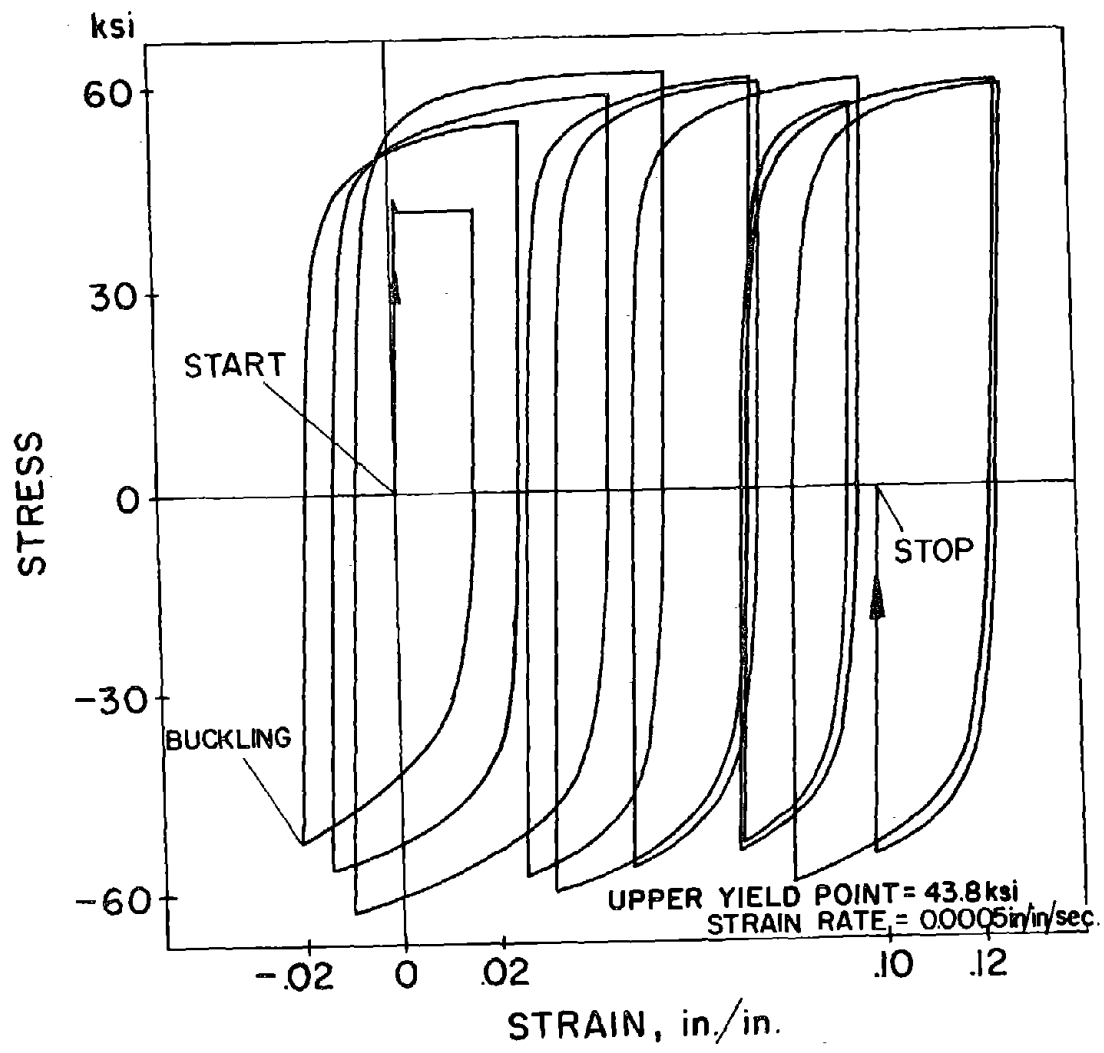


FIGURE B17 - CYCLIC STRESS-STRAIN CURVE FOR A SINGLE GAGE OF A SPECIMEN TAKEN FROM W6X12





APPENDIX C

INPUT FORMAT AND FORTRAN LISTING  
FOR SHEAR YIELD ELEMENT

INPUT INSTRUCTIONS

The number of words of information per element - 104.

A. CONTROL INFORMATION FOR GROUP (715) - ONE CARD.

- Columns            5: Punch 9 (to indicate that group consists of shear yield elements).
- 6 - 10: Number of elements in group.
- 11 - 15: Number of different element stiffness types (max. 40).
- 16 - 20: Number of different end eccentricity types (max. 15).
- 21 - 25: Number of different yield surfaces for cross sections (max. 40).
- 26 - 30: Number of different fixed end force patterns (max. 35).
- 31 - 35: Number of different initial element force patterns (max. 30).

B. STIFFNESS TYPES (I5,6F10.0,3F5.0,/,F10.0) - TWO CARDS FOR EACH STIFFNESS TYPE.

- Columns    1 - 5: Stiffness type number.
- 6 - 15: Young's modulus of elasticity.
- 16 - 25: Uniaxial strain hardening modulus, as a proportion of Young's modulus.
- 26 - 35: Depth of the wide flange beam.
- 36 - 45: Thickness of wide flange beam flanges.
- 46 - 55: Width of flange.
- 56 - 65: Web thickness.
- 66 - 70: Flexural stiffness factor,  $f_{ij}$  (see note below).

71 - 75: Flexural stiffness factor  $f_{jj}$  (see note below).

76 - 80: Flexural stiffness factor  $f_{ij}$  (see note below).

1 - 10: Poisson's ratio

Note: Note that the flexural stiffness factors are used to compute the bending component of deflection as described in Chapter 3. Therefore, these factors must reflect the degree of rotational constraint provided by other attached elements as well as any variation in element properties and dimensions. If this is not done the warping restraint provided in this element may produce erroneous results.

C. END ECCENTRICITIES (I5,4F10.0) - ONE CARD FOR EACH END ECCENTRICITY TYPE.

Omit if there are no end eccentricities. See Fig. B2.6 for explanation. All eccentricities are measured from the node to the element end.

Columns 1 - 5: End eccentricity type number, in sequence beginning with 1.

6 - 15:  $X_i$  = X eccentricity at end i.

16 - 25:  $X_j$  = X eccentricity at end j.

26 - 35:  $Y_i$  = Y eccentricity at end i.

36 - 45:  $Y_j$  = Y eccentricity at end j.

D. CROSS SECTION YIELD SURFACES (I5,5X,2F10.0,40X,F10.0) - ONE CARD FOR EACH YIELD SURFACE.

Columns 1 - 5: Yield surface number, in sequence beginning with 1.

11 - 20: Positive (sagging) yield moment  $M_{y+}$ .

21 - 30: Negative (hogging) yield moment  $M_{y-}$ .

71 - 80: Shear yield force. A very large number is assumed if left at zero.

E. FIXED END FORCE PATTERNS (2I5,7F10.0) - ONE CARD FOR EACH FIXED END FORCE PATTERN.

Omit if there are no fixed end forces. See Fig. B2.5.

Columns 1 - 5: Pattern number, in sequence beginning with 1.

10: Axis code, as follows.

Code = 0: Forces are in the element coordinate system, as in Fig. B2.5a.

Code = 1: Forces are in the global coordinate system, as in Fig. B2.5b.

- 11 - 20: Clamping force,  $F_i$ .
- 21 - 30: Clamping force,  $V_i$ .
- 31 - 40: Clamping moment,  $M_i$ .
- 41 - 50: Clamping force,  $F_j$ .
- 51 - 60: Clamping force,  $V_j$ .
- 61 - 70: Clamping moment,  $M_j$ .
- 71 - 80: Live load reduction factor, for computation of live load forces to be applied to nodes. See Section B2.5, Appendix B2 for explanation.

F. INITIAL ELEMENT FORCE PATTERNS (I5,6F10.0) - ONE CARD FOR EACH INITIAL FORCE PATTERN.

Omit if there are no initial forces. See Fig. B2.5a.

- Columns
- 1 - 5: Pattern number, in sequence beginning with 1.
  - 6 - 15: Initial axial force,  $F_i$ .
  - 16 - 25: Initial shear force,  $V_i$ .
  - 26 - 35: Initial moment,  $M_i$ .
  - 36 - 45: Initial axial force,  $F_j$ .
  - 46 - 55: Initial shear force,  $V_j$ .
  - 56 - 65: Initial moment,  $M_j$ .

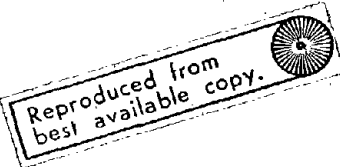
G. ELEMENT GENERATION COMMANDS (I2I5,2F5.0,I5,F5.0) - ONE CARD FOR EACH GENERATION COMMAND.

Elements must be specified in increasing numerical order. Cards for the first and last elements must be included. See NOTE 7 for explanation of generation procedure.

- Columns
- 1 - 5: Element number, or number of first element in a sequentially numbered series of elements to be generated by this command.
  - 6 - 10: Node number at element end  $i$ .
  - 11 - 15: Node number at element end  $j$ .
  - 16 - 20: Node number increment for element generation. If zero or blank, assumed to be equal to 1.

- 21 - 25: Stiffness type number.
- 26 - 30: End eccentricity type number. Leave blank or punch zero if there is no end eccentricity.
- 31 - 35: Yield surface number for element end i.
- 36 - 40: Yield surface number for element end j.
- 45: Code for including geometric stiffness. Punch 1 if geometric stiffness is to be included. Leave blank or punch zero if geometric stiffness is to be ignored.
- 50: Time history output code. If a time history of element results is not required for the element covered by this command, punch zero or leave blank. If a time history printout, at the intervals specified on card D1, is required, punch 1.
- 51 - 55: Fixed end force pattern number for static dead loads on element. Leave blank or punch zero if there are no dead loads. See note below.
- 56 - 60: Fixed end forces pattern number for static live loads on element. Leave blank or punch zero there are no live loads.
- 61 - 65: Scale factor to be applied to fixed end forces due to static dead loads.
- 66 - 70: Scale factor to be applied to fixed end forces due to static live loads.
- 71 - 75: Initial force pattern number. Leave blank or punch zero if there are no initial forces.
- 76 - 80: Scale factor to be applied to initial element forces.

Note: If the static load code, Card C1, is zero but fixed end forces are still specified for some elements, an inconsistency results. In effect, any such fixed end forces will be treated as initial element forces.



```

SUBROUTINE RESPO (NCCF,NINFC,KBAL,KPP,CCMS,DDISM,DD,TIME,VELM,DFACRES 10
L,DELTA)                                RES 20
*****                                RES 30
SHEAR YIELDING ELEMENT -- STATE DETERMINATION  RES 40
CHARLES RICEFR                            RES 50
REVISED FROM ELEMENT 5 -- FEBRUARY 1974    RES 60
*****                                RES 70
COMMON /INFL/ IMEM,KST,LM(6),KCECH,FL,CCSA,SINA,A(2,6),EK11,  RES 80
1      FK22,EK12,PSH,EAL,EK11F,EK22F,EC(4),KCOYX(2),    RES 90
2      KLOY(2),EMTCT(2),SFCT(2),FIC(2),FATCT(2),SENF(M),RES 100
3      SENN(8),TENR(8),TENN(8),FEAC(2),PFAC(2),EMEP(2),  RES 110
4      SDACT(1),PMY(2,2),NCDI,NCDJ,KCUTOI,PR1Z,PR21,    RES 120
5      SK11,SK22,SK12,SK11F,SK22F,VP(2),REST(96)      RES 130
COMMON /WORK/ DVR(2),DPR(2),DBM(2),BMTCT(2),BML(2),BML(2),  RES 140
1      DVAX,DFAX,FACAC,FACTOR,FA,CSF,BMIUB,BMJUB,SFUB,  RES 150
2      SDW1,SDWJ,SDFC,KCDE(2),VT,EMT(2),VEL(2),WCRK,  RES 160
3      SPYLD(2),W1596)                                RES 170
COMMON/THIST/THCUT(10),THCUT(20),THP,TSAVE,NELTH,NSTH,NF7,ISE  RES 180
DIMENSION CCM(1), CCMS(1), DDISM(1), DE(1), VELM(1), NCD(2)  RES 190
EQUIVALENCE (IMEM,CCM(1)), (NCDI,NCD(1))              RES 200
KAT=C                                                 RES 210
DO 10 J=1,NINFC                                     RES 220
10 CCM(J)=CCMS(J)                                    RES 230
KCOYX(1)=KCOY(1)                                    RES 240
KCOYX(2)=KCOY(2)                                    RES 250
IF (IMEM.EC.1) IFED=0                                RES 260
DEFORATION INCREMENTS                               RES 270
IF (EC(1).EQ.1.23456710) GO TO 20                  RES 280
DDISM(1)=DDISM(1)-EC(3)*DDISM(1)                   RES 290
DDISM(2)=DDISM(2)+EC(1)*DDISM(2)                   RES 300
DDISM(4)=DDISM(4)-EC(4)*DDISM(4)                   RES 310
DDISM(5)=DDISM(5)+EC(2)*DDISM(5)                   RES 320
20 DVAX=CCM(4)-DDISM(1)+SINA*(DDISM(5)-DDISM(2))    RES 330
ROT=SINA*(DDISM(4)-DDISM(1))+CSA*(DDISM(2)-DDISM(5))/FL  RES 340
DVR(1)=DDISM(3)+RCT                                  RES 350
DVR(2)=DDISM(6)+RCT                                  RES 360
AXIAL FORCE INCREMENT                                RES 370
DFAX=EAL*DVAX                                        RES 380
FTCT(1)=FTCT(1)+DFAX                                RES 390
FTCT(2)=FTCT(2)+DFAX                                RES 400
LINEAR MOMENT INCREMENTS                            RES 410
CALL BXCAL9                                          RES 420

```

```

BML(1)=EMEP(1)+DBM(1)                                RES 570
BML(2)=EMEP(2)+DBM(2)                                RES 580
EMFL(1)=EMTCT(1)-BMEP(1)                            RES 590
EMFL(2)=EMTCT(2)-BMEP(2)                            RES 600
TRACE OUT NONLINEAR PATH                             RES 610
NOTE THAT CONTINUATION OF YIELDING IS CHECKED BY ASSUMING ELASTIC  RES 620
BEHAVIOR AND DETERMINING IF THE YIELD SURFACE IS PENETRATED  RES 630
VI=(BMEP(1)+2*BMEP(2))/FL                            RES 640
BMT(1)=BMEP(1)                                        RES 650
BMT(2)=BMEP(2)                                        RES 660
KCOY(1)=C                                             RES 670
KCOY(2)=0                                             RES 680
CALL BXCAL9                                          RES 690
FACAC=0.                                              RES 700
KIAL=0                                               RES 710
30 FACTOR=1.-FACAC                                    RES 720
KCOE(1)=KCOY(1)                                       RES 730
KCOE(2)=KCOY(2)                                       RES 740
25 FORMAT (2HOP,4110)                                RES 750
PLASTIC HINGE ROTATIONS                               RES 760
KYY=KCOY(1)+KCOY(2)+1                                RES 770
GO TO (60,40,50,400,60,95,50) ,KYY                 RES 780
40 DPR(1)=DVR(1)+.9921*DVR(2)                        RES 790
DPR(2)=DVR(2)+.9912*DVR(1)                          RES 800
GO TO 60                                              RES 810
45 DPR(1)=DVR(1)+.5K12/5K11)*DVR(2)                 RES 820
DPR(2)=DVR(2)+(.5K12/5K22)*DVR(1)                   RES 830
GO TO 60                                              RES 840
50 DPR(1)=DVR(1)                                       RES 850
DPR(2)=DVR(2)                                       RES 860
60 KFAC=0                                             RES 870
GO 100 IEND=1,2                                       RES 880
KYY=KCOY(IEND)+1                                       RES 890
GO TO (65,90,65,90) ,KYY                             RES 900
ELASTIC, GET FACTOR FOR STATE CHANGE                 RES 910
65 IF (DPR(IEND)) 70,100,80                            RES 920
70 FAC=(PMY(IEND,2)-BMEP(IEND))/DBM(IEND)            RES 930
IF (FAC.GT.FACTOR) GO TO 100                          RES 940
IF ((IEND.EQ.2).AND.(KCOY(1)-KCOE(1)).NE.C).AND.(FAC.NE.FACTOR)  RES 950
1 KCOY(1)=KCOY(1)-1                                    RES 960
IF (FAC.LT.0.C) CALL EXIT                             RES 970
FACTOR=FAC                                             RES 980
BMY=BMY(IEND,2)                                       RES 990
KCOY(IEND)=KCOY(IEND)+1                               RES 1000
KFAC=IEND                                             RES 1010
GO TO 100                                             RES 1020
80 FAC=(SMY(IEND,1)-BMEP(IEND))/DBM(IEND)            RES 1030
IF (FAC.GT.FACTOR) GO TO 100                          RES 1040
IF ((IEND.EQ.2).AND.(KCOY(1)-KCOE(1)).NE.C).AND.(FAC.NE.FACTOR)  RES 1050

```

```

1 KCDY(1)=KCDY(1)-1
IF (FAC.LT.0.0) CALL EXIT
FACTF=FACT
EMY=EMY(IEND,1)
KCDY(IEND)=KCDY(IEND)+1
KFAC=IEND
CC TO 100
90 CONTINUE
C
100 CONTINUE
C IF BOTH CODES ARE RESET DUE TO BEING YIELD CHECK WHICH YIELDS
C FIRST
KYY=KCDY(1)+KCDY(2)-KCODE(1)-KCODE(2)
IF (KYY.NE.2) GO TO 103
C KYY IS LESS THAN 2 UNLESS BOTH YIELD AT THE SAME TIME OR FACTOR=2
IF (ABS(DRM(1)).GT.495(DRM(2))) KCDY(2)=KCDY(2)-1
IF (ABS(DRM(1)).LT.495(DRM(2))) KCDY(1)=KCDY(1)-1
103 CONTINUE
C INSERT SHEAR YIELD CHECK
SHEAF=FACTCP
IF (FACTCP.GT.1.0) SHEAF=1.0
BMT(1)=BMT(1)+SHEAF*DRM(1)
BMT(2)=BMT(2)+SHEAF*DRM(2)
DELSHR=(BMT(1)-BMEF(1)+BMT(2)-BMEF(2))/FL
VT=VT+DELSHR*SHEAF
IF (KCDY(1).GE.2) GO TO 108
C ELEMENT IS ELASTIC IN SHEAR -- CHECK FOR START OF YIELDING
IF (VT.LE.0.0) GO TO 104
IF (VT.LE.VP(2)) GO TO 105
GO TO 104
104 IF (VT.GE.VP(1)) GO TO 105
GO TO 104
105 CONTINUE
C ELEMENT IS STARTING TO YIELD IN SHEAR
FAC=1.0
IF (DELSHR.EQ.0.0) GO TO 106
IF (VT.LE.0.0) FAC=1.-(VT-VP(2))/(DELSHR*SHEAF)
IF (VT.GT.0.0) FAC=1.-(VT-VP(1))/(DELSHR*SHEAF)
106 CONTINUE
FACTR=FACT*SHEAF
KFAC=0.
KCDY(1)=KCODE(1)+2
KCDY(2)=KCODE(2)+2
GO TO 104
104 CONTINUE
KAT=KAT+1
IF (KAT.GT.16) CALL EXIT
C SHEAR CHECK IS FINISHED FOR THIS CYCLE CONTINUE ON CYCLE
C UPDATE SHEAR FOR YIELD CHECK
IF (KCDY(1).GE.2) GO TO 104
DELSHR=FACTCP*(DRM(1)+DRM(2))/FL
105 CONTINUE
C
C UPDATE MOMENTS AND HINGE ROTATIONS
C
CC TO 140 IFAD=1,2

```

```

RES 1130
RES 1140
RES 1150
RES 1160
RES 1170
RES 1180
RES 1190
RES 1200
RES 1210
RES 1220
RES 1230
RES 1240
RES 1250
RES 1260
RES 1270
RES 1280
RES 1290
RES 1300
RES 1310
RES 1320
RES 1330
RES 1340
RES 1350
RES 1360
RES 1370
RES 1380
RES 1390
RES 1400
RES 1410
RES 1420
RES 1430
RES 1440
RES 1450
RES 1460
RES 1470
RES 1480
RES 1490
RES 1500
RES 1510
RES 1520
RES 1530
RES 1540
RES 1550
RES 1560
RES 1570
RES 1580
RES 1590
RES 1600
RES 1610
RES 1620
RES 1630
RES 1640
RES 1650
RES 1660
RES 1670
RES 1680

```

```

IF (IEND.EQ.KFAC) GO TO 130
IF ((KCDY(IEND).NE.0).AND.(KCDY(IEND).NE.2)) GO TO 110
BMEF(IEND)=BMEF(IEND)+FACTCP*DRM(IEND)
CC TO 140
110 DPPP=FACTOR*DPPR(IEND)
PRTCT(IEND)=PRTCT(IEND)+DPPP
IF (DPPP.LT.0.) GO TO 120
FRAC(IEND)=FRAC(IEND)+DPPP
GO TO 140
120 DRACN(IEND)=DRACN(IEND)+DPPP
CC TO 140
130 BMEF(IEND)=BMEF(IEND)
140 CONTINUE
IF (KCDY(1).LT.2) GO TO 107
C APPLY ISOTROPIC HARDENING EFFECT TO SHEAR YIELD SURFACE
IF (VT.GT.0.0) VP(1)=(EMEP(1)+EMEP(2))/FL
IF (VT.LE.0.0) VP(2)=(EMEP(1)+EMEP(2))/FL
107 CONTINUE
C
C CHECK COMPLETION OF CYCLE
C
FACTC=FACTCP*FACTF
152 FORMAT (2F04.4(1E20.10,7))
IF (FACTC.GT.0.99995) GO TO 150
CALL BMCALC
GO TO 150
C
C ELASTIC AND TOTAL FORCES
C
150 BEMTCT(1)=BEMTCT(1)
BEMTCT(2)=BEMTCT(2)
BMTCT(1)=BMEF(1)+EMEL(1)+(EK11*CVR(1)+EK12*CVR(2))*PSH
EMTCT(2)=BMEF(2)+EMEL(2)+(EK12*CVR(1)+EK22*CVR(2))*PSH
DSF=(BMTCT(1)-BEMTCT(1)+EMTCT(2)-BEMTCT(2))/FL
SFTCT(1)=SFTCT(1)+DSF
SFTCT(2)=SFTCT(2)+DSF
C
C UNBALANCED LOADS DUE TO YIELD
C
IF ((KCDY(1).NE.KCDYX(1)).OR.(KCDY(2).NE.KCDYX(2))) KPAL=1
FCUR=0.
IF (KPAL.EQ.0) GO TO 160
FVJUB=FVL(1)-BMEF(1)
EMJUB=FVL(2)-BMEF(2)
CC TO 170
160 BVJUB=0.
BVJUB=0.
C
C DEFORMATION RATES FOR DAMPING
C
170 IF (DFAC.EQ.0.0.AND.DELTA.EQ.0.0) GO TO 200
IF (TIME.EQ.0.) GO TO 210
KEAL=1
IF (EC(1).EQ.1.23456E10) GO TO 180
VELM(1)=VELM(1)-EC(3)*VELM(3)
VELM(2)=VELM(2)+EC(1)*VELM(2)
RES 1690
RES 1700
RES 1710
RES 1720
RES 1730
RES 1740
RES 1750
RES 1760
RES 1770
RES 1780
RES 1790
RES 1800
RES 1810
RES 1820
RES 1830
RES 1840
RES 1850
RES 1860
RES 1870
RES 1880
RES 1890
RES 1900
RES 1910
RES 1920
RES 1930
RES 1940
RES 1950
RES 1960
RES 1970
RES 1980
RES 1990
RES 2000
RES 2010
RES 2020
RES 2030
RES 2040
RES 2050
RES 2060
RES 2070
RES 2080
RES 2090
RES 2100
RES 2110
RES 2120
RES 2130
RES 2140
RES 2150
RES 2160
RES 2170
RES 2180
RES 2190
RES 2200
RES 2210
RES 2220
RES 2230
RES 2240

```



```

C *****TH9 50
C SHEAR YIELDING ELEMENT -- REORGANIZED ELEMENT SUBROUTINE TH9 60
C CHARLES ROEDER TH9 70
C REVISED FROM ELEMENT 5 -- JUNE 1976 TH9 80
C *****TH9 90
C REORGANIZED TIME HISTORY ELEMENT, BEAM ELEMENTS TH9 100
C IF (NS.EQ.1) GO TO 20 TH9 110
C PRINT 10, ITHOUT(1), ITHOUT(3) TH9 120
C LC FORMAT(10HIFULLS FOR CRCLP,13, TH9 130
C 1 2RH, BEAM ELEMENTS, ELEMENT NO.,14//5X, TH9 140
C 2 5H TIME,4X,4HNODE,7X,5HYIELD,6X,7HEERING,7X,5HSHEAR, TH9 150
C 3 7X,5HAXIAL,12X,2HPLASTIC HINGE ROTATIONS/5X, TH9 160
C 4 5H ,4X,4H NO.,3X,5H COEF,6X,7H ELEMENT,7X,5HFORCE, TH9 170
C 5 7X,5HFORCE,12X,7HCURRENT,4X,5HACC. PCS.,2X,9HCC. NEG./ TH9 180
C 20 PRINT 30, ITHOUT(13), ITHOUT(16), ITHOUT(4), ITHOUT(1), I-1, 11, 2), ITHOUT(19) TH9 190
C 1(2), ITHOUT(5), ITHOUT(1), I=2, 12, 2) TH9 200
C 30 FORVAT (10H,08.2,19,17.5X,2F12.2,37,5F12.5/5X,18,17,2X,2F12.2,3X,3TH9 210
C IF(12.5) TH9 220
C 31 (15E+0.0) GO TO 40 TH9 230
C WRITE (INF7) ITHOUT(13), ITHOUT(6), ITHOUT(4), ITHOUT(1), I=1, 11, 2), ITHOUT(19) TH9 240
C IUT(7), ITHOUT(5), ITHOUT(1), I=2, 12, 2) TH9 250
C 40 CONTINUE TH9 260
C RETURN TH9 270
C END TH9 280
C SUBROUTINE STIFF (MSTEP,NCF,NINFC,CCMS,FK,CFAC) TH9 290
C *****ST9 300
C SHEAR YIELDING ELEMENT -- STIFFNESS MODIFICATION ROUTINE ST9 310
C CHARLES ROEDER ST9 320
C REVISED FROM ELEMENT 5 -- FEBRUARY 1976 ST9 330
C *****ST9 340
C COMMON /INFLY /MSTEP,NCF,NINFC,CCMS,FK,CFAC ST9 350
C 1 SK22,FK12,PSH,EAL,FK11H,FK22H,EC(4),KCOYX(2), ST9 360
C 2 KORY(2),PMCT(2),SHIT(2),FICT(2),FRCT(2),SENF(2), ST9 370
C 3 SENK(2),TENP(2),TEPN(2),FRAC(2),PRACK(2),PREP(2), ST9 380
C 4 SDACT(2),RBY(2,2),ACDI,NCOJ,KGUTDI,FR12,FR21, ST9 390
C 5 SK11,SK22,SK12,SK11H,SK22H,REST(CE) ST9 400
C COMMON /ACRKY /ST(2,2),ST1(2,2),ATK16,2),AA(2,6),PFL,AXK,FK, ST9 410
C 1 FFK16,5),N(1929) ST9 420
C DIMENSION CCM(1),CCMS(1),FK(6,6) ST9 430
C EQUIVALENCE(LINEX,CCM(1)) ST9 440
C STIFFNESS FORMULATION, BEAM ELEMENTS ST9 450

```

```

C CC 10 J=3,39 ST9 250
C 10 CCM(1)=CCMS(J) ST9 260
C SD 15 I=98,103 ST9 270
C 15 CCM(I)=CCMS(I) ST9 280
C C CURRENT FLEXURAL STIFFNESS, ELASTIC-PLASTIC PART ST9 290
C CALL FSTF9 (ST,KOXY) ST9 300
C PREVIOUS STIFFNESS ST9 310
C IF (MSTEP.LT.2) GO TO 30 ST9 320
C CALL FSTF9 (ST,KOXY) ST9 330
C STIFFNESS DIFFERENCE ST9 340
C DC 20 I=1,4 ST9 350
C 20 ST(I,1)=ST(I,1)-STT(I,1) ST9 360
C CALL MULTST (A,ST,ATK,FK,6,2) ST9 370
C RETURN ST9 380
C ORIGINAL STIFFNESS AT STEP ZERO, BETA-C CORRN AT STEP 1 ST9 390
C 30 FAC=1. ST9 400
C IF (MSTEP.EQ.1) FAC=DFAC ST9 410
C CC=(1.+PSH)*FAC ST9 420
C DC 40 I=1,4 ST9 430
C 40 ST(I,1)=ST(I,1)*CC ST9 440
C CALL MULTST (A,ST,ATK,FK,6,2) ST9 450
C IF (FAC.EQ.0.) GO TO 70 ST9 460
C EAL=EAL*FAC ST9 470
C AXK=EAL*CCSA**2 ST9 480
C FK(1,1)=FK(1,1)+AXK ST9 490
C FK(1,4)=FK(1,4)-AXK ST9 500
C FK(4,4)=FK(4,4)+AXK ST9 510
C AXK=EAL*SINA**2 ST9 520
C FK(2,2)=FK(2,2)+AXK ST9 530
C FK(2,5)=FK(2,5)-AXK ST9 540
C FK(5,5)=FK(5,5)+AXK ST9 550
C AXK=EAL*SINA*CCSA ST9 560
C FK(1,2)=FK(1,2)+AXK ST9 570
C FK(1,5)=FK(1,5)-AXK ST9 580
C FK(2,4)=FK(2,4)-AXK ST9 590
C FK(4,5)=FK(4,5)+AXK ST9 600
C IF (RC(1),SO.1,27456E10) GO TO 50 ST9 610
C EC3=(TSA*EC(3)-SINA*EC(1)) ST9 620
C EC4=SINA*EC(2)-CCSA*EC(4) ST9 630
C AXK=CCSA*EC3*FAL ST9 640
C FK(1,3)=FK(1,3)-AXK ST9 650
C FK(3,4)=FK(3,4)+AXK ST9 660
C AXK=SINA*EC3*EAL ST9 670
C FK(2,3)=FK(2,3)-AXK ST9 680
C FK(3,5)=FK(3,5)+AXK ST9 690
C FK(3,3)=FK(3,3)+EAL*EC3**2 ST9 700
C AXK=CCSA*EC4*EAL ST9 710

```





```

90 FORMAT (I4,2(F10.2,F10.2,1X))
C
C YIELD MOMENT TYPES
C
100 PRINT 110
110 FORMAT(////10# YIELD MOMENT TYPES//
1 5# TYPE,5X,8#POSITIVE,5X,8#NEGATIVE,7X,5#SHEAR/
2 5# NC.,5X,8# MOMENT ,5X,8# MOMENT ,7X,5#YIFLC/)
DC 140 N=1,NSLDF
READ 120, I,EMMY(N,1),EMMY(N,2),EMMY(N,3)
PRINT 130, N,EMMY(N,1),EMMY(N,2),EMMY(N,3)
120 FORMAT (I5,5X,2(F10.3,40X,F10.0)
12C FORMAT (I4,3F13.2)
140 EMMY(N,2)=-ABS(EMMY(N,2))
C
C FIXED END FORCE PATTERNS
C
IF (NFEF.EC.0) GC TO 190
PRINT 150
150 FORMAT(////25# FIXED END FORCE PATTERNS//
1 8# PATTERN,3X,4#AXIS,7X,5#AXIAL,7X,5#SHEAR,6X,6#MOMENT,
2 7X,5#AXIAL,7X,5#SHEAR,6X,6#MOMENT,5X,8#LL. PEJ./
3 8# NC. ,3X,4#CODE,7X,SHAT 1,7X,SHAT 1,6X,6# AT I ,
4 7X,SHAT J,7X,SHAT J,6X,6# AT J ,5X,8# FACILR //)
DC 160 N=1,NFEF
READ 170, I,KDFEF(N),(FEF(N,J),J=1,7)
160 PRINT 190, N,KDFEF(N),(FEF(N,J),J=1,7)
170 FORMAT (2I5,7F10.0)
180 FORMAT (I5,I0,F12.2,6F12.2,F12.3)
C
C INITIAL FORCE PATTERNS
C
190 IF (NIAT.EC.0) GC TO 240
PRINT 200
200 FORMAT(////28# INITIAL END FORCE PATTERNS //
1 6# PATTERN,7X,SHAXIAL,7X,5#SHEAR,6X,6#MOMENT,7X,5#AXIAL,
2 7X,5#SHEAR,6X,6#MOMENT/
3 8# NC. ,7X,SHAT 1,7X,SHAT 1,6X,6# AT I ,7X,SHAT J,
4 7X,SHAT J,6X,6# AT J //)
DC 210 N=1,NIAT
READ 220, I,(FINIT(N,J),J=1,6)
210 PRINT 230, N,(FINIT(N,J),J=1,6)
220 FORMAT (I5,6F10.0)
230 FORMAT (I5,3X,6F12.2)
C
C ELEMENT SPECIFICATION
C
240 PRINT 250
250 FORMAT(////28# ELEMENT SPECIFICATION//
1 3X,4#ELEM,3X,4#NCCE,2X,4#NCCE,2X,4#NCCE,2X,4#STIF,2X,4#ECCYINR
2 2X,14#YIELD MOMENTS,2X,4#ECCM,2X,4#TIME,3X,
3 12#FEF PATTERNS,3X,17#FEF SCALE FACTORS,3X,
4 16# INITIAL FORCES //)
5 3X,4# NC.,3X,4# I ,2X,4# J ,2X,4#DIFF,2X,4#TYPE,2X,4#TYPEINR
6 2X,14# END I END J ,2X,4#STIF,2X,4#LIST,3X,
7 12# DL LL ,3X,17# DL LL ,3X,

```

```

IN9 780
IN9 790
IN9 800
IN9 810
IN9 820
IN9 830
IN9 840
IN9 850
IN9 860
IN9 870
IN9 880
IN9 890
IN9 900
IN9 910
IN9 920
IN9 930
IN9 940
IN9 950
IN9 960
IN9 970
IN9 980
IN9 990
IN9 1000
IN9 1010
IN9 1020
IN9 1030
IN9 1040
IN9 1050
IN9 1060
IN9 1070
IN9 1080
IN9 1090
IN9 1100
IN9 1110
IN9 1120
IN9 1130
IN9 1140
IN9 1150
IN9 1160
IN9 1170
IN9 1180
IN9 1190
IN9 1200
IN9 1210
IN9 1220
IN9 1230
IN9 1240
IN9 1250
IN9 1260
IN9 1270
IN9 1280
IN9 1290
IN9 1300
IN9 1310
IN9 1320
IN9 1330

```

```

8 17# NC. SCALE FAC./)
C
C _ CC 260 J=32,98
260 COX(J)=0.
KCOX(1)=0
KCOX(2)=0
KCOY(1)=0
KCOY(2)=0
KST=0
C
IMEM=1
270 READ 280, INEL,INOD1,INODJ,IINC,IIMBT,IFCC,IKSFI,IKSFJ,IKGM,IKDT,
IKFOL,IKFLL,FFCL,FLL,FINIT,FFINIT
280 FORMAT (I2I5,2F5.0,15,F5.0)
C
IF (INEL.GT.IMEM) GC TO 320
290 ACCI=INCDI
ACDJ=INCDJ
INC=IINC
IF (IINC.EC.0) INC=1
IMBT=IIMBT
IFCC=IIFCC
KSFJ=IKSFJ
KSFJ=IKSFJ
KGECM=IKGM
KCLDT=IKDT
YNG=YESNC(7)
IF (KGECM.NE.0) YAG=YESNC(11)
YNT=YESNC(2)
IF (KCLDT.NE.0) YNT=YESNC(11)
KFOL=IKFOL
KFL=IKFLL
FCL=FFCL
FLL=FFLL
FLLF=1.
IF (KFL.EC.0) GC TO 300
FLLF=FFF(IKFLL,7)
IF (FLLF.EC.0) FLLF=1.E-6
300 INITE=FINIT
FINIT=FFINIT
ASTT=AST(1)
IF (INEL.NE.IMEM) 270,320
C
310 NOD1=NOD1+INC
ACDJ=ACDJ+INC
ASTT=AST(2)
C
320 PRINT 330, ASTT,IMEM,ACCI,ACDJ,INC,IMBT,IFCC,KSF1,KSFJ,YNG,YNT,KFDINS
IL,KFLL,FOL,FLLM,INIT,FINIT
330 FORMAT (A2,I4,I7,A16,2I7,5X,A9,2X,A4,I7,I6,F11.2,F10.2,I7,F11.2)
C
INITIALIZE SHEAR STIFFNESS PROPERTIES
SK11=0.0
SK12=0.0
SK22=0.0
SK11F=0.0
SK12H=0.0

```

```

IN9 1340
IN9 1350
IN9 1360
IN9 1370
IN9 1380
IN9 1390
IN9 1400
IN9 1410
IN9 1420
IN9 1430
IN9 1440
IN9 1450
IN9 1460
IN9 1470
IN9 1480
IN9 1490
IN9 1500
IN9 1510
IN9 1520
IN9 1530
IN9 1540
IN9 1550
IN9 1560
IN9 1570
IN9 1580
IN9 1590
IN9 1600
IN9 1610
IN9 1620
IN9 1630
IN9 1640
IN9 1650
IN9 1660
IN9 1670
IN9 1680
IN9 1690
IN9 1700
IN9 1710
IN9 1720
IN9 1730
IN9 1740
IN9 1750
IN9 1760
IN9 1770
IN9 1780
IN9 1790
IN9 1800
IN9 1810
IN9 1820
IN9 1830
IN9 1840
IN9 1850
IN9 1860
IN9 1870
IN9 1880
IN9 1890

```

```

VF(1)=999999.0
VP(2)=-VP(1)
C
CCLNT=NUMBER OF ELEMENT TIME HISTORIES
C
IF (KOUTGT.NP.0) NELTH=NELTH+1
C
LOCATION MATRIX
C
DO 340 I=1,2
  LM(I)=10(NCDI,I)
340 CALL EAND
C
ELEMENT PROPERTIES
C
XL=X(NCDJ)-X(NCDI)
YL=Y(NCDJ)-Y(NCDI)
IF (IECC.EC.0) GO TO 360
DO 350 I=1,4
  EC(I)=ECC(IECC,I)
  XL=XL-EC(1)+EC(2)
  YL=YL-EC(3)+EC(4)
350 FL=SQRT(XL**2+YL**2)
  COSA=XL/FL
  SINA=YL/FL
  YMOD=FTYP(IMBT,1)
  PSH=FTYP(IMBT,2)
  PPSH=1.-PSH
  PSH=PSH/PPSH
  C=FTYP(IMBT,3)-FTYP(IMBT,4)
  TF=FTYP(IMBT,4)
  F=FTYP(IMBT,5)
  IW=FTYP(IMBT,6)
  EIL=(YMOD*PPSH/FL)*((B*(1.-TF)**3)/12.+1E*TF**2/2.)+(E*TF**3/6.)
  AREA=2.*TF*B+TW*(C.-TF)
  EAL=YMOD*AREA/FL
  FACL=FTYP(IMBT,7)
  FACR=FTYP(IMBT,8)
  FACLR=FTYP(IMBT,9)
  IF (FACL.EC.0.) FACI=1.E-6
  IF (FACR.EC.0.) FACR=1.E-6
  IF ((1+D).EQ.0.) GO TO 370
  SHFAC=EIL/(FTYP(IMBT,1))/(2.*F*(1.+FTYP(IMBT,1C)))*TW*COFL*PPSH
  UET=FACL*FACR-FACLR**2
  FI=(FACR/DET)+SHFAC
  FJJ=FACL/DET+SHFAC
  FIJ=-FACLR/DEI+SHFAC
  STIFFNESS WITH SHEAR YIELD
  P=FTYP(IMBT,2)
  IF ((D.LE.0.00001).OR.(FTYP(IMBT,6).LE.0.01)) GO TO 375
  EILF=EIL/PPSH
375 CONTINUE
  DET=FII*FJJ-FIJ**2
  FACP=FII/DET

```

```

INS 1900
INS 1910
INS 1920
INS 1930
INS 1940
INS 1950
INS 1960
INS 1970
INS 1980
INS 1990
INS 2000
INS 2010
INS 2020
INS 2030
INS 2040
INS 2050
INS 2060
INS 2070
INS 2080
INS 2090
INS 2100
INS 2110
INS 2120
INS 2130
INS 2140
INS 2150
INS 2160
INS 2170
INS 2180
INS 2190
INS 2200
INS 2210
INS 2220
INS 2230
INS 2240
INS 2250
INS 2260
INS 2270
INS 2280
INS 2290
INS 2300
INS 2310
INS 2320
INS 2330
INS 2340
INS 2350
INS 2360
INS 2370
INS 2380
INS 2390
INS 2400
INS 2410
INS 2420
INS 2430
INS 2440
INS 2450

```

```

FACL=FJJ/DET
FACLR=-FII/DET
370 EK11=EIL*FACL
EK22=EIL*FACR
EK12=EIL*FACLR
EK11F=EK11-EK12**2/EK22
EK22F=EK22-EK12**2/EK11
IF ((D.LE.0.00001).OR.(1+D)**2 .LE.0.01) GO TO 377
C DEVELOPE SHEAR YIELD STIFFNESS TERMS -- ASSUME NO CROSSSECTIONAL
C WARPING AT ENDS -- REF. PLANTENA, SANDWICH CONSTRUCTION,WILEY
C , 1966
S=TW*(D**2)*YMOD*FTYP(IMBT,2)/((C.-TF)**2.0)
SF=B*TF*YMOD/(2.*C*(1.+FTYP(IMBT,10)))
FF=B*YMOD*(TF**3)/12.0
D=B*YMOD*TF*(D**2)/2.0
ALPHA=SQRT(S*SF/(D*FF*(S+2.*SF)))
C SOLVE FOR STIFFNESS COEFFICIENTS
EPAL=EXP(ALPHA*FL)
WSIL=(2.0*(1.-EPAL)**2)/(ALPHA*S*(1.-EPAL**2))+FL/S
WS2L=-ALPHA*PPSH*2.0*((1.-EPAL)**2)/(S*SF*(1.-EPAL**2))
WS2PM=(ALPHA**2)*FF/(S*SF*FL)
FACL=FTYP(IMBT,7)
FACR=FTYP(IMBT,8)
FACLR=FTYP(IMBT,9)
IF (FACL.EC.0.) FACI=1.E-6
IF (FACR.EC.0.) FACR=1.E-6
DET=FACL*FACR-FACLR**2
F22=FACL*PPSH/(DET*EIL)
F11=FACR*PPSH/(DET*EIL)
F11=(FACL*PPSH)/(DET*EIL)-WS2PM*(WSIL+WS2L)/(FL*FL)
FJJ=(FACR*PPSH)/(DET*EIL)-WS2PM*(WSIL+WS2L)/(FL*FL)
FIJ=-FACLR*PPSH/(DET*EIL)-WS2PM*(WSIL+WS2L)/(FL*FL)
DFT=FII*FJJ-FIJ**2
SK11=FII/DET-(D*EK11)/PPSH
SK22=FJJ/DET-(D*EK22)/PPSH
SK12=-FIJ/DET-(D*EK12)/PPSH
C NOTE THAT WHEN THE FLANGE HAS YIELDED IT CAN NO LONGER PROVIDE
C WARPING RESISTANCE
C HINGE AT RIGHT END
WS1L=(1.+D)/(S*FL)*(1./(ALPHA*S*FL))
WS2L=1./(ALPHA*FL*(S+2.*SF))
WS10PM=2.0
WS20PM=(1.-EPAL)/(FL*(S+2.*SF))*(1.-EPAL**2)
DFT=FACL*FACR-FACLR**2
F11=(FACR*PPSH)/(DET*EIL)-WS10PM-WS20PM*(WSIL+WS2L)/(FL*FL)
FIJ=-FACLR*PPSH/(DET*EIL)-WS10PM-WS20PM*(WSIL+WS2L)/(FL*FL)
FJJ=(FACR*PPSH)/(DET*EIL)-WS10PM-WS20PM*(WSIL+WS2L)/(FL*FL)
F11=-FACLR*PPSH/(DET*EIL)-WS10PM-WS20PM*(WSIL+WS2L)/(FL*FL)
DFT=FII*FJJ-FIJ**2
S11=FJJ/DET-EK11*F/PPSH
S22=FII/DET-EK22*F/PPSH
S12=-FIJ/DET-EK12*F/PPSH
S11=-FJJ/DET-EK11*F/PPSH
S22=-S22-S12**2/S11
INS 2460
INS 2470
INS 2480
INS 2490
INS 2500
INS 2510
INS 2520
INS 2530
INS 2540
INS 2550
INS 2560
INS 2570
INS 2580
INS 2590
INS 2600
INS 2610
INS 2620
INS 2630
INS 2640
INS 2650
INS 2660
INS 2670
INS 2680
INS 2690
INS 2700
INS 2710
INS 2720
INS 2730
INS 2740
INS 2750
INS 2760
INS 2770
INS 2780
INS 2790
INS 2800
INS 2810
INS 2820
INS 2830
INS 2840
INS 2850
INS 2860
INS 2870
INS 2880
INS 2890
INS 2900
INS 2910
INS 2920
INS 2930
INS 2940
INS 2950
INS 2960
INS 2970
INS 2980
INS 2990
INS 3000
INS 3010

```

```

C HINGE AT END 1 (LEFT END)
WS10PM=WS1LPM
WS1LPM=0.0
F11=WS2LPM
WS2LPM=WS20PM
WS20PM=F11
DET=FACL*F/CR-FACLR**2
F11=(FACL*PPSH)/(DET*EIL)-WS10PM-WS20PM*(WS1L+WS2L)/(FL*FL)
F1J=(FACLR*PPSH)/(DET*FIL)-WS10PM-WS20PM*(WS1L+WS2L)/(FL*FL)
FJJ=(FACL*PPSH)/(DET*EIL)-WS1LPM-WS2LPM*(WS1L+WS2L)/(FL*FL)
FJI=(FACLR*PPSH)/(DET*EIL)-WS1LPM-WS2LPM*(WS1L+WS2L)/(FL*FL)
DET=F11*FJJ-F1J*FJI
S11=FJJ/DET-EK11*F/PPSH
S22=F11/DET-EK22*F/PPSH
S12=-F1J/DET-EK12*F/PPSH
S21=-FJI/DET-EK12*F/PPSH
SK11=S11-C12*E21/S22
372 FORMAT (1H,SE20.10,/,1F0,SE20.10 )
377 CONTINUE
C
C YIELD MOMENTS
C
EMV(1,1)=-EMMY(KSFI,2)*PPSH
BMY(1,2)=-BMMY(KSFI,1)*PPSH
BMY(2,1)=BMMY(KSFJ,1)*PPSH
BMY(2,2)=EMMY(KSFJ,2)*PPSH
VP(1)=ABS(BMMY(KSFI,3))*PPSH
IF (ABS(BMMY(KSFJ,3))>.LT.VP(1)) VP(1)=ABS(BMMY(KSFJ,3))*PPSH
VP(2)=-VP(1)
C
C DISPLACEMENT TRANSFORMATION
C
A(1,1)=-SINA/FL
A(1,2)=CCSA/FL
A(1,3)=1.
A(1,4)=-A(1,1)
A(1,5)=-A(1,2)
A(1,6)=0.
A(2,1)=A(1,1)
A(2,2)=A(1,2)
A(2,3)=0.
A(2,4)=A(1,4)
A(2,5)=A(1,5)
A(2,6)=1.
IF (IECC.EQ.0) GO TO 380
A(2,3)=(SINA*EC(2)+CCSA*EC(1))/FL
A(1,3)=1.+A(2,3)
A(1,4)=(-SINA*EC(4)-CCSA*EC(2))/FL
A(2,6)=1.+A(1,6)
CC TO 390
390 EC(1)=1.21456E10
390 CONTINUE
C
C LOADS DUE TO FIXED END FORCES
INS 3020
IN9 3030
IN9 3040
IN9 3050
IN9 3060
IN9 3070
IN9 3080
IN9 3090
IN9 3100
IN9 3110
IN9 3120
IN9 3130
IN9 3140
IN9 3150
IN9 3160
IN9 3170
IN9 3180
IN9 3190
IN9 3200
IN9 3210
IN9 3220
IN9 3230
IN9 3240
IN9 3250
IN9 3260
IN9 3270
IN9 3280
IN9 3290
IN9 3300
IN9 3310
IN9 3320
IN9 3330
IN9 3340
IN9 3350
IN9 3360
IN9 3370
IN9 3380
IN9 3390
IN9 3400
IN9 3410
IN9 3420
IN9 3430
IN9 3440
IN9 3450
IN9 3460
IN9 3470
IN9 3480
IN9 3490
IN9 3500
IN9 3510
IN9 3520
IN9 3530
IN9 3540
IN9 3550
IN9 3560
IN9 3570

```

```

C
DC 400 I=1,6
SFF(I)=0.
400 SFFF(I)=0.
IF (KFOL*KFLL.FC.0) GO TO 530
CC 410 I=1,6
DC 410 J=1,6
410 GA(I,J)=0.
GA(1,1)=CCSA
CA(1,2)=SINA
CA(2,1)=-SINA
GA(2,2)=CCSA
CA(2,2)=1.
GA(4,4)=CCSA
CA(4,5)=SINA
CA(5,4)=-SINA
GA(5,5)=CCSA
CA(5,5)=1.
C
IF (KFOL.EQ.0) GO TO 450
DC 420 I=1,6
420 FFEF(I)=FEF(KFOL,I)*FOL
IF (KCFEF(KFOL).EQ.0) CC TO 430
CALL MULT (GA,FFEF,SFF,6,6,1)
CC TO 450
430 CC 440 I=1,6
440 SFF(I)=FFEF(I)
C
450 IF (KFLL.EQ.0) GO TO 490
CC 460 I=1,6
FLL=FLLF*FLLM
IF (I.EQ.3) (FLL.EQ.4) FLL=FLLM
460 FFEF(I)=FEF(KFLL,I)*FLL
IF (KCFEF(KFLL).EQ.0) CC TO 470
CALL MULT (GA,FFEF,SFFF,6,6,1)
CC TO 490
470 CC 480 I=1,6
480 SFFF(I)=FFEF(I)
C
490 CC 500 I=1,6
500 FF(I)=SFF(I)+SFFF(I)
C
CALL MULTT (GA,FF,CC,6,6,1)
IF (IECC.EQ.0) GO TO 510
DD(2)=DD(2)-DD(1)*EC(2)+DD(2)*EC(1)
DD(6)=DD(6)-DD(4)*EC(4)+DD(5)*EC(2)
510 CALL SPURCE (DD)
C
C MODIFY TO GET INITIAL ELEMENT FORCES
C
CC 520 I=1,6
FLL=1./FLLF
IF (I.EQ.3) (FLL.EQ.4) FLL=1.
520 SFF(I)=FF(I)+SFFF(I)*FLL
C
C INITIAL FORCES
INS 3580
INS 3590
INS 3600
INS 3610
INS 3620
INS 3630
INS 3640
INS 3650
INS 3660
INS 3670
INS 3680
INS 3690
INS 3700
INS 3710
INS 3720
INS 3730
INS 3740
INS 3750
INS 3760
INS 3770
INS 3780
INS 3790
INS 3800
INS 3810
INS 3820
INS 3830
INS 3840
INS 3850
INS 3860
INS 3870
INS 3880
INS 3890
INS 3900
INS 3910
INS 3920
INS 3930
INS 3940
INS 3950
INS 3960
INS 3970
INS 3980
INS 3990
INS 4000
INS 4010
INS 4020
INS 4030
INS 4040
INS 4050
INS 4060
INS 4070
INS 4080
INS 4090
INS 4100
INS 4110
INS 4120
INS 4130

```

```

C
530 DC 540 I=1,6          IN9 4140
540 S5FF(1)=0.          IN9 4150
      IF (INIT.EQ.0) GC TC 550 IN9 4160
      DC 550 I=1,5       IN9 4170
      S5FF(1)=FINIT(INIT,I)*FINI IN9 4180
550 SFF(1)=SFF(1)+S5FF(1) IN9 4190
      IN9 4200
C          IN9 4210
C INITIALIZE ELEMENT FORCES IN9 4220
C          IN9 4230
560 BMEP(1)=SFF(1)*PPSH IN9 4240
      BMEP(2)=SFF(5)*PPSH IN9 4250
      FTOT(1)=SFF(1) IN9 4260
      FICT(2)=SFF(4) IN9 4270
      SFTOT(1)=SFF(2) IN9 4280
      SFTOT(2)=SFF(5) IN9 4290
      BMTCT(1)=SFF(3) IN9 4300
      BMTOT(2)=SFF(4) IN9 4310
C          IN9 4320
C INITIALIZE ENVELOPES IN9 4330
C          IN9 4340
      FF(1)=S5FF(3) IN9 4350
      FF(2)=S5FF(6) IN9 4360
      FF(3)=S5FF(2) IN9 4370
      FF(4)=S5FF(5) IN9 4380
      FF(5)=S5FF(1) IN9 4390
      FF(6)=S5FF(4) IN9 4400
      DO SFC I=1,6 IN9 4410
      IF (FF(I).LT.0.) GC TC 570 IN9 4420
      SENP(I)=FF(I) IN9 4430
      SENN(I)=0. IN9 4440
      GC TC 580 IN9 4450
570 SENN(I)=FF(I) IN9 4460
      SENP(I)=0. IN9 4470
580 CONTINUE IN9 4480
C          IN9 4490
C CALL FINISH IN9 4500
C          IN9 4510
C GENERATE MISSING ELEMENTS IN9 4520
C          IN9 4530
      IF (IMEM.EQ.NMEM) RETLRN IN9 4540
      IMEM=IMEM+1 IN9 4550
      IF (IMEM.EQ.INFL) GC TC 250 IN9 4560
      CC TC 310 IN9 4570
C          IN9 4580
C END IN9 4590
      SLRROUTINE CUT9 (CCMS,AINFC) CL9 10
      *****DU9 20
C          CL9 30
C SHEAR YIELDING ELEMENT -- ENVELOPE OUTPUT SUBROUTINE CUS 40
C          CUS 50
C CHARLES RICEDEP CUS 60
C          CUS 70
C REVISED FROM ELEMENT 5 -- JUNE 1974 CL9 80
C          CUS 90
C *****DU9 100

```

```

C          CUS 110
      COMMON /INFL/ IMEM,KST,LM(2),KCECM,FL,CCSA,STRA,IA(2,6),EK11, CUS 120
      1 FK22,EK12,PSH,EAL,FK11F,EK22F,EC(4),KDDYX(2), CUS 130
      2 KDDY(2),BMTCT(2),SFTCT(2),FTCT(2),FRTCT(2),SFNP(2), CUS 140
      3 SENN(6),TENP(2),TENN(2),PPACP(2),PRACN(2),BMEP(2), CUS 150
      4 SDACT(3),ENY(2,2),NECI,NCCJ,NCUTCT,FF12,PP21, CUS 160
      5 REST(103) CUS 170
C          CUS 180
      DIMENSION COM(1),CCMS(1) CUS 190
      EQUIVALENCE(IMEM,COM(1)) CUS 200
C          CUS 210
      FINAL ENVELOPE OUTPUT, BEAM ELEMENTS CUS 220
C          CUS 230
      DO IC J=1,AINFC CUS 240
      10 COM(J)=CCMS(J) CUS 250
C          CUS 260
      IF (IMEM.EQ.1) PRINT 20 CUS 270
      20 FORMAT(23H BEAM ELEMENTS (TYPE 91)/// CUS 280
      1 5H ELEM,2X,4HNODE,17X,7HENDING,14X,4HSEPAR,14X,5HAXIAL, CUS 290
      2 13X,4HPL FINGE,12X,9H ACCUM / CUS 300
      3 5H NC,7X,4H NC,17X,7H NCAENT,3X,4HTIME,7X,5HCFCE,3X, CUS 310
      4 4HTIME,7X,5HCFCE,3X,4HTIME,3X,4HROTATION,3X,4HTIME, CUS 320
      5 5X,4HROTATION) CUS 330
C          CUS 340
      PRINT 30, IMEM,NCCI,(SENP(1),TENP(1),I=1,7,2),PPACP(1),(SENN(1),TECL CUS 350
      1AN(1),I=1,7,2),PRACN(1),NCCJ,(SENP(1),TENP(1),I=2,6,2),PPACP(2),(C CUS 360
      2FAN(1),TENN(1),I=2,6,2),PRACN(2) CUS 370
      20 FORMAT(14,17,5X,4HPOSITIVE,3(F12.2,F7.3),F14.5,F7.3,F14.5/ CUS 380
      1 16X,4HNegative,3(F12.2,F7.3),F14.5,F7.3,F14.5/ CUS 390
      2 7X,14,5X,4HPOSITIVE,3(F12.2,F7.3),F14.5,F7.2,F14.5/ CUS 400
      3 16X,4HNegative,3(F12.2,F7.3),F14.5,F7.3,F14.5/) CUS 410
C          CUS 420
      RETURN CUS 430
      END CUS 440
      SLRROUTINE FST19 (ST,KCS) CUS 10
C          FSS 20
      *****FSS 30
C          FSS 40
      POPM 2 * 2 FLEXURAL STIFFNES FSS 50
C          FSS 60
      SHEAR YIELDING ELEMENT -- STIFFNESS ASSIGNMENT SUBROUTINE FSS 60
C          FSS 70
      REVISED JUNE 1974 FSS 70
C          FSS 80
C          FSS 90
C CHARLES RICEDEP FSS 100
C          FSS 110
      *****FSS 120
      COMMON /INFL/ SPAC(24),EK11,EK22,EK12,PSH,EAL,EK11F,EK22F, CUS 130
      1 GAP(6),SK11,SK22,SK12,SK11F,SK22F,REST(58) FSS 140
      DIMENSION ST(2,2),KCD(2) FSS 150
      KYY=KCD(1)+1 FSS 160
      DO IC (10,20,30,40),KYY FSS 170
      10 NE SHEAR YIELD PLUS KCD(2) EQUALS 1 OR C CUS 180
      20 ELASTIC END 1 FSS 190
      30 IF (KCD(2).EQ.1) GC TC 15 FSS 200
      40 ENTIRELY ELASTIC FSS 210
      50 ST(1,1)=FK11 FSS 220

```



## APPENDIX D

### INPUT FORMAT AND FORTRAN LISTING FOR POST BUCKLING TRUSS ELEMENT

#### INPUT INSTRUCTIONS

The number of words of information per element = 52.

#### A. CONTROL INFORMATION FOR GROUP (4I5) - ONE CARD.

- Columns            5: Punch 7 (to indicate that the group consists of the post buckling elements).
- 6 - 10: Number of elements in group.
- 11 - 15: Number of different element stiffness types (max. 40).
- 16 - 20: Number of different fixed end force patterns (max. 40).

#### B. STIFFNESS TYPES (I5,7F10.0/,7F10.0) - TWO CARDS PER STIFFNESS TYPE (see Fig. D1).

##### CARD 1

- 1 - 5: Stiffness number.
- 6 - 15: Young's modulus of elasticity.
- 16 - 25: Cross sectional area.
- 26 - 35: Yield stress (yields only in tension).
- 36 - 45: Buckling load -  $P_{cr}$ .
- 46 - 55: Displacement coordinate -  $U_1$ .
- 56 - 65: Displacement coordinate -  $U_B$ .
- 66 - 75: Post buckling load - POSTBL.

##### CARD 2

- 1 - 10: Force coordinate  $F_1'$ .
- 11 - 20: Slope of zone 5 as a proportion of elastic zone 1 slope.
- 21 - 30: Slope of zone 8 as a proportion of elastic zone 1 slope.

- 31 - 40: Zone 6 pivotal point force coordinate  $F_6$ .
- 41 - 50: Zone 7 pivotal point force coordinate  $F_7$ .
- 51 - 60: Zone 6 pivotal point displacement coordinate  $U_6$ .
- 61 - 70: Zone 7 pivotal point displacement coordinate  $U_7$ .
- 71 - 80: Buckling load - PCRF - for later cycles after permanently kinked.

C. FIXED END FORCE PATTERNS (2I5,4F10.0) - ONE CARD FOR EACH FIXED END FORCE PATTERN.

Omit if there are no fixed end forces. See Fig. B1.5.

Columns 1 - 5: Pattern number, in sequence beginning with 1.

10: Axis code, as follows.

Code = 0: Forces are in the element coordinate system, as in Fig. B1.5a.

Code = 1: Forces are in the global coordinate system, as in Fig. B1.5b.

11 - 20: Clamping force  $F_j$ .

21 - 30: Clamping force  $V_j$ .

31 - 40: Clamping force  $F_j$ .

41 - 50: Clamping force  $V_j$ .

D. ELEMENT GENERATION COMMANDS (9I5,2F5.0,F10.0) - ONE CARD FOR EACH GENERATION COMMAND.

Elements must be specified in increasing numerical order. Cards for the first and last elements must be included. See NOTE 7 for explanation of generation procedure.

Columns 1 - 5: Element number, or number of first element in a sequentially numbered series of elements to be generated by this command.

6 - 10: Node number at element end  $i$ .

11 - 15: Node number at element end  $j$ .

16 - 20: Node number increment for element generation. If zero or blank, assumed to be equal to 1.

21 - 25: Stiffness type number.



- 30: Code for including geometric stiffness. Punch 1 if geometric stiffness is to be included. Leave blank or punch zero if geometric stiffness is to be ignored.
- 35: Time history output code. If a time history of element results is not required for the elements covered by this command, punch zero or leave blank. If a time history printout, at the intervals specified on card D1, is required, punch 1.
- 36 - 40: Fixed end force pattern number for static dead loads on element. Leave blank if there are no dead loads. See note below.
- 41 - 45: Fixed end force pattern number for static live loads on element. Leave blank if there are no live loads.
- 46 - 50: Scale factor to be applied to fixed end forces due to static dead loads. Leave blank if there are no dead loads.
- 51 - 55: Scale factor to be applied to fixed end forces due to static live loads. Leave blank if there are no live loads.
- 56 - 65: Initial axial force on element, tension positive.

Note: If the static load code, Card C1, is zero but fixed end forces are still specified for some elements, an inconsistency results. In effect, any such fixed end forces will be treated as initial element forces.

#### NOTES ON THE PHILOSOPHY BEHIND THE ELEMENT

1. This element is a model of brace behavior which permits the user to describe the inelastic behavior. The behavior may be found by a theory of brace behavior, by judgment, or by experimental results. The input parameters are described in Fig. D1. The general zonal behavior is described in Fig. D2. Figure D3 shows the procedure used in the deterioration in buckling load.

2. In a given time step the brace must lengthen, shorten, or remain unchanged. It is not possible to lengthen during part of the step and shorten during the rest of the step. This means that the

brace must continue to lengthen or shorten during a time step, or it may reverse itself. There are no other possibilities.

3. Zones 1, 6, and 7 are elastic zones. The brace can reverse itself on these zones.

4. Zones 3, 4, 5, and 8 are plastic zones. Thus, the brace must enter zones 6 or 7 when reversing from these plastic zones.

5. Zone 2 is also an inelastic zone. The brace can reverse from this zone only by entering zone 1.

6. Zone 9 is an inelastic zone. However, when zone 9 is reached the brace is nearly straight. Therefore, it would be unrealistic to reverse on to zone 7 from any point on zone 9. As a result partial reversal is permitted on zone 9. Zone 9 may unload until a critical force level is reached and then unloading progresses along zone 7. This is slightly different from the Nilforoushan approach. He creates a new zone which is parallel to zone 1 until  $R_{el} = 0.0$  and he then progresses along zone 7. The difference between these two methods is relatively minor, because metal braces have relatively high axial stiffness. Thus the stiffness of zone 9 is quite similar to the stiffness of zone 1, and the dissipated energy between zones 9 and 1 is trivial. There is no theoretical basis for either approach; they are based on judgment. This approach could easily be changed in the program.

7. Zone 6 may pass directly to zone 1 if it intersects zone 1 before it intersects zone 7. Zone 7 may pass directly to zone 1 if it intersects 1 before it reaches zone 8. This is another minor difference from the Nilforoushan model. He requires the brace to phase through zone 9 when going from 7 to 1. The difference is minor because this new zone 9 will be of very high stiffness.



-293-

```

SUBROUTINE RESPT (KDFE,MINFC,KBAL,KPP,COMS,CDISM,DD,TIME,      PE7 10
1  VELM,DFAC,DELTA)                                          RE7 20
COMMON /INFEL/ IMEM,KST,LM(4),KCECM,EALD,EALE,FL,CCSA,SINA,    RE7 30
1  N(7),NDD,C5,C8,PYP,F6,U6,F7,U7,IHIST,                      RE7 40
2  IFUT,STHIST,TSTR,RSTR,U1,CP,FCSTBL,FCR,UCLD,PCLD,          RE7 50
3  CELD,F1PRM,UNEW,RNEW,PFL,CF,CKNST,KCLD,T,REST(10)         RE7 60
4  PCPM,SDFC,REM(148)                                         RE7 70
COMMON /WORK/ EAL,DSL,DSEP,DSL,FAC,FACTOR,FAACC,DSEP,PCUT(1692) RE7 80
COMMON /THIST/THCUT(10),THCUT(20),IIPF,ISAVE,NETI,ASTH,NF7,ISE RE7 90
DIMENSION COM(1),COMS(1),DDISM(1),DD(1),VELM(1)             RE7 100
EQUIVALENCE (IMEM,COM(1))                                    RE7 110
EQUIVALENCE (ICLD,IHIST)                                     RE7 120
*****PE7 130
PCST BUCKLING TRUSS ELEMENT -- STATE DETERMINATION          RE7 140
C                                                              RE7 150
C                                                              RE7 160
C                                                              RE7 170
C CHARLES RCEDER                                             RE7 180
C                                                              RE7 190
C REVISED OCTOBER 30 , 1976                                 RE7 200
C                                                              RE7 210
*****PE7 210
C FALE = E.A / L                                             RE7 220
C FL = LENGTH                                               RE7 230
C CE = SLOPE OF ZONE 5                                       RE7 240
C CA = SLOPE OF ZONE 6                                       RE7 250
C (U6,F6) = COORDINATES OF ZONE 6 INTERSECTION POINT       RE7 260
C (U7,F7) = COORDINATES OF ZONE 7 INTERSECTION POINT       RE7 270
C IHIST = IOLD= ZONE FOR LAST TIME STEP                       RE7 280
C IFUT = ZONE FOR NEXT TIME STEP                             RE7 290
C STHIST = ACCUMULATED TENSILE ELONGATION AT TIME T         RE7 300
C TSTR = ELONGATION AT YIELD = (PYP L) / (A E)              RE7 310
C RSTR = ELONGATION AT FIRST BUCKLING = (RCP L) / (A E)     RE7 320
C U1 = ELONGATION AT COMPRESSIVE INSTABILITY                RE7 330
C (UB,PCSTBL) = COORDINATES FOR INTERSECTION OF ZONES 6 AND 7 RE7 340
C UCLD = OLD ELONGATION                                       RE7 350
C UNEW = NEW ELONGATION                                       RE7 360
C CP = AXIAL STIFFNESS OF NEXT TIME STEP                    RE7 370
C PCLD = AXIAL FORCE FOR LAST TIME STEP                      RE7 380
C RNEW = AXIAL FORCE FOR NEXT TIME STEP                      RE7 390
C COLD = AXIAL STIFFNESS OF LAST TIME STEP                  RE7 400
C SLIN = AXIAL FORCE IF THE BRACE REMAINS ON THE PRESENT ZONE RE7 410
C DV = CHANGE IN LENGTH OF THE BRACE IN THE LAST TIME STEP RE7 420
C SU = CORRECTION NECESSARY TO ACCOLAT FOR ZONE CHANGE     RE7 430
C PZERO, FCR, FRC, CRF, DEL = WORK VARIABLELS -- THEY HAVE NO RE7 440
C UNLDR MEANING                                              RE7 450
C INITIALIZE VALUES                                         RE7 460
C DC IC I=1,MINFC                                           RE7 470
10 COM(1)=COMS(1)                                           RE7 480
C KST=C                                                       RE7 490
C ICLD=IFUT                                                  RE7 500
C PCLD=PCPM                                                  RE7 510
C LCLD=UNEW                                                  RE7 520
C CCLD=CF                                                    RE7 530
C DSUB=0.0                                                   RE7 540
C IF (IMEV,EG.1) IMED=0                                       RE7 550
C DETERMINE EXTENSION INCREMENT OF EAR                      RE7 560
DV=CP*SA*(DDISM(1)-DDISM(1))+STNA*(CDISM(4)-CDISM(2))      RE7 570
LNEW=UNEW+DV                                                RE7 580
SLIN=PNW+DF*DV                                               RE7 590
RELD=UNEW-STHIST                                             RE7 600
C DETERMINE NEW ZONE FROM OLD ZONE                           RE7 610
GO TO (50,50,70,80,90,100,110,120,130), IHIST              RE7 620
ICLD = 1 OF 2                                               RE7 630
C 50 IF (RELD,GE,TSTR) GO TO 220                             RE7 640
IF (RELD,CF,RSTR) GO TO 210                                 RE7 650
IF (RELD,GE,UE) GO TO 230                                   RE7 660
IF (RELD,CF,U1) GO TO 240                                  RE7 670
GO TO 250                                                    RE7 680
C ICLD = 2                                                  RE7 690
C 70 IF (UNEW,GT,UCLD) GO TO 55                               RE7 700
IF (RELD,GE,UE) GO TO 230                                   RE7 710
IF (RELD,GE,U1) GO TO 240                                   RE7 720
GO TO 250                                                    RE7 730
C ICLD = 4                                                  RE7 740
C 80 IF (UNEW,GT,UCLD) GO TO 55                               RE7 750
IF (RELD,GE,U1) GO TO 240                                   RE7 760
GO TO 250                                                    RE7 770
C ICLD = 5                                                  RE7 780
C 90 IF (UNEW,GT,UCLD) GO TO 55                               RE7 790
GO TO 250                                                    RE7 800
C CHECK TO SEE IF BRACE REMAINS ON ZONE 6 OR DIRECTLY TO 1 OR THRU RE7 810
C BRACE IS LENGTHENING FROM ZONES 3, 4, 5, 6, OR 7         RE7 820
95 IF (RELD,GE,TSTR) GO TO 220                              RE7 830
DEL=(PCLD/(F6-PCLD))*(L6+DV-RELD)                          RE7 840
PZERO=UCLD+DEL                                              RE7 850
FCR=PFLD*FALE                                               RE7 860
FRC=PCLD+DV*F6/(L6+STHIST-PZERO)                           RE7 870
IF ((PZERO,CE,STHIST).AND.(FCR,GE,FRC)) GO TO 210          RE7 880
IF (DEL,GT,DV) GO TO 260                                     RE7 890
C 56 FORMAT (56H**WARNING** QUESTIONABLE ZONE CHANGE CHECK INPLT DATE RE7 900
1A )                                                         RE7 910
C CHECK TO SEE IF BRACE STOPS IN ZONE 7 OR GOES ON TO 1, 5, OR 6 RE7 920
97 FRC=(UNEW-PZERO)*F7/(STHIST-PZERO+U7)                   RE7 930
FCR=(RELD-U1)*CP+IIPM                                       RE7 940
IF ((RELD,LT,0.0).AND.(FRC,CE,FCR)) GO TO 260              RE7 950
FCR=PIPRM-LIACD                                             RE7 960
CRF=F7*(STHIST-PZERO)/(STHIST-PZERO+U7)                    RE7 970
IF ((CRF,CE,FCR).AND.(RELD,GT,0.0)) GO TO 250              RE7 980
C 99 FCR=RELD*FALE                                           RE7 990
IF (FRC,LE,FCR) GO TO 210                                   RE7 1000
GO TO 270                                                    RE7 1010
C ICLD = 6                                                  RE7 1020
C 100 IF ((UNEW,GE,UCLD).AND.(SLIN,LE,0.0)) GO TO 101      RE7 1030
IF (UNEW,GE,UCLD) GO TO 55                                  RE7 1040
PZERO=UCLD-FCLD/CF-STHIST                                   RE7 1050
GO TO 135                                                    RE7 1060
C 101 EALD=SLIN/FALE                                         RE7 1070
IF (RELD,GE,EALD) GO TO 210                                 RE7 1080
GO TO 260                                                    RE7 1090
C ICLD = 7                                                  RE7 1100
C 110 PZERO=UCLD-(PCLD/CF)-STHIST                            RE7 1110
IF (LIN,LE,0.0) GO TO 135                                   RE7 1120

```

```

IF (RELD.GE.TSTP) GO TO 220
IF (UNEW.LE.UCLD) GO TO 270
PZERC=PZERC+STHIST
GO TO 27
C
129 FRC=FALE*RELD
IF (RELD.GE.TSTP) GO TO 220
IF (RELD.GE.0.9) GO TO 290
IF (UNFW.GE.UCLD) GO TO 280
PZERC=UCLD-STHIST-(POLD*(STHIST+U7-UCLD))/(F7-PELD)
IF (UNEW.GT.PZERC) GO TO 270
GO TO 135
C
128 IFLD = 9
C
ZONE 9 IS AN INELASTIC ZONE. HOWEVER, THE BRACE IS NEARLY
C STRAIGHT WHEN IT ENTERS ZONE 9. THEREFORE, IT WOULD NOT BE
C REALISTIC TO REVERSE DIRECTLY ON TO ZONE 7 FROM JUST ANY POINT ON
C ZONE 9. FOR EXAMPLE, IF POLD IS GREATER THAN F7 A TOTALLY
C UNREALISTIC NEGATIVE SLOPE WOULD RESULT. THEREFORE, I AM
C PERMITTING REVERSAL ON ZONE 9 UNTIL F IS LESS THAN 0.5 F7 AND THE
C INTERSECTION WITH ZONE 9. THIS WILL PREVENT THE STIFFNESS FROM
C BEING NEGATIVE OR EXCESSIVELY SMALL WHEN THE BRACE IS NEARLY
C STRAIGHT. IT IS AN ARBITRARY DECISION AND CAN BE CHANGED BY
C CHANGING THE TWO CARDS AFTER STATEMENT 130.
130 IF (SLIN.GE.PYP) GO TO 220
FRC=FPRM-CR*UI
PCR=C.50*F7
IF (FRC.LE.CP) FRC=FRC
IF ((SLIN.LE.FRC).AND.(UNEW.LE.UCLD).AND.(SLIN.LE.FRC)) GO TO 132
GO TO 290
131 LEL=(POLD-FRC)/CF
PZERC=UCLD-DEL-FRC*(STHIST+U7-UCLD+DEL)/(F7-FRC)-STHIST
IF (RELD.GT.PZERC) GO TO 270
C
BRACE IS COMPRESSING ON TO ZONE 6 AND POSSIBLY INTERSECTS 3,4,OR
C BRACE IS SHORTENING FROM ZONES 7, 8, OR 9
135 FCP=(F7/106-PZERC)/(RELD-PZERC)
FRC=PCSTBL+CP*(RELD-UI)
IF (FCP.GT.FRC) GO TO 280
IF (RELD.LE.UI) GO TO 250
IF ((RELD.GE.UI).AND.(FRC.LE.PCR)) GO TO 230
FRC=PCSTBL+(RELD-UI)*(PCR-PCSTBL)/(CR-L1)
IF ((RELD.GE.L1).AND.(FRC.LE.FRC)) GO TO 240
GO TO 260
C
GO TO NEW ZONE AND DETERMINE SU
IFUT = 1
C
210 IFUT=1
CF=SAFE
IF (ICLD.EC.1) SU=0.0
IF (ICLD.NE.1) SU=SLIN-RELD*EALL
GO TO 350
C
IFUT = 2
220 IFL=2
CF=0.0
STHIST=UNEW-TSTR
IF (ICLD.EC.2) SU=0.0
IF (ICLD.NE.2) SU=SLIN-PYP
GO TO 350
RE7 1130
RE7 1140
RE7 1150
RE7 1160
RE7 1170
RE7 1180
RE7 1190
RE7 1200
RE7 1220
RE7 1230
RE7 1240
RE7 1250
RE7 1260
RE7 1270
RE7 1280
RE7 1290
RE7 1300
RE7 1310
RE7 1320
RE7 1330
RE7 1340
RE7 1350
RE7 1360
RE7 1370
RE7 1380
RE7 1390
RE7 1400
RE7 1410
RE7 1420
RE7 1430
RE7 1440
RE7 1450
RE7 1460
RE7 1470
RE7 1480
RE7 1490
RE7 1500
RE7 1510
RE7 1520
RE7 1530
RE7 1540
RE7 1550
RE7 1560
RE7 1570
RE7 1580
RE7 1590
RE7 1600
RE7 1610
RE7 1620
RE7 1630
RE7 1640
RE7 1650
RE7 1660
RE7 1670
RE7 1680
RE7 1690
RE7 1700
RE7 1710
RE7 1720
RE7 1730
RE7 1740
RE7 1750
RE7 1760
RE7 1770
RE7 1780
RE7 1790
RE7 1800
RE7 1810
RE7 1820
RE7 1830
RE7 1840
RE7 1850
RE7 1860
RE7 1870
RE7 1880
RE7 1890
RE7 1900
RE7 1910
RE7 1920
RE7 1930
RE7 1940
RE7 1950
RE7 1960
RE7 1970
RE7 1980
RE7 1990
RE7 2000
RE7 2010
RE7 2020
RE7 2030
RE7 2040
RE7 2050
RE7 2060
RE7 2070
RE7 2080
RE7 2090
RE7 2100
RE7 2110
RE7 2120
RE7 2130
RE7 2140
RE7 2150
RE7 2160
RE7 2170
RE7 2180
RE7 2190
RE7 2200
RE7 2210
RE7 2220
RE7 2230
RE7 2240
C
230 IFUT=3
IFL=3
CF=0.0
IF (ICLD.EC.3) SU=0.0
IF (ICLD.NE.3) SU=SLIN-PCR
GO TO 350
C
IFUT = 4
240 IFUT=4
IF (ICLD.NE.4)
ICF=(PCR-PCSTBL)/(CB-UI)
IF (ICLD.EC.4) SU=0.0
IF (ICLD.NE.4) SU=SLIN-CF*(RELD-L1)-PCSTBL
GO TO 350
C
IFUT = 5
250 IFUT=5
CF=CS
IF (ICLD.EC.5) SU=0.0
IF (ICLD.NE.5) SU=SLIN-(RELD-L1)*CF-PCSTBL
GO TO 350
C
IFUT = 6
260 IFUT=6
IF (ICLD.GE.7) SU=SLIN-FRC
IF (ICLD.EC.6) SU=0.0
IF (ICLD.NE.6) SU=SLIN-((F6-POLD)/(STHIST+U6-UCLD)+CV)-POLD
GO TO 250
C
IFUT = 7
270 IFL=7
IF (ICLD.EC.7) PRINT 56
IF (ICLD.EC.7) SU=0.0
IF (ICLD.EC.8) SU=SLIN-(F7-PELD)*CV/(L7+STHIST-UCLD)-POLD
IF (ICLD.EC.9) SU=SLIN-FCH+(F7*(CV+DEL)/(L7+STHIST-PZERC))
IF (ICLD.NE.9) SU=SLIN-(F7*(CV-DEL)/(L7+STHIST-PZERC))
IF (ICLD.NE.6) GO TO 250
PZERC=UCLD+(FC/L7*(RELD-SLIN))*CV
SU=SLIN-(UNEW-PZERC)/(F7/(STHIST+U7-PZERC))
GO TO 350
C
IFUT = 8
280 IFUT=8
IF (ICLD.LE.4) PRINT 96
CF=CR
IF (ICLD.EC.8) SU=0.0
IF (ICLD.NE.8) SU=SLIN+CR*(UI-RELD)-F1PRM
GO TO 350
C
IFUT = 9
290 IFUT=9
IF (ICLD.LE.4) PRINT 96
CF=(PYP-F1PRM+(UI*CF))/TSTR
IF (ICLD.EC.9) SU=0.0
IF (ICLD.NE.9) SU=SLIN-(PYP-F1PRM+UI*CF)*(UNEW-STHIST)/TSTR
GO TO 350
1) IF (PRM-CR*LI)
GO TO 350
350 PNEW=SLIN-SL
PFL=PNEW
IF (ICLD.EC.IFUT) GO TO 375
DSU=SU
KST=1
RE7 1690
RE7 1700
RE7 1710
RE7 1720
RE7 1730
RE7 1740
RE7 1750
RE7 1760
RE7 1770
RE7 1780
RE7 1790
RE7 1800
RE7 1810
RE7 1820
RE7 1830
RE7 1840
RE7 1850
RE7 1860
RE7 1870
RE7 1880
RE7 1890
RE7 1900
RE7 1910
RE7 1920
RE7 1930
RE7 1940
RE7 1950
RE7 1960
RE7 1970
RE7 1980
RE7 1990
RE7 2000
RE7 2010
RE7 2020
RE7 2030
RE7 2040
RE7 2050
RE7 2060
RE7 2070
RE7 2080
RE7 2090
RE7 2100
RE7 2110
RE7 2120
RE7 2130
RE7 2140
RE7 2150
RE7 2160
RE7 2170
RE7 2180
RE7 2190
RE7 2200
RE7 2210
RE7 2220
RE7 2230
RE7 2240

```

```

C      KEAL=1
      DEFORMATION RATE FOR DAMPING
375 IF (DFAC.EQ.0.0.AND.DELTA.EQ.0.0) GO TO 400
      IF (TIME.EQ.0.0) GO TO 450
      KBAL=1
      DV=COSAP(VELM(3)-VELM(1))*SINA+(VELM(4)-VELM(2))
C      BETA = 0 DAMPING FORCE
      IF (DFAC.EQ.0.0) GO TO 390
      DSUB=DSUB+DFAC*EALE*DV
C      STRUCTURAL DAMPING FORCE
350 IF (DELTA.EQ.0.0) GO TO 400
      DSL=DELTA*SIGN(ABS(SLIN),DV)
      DSUB=DSUB-DSL*SCFC
      SCFC=DSL
C      UNBALANCED LOAD VECTOR
400 IF (KBAL.EQ.0) GO TO 450
      DD(1)=DSUB*CCSA
      DD(4)=DSUB*SINA
      DD(1)=-DD(3)
      DD(2)=-DD(4)
C      PRINT TIME HISTORY
450 ISAVE=0
      IF (KPR.LT.0) GO TO 475
      IF (KPR.EQ.0.OR.KCUTDT.EQ.0) GO TO 525
      IF (11HP.GT.1) GO TO 490
475 IF (11MED.NE.0) GO TO 480
      KKPR=(ABS(KPR)
      PRINT 475, KKPR, TIME
478 FORMAT(///18H RESULTS FOR GROUP,12,28H, POST BUCKLING TRUSS ELEMENT
1      ,10HTS, TIME=,F8.3,/,5X,5H ELEM,3X,4HNODE,3X,4HNOCE,3X,5HPHASE
2      ,8X,5HAXIAL,4X,9H LATEST,2X,14HACCLM, FLASTIC,/, 5X,5H NC.,
3      3X,4H I ,3X,4H J ,2X,5H CODE,2X,5HFORCE,4X,4HEXTENSION,6X,
4      9HEXTENSION/)
      11ED=1
480 PRINT 485, 11FW,NDD1,NDDJ,11FUT,11FNEW,11UNEW,11STHIST
485 FORMAT (19,217,(8,F14.2,2F13.5)
490 IF (11HP.LT.1.CF.KCUTDT.EQ.0) GO TO 525
C      SET TIME HISTORY IN THIS
      KKPR=(ABS(KPR)
      11HOLT(1)=KKPR
      11HOLT(2)=7
      11HCUT(3)=11FV
      11HOLT(4)=NDD1
      11HCUT(5)=NDDJ
      11HOLT(6)=11FUT
      11HOLT(1)=11FNEW
      11HCUT(2)=11UNEW
      11HOLT(3)=11STHIST
      11HCUT(4)=11TIME
      ISAVE=1
525 CONTINUE
      IF (11NEW.LT.REST(1)) REST(2)=11TIME
      IF (11NEW.LT.REST(1)) REST(1)=11FNEW
      IF (11NEW.GT.REST(3)) REST(4)=11TIME
      IF (11NEW.GT.REST(3)) REST(3)=11FNEW
      IF (11ELD.GT.REST(5)) REST(6)=11TIME
      IF (11ELD.LT.REST(5)) REST(5)=11ELD
      IF (11ELD.LT.REST(7)) REST(7)=11TIME
      IF (11ELD.LT.REST(7)) REST(7)=11ELD
      REST(5)=11STHIST
      IF ((11FUT.EQ.(3.CF.4.CF.5)).AND.(11ELD.NE.(3.CF.4.CF.5)))
1      REST(10)=REST(10)+11ELD-11FUT
      IF ((11FUT.EQ.(3.CF.4.CF.5)).AND.(11ELD.EQ.(3.CF.4.CF.5)))
1      REST(10)=REST(10)+11NEW-UCLD
      IF (11FUT.EQ.6) CF=(11F6-11NEW)/(11L6+11STHIST-11NEW)
      IF (11FUT.EQ.7) CF=(11F7-11NEW)/(11STHIST+11U7-11NEW)
C      ADJUST PCP FOR SUBSEQUENT CYCLES
      IF ((11FUT.LF.5).AND.(11FLT.CF.3)) GO TO 549
      GO TO 549
529 IF (11NEW.LT.11PCRM) GO TO 530
      ESTR=(11CRM/11PCF)*11ESTR
      PCF = 11CRM
      GO TO 540
530 ESTR=(11NEW/11PCR)*11ESTR
      PCR=11NEW
540 CONTINUE
C      UPDATE CCMS
      CO 550 I-1,N11FC
550 COMS(1)=COMI1
      RE11PW
      11N0
      SUBROUTINE INFL7 (KCCNT,FCOCT,ACCF,N11FC,IC,X,Y,NX)
C
      COMMON /INFL7 INFM,KST,LM(4),KKECM,EALEP,EALE,FL,CCSA,SINA,
1      NDD1,NDDJ,C5,C6,P1P,F6,L6,F7,U7,11HIST,
2      11FUT,11STHIST,11STR,11STR,U1,UP,11PS1R1,11CF,UCLD,11ELD,
3      CCLD,11PRM,11UNEW,11FNEW,11FLL,CF,CNST,KCUTDT,REST(10),
4      11CPM,11SFC,11RFM(148)
      COMMON /WCRK/11TYP(40,15),KKEUC(40),11FEP(40,4),KDFEP(40),DD(4),
1      GATA(4),11FFP(4),11SFF(4),11SSFF(4),N11EV,N11ET,11FEF,
2      GNEL,INEL,11NDD1,11NDDJ,11AC,11JNC,11MBT,11MBT,11KGM,
3      11KCT,11KFDL,11KFL,11KFL,11KFL,11KFL,11KFL,11KFL,11KFL,
4      11INIT,11FINIT,11XL,11YL,11AREA,11(1102)
      COMMON/11H/11HCUT(10),11HOLT(20),11HP,11SAVE,NELT,NCTP,NF7,11SE
C
      DIMENSION KCONT(11),IC(INN,11),X(11),Y(11),COM(1)
      DIMENSION AST(2),YESAC(2)
      DATA AST /2H ,2H 9/
      DATA YESAC/4H YES,4H NO /
      *****
C
C      POST BUCKLING TRUSS ELEMENT -- INFL7 SUBROUTINE
C
C      CHARLES FEEFFE
C
C      REVISED OCTOBER 20 , 1976
C
C      *****
C
C      *****
C
C      THIS SUBROUTINE IS REVISED SLIGHTLY FROM INEL1. INEL INITIALIZES
      AND READS ELEMENT DATA. THE INITIAL DATA IS NOT VERY
      DIFFERENT FOR THE POST BUCKLING MODEL .

```



Reproduced from  
best available copy.

```

IFINIT
180 FORMAT (A2,14,17,316,3X,A4,2X,A4,17,16,F11.2,F10.2,F11.2)
C
C COUNT NUMBER OF ELEMENT TIME HISTORIES
C
C IF (KOUTD.NE.0) NELTH=NELTH+1
C
C LOCATION MATRIX
C
C CC 190 I=1,2
C LM(L)=IG(NDD1,L)
190 LM(L+2)=IG(NDDJ,L)
CALL EANC
C
C ELEMENT PROPERTIES
C
C XL=X(NDDJ)-X(NDD1)
C YL=Y(NDDJ)-Y(NDD1)
C FL=SQRT(XL**2+YL**2)
C CQSA=XL/FL
C SINA=YL/FL
C
C IHIST = NUMBER DEFINING THE PART OF THE CYCLIC CURVED WHICH IS
C OCCUPIED DURING THIS TIME STEP. SHIST - HISTORY OF
C PERMANENT DEFORMATION OF MEMBER.
C
C IHIST = 1
C 1STH = (FTYP(IMBT,3)*FL)/FTYP(IMBT,1)
C BSTR=FTYP(IMBT,4)*FL/(FTYP(IMBT,2)*FTYP(IMBT,1))
C LNEW=0.0
C F1PRM=FTYP(IMBT,5)
C U1=FTYP(IMBT,5)
C U2=FTYP(IMBT,6)
C POSTRL=FTYP(IMBT,7)
C PCR=FTYP(IMBT,4)
C PCRM = FTYP(IMBT,15)
C IFUT=1
C SHI*1 = 0.0
C AREA=FTYP(IMBT,2)
C DPA=AREA*FTYP(IMBT,3)
C EALEP = 0.0
C FALE = FTYP(IMBT,1) * AREA / FL
C C5=FTYP(IMBT,9)*FALE
C C6=FTYP(IMBT,10)*FALE
C F6=FTYP(IMBT,11)
C F7=FTYP(IMBT,12)
C U6=FTYP(IMBT,13)
C U7=FTYP(IMBT,14)
C CF=EALE
C CCLD=CF
C
C LOADS DUE TO FIXED END FORCES
C
C SFFF=0.
C IF (KFCL+KELL.EC.0) GO TO 310
C DO 200 I=1,NDF
C DO 200 J=1,NDDF
200 GA(I,J)=0.

```

```

IN7 1640
IN7 1450
IN7 1460
IN7 1470
IN7 1480
IN7 1490
IN7 1500
IN7 1510
IN7 1520
IN7 1530
IN7 1540
IN7 1550
IN7 1560
IN7 1570
IN7 1580
IN7 1590
IN7 1600
IN7 1610
IN7 1620
IN7 1630
IN7 1640
IN7 1650
IN7 1660
IN7 1670
IN7 1680
IN7 1690
IN7 1700
IN7 1710
IN7 1720
IN7 1730
IN7 1740
IN7 1750
IN7 1760
IN7 1770
IN7 1780
IN7 1790
IN7 1800
IN7 1810
IN7 1820
IN7 1830
IN7 1840
IN7 1850
IN7 1860
IN7 1870
IN7 1880
IN7 1890
IN7 1900
IN7 1910
IN7 1920
IN7 1930
IN7 1940
IN7 1950
IN7 1960
IN7 1970
IN7 1980
IN7 1990

```

```

CA(1,1)=CCSA
GA(1,2)=SINA
CA(2,1)=-SINA
GA(2,2)=CCSA
CA(3,2)=CQSA
CA(3,4)=SINA
CA(4,3)=-SINA
CA(4,4)=CCSA
CC 210 I=1,4
SFF(I)=0.
210 SFFF(I)=0.
IF (KFCL.EC.0) GO TO 250
CC 220 I=1,4
220 FFFF(I)=FEF(KFCL,I)*FCL
IF (KDFEF(KFCL).EC.0) GO TO 220
CALL MLTI (CA,FFFF,SFF,4,4,1)
CC TO 250
230 DD 240 I=1,4
240 SFF(I)=FFFF(I)
C
250 IF (KELL.EC.0) GO TO 290
DD 260 I=1,4
260 FFFF(I)=FEF(KELL,I)*FLL
IF (KDFEF(KELL).EC.0) GO TO 270
CALL MLTI (CA,FFFF,SFFF,4,4,1)
CC TO 290
270 DD 280 I=1,4
280 SFFF(I)=FFFF(I)
C
290 DD 300 I=1,4
300 SFFF(I)=SFFF(I)+SFF(I)
C
CALL MLTI (CA,SFFF,CC,4,4,1)
CALL SFORCE (CD)
C
C INITIALIZE ELEMENT FORCE
C
C STATE=(SFFF(3)-SFFF(1))*C.5
310 FNEW=FINIT+SFFF
FLL=FNFW
IF (FINIT.LT.0.) GO TO 320
REST(1)=FINIT
REST(2)=0.0
CC TO 330
320 REST(3)=FINIT
REST(4)=0.0
C
330 CALL FINISH
C
C GENERATE MISSING ELEMENTS
C
IF (IMEM.EC.NMEM) RETURN
IMEM=IMEM+1
IF (IMEM.EC.INEL) GO TO 150
CD TO 160
IN7 2000
IN7 2010
IN7 2020
IN7 2030
IN7 2040
IN7 2050
IN7 2060
IN7 2070
IN7 2080
IN7 2090
IN7 2100
IN7 2110
IN7 2120
IN7 2130
IN7 2140
IN7 2150
IN7 2160
IN7 2170
IN7 2180
IN7 2190
IN7 2200
IN7 2210
IN7 2220
IN7 2230
IN7 2240
IN7 2250
IN7 2260
IN7 2270
IN7 2280
IN7 2290
IN7 2300
IN7 2310
IN7 2320
IN7 2330
IN7 2340
IN7 2350
IN7 2360
IN7 2370
IN7 2380
IN7 2390
IN7 2400
IN7 2410
IN7 2420
IN7 2430
IN7 2440
IN7 2450
IN7 2460
IN7 2470
IN7 2480
IN7 2490
IN7 2500
IN7 2510
IN7 2520
IN7 2530
IN7 2540
IN7 2550

```

```

END IN7 2560
SUBROUTINE ST1F7 (MSTEP,NOCF,NINFC,CCMS,FK,CFAC) ST7 10
COMMON /INFL/ IMEM,KST,LV(4),KGECA,FALEP,EALC,FL,CCSA,SINA, ST7 20
1 NOC1,NOC2,CS,CR,PYP,FE,UC,F7,U7,IHIST, ST7 30
2 IFLY,STHIST,TSTR,ESTR,UI,UE,FCSTEL,FCR,UCLD,PCLD, ST7 40
3 COLD,FIPRM,UNEM,PNEM,PFL,CF,CCNST,KELTOT,REST(160) ST7 50
COMMON /WCP/ SST(2,2),AA(2,4),AATK(4,2),FFK(4,4),K(160) ST7 60
DIMENSION CCM(1),CCMS(1),FK(4,4) ST7 70
EQUIVALENCE (IMEM,CCM(1)) ST7 80
*****ST7 90
POST BUCKLING TRUSS ELEMENT -- STIFFNESS MODIFICATION SUBROUTINE ST7 100
CHARLES RICEBER ST7 110
REVISED FEBRUARY 12, 1976 ST7 120
*****ST7 130
DO 10 J=3,NINFC ST7 140
CCM(J)=CCMS(J) ST7 150
IF (MSTEP,CF,C) GO TO 40 ST7 160
CCNST=CALE ST7 170
COLD=FALE ST7 180
CC 10 500 ST7 190
40 IF (MSTEP,FC,1) CCNST=FALE*CFAC ST7 200
IF (MSTEP,FC,1) GO TO 500 ST7 210
THE SHAPE OF THE CYCLIC FORCE - DISPLACEMENT CURVE CAN ST7 220
BE CHANGED BY CHANGING THE INPUT VARIABLES. HOWEVER, ST7 230
CARE MUST BE TAKEN TO ASSURE THAT THE INFLT BEHAVIOR ST7 240
RESEMBLES BRACE BEHAVIOR. INFLT SUCH AS NEGATIVE P6 OR F7 ST7 250
COULD GIVE STRANGE RESULTS. ST7 260
200 CCNST=CF-COLD ST7 270
500 FK(1,1)=CCNST*LESA**2 ST7 280
FK(1,2)=CCNST*SINA*CCSA ST7 290
FK(1,3)=-FK(1,1) ST7 300
FK(1,4)=-FK(1,2) ST7 310
FK(2,2)=CCNST*SINA**2 ST7 320
FK(2,3)=FK(1,4) ST7 330
FK(2,4)=-FK(2,2) ST7 340
FK(3,3)=FK(1,1) ST7 350
FK(3,4)=FK(1,2) ST7 360
FK(4,4)=FK(2,2) ST7 370
DO 600 I=2,4 ST7 380
JJ=I-1 ST7 390
DO 650 J=1,JJ ST7 400
FK(1,J)=FK(J,1) ST7 410
COMPUTE GEOMETRIC STIFFNESS ST7 420
600 IF (KGECA,FC,C) GO TO 700 ST7 430
IF (MSTEP,FC,1) GO TO 700 ST7 440
DO 620 I=1,4 ST7 450
SST(I,1)=PFL ST7 460
DO 630 I=1,4 ST7 470
AA(I,1)=C,C ST7 480
AA(I,2)=-SINA ST7 490
AA(I,3)=CCSA ST7 500
AA(I,4)=SINA ST7 510

```

```

AA(2,4)=-CCSA ST7 520
CALL MULTST (AA,CFST,AATK,FFK,4,2) ST7 530
DO 650 I=1,16 ST7 540
650 FFK(I,1)=FK(I,1)*FFK(I,1) ST7 550
700 CONTINUE ST7 560
RTIURN ST7 570
END ST7 580
SUBROUTINE CUT7 (CCMS,NINFC) ST7 590
COMMON /INFL/ IMEM,KST,LV(4),KGECA,FALEP,EALC,FL,CCSA,SINA, ST7 600
1 NOC1,NOC2,CS,CR,PYP,FE,UC,F7,U7,IHIST, ST7 610
2 IFLY,STHIST,TSTR,ESTR,UI,UE,FCSTEL,FCR,UCLD,PCLD, ST7 620
3 COLD,FIPRM,UNEM,PNEM,PFL,CF,CCNST,KELTOT,REST(160) ST7 630
DIMENSION CCM(1),CCMS(1) ST7 640
EQUIVALENCE (IMEM,CCM(1)) ST7 650
*****CUT7 80
POST BUCKLING TRUSS ELEMENT -- ENVELOPE OUTPUT SUBROUTINE ST7 90
CHARLES RICEBER ST7 100
REVISED JANUARY 19, 1976 ST7 110
*****CUT7 120
ENVELOPE OUTPUT FOR POST BUCKLING TRUSS ELEMENTS ST7 130
DO 10 J=1,NINFC ST7 140
10 CCM(J)=CCMS(J) ST7 150
IF (IMEM,FC,1) PRINT 20 ST7 160
20 FORMAT (38H POST BUCKLING TRUSS ELEMENTS (TYPE 7) ,// ST7 170
1 5H ELEM,7X,4HNODE,14X,20HMAXIMUM AXIAL FORCES , ST7 180
2 16X,18HMAXIMUM EXTENSIONS,12X,25HACCUM. PLASTIC EXTENSIONS,// ST7 190
3 5H NO.,3X,4H I ,3X,4H J ,6X,2HCUMPN,4X,4HTIME,5X, ST7 200
4 7HTENSION ,2X,4HTIME,5X,8HPOSITIVE,3X,4HTIME, ST7 210
5 3X,8HNEGATIVE,3X,4HTIME,7X,8HPOSITIVE,5X,8HNEGATIVE// ST7 220
PRINT 30,IMEM,NOC1,NOC2, (REST(1),I=1,10) ST7 230
30 FORMAT(14,17,17,2X,2(F11.2,F7.2),2X,2(F11.5,F7.2),2X,2F13.5) ST7 240
RETURN ST7 250
END ST7 260
SUBROUTINE THP7 (AS) ST7 270
COMMON /THIST/ ITHOUT(10),ITHOUT(20),ITHP,ISAVE,MLLTH,NSTH,NF7,ISE ST7 280
*****THP7 30
POST BUCKLING TRUSS ELEMENT -- REORGANIZED OUTPUT SUBROUTINE. ST7 40
CHARLES RICEBER ST7 50
REVISED FEBRUARY 12, 1976 ST7 60
*****THP7 70
REORGANIZED TIME HISTORY OUTPUT ST7 80
IF (AS,GT,1) GO TO 20 ST7 90
PRINT 10,ITHOUT(1),ITHOUT(3) ST7 100
10 FORMAT(10HRESULTS FOR GROUP,13,29) POST BUCKLING TRUSS ELEMENTS, ST7 110
1 13H, ELEMENT NO.,14,7X,5H TIME,3X,4HNODE,3X, ST7 120
2 5H, SH,SHAXIAL,4X,9H TOTAL ,3X,14HACCUM. PLASTIC,7,5X, ST7 130
3 3H ,3X,4H I ,3X,4H J ,3X,5H CODE,6X,8HCODE,4X, ST7 140
4 8HEXTENSION,6X,8HEXTENSION ST7 150
20 PRINT 10, ITHOUT(4),(ITHOUT(1),I=4,2),(ITHOUT(1),I=1,2) ST7 160
30 FORMAT (10H,FR,3,17,18,F14.2,3F13.5) ST7 170
IF (ISE,FC,0) GO TO 40 ST7 180
WRITE (INF,7) ITHOUT(4),(ITHOUT(1),I=4,2),(ITHOUT(1),I=1,2) ST7 190
40 CONTINUE ST7 200
RTIURN ST7 210
END ST7 220

```



### ZONE NUMBERING AND DEFINING VALUES

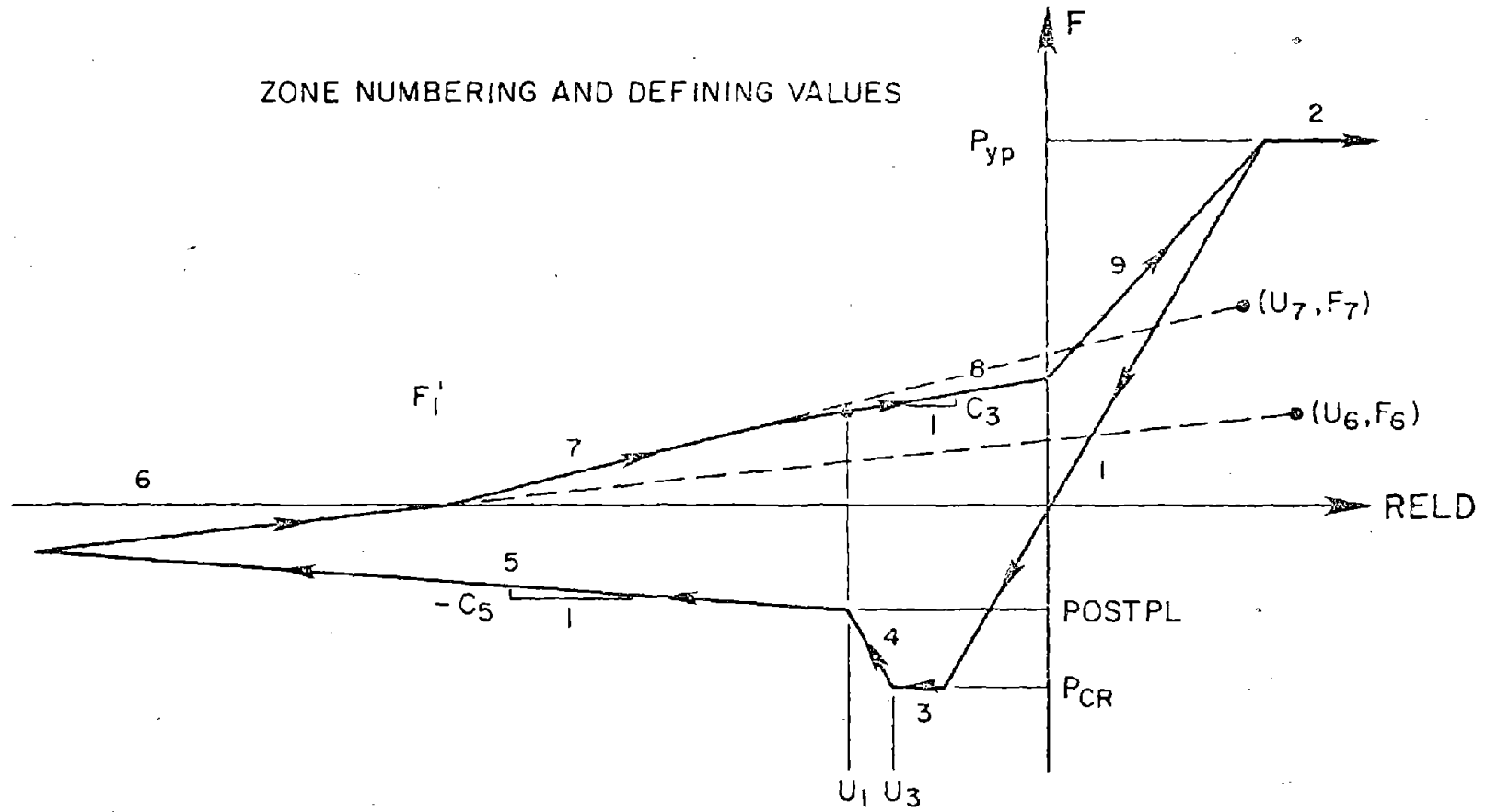


FIGURE D1 - DEFINITION OF INPUT PARAMETERS

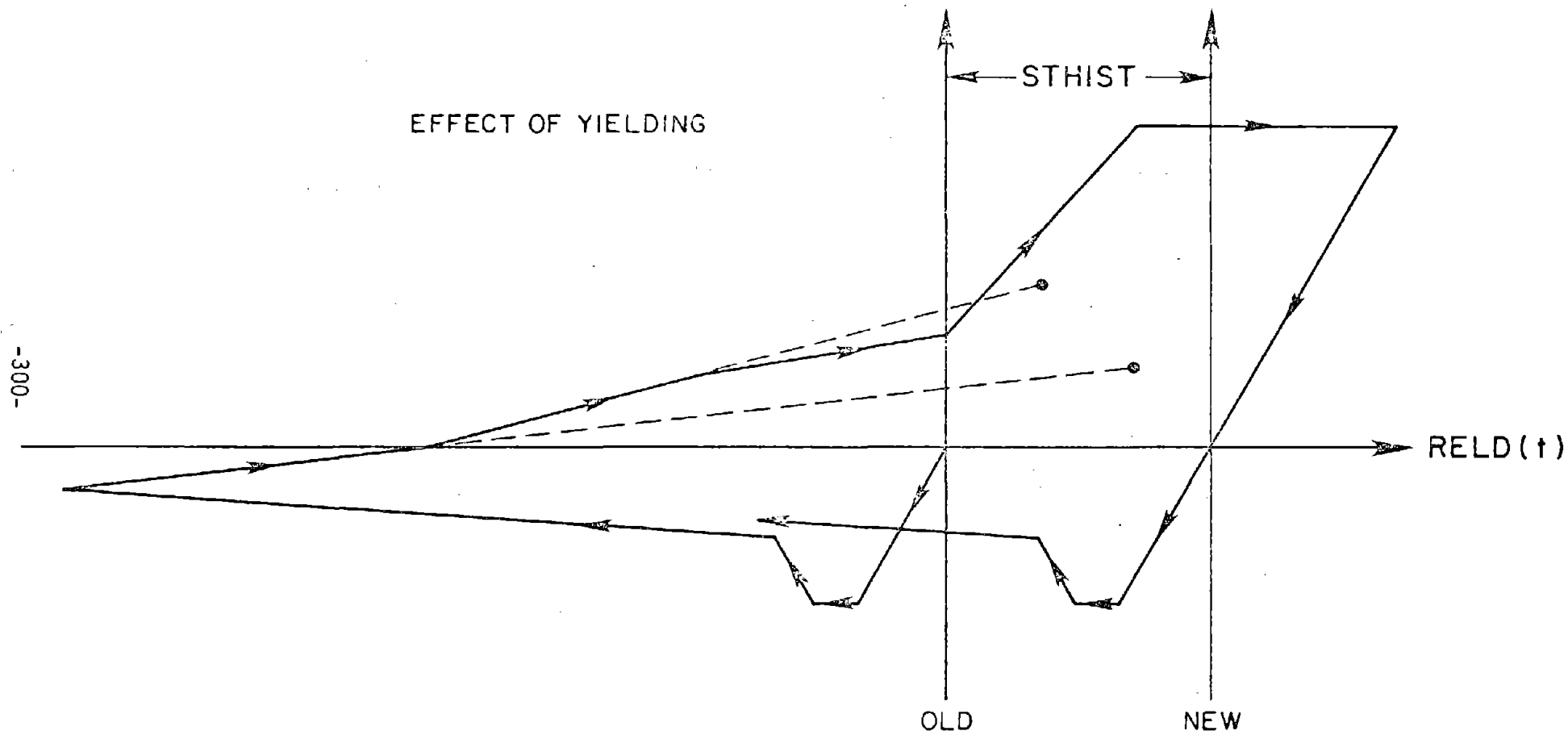


FIGURE D2 - MODIFICATION OF THE CRITICAL PARAMETERS DUE TO YIELDING OF THE BRACE

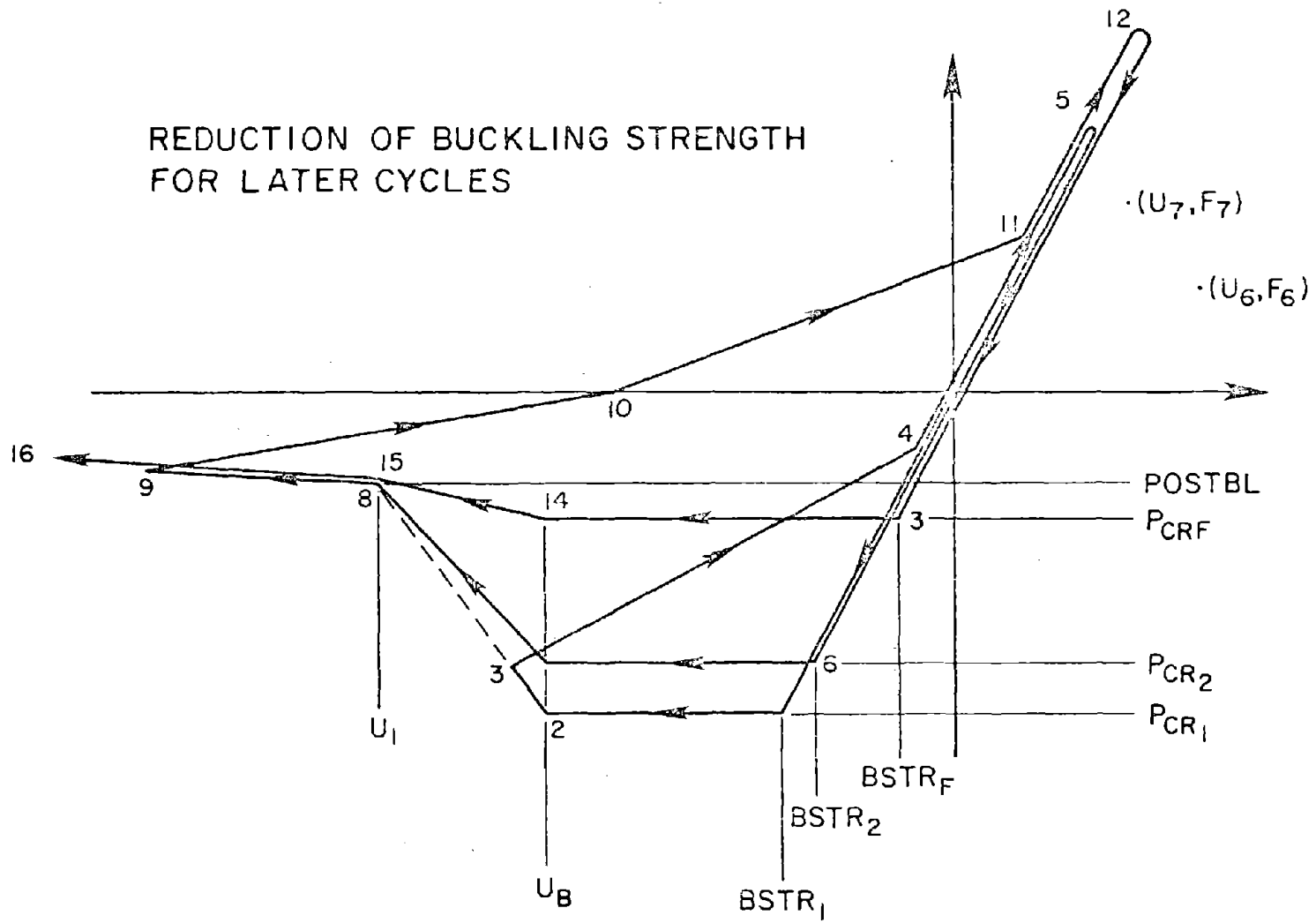
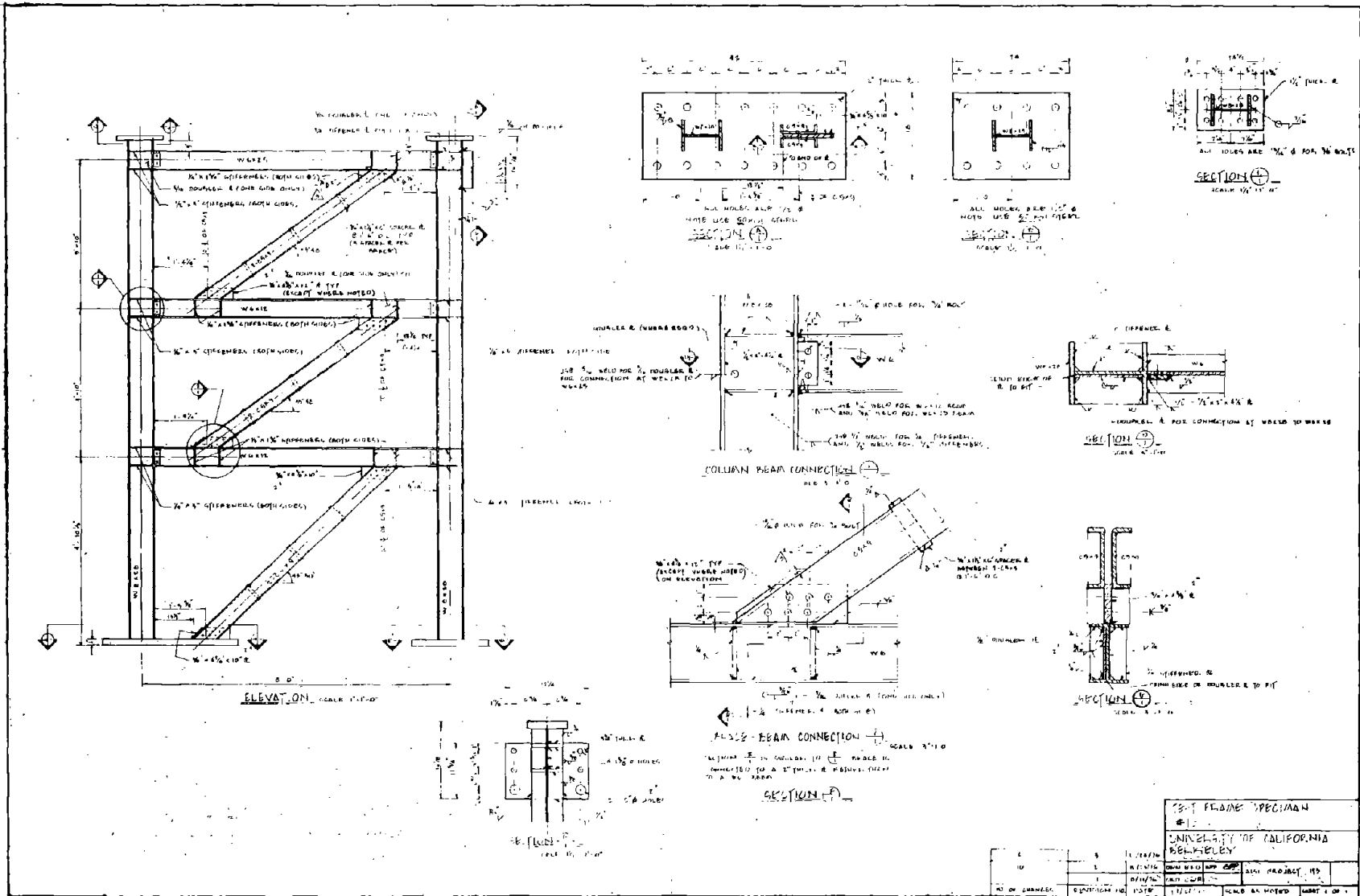


FIGURE D3 - BUCKLING BEHAVIOR DURING LATER CYCLES



Reproduced from  
best available copy.



-303-

FIGURE E1 - WORKING DRAWINGS OF TEST FRAME 1

TEST FRAME SPECIMAN					
UNIVERSITY OF CALIFORNIA					
BERKELEY					
NO. OF SHEETS	SHEET NO.	DATE	SCALE	BY	CHECKED

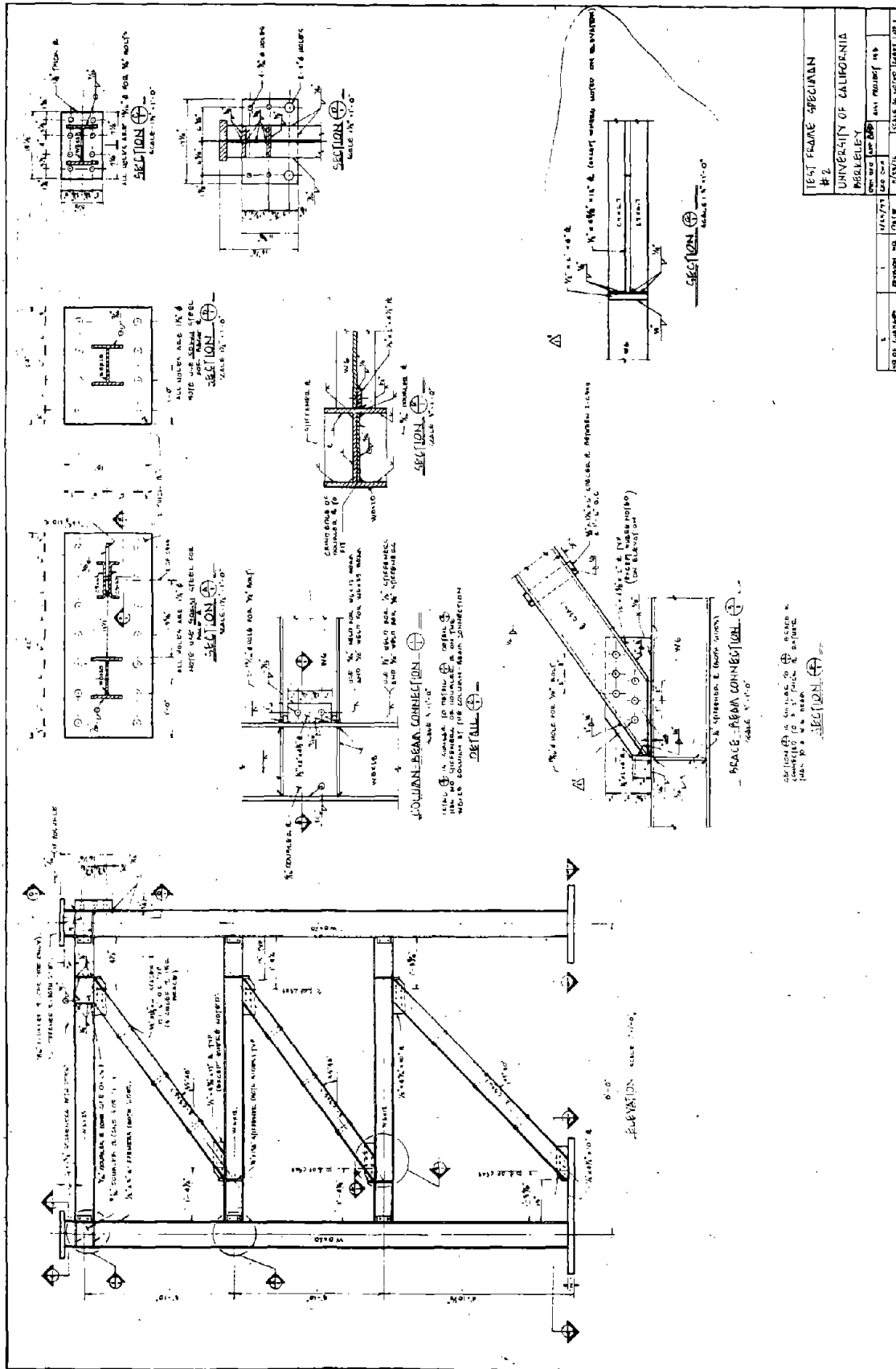
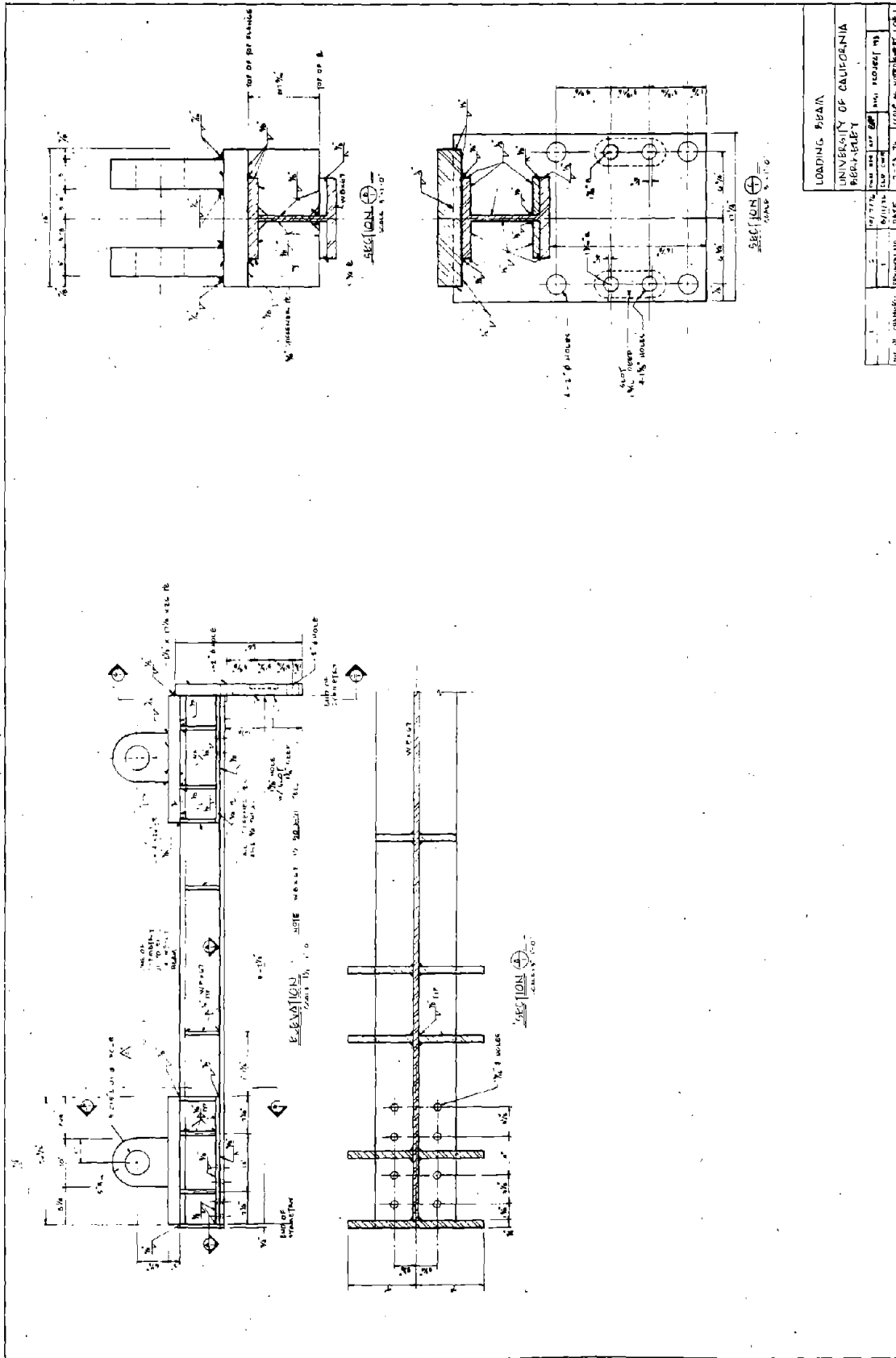


FIGURE E2 - WORKING DRAWINGS OF TEST FRAME 2



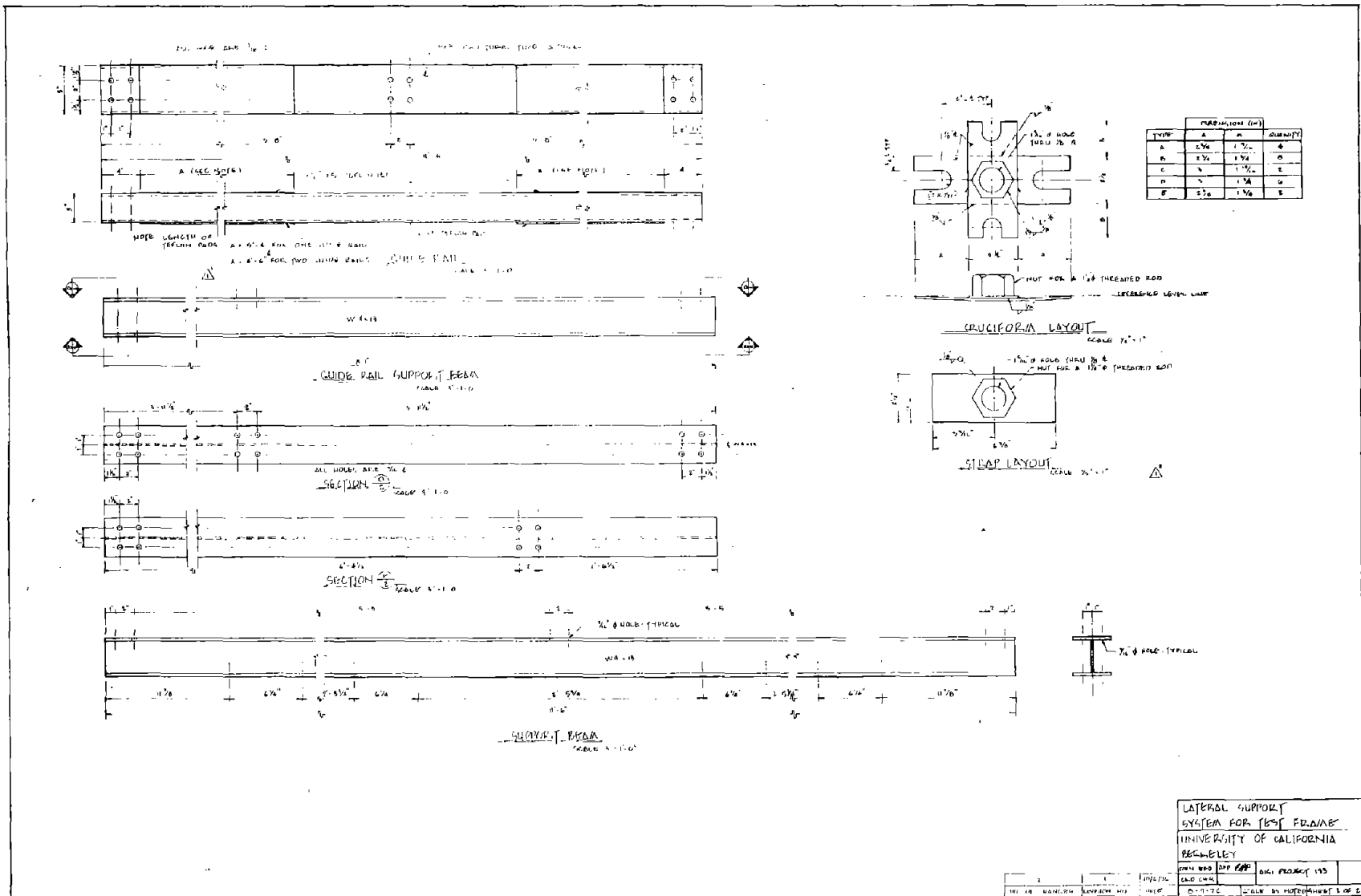
LOADING BEAM	
UNIVERSITY OF CALIFORNIA	
BERKELEY	
DATE	APPROVED BY
DESIGNED BY	CHECKED BY
DRAWN BY	DATE

FIGURE E3 - WORKING DRAWINGS OF THE LOADING BEAM





Reproduced from  
best available copy.



-307-

FIGURE E5 - WORKING DRAWINGS OF THE LATERAL SUPPORT FRAME



EARTHQUAKE ENGINEERING RESEARCH CENTER REPORTS

NOTE: Numbers in parentheses are Accession Numbers assigned by the National Technical Information Service; these are followed by a price code. Copies of the reports may be ordered from the National Technical Information Service, 5285 Port Royal Road, Springfield, Virginia, 22161. Accession Numbers should be quoted on orders for reports (PB--- ---) and remittance must accompany each order. Reports without this information were not available at time of printing. Upon request, EERC will mail inquirers this information when it becomes available.

- EERC 67-1 "Feasibility Study of Large-Scale Earthquake Simulator Facility," by J. Penzien, J. G. Bouwkamp, R. W. Clough, and D. Rea - 1967 (PB 187 905)A07
- EERC 68-1 Unassigned
- EERC 68-2 "Inelastic Behavior of Beam-to-Column Subassemblages under Repeated Loading," by V. V. Bertero - 1968 (PB 184 888)A05
- EERC 68-3 "A Graphical Method for Solving the Wave Reflection-Refraction Problem," by H. D. McNiven and Y. Mengi - 1968 (PB 187 943)A03
- EERC 68-4 "Dynamic Properties of McKinley School Buildings," by D. Rea, J. G. Bouwkamp, and R. W. Clough - 1968 (PB 187 902)A07
- EERC 68-5 "Characteristics of Rock Motions during Earthquakes," by H. B. Seed, I. M. Idriss, and F. W. Kiefer - 1968 (PB 188 338)A03
- EERC 69-1 "Earthquake Engineering Research at Berkeley," - 1969 (PB 187 906)A11
- EERC 69-2 "Nonlinear Seismic Response of Earth Structures," by M. Dibaj and J. Penzien - 1969 (PB 187 904)A08
- EERC 69-3 "Probabilistic Study of the Behavior of Structures during Earthquakes," by R. Ruiz and J. Penzien - 1969 (PB 187 886)A06
- EERC 69-4 "Numerical Solution of Boundary Value Problems in Structural Mechanics by Reduction to an Initial Value Formulation," by N. Distefano and J. Schujman - 1969 (PB 187 942)A02
- EERC 69-5 "Dynamic Programming and the Solution of the Biharmonic Equation," by N. Distefano - 1969 (PB 187 941)A03
- EERC 69-6 "Stochastic Analysis of Offshore Tower Structures," by A. K. Malhotra and J. Penzien - 1969 (PB 187 903)A09
- EERC 69-7 "Rock Motion Accelerograms for High Magnitude Earthquakes," by H. B. Seed and I. M. Idriss - 1969 (PB 187 940)A02
- EERC 69-8 "Structural Dynamics Testing Facilities at the University of California, Berkeley," by R. M. Stephen, J. G. Bouwkamp, R. W. Clough and J. Penzien - 1969 (PB 189 111)A04
- EERC 69-9 "Seismic Response of Soil Deposits Underlain by Sloping Rock Boundaries," by H. Dezfulian and H. B. Seed - 1969 (PB 189 114)A03
- EERC 69-10 "Dynamic Stress Analysis of Axisymmetric Structures under Arbitrary Loading," by S. Ghosh and E. L. Wilson - 1969 (PB 189 026)A10
- EERC 69-11 "Seismic Behavior of Multistory Frames Designed by Different Philosophies," by J. C. Anderson and V. V. Bertero - 1969 (PB 190 662)A10
- EERC 69-12 "Stiffness Degradation of Reinforcing Concrete Members Subjected to Cyclic Flexural Moments," by V. V. Bertero, B. Bresler, and H. Ming Liao - 1969 (PB 202 942)A07
- EERC 69-13 "Response of Non-Uniform Soil Deposits to Travelling Seismic Waves," by H. Dezfulian and H. B. Seed - 1969 (PB 191 023)A03
- EERC 69-14 "Damping Capacity of a Model Steel Structure," by D. Rea, R. W. Clough, and J. G. Bouwkamp - 1969 (PB 190 663)A06
- EERC 69-15 "Influence of Local Soil Conditions on Building Damage Potential during Earthquakes," by H. B. Seed and I. M. Idriss - 1969 (PB 191 036)A03

- EERC 69-16 "The Behavior of Sands under Seismic Loading Conditions," by M. L. Silver and H. B. Seed - 1969 (AD 714 982)A07
- EERC 70-1 "Earthquake Response of Gravity Dams," by A. K. Chopra - 1970 (AD 709 640)A03
- EERC 70-2 "Relationships between Soil Conditions and Building Damage in the Caracas Earthquake of July 29, 1967," by H. B. Seed, I. M. Idriss, and H. Dezfulian - 1970 (PB 195 762)A05
- EERC 70-3 "Cyclic Loading of Full Size Steel Connections," by E. P. Popov and R. M. Stephen - 1970 (PB 213 545)A04
- EERC 70-4 "Seismic Analysis of the Charaima Building, Caraballeda, Venezuela," by Subcommittee of the SEAONC Research Committee: V. V. Bertero, P. F. Fratessa, S. A. Mahin, J. H. Sexton, A. C. Scordelis, E. L. Wilson, L. A. Wyllie, H. B. Seed, and J. Penzien, Chairman - 1970 (PB 201 455)A06
- EERC 70-5 "A Computer Program for Earthquake Analysis of Dams," by A. K. Chopra and P. Chakrabarti - 1970 (AD 723 994)A05
- EERC 70-6 "The Propagation of Love Waves Across Non-Horizontally Layered Structures," by J. Lysmer and L. A. Drake - 1970 (PB 197 896)A03
- EERC 70-7 "Influence of Base Rock Characteristics on Ground Response," by J. Lysmer, H. B. Seed, and P. B. Schnabel - 1970 (PB 197 897)A03
- EERC 70-8 "Applicability of Laboratory Test Procedures for Measuring Soil Liquefaction Characteristics under Cyclic Loading," by H. B. Seed and W. H. Peacock - 1970 (PB 198 016)A03
- EERC 70-9 "A Simplified Procedure for Evaluating Soil Liquefaction Potential," by H. B. Seed and I. M. Idriss - 1970 (PB 198 009)A03
- EERC 70-10 "Soil Moduli and Damping Factors for Dynamic Response Analysis," by H. B. Seed and I. M. Idriss - 1970 (PB 197 869)A03
- EERC 71-1 "Koyna Earthquake of December 11, 1967 and the Performance of Koyna Dam," by A. K. Chopra and P. Chakrabarti - 1971 (AD 731 496)A06
- EERC 71-2 "Preliminary In-Situ Measurements of Anelastic Absorption in Soils using a Prototype Earthquake Simulator," by R. D. Borcherdt and P. W. Rodgers - 1971 (PB 201 454)A03
- EERC 71-3 "Static and Dynamic Analysis of Inelastic Frame Structures," by F. L. Porter and G. H. Powell - 1971 (PB 210 135)A06
- EERC 71-4 "Research Needs in Limit Design of Reinforced Concrete Structures," by V. V. Bertero - 1971 (PB 202 943)A04
- EERC 71-5 "Dynamic Behavior of a High-Rise Diagonally Braced Steel Building," by D. Rea, A. A. Shah, and J. G. Bouwkamp - 1971 (PB 203 584)A06
- EERC 71-6 "Dynamic Stress Analysis of Porous Elastic Solids Saturated with Compressible Fluids," by J. Ghaboussi and E. L. Wilson - 1971 (PB 211 396)A06
- EERC 71-7 "Inelastic Behavior of Steel Beam-to-Column Subassemblages," by H. Krawinkler, V. V. Bertero, and E. P. Popov - 1971 (PB 211 355)A14
- EERC 71-8 "Modification of Seismograph Records for Effects of Local Soil Conditions," by P. Schnabel, H. B. Seed, and J. Lysmer - 1971 (PB 214 450)A03
- EERC 72-1 "Static and Earthquake Analysis of Three Dimensional Frame and Shear Wall Buildings," by E. L. Wilson and H. H. Dovey - 1972 (PB 212 904)A05
- EERC 72-2 "Accelerations in Rock for Earthquakes in the Western United States," by P. B. Schnabel and H. B. Seed - 1972 (PB 213 100)A03
- EERC 72-3 "Elastic-Plastic Earthquake Response of Soil-Building Systems," by T. Minami - 1972 (PB 214 868)A08
- EERC 72-4 "Stochastic Inelastic Response of Offshore Towers to Strong Motion Earthquakes," by M. K. Kaul - 1972 (PB 215 713)A05

- EERC 72-5 "Cyclic Behavior of Three Reinforced Concrete Flexural Members with High Shear," by E. P. Popov, V. V. Bertero, and H. Krawinkler - 1972 (PB 214 555)A05
- EERC 72-6 "Earthquake Response of Gravity Dams Including Reservoir Interaction Effects," by P. Chakrabarti and A. K. Chopra - 1972 (AD 762 330)A08
- EERC 72-7 "Dynamic Properties of Pine Flat Dam," by D. Rea, C. Y. Liaw, and A. K. Chopra - 1972 (AD 763 928)A05
- EERC 72-8 "Three Dimensional Analysis of Building Systems," by E. L. Wilson and H. H. Dovey - 1972 (PB 222 438)A06
- EERC 72-9 "Rate of Loading Effects on Uncracked and Repaired Reinforced Concrete Members," by S. Mahin, V. V. Bertero, D. Rea and M. Atalay - 1972 (PB 224 520)A08
- EERC 72-10 "Computer Program for Static and Dynamic Analysis of Linear Structural Systems," by E. L. Wilson, K.-J. Bathe, J. E. Peterson and H. H. Dovey - 1972 (PB 220 437)A04
- EERC 72-11 "Literature Survey - Seismic Effects on Highway Bridges," by T. Iwasaki, J. Penzien, and R. W. Clough - 1972 (PB 215 613)A19
- EERC 72-12 "SHAKE - A Computer Program for Earthquake Response Analysis of Horizontally Layered Sites," by P. B. Schnabel and J. Lysmer - 1972 (PB 220 207)A06
- EERC 73-1 "Optimal Seismic Design of Multistory Frames," by V. V. Bertero and H. Kamil - 1973
- EERC 73-2 "Analysis of the Slides in the San Fernando Dams during the Earthquake of February 9, 1971," by H. B. Seed, K. L. Lee, I. M. Idriss, and F. Makdisi - 1973 (PB 223 402)A14
- EERC 73-3 "Computer Aided Ultimate Load Design of Unbraced Multistory Steel Frames," by M. B. El-Hafez and G. H. Powell - 1973 (PB 248 315)A09
- EERC 73-4 "Experimental Investigation into the Seismic Behavior of Critical Regions of Reinforced Concrete Components as Influenced by Moment and Shear," by M. Celebi and J. Penzien - 1973 (PB 215 884)A09
- EERC 73-5 "Hysteretic Behavior of Epoxy-Repaired Reinforced Concrete Beams," by M. Celebi and J. Penzien - 1973 (PB 239 568)A03
- EERC 73-6 "General Purpose Computer Program for Inelastic Dynamic Response of Plane Structures," by A. Kanaan and G. H. Powell - 1973 (PB 221 260)A08
- EERC 73-7 "A Computer Program for Earthquake Analysis of Gravity Dams Including Reservoir Interaction," by P. Chakrabarti and A. K. Chopra - 1973 (AD 766 271)A04
- EERC 73-8 "Behavior of Reinforced Concrete Deep Beam-Column Subassemblages under Cyclic Loads," by O. Küstü and J. G. Bouwkamp - 1973 (PB 246 117)A12
- EERC 73-9 "Earthquake Analysis of Structure-Foundation Systems," by A. K. Vaish and A. K. Chopra - 1973 (AD 766 272)A07
- EERC 73-10 "Deconvolution of Seismic Response for Linear Systems," by R. B. Reimer - 1973 (PB 227 179)A08
- EERC 73-11 "SAP IV: A Structural Analysis Program for Static and Dynamic Response of Linear Systems," by K.-J. Bathe, E. L. Wilson, and F. E. Peterson - 1973 (PB 221 967)A09
- EERC 73-12 "Analytical Investigations of the Seismic Response of Long, Multiple Span Highway Bridges," by W. S. Tseng and J. Penzien - 1973 (PB 227 816)A10
- EERC 73-13 "Earthquake Analysis of Multi-Story Buildings Including Foundation Interaction," by A. K. Chopra and J. A. Gutierrez - 1973 (PB 222 970)A03
- EERC 73-14 "ADAP: A Computer Program for Static and Dynamic Analysis of Arch Dams," by R. W. Clough, J. M. Raphael, and S. Mojtahedi - 1973 (PB 223 763)A09
- EERC 73-15 "Cyclic Plastic Analysis of Structural Steel Joints," by R. B. Pinkney and R. W. Clough - 1973 (PB 226 843)A08
- EERC 73-16 "QUAD-4: A Computer Program for Evaluating the Seismic Response of Soil Structures by Variable Damping Finite Element Procedures," by I. M. Idriss, J. Lysmer, R. Hwang, and H. B. Seed - 1973 (PB 229 424)A05

- EERC 73-17 "Dynamic Behavior of a Multi-Story Pyramid Shaped Building," by R. M. Stephen, J. P. Hollings, and J. G. Bouwkamp - 1973 (PB 240 718)A06
- EERC 73-18 "Effect of Different Types of Reinforcing on Seismic Behavior of Short Concrete Columns," by V. V. Bertero, J. Hollings, O. Küstü, R. M. Stephen, and J. G. Bouwkamp - 1973
- EERC 73-19 "Olive View Medical Center Materials Studies, Phase I," by B. Bresler and V. V. Bertero - 1973 (PB 235 986)A06
- EERC 73-20 "Linear and Nonlinear Sesismic Analysis Computer Programs for Long Multiple-Span Highway Bridges," by W. S. Tseng and J. Penzien - 1973
- EERC 73-21 "Constitutive Models for Cyclic Plastic Deformation of Engineering Materials," by J. M. Kelly and P. P. Gillis - 1973 (PB 226 024)A03
- EERC 73-22 "DRAIN-2D User's Guide," by G. H. Powell - 1973 (PB 227 016)A05
- EERC 73-23 "Earthquake Engineering at Berkeley - 1973 " 1973 (PB 226 033)A11
- EERC 73-24 Unassigned
- EERC 73-25 "Earthquake Response of Axisymmetric Tower Structures Surrounded by Water," by C. Y. Liaw and A. K. Chopra - 1973 (AD 773 052)A09
- EERC 73-26 "Investigation of the Failures of the Olive View Stairtowers during the San Fernando Earthquake and Their Implications on Seismic Design," by V. V. Bertero and R. G. Collins - 1973 (PB 235 106)A13
- EERC 73-27 "Further Studies on Seismic Behavior of Steel Beam-Column Subassemblages," by V. V. Bertero, H. Krawinkler, and E. P. Popov - 1973 (PB 234 172)A06
- EERC 74-1 "Seismic Risk Analysis," by C. S. Oliveira - 1974 (PB 235 920)A06
- EERC 74-2 "Settlement and Liquefaction of Sands under Multi-Directional Shaking," by R. Pyke, C. K. Chan, and H. B. Seed - 1974
- EERC 74-3 "Optimum Design of Earthquake Resistant Shear Buildings," by D. Ray, K. S. Pister, and A. K. Chopra - 1974 (PB 231 172)A06
- EERC 74-4 "LUSH - A Computer Program for Complex Response Analysis of Soil-Structure Systems," by J. Lysmer, T. Udaka, H. B. Seed, and R. Hwang - 1974 (PB 236 796)A05
- EERC 74-5 "Sensitivity Analysis for Hysteretic Dynamic Systems: Applications to Earthquake Engineering," by D. Ray - 1974 (PB 233 213)A06
- EERC 74-6 "Soil Structure Interaction Analyses for Evaluating Seismic Response," by H. B. Seed, J. Lysmer, and R. Hwang - 1974 (PB 236 519)A04
- EERC 74-7 Unassigned
- EERC 74-8 "Shaking Table Tests of a Steel Frame - A Progress Report," by R. W. Clough and D. Tang - 1974 (PB 240 869)A03
- EERC 74-9 "Hysteretic Behavior of Reinforced Concrete Flexural Members with Special Web Reinforcement," by V. V. Bertero, E. P. Popov, and T. Y. Wang - 1974 (PB 236 797)A07
- EERC 74-10 "Applications of Realiability-Based, Global Cost Optimization to Design of Earthquake Resistant Structures," by E. Vitiello and K. S. Pister - 1974 (PB 237 231)A06
- EERC 74-11 "Liquefaction of Gravelly Soils under Cyclic Loading Conditions," by R. T. Wong, H. B. Seed, and C. K. Chan - 1974 (PB 242 042)A03
- EERC 74-12 "Site-Dependent Spectra for Earthquake-Resistant Design," by H. B. Seed, C. Ugas, and J. Lysmer - 1974 (PB 240 953)A03
- EERC 74-13 "Earthquake Simulator Study of a Reinforced Concrete Frame," by P. Hidalgo and R. W. Clough - 1974 (PB 241 944)A13
- EERC 74-14 "Nonlinear Earthquake Response of Concrete Gravity Dams," by N. Pal - 1974 (AD/A 006 583)A06

- EERC 74-15 "Modeling and Identification in Nonlinear Structural Dynamics - I. One Degree of Freedom Models," by N. Distefano and A. Rath - 1974 (PB 241 548)A06
- EERC 75-1 "Determination of Seismic Design Criteria for the Dumbarton Bridge Replacement Structure, Vol. I: Description, Theory and Analytical Modeling of Bridge and Parameters," by F. Baron and S.-H. Pang - 1975 (PB 259 407)A15
- EERC 75-2 "Determination of Seismic Design Criteria for the Dumbarton Bridge Replacement Structure, Vol. II: Numerical Studies and Establishment of Seismic Design Criteria," by F. Baron and S.-H. Pang - 1975 (PB 259 408)A11 [For set of EERC 75-1 and 75-2 (PB 241 454)A09]
- EERC 75-3 "Seismic Risk Analysis for a Site and a Metropolitan Area," by C. S. Oliveira - 1975 (PB 248 134)A09
- EERC 75-4 "Analytical Investigations of Seismic Response of Short, Single or Multiple-Span Highway Bridges," by M.-C. Chen and J. Penzien - 1975 (PB 241 454)A09
- EERC 75-5 "An Evaluation of Some Methods for Predicting Seismic Behavior of Reinforced Concrete Buildings," by S. A. Mahin and V. V. Bertero - 1975 (PB 246 306)A16
- EERC 75-6 "Earthquake Simulator Story of a Steel Frame Structure, Vol. I: Experimental Results," by R. W. Clough and D. T. Tang - 1975 (PB 243 981)A13
- EERC 75-7 "Dynamic Properties of San Bernardino Intake Tower," by D. Rea, C.-Y. Liaw and A. K. Chopra - 1975 (AD/A 008 406)A05
- EERC 75-8 "Seismic Studies of the Articulation for the Dumbarton Bridge Replacement Structure, Vol. 1: Description, Theory and Analytical Modeling of Bridge Components," by F. Baron and R. E. Hamati - 1975 (PB 251 539)A07
- EERC 75-9 "Seismic Studies of the Articulation for the Dumbarton Bridge Replacement Structure, Vol. 2: Numerical Studies of Steel and Concrete Girder Alternates," by F. Baron and R. E. Hamati - 1975 (PB 251 540)A10
- EERC 75-10 "Static and Dynamic Analysis of Nonlinear Structures," by D. P. Mondkar and G. H. Powell - 1975 (PB 242 434)A08
- EERC 75-11 "Hysteretic Behavior of Steel Columns," by E. P. Popov, V. V. Bertero, and S. Chandramouli - 1975 (PB 252 365)A11
- EERC 75-12 "Earthquake Engineering Research Center Library Printed Catalog" - 1975 (PB 243 711)A26
- EERC 75-13 "Three Dimensional Analysis of Building Systems (Extended Version)," by E. L. Wilson, J. P. Hollings, and H. H. Dovey - 1975 (PB 243 989)A07
- EERC 75-14 "Determination of Soil Liquefaction Characteristics by Large-Scale Laboratory Tests," by P. De Alba, C. K. Chan, and H. B. Seed - 1975 (NUREG 0027)A08
- EERC 75-15 "A Literature Survey - Compressive, Tensile, Bond and Shear Strength of Masonry," by R. L. Mayes and R. W. Clough - 1975 (PB 246 292)A10
- EERC 75-16 "Hysteretic Behavior of Ductile Moment-Resisting Reinforced Concrete Frame Components," by V. V. Bertero and E. P. Popov - 1975 (PB 246 388)A05
- EERC 75-17 "Relationships Between Maximum Acceleration, Maximum Velocity, Distance from Source, Local Site Conditions for Moderately Strong Earthquakes," by H. B. Seed, R. Murarka, J. Lysmer, and I. M. Idriss - 1975 (PB 248 172)A03
- EERC 75-18 "The Effects of Method of Sample Preparation on the Cyclic Stress-Strain Behavior of Sands," by J. Mulilis, C. K. Chan, and H. B. Seed - 1975 (Summarized in EERC 75-28)
- EERC 75-19 "The Seismic Behavior of Critical Regions of Reinforced Concrete Components as Influenced by Moment, Shear and Axial Force," by M. B. Atalay and J. Penzien - 1975 (PB 258 842)A11
- EERC 75-20 "Dynamic Properties of an Eleven Story Masonry Building," by R. M. Stephen, J. P. Hollings, J. G. Bouwkamp, and D. Jurukovski - 1975 (PB 246 945)A04
- EERC 75-21 "State-of-the-Art in Seismic Strength of Masonry - An Evaluation and Review," by R. L. Mayes and R. W. Clough - 1975 (PB 249 040)A07
- EERC 75-22 "Frequency Dependent Stiffness Matrices for Viscoelastic Half-Plane Foundations," by A. K. Chopra, P. Chakrabarti, and G. Dasgupta - 1975 (PB 248 121)A07

- EERC 75-23 "Hysteretic Behavior of Reinforced Concrete Framed Walls," by T. Y. Wang, V. V. Bertero, and E. P. Popov - 1975
- EERC 75-24 "Testing Facility for Subassemblages of Frame-Wall Structural Systems," by V. V. Bertero, E. P. Popov, and T. Endo - 1975
- EERC 75-25 "Influence of Seismic History on the Liquefaction Characteristics of Sands," by H. B. Seed, K. Mori, and C. K. Chan - 1975 (Summarized in EERC 75-28)
- EERC 75-26 "The Generation and Dissipation of Pore Water Pressures during Soil Liquefaction," by H. B. Seed, P. P. Martin, and J. Lysmer - 1975 (PB 252 648)A03
- EERC 75-27 "Identification of Research Needs for Improving Aseismic Design of Building Structures," by V. V. Bertero - 1975 (PB 248 136)A05
- EERC 75-28 "Evaluation of Soil Liquefaction Potential during Earthquakes," by H. B. Seed, I. Arango, and C. K. Chan - 1975 (NUREG 0026)A13
- EERC 74-29 "Representation of Irregular Stress Time Histories by Equivalent Uniform Stress Series in Liquefaction Analyses," by H. B. Seed, I. M. Idriss, F. Makdisi, and N. Banerjee - 1975 (PB 252 635)A03
- EERC 75-30 "FLUSH - A Computer Program for Approximate 3-D Analysis of Soil-Structure Interaction Problems," by J. Lysmer, T. Udaka, C.-F. Tsai, and H. B. Seed - 1975 (PB 259 332)A07
- EERC 75-31 "ALUSH - A Computer Program for Seismic Response Analysis of Axisymmetric Soil-Structure Systems," by E. Berger, J. Lysmer, and H. B. Seed - 1975
- EERC 75-32 "TRIP and TRAVEL - Computer Programs for Soil-Structure Interaction Analysis with Horizontally Travelling Waves," by T. Udaka, J. Lysmer, and H. B. Seed - 1975
- EERC 75-33 "Predicting the Performance of Structures in Regions of High Seismicity," by J. Penzien - 1975 (PB 248 130)A03
- EERC 75-34 "Efficient Finite Element Analysis of Seismic Structure-Soil-Direction," by J. Lysmer, H. B. Seed, T. Udaka, R. N. Hwang, and C.-F. Tsai - 1975 (PB 253 570)A03
- EERC 75-35 "The Dynamic Behavior of a First Story Girder of a Three-Story Steel Frame Subjected to Earthquake Loading," by R. W. Clough and L.-Y. Li - 1975 (PB 248 841)A05
- EERC 75-36 "Earthquake Simulator Story of a Steel Frame Structure, Volume II - Analytical Results," by D. T. Tang - 1975 (PB 252 926)A10
- EERC 75-37 "ANSR-I General Purpose Computer Program for Analysis of Non-Linear Structural Response," by D. P. Mondkar and G. H. Powell - 1975 (PB 252 386)A08
- EERC 75-38 "Nonlinear Response Spectra for Probabilistic Seismic Design and Damage Assessment of Reinforced Concrete Structures," by M. Murakami and J. Penzien - 1975 (PB 259 530)A05
- EERC 75-39 "Study of a Method of Feasible Directions for Optimal Elastic Design of Frame Structures Subjected to Earthquake Loading," by N. D. Walker and K. S. Pister - 1975 (PB 247 781)A06
- EERC 75-40 "An Alternative Representation of the Elastic-Viscoelastic Analogy," by G. Dasgupta and J. L. Sackman - 1975 (PB 252 173)A03
- EERC 75-41 "Effect of Multi-Directional Shaking on Liquefaction of Sands," by H. B. Seed, R. Pyke, and G. R. Martin - 1975 (PB 258 781)A03
- EERC 76-1 "Strength and Ductility Evaluation of Existing Low-Rise Reinforced Concrete Buildings - Screening Method," by T. Okada and B. Bresler - 1976 (PB 257 906)A11
- EERC 76-2 "Experimental and Analytical Studies on the Hysteretic Behavior of Reinforced Concrete Rectangular and T-Beams," by S.-Y. M. Ma, E. P. Popov, and V. V. Bertero - 1976 (PB 260 843)A12
- EERC 76-3 "Dynamic Behavior of a Multistory Triangular-Shaped Building," by J. Petrovski, R. M. Stephen, E. Gartenbaum, and J. G. Bouwkamp - 1976
- EERC 76-4 "Earthquake Induced Deformations of Earth Dams," by N. Serff and H. B. Seed - 1976
- EERC 76-5 "Analysis and Design of Tube-Type Tall Building Structures," by H. de Clercq and G. H. Powell - 1976 (PB 252 220)A10



- EERC 76-6 "Time and Frequency Domain Analysis of Three-Dimensional Ground Motions, San Fernando Earthquake," by T. Kubo and J. Penzien - 1976 (PB 260 556)A11
- EERC 76-7 "Expected Performance of Uniform Building Code Design Masonry Structures," by R. L. Mayes, Y. Omote, S. W. Chen, and R. W. Clough - 1976
- EERC 76-8 "Cyclic Shear Tests on Concrete Masonry Piers, Part I - Test Results," by R. L. Mayes, Y. Omote, and R. W. Clough - 1976 (PB 264 424)A06
- EERC 76-9 "A Substructure Method for Earthquake Analysis of Structure-Soil Interaction," by J. A. Gutierrez and A. K. Chopra - 1976 (PB 247 783)A08
- EERC 76-10 "Stabilization of Potentially Liquefiable San Deposits using Gravel Drain Systems," by H. B. Seed and J. R. Booker - 1976 (PB 248 820)A04
- EERC 76-11 "Influence of Design and Analysis Assumptions on Computed Inelastic Response of Moderately Tall Frames," by G. H. Powell and D. G. Row - 1976
- EERC 76-12 "Sensitivity Analysis for Hysteretic Dynamic Systems: Theory and Applications," by D. Ray, K. S. Pister, and E. Polak - 1976 (PB 262 859)A04
- EERC 76-13 "Coupled Lateral Torsional Response of Buildings to Ground Shaking," by C. L. Kan and A. K. Chopra - 1976 (PB 257 907)A09
- EERC 76-14 "Seismic Analyses of the Banco de America," by V. V. Bertero, S. A. Mahin, and J. A. Hollings - 1976
- EERC 76-15 "Reinforced Concrete Frame 2: Seismic Testing and Analytical Correlation," by R. W. Clough and J. Gidwani - 1976 (PB 261 323)A08
- EERC 76-16 "Cyclic Shear Tests on Masonry Piers, Part II - Analysis of Test Results," by R. L. Mayes, Y. Omote, and R. W. Clough - 1976
- EERC 76-17 "Structural Steel Bracing Systems: Behavior under Cyclic Loading," by E. P. Popov, K. Takanashi, and C. W. Roeder - 1976 (PB 260 715)A05
- EERC 76-18 "Experimental Model Studies on Seismic Response of High Curved Overcrossings," by D. Williams and W. G. Godden - 1976
- EERC 76-19 "Effects of Non-Uniform Seismic Disturbances on the Dumbarton Bridge Replacement Structure," by F. Baron and R. E. Hamati - 1976
- EERC 76-20 "Investigation of the Inelastic Characteristics of a Single Story Steel Structure using System Identification and Shaking Table Experiments," by V. C. Matzen and H. D. McNiven - 1976 (PB 258 453)A07
- EERC 76-21 "Capacity of Columns with Splice Imperfections," by E. P. Popov, R. M. Stephen and R. Philbrick - 1976 (PB 260 378)A04
- EERC 76-22 "Response of the Olive View Hospital Main Building during the San Fernando Earthquake," by S. A. Mahin, V. V. Bertero, A. K. Chopra, and R. Collins," - 1976
- EERC 76-23 "A Study on the Major Factors Influencing the Strength of Masonry Prisms," by N. M. Mostaghel, R. L. Mayes, R. W. Clough, and S. W. Chen - 1976
- EERC 76-24 "GADFLEA - A Computer Program for the Analysis of Pore Pressure Generation and Dissipation during Cyclic or Earthquake Loading," by J. R. Booker, M. S. Rahman, and H. B. Seed - 1976 (PB 263 947)A04
- EERC 76-25 "Rehabilitation of an Existing Building: A Case Study," by B. Bresler and J. Axley - 1976
- EERC 76-26 "Correlative Investigations on Theoretical and Experimental Dynamic Behavior of a Model Bridge Structure," by K. Kawashima and J. Penzien - 1976 (PB 263 388)A11
- EERC 76-27 "Earthquake Response of Coupled Shear Wall Buildings," by T. Srichatrapimuk - 1976 (PB 265 157)A07
- EERC 76-28 "Tensile Capacity of Partial Penetration Welds," by E. P. Popov and R. M. Stephen - 1976 (PB 262 899)A03
- EERC 76-29 "Analysis and Design of Numerical Integration Methods in Structural Dynamics," by H. M. Hilber - 1976 (PB 264 410)A06

- EERC 76-30 "Contribution of a Floor System to the Dynamic Characteristics of Reinforced Concrete Buildings," by L. E. Malik and V. V. Bertero - 1976
- EERC 76-31 "The Effects of Seismic Disturbances on the Golden Gate Bridge," by F. Baron, M. Arikan, R. E. Hamati - 1976
- EERC 76-32 "Infilled Frames in Earthquake-Resistant Construction," by R. E. Klingner and V. V. Bertero - 1976 (PB 265 892)A13
- UCB/EERC-77/01 "PLUSH - A Computer Program for Probabilistic Finite Element Analysis of Seismic Soil-Structure Interaction," by M. P. Romo Organista, J. Lysmer, and H. B. Seed - 1977
- UCB/EERC-77/02 "Soil-Structure Interaction Effects at the Humboldt Bay Power Plant in the Ferndale Earthquake of June 7, 1975," by J. E. Valera, H. B. Seed, C.-F. Tsai, and J. Lysmer - 1977 ( B 265 795)A04
- UCB/EERC-77/03 "Influence of Sample Disturbance on Sand Response to Cyclic Loading," by K. Mori, H. B. Seed, and C. K. Chan - 1977 (PB 267 352)A04
- UCB/EERC-77/04 "Seismological Studies of Strong Motion Records," by J. Shoja-Taheri - 1977 (PB 269 655)A10
- UCB/EERC-77/05 "Testing Facility for Coupled Shear Walls," by L.-H. Lee, V. V. Bertero, and E. P. Popov - 1977
- UCB/EERC-77/06 "Developing Methodologies for Evaluating the Earthquake Safety of Existing Buildings," No. 1 - B. Bresler; No. 2 - B. Bresler, T. Okada, and D. Zisling; No. 3 - T. Okada and B. Bresler; No. 4 - V. V. Bertero and B. Bresler - 1977 (PB 267 354)A08
- UCB/EERC-77/07 "A Literature Survey - Transverse Strength of Masonry Walls," by Y. Omote, R. L. Mayes, S. W. Chen, and R. W. Clough - 1977
- UCB/EERC-77/08 "DRAIN-TABS: A Computer Program for Inelastic Earthquake Response of Three Dimensional Buildings," by R. Guendelman-Israel and G. H. Powell - 1977
- UCB/EERC-77/09 "SUBWALL: A Special Purpose Finite Element Computer Program for Practical Elastic Analysis and Design of Structural Walls with Substructure Option," by D. Q. Le, H. Petersson, and E. P. Popov - 1977
- UCB/EERC-77/10 "Experimental Evaluation of Seismic Design Methods for Broad Cylindrical Tanks," by D. P. Clough - 1977
- UCB/EERC-77/11 "Earthquake Engineering Research at Berkeley - 1976," - 1977
- UCB/EERC-77/12 "Automated Design of Earthquake Resistant Multistory Steel Building Frames," by N. D. Walker, Jr. - 1977
- UCB/EERC-77/13 "Concrete Confined by Rectangular Hoops and Subjected to Axial Loads," by J. Vallenias, V. V. Bertero, and E. P. Popov - 1977
- UCB/EERC-77/14 "Seismic Strain Induced in the Ground during Earthquakes," by Y. Sugimura - 1977
- UCB/EERC-77/15 "Bond Deterioration under Generalized Loading," by V. V. Bertero, E. P. Popov, and S. Viwathanatepa - 1977
- UCB/EERC-77/16 "Computer-Aided Optimum Design of Ductile Reinforced Concrete Moment-Resisting Frames," by S. W. Zagajeski and V. V. Bertero - 1977
- UCB/EERC-77/17 "Earthquake Simulation Testing of a Stepping Frame with Energy-Absorbing Devices," by J. M. Kelly and D. F. Tsztoo - 1977
- UCB/EERC-77/18 "Inelastic Behavior of Eccentrically Braced Steel Frames under Cyclic Loadings," by C. W. Roeder and E. P. Popov - 1977